92-07067/

TEMPERATURE DEPENDENT STEADY-STATE PERMEABILITY AND HYSTERISIS TESTS

[Part of Energy, Mines and Resources Cost-shared Energy Conversion Program and Part of the Program of the Federal Panel on Energy R&D (PERD)]

Prepared by

Hycal Energy Research Laboratories Ltd.
and
Petro-Canada

DSS File No. 006SQ. 23440-9-9259
DSS Contract Serial No. 23440-9-9259/01-SQ
CANMET Scientific Authority: Dr. K.N. Jha

March 1992

MICROMEDIA

SUMMARY

Two high temperature, reservoir condition steady state relative permeability tests were conducted using supplied frozen preserved core material from the 289.84 - 292.95 meter interval of Petro-Canada Hangingstone area well 1-34-84-11 W4M. The tests were performed isothermally at a temperature of 200 ^{O}C with 2000 kPag backpressure and 6200 kPag overburden pressure. Synthetic produced water and cleaned (<1% BS&W) Hangingstone bitumen were utilized for the steady state displacement tests. Oil-water steady state relative permeability curves were generated in both the imbibition and drainage directions in both tests to observe potential relative permeability hysterisis effects. Major results of the study are summarized as follows:

	Test #1	Test #2
Well #	1-34-84-11 W4M	1-34-84-11 W4M
Core ID#	P5	P6
Depth (meters)	289.84	292.65
Sw_i (fraction)	0.058	0.030
So_i (fraction)	0.942	0.970
Ko_i $(\mu m)^2 \times 10^{-3}$	1544.6	1491.94
mD	1565.0	1511.60
K_{abs} (air)		
$(\mu m)^2 \times 10^{-3}$	3048.3	2533.6
mD	3088.5	2567.0
K_{abs}* (fluid)		
$(\mu m)^2 \times 10^{-3}$	1930.8	1864.9
mD	1956.3	1889.5
K_{ro} at Sw_i	0.800	0.800

	Test #1	Test #2
Percent Recovery of Oil by Waterflood	67.0	64.3
Post Waterflood Sor	0.311	0.346
Post Waterflood Sw_{max}	0.689	0.654
Post Waterflood K_w		
$(\mu m)^2 \times 10^{-3}$	120.62	171.01
mD	122.21	173.26
K_{rw} at S_{or}	0.0625	0.0917
Post Hysteresis Oilflood O_{max}	0.861	0.894
Post hysteresis Oilflood S_{wr}	0.139	0.103
Post Oilflood K_o		
$(\mu m)^2 \times 10^{-3}$	1299.2	1445.3
mD	1316.3	1464.4
Pre-test Porosity (%)	39.5	40.4
Post-test Porosity (%)	38.0	39.1

* K_{abs} (fluid) estimated assuming $k_o = 0.80\ k_{abs}$

1. The configuration of the water-oil relative permeability curves, low endpoint permeability to water, high residual oil saturation and trapping phenomena resulting in a higher irreducible water saturation after testing would suggest water wet behavior at 200°C for both core tests.

2. Residual oil saturations ranged between 30 and 35 % after waterflooding at 200 °C indicating recoveries of approximately 65 % of the oil in place by hot waterflooding. Steamflooding at 200 °C, or at higher temperatures, will result in a substantial additional reduction in residual oil saturation.

3. Substantial physical hysteresis was observed in the wetting (oil) phase in both tests. Much less hysteresis was observed in the water phase. Individual phase relative permeabilities were greater when their saturation was increasing than when decreasing.

4. At the temperature level tested (200°C) and the time of duration of the studies (4-5 months/core) no significant evidence of thermally induced formation damage was apparent. Higher temperatures, longer exposure times and actual exposure to a vapor steam phase may result in a greater propensity for damage.

5. The in-situ formation of stable emulsions was observed in both tests. Severity of emulsions was greatest at approximately 40% water, 60% oil simultaneous flow ratios. Maximum emulsification of water in the oil phase observed in this study was about 25 - 27% (by mass). Emulsification level increased fairly linearly with fraction of injected water up to a local maximum of about a 40% injected fraction and then declined to about a 15 - 18% in-situ emulsification level for higher injection ratios. This local maximum may be initiated by an increased in-situ turbulence at these particular saturation levels. An increase in emulsification problems during the water saturation decreasing cycles is apparent, but there is insufficient data available with only the two tests which were conducted to be conclusive.

6. The experimental data for the two relative permeability tests contain a degree of experimental scatter and non-linearity. The data for each test were regressed utilizing a power law formulation of the form:

$$kr_i = k_{max_i} \, (Se_i)^{E_i}_{i=o,w}$$

where i = o, w (oil or water phases)

kr_i = Calculated (regressed) oil or water relative permeability

$kmax_i$ = Endpoint maximum oil or water phase relative permeability value

E_i = Power law constant (regressed)

Se_w = $(Sw - Sw_{min})/(Sw_{max} - Sw_{min})$

Se_o = $1 - Se_w$

These equations will generate smooth, monotonic approximations to the experimental data. Accuracy of the fits may be improved by the use of a more complex functional form (i.e., cubic splines). Regression constants for each test follow:

Test #1	Phase of Test	Fluid Phase	"$Kmax_i$"	E_i
1	water sat^n increasing	oil	0.800	5.263
1	water sat^n increasing	water	0.0625	2.81
1	water sat^n decreasing	oil	0.673	3.511
1	water sat^n decreasing	water	0.0625	2.89
2	water sat^n increasing	oil	0.800	4.839
2	water sat^n increasing	water	0.0917	2.53
2	water sat^n decreasing	oil	0.775	2.097
2	water sat^n decreasing	water	0.0917	2.72

A comparison of the simulator performances of the steady-state and unsteady-state relative permeability curves was conducted. For each case all model input parameters were assumed to be the same, with the exception of the oil-water relative permeability data.

The simulation study indicated that the steady-state permeability curves resulted in less oil production, less water production, and longer production cycles than the unsteady-state permeability curves. However, the differences in the results of the two cases were small, and were considered to be within engineering tolerance.

The similarity between the two simulation cases suggests that the shape of the relative permeability curve does not affect the results as much as the curve endpoints. Both runs used the same temperature dependent end points that were determined in the unsteady-state experiment.

The shape of the water-oil hysterisis envelope differs from data found in the published literature. Also, most published information suggests that the steady-state oil relative permeability curve is above the unsteady-state curve at the same saturation. This study indicates the contrary.

The effect of emulsion flow and core preservation techniques on relative permeabilities cannot be accounted for in an inadequate reservoir model. These effects are beyond the scope of this study and cannot be evaluated at present.

RESUME

Deux essais de perméabilité relative en régime permanent à haute température furent réalisés en utilisant des échantillons préservés de carottes gelées provenant des intervalles 289.84 à 292.95 mètres du puit 1-34-84-11 W4M situé à Hangingstone en Alberta. Les essais furent performés de façon isothermale à une température de 200 ^{O}C, une pression de confinement de 200 kPag et une pression de mort terrain de 6200 kPag. De l'eau de production reconstruite synthétiquement et du bitume propre (<1% BS&W) furent utilisés pour les essais de déplacement en régime permanent. Afin d'observer le potentiel d'hystérèse de la perméabilité relative, les courbes pétrole-eau de perméabilité relative en régime permanent ont été générées dans les directions d'imbibition et de drainage pour les deux essais. Les résultats principaux de l'étude sont les suivants:

	Essai #1	Essai #2
Puits No.	1-34-84-11 W4M	1-34-84-11 W4M
Carotte No.	P5	P6
Profondeur (mètre)	289.84	292.65
Sw_i (fraction)	0.058	0.030
So_i (fraction)	0.942	0.970
Ko_i $(\mu m)^2 \times 10^{-3}$ mD	1544.6 1565.0	1491.94 1511.60
K_{abs} (air) $(\mu m)^2 \times 10^{-3}$ mD	3048.3 3088.5	2533.6 2567.0
K_{abs} * (fluide) $(\mu m)^2 \times 10^{-3}$ mD	1930.8 1956.3	1864.9 1889.5
K_{ro} à Sw_i	0.800	0.800

	Essai #1	Essai #2
Récupération de Pétrole par Injection d'eau (%)	67.0	64.3
Sor après Injection d'eau	0.311	0.346
Sw_{max} après Injection d'eau	0.689	0.654
K_w après Injection d'eau $(\mu m)^2 \times 10^{-3}$ mD	120.62 122.21	171.01 173.26
K_{rw} à S_{or}	0.0625	0.0917
O_{max} après Hystérèse du Pétrole	0.861	0.894
S_{wr} après Hystérèse du Pétrole	0.139	0.103
K_o après Hystérèse du Pétrole $(\mu m)^2 \times 10^{-3}$ mD	1299.2 1316.3	1445.3 1464.4
Porosité de Pré-Test (%)	39.5	40.4
Porosité d'Après-Test (%)	38.0	39.1

* K_{abs} (fluide) est estimé en assumant $k_o = 0.80\ k_{abs}$

1. La configuration des courbes de perméabilité relative de eau-pétrole, la faible valeur de la limite inférieure de la perméabilité à l'eau, la grande saturation résiduelle en pétrole et le phénomène d'entrappement résultant en une saturation résiduelle en eau supérieure après les essais suggèrent un comportement de mouillage par l'eau à 200°C pour les deux essais effectués sur les carottes.

2. Les saturations résiduelles en pétrole varient entre 30 et 35 % après l'injection d'eau à 200 ^{O}C. Ceci nous indique des récupérations d'environ 65 % du pétrole en place par injection d'eau chaude. L'injection de vapeur à 200 ^{O}C ou plus résultera donc, en des réductions additionelles fort substantielles de la saturation en pétrole résiduel.

3. De substantielles hystérèses physiques ont été observées lors de la phase de mouillage par le pétrole dans les deux essais. Toutefois, durant la phase de mouillage par l'eau, les hystérèses observées etaient moindres. Les valeurs de perméabilité relative durant les phases individuelles étaient plus grandes quand la saturation augmentait que lorsqu'elle diminuait.

4. Au niveau de température testé (200°C) et avec la durée des études (4-5 mois/carotte), nous n'avons remarqué aucune évidence significative de dommages induits par la chaleur sur la formation. Des températures plus élevées, des temps d'exposition plus longs, alliés à une exposition à la vapeur d'eau pourraient cependant résulter en une plus grande propension aux dommages.

5. La formation in-situ d'émulsions stables a été observée dans les deux essais. La formation d'émulsion était plus grande à un ratio approximativement égal à 40% eau - 60% pétrole. L'émulsion maximale de l'eau dans la phase de pétrole observée lors de cette étude a été d'environ 25 à 27% par masse. Le niveau d'émulsion augmente de façon généralement linéaire avec la fraction d'eau injectée jusqu'à un niveau local maximal de fraction injectée d'environ 40%. Pour des ratios d'injection supérieurs à 40%, le niveau d'émulsion in-situ diminue à environ 15 à 18%. Ce maximum local peut être engendré en augmentant la turbulence in-situ aux niveaux de saturation en question. Une augmentation des problèmes d'émulsion durant les cycles décroissants de saturation d'eau est apparente, mais le nombre de données provenant de ces deux essais est insuffisant pour mener à une conclusion.

6. Les données expérimentales pour les deux essais de perméabilité relative contiennent un certain degré de dispersion expérimentale et de non-linéarité. Les données de chaque essai ont été régressées en utilisant une formule exponentielle de la forme suivante:

$$kr_i = k_{max_i} (Se_i)^{Ei}{}_{i=o,w}$$

où i = o, w (pétrole ou eau)

kr_i = perméabilité relative calculée du pétrole ou de l'eau

$kmax_i$ = valeur maximale de perméabilité relative du pétrole ou de l'eau

E_i = constante calculée de la loi exponentielle

Se_w = $(Sw - Sw_{min}) / (Sw_{max} - Sw_{min})$

Se_o = $1 - Se_w$

Ces équations génèrent des approximations douces et monotones des données expérimentales. La précision des ajustements peut être améliorée en utilisant des fonctions plus complexes (i.e. spirales cubiques). Les constantes de régression pour chaque essai sont les suivantes:

Essai #	Phase de l'essai	Type de Fluide	"$Kmax_i$"	E_i
1	saturation d'eau croissante	pétrole	0.800	5.263
1	saturation d'eau croissante	eau	0.0625	2.81
1	saturation d'eau décroissante	pétrole	0.673	3.511
1	saturation d'eau décroissante	eau	0.0625	2.89
2	saturation d'eau croissante	pétrole	0.800	4.839
2	saturation d'eau croissante	eau	0.0917	2.53
2	saturation d'eau décroissante	pétrole	0.775	2.097
2	saturation d'eau décroissante	eau	0.0917	2.72

Une comparaison a été établie entre les courbes de perméabilité relative en régime permanent et en régime irrégulier, obtenues par simulation. Dans chaque cas, on a présumé que tous les paramètres d'entrée des modèles étaient les mêmes, à l'exception des données sur la perméabilité relative eau-pétrole.

L'essai a démontré que les courbes de perméabilité en régime permanent entraînaient une production de pétrole et d'eau plus faible et des cycles de production plus longs que les courbes de perméabilité en régime irrégulier. Cependant, les écarts constatés entre les résultats dans les deux cas étaient faibles et se situaient en deçà des écarts admissibles.

La similarité existant entre les deux cas de simulation semble indiquer que la forme de la courbe de perméabilité relative n'a pas autant d'effet sur les résultats que les valeurs limites de la courbe. Dans les deux cas, on a utilisé les mêmes valeurs limites dépendant de la température que celles ayant été déterminées dans l'expérience en régime irrégulier.

La forme des courbes de l'hystérèse pétrole-eau diffère des données que l'on retrouve dans les publications techniques. De plus, la plupart des publications suggèrent que la courbe de perméabilité relative du pétrole en régime permanent est au-dessus de la courbe en régime irrégulier au même niveau de saturation. La présente étude démontre le contraire.

On ne peut tenir compte des effets sur la perméabilité relative de l'écoulement de l'émulsion et des techniques de stockage des échantillons dans un modèle de gisement inadéquat. Ces effets dépassent la portée de la présente étude et ne peuvent être évalués pour l'instant.

TABLE OF CONTENTS

Page

SUMMARY i
RESUME vi
TABLE OF CONTENTS xi
LIST OF TABLES xii
LIST OF FIGURES xiv
LIST OF APPENDICES xx
INTRODUCTION 1

PART A: LABORATORY EXPERIMENT
- DESCRIPTION OF EQUIPMENT 6
- EXPERIMENTAL PROCEDURE 10
  - Preliminary Preparations 10
  - Displacement Tests 11
  - Effluent Separation - Emulsion Determination 14
- RESULTS AND DISCUSSION 16
  - Preliminary Work 16
  - High Temperature Steady State Test #1 16
  - High Temperature Steady State Test #2 23
  - Smooth Regression Equations for Relative Permeability 29
  - General Discussion 34
  - Data Diskette Summary 36
- CONCLUSIONS 37
- TABLES 38
- FIGURES 53

PART B: NUMERICAL SIMULATION
- BACKGROUND INFORMATION 113
  - Numerical Modelling of the Cyclic Steam Stimulation Process 113
  - Source of Relative Permeability Data 113
  - Model Configuration 113
  - Model Calibration 114
- RESULTS AND DISCUSSION 114
  - Model Performance Comparison 114
  - Analysis of Results 115
  - General Discussion 115
- CONCLUSIONS 118
- TABLES 119
- FIGURES 121

REFERENCES 128
APPENDIX A 129

LIST OF TABLES

Page

TABLE 1: Water Analysis 38

TABLE 2: Supplied Preserved Core Samples 39

TABLE 3: Clean Oil Viscosity Data 40

TABLE 4: Test #1 - Core and Run Parameters 41

TABLE 5: Test #1 - Water Saturation Increasing Relative Permeability Results 42

TABLE 6: Test #1 - Water Saturation Decreasing Relative Permeability Results 43

TABLE 7: Test #1 - Water Saturation Increasing Test - Measured Emulsion Parameters 44

TABLE 8: Test #1 - Water Saturation Decreasing Test - Measured Emulsion Parameters 45

TABLE 9: Steady State Test #1 - Pre/Post Test Core Parameters 46

TABLE 10: Test #2 - Core and Run Parameters 47

TABLE 11: Test #2 - Water Saturation Increasing Relative Permeability Results 48

TABLE 12: Test #2 - Water Saturation Decreasing Relative Permeability Results 49

TABLE 13: Test #2 - Water Saturation Increasing Test - Measured Emulsion Parameters 50

TABLE 14: Test #2 - Water Saturation Decreasing Test - Measured Emulsion Parameters 51

TABLE 15: Steady State Test #2 - Pre/Post Test Parameters 52

LIST OF TABLES (Cont'd)

Page

TABLE 16: THERM Model Properties 119

TABLE 17: Thermal Model Data Summary..... 120

LIST OF FIGURES

		Page
FIGURE 1:	High Temperature Relative Permeability Apparatus Flow Schematic	53
FIGURE 2:	High Temperature Coreholder Schematic	54
FIGURE 3:	Dead Oil Viscosity vs Temperature - Cartesian Co-ordinates	55
FIGURE 4:	Dead Oil Viscosity vs Temperature - Log μ vs 1/K Co-ordinates	56
FIGURE 5:	Steady State Test #1 - Water Saturation Increasing, Oil-Water Relative Permeability vs Saturation (Cartesian Co-ordinates)	57
FIGURE 6:	Steady State Test #1 - Water Saturation Increasing, Oil-Water Relative Permeability vs Saturation (Semi-Log Co-ordinates)	58
FIGURE 7:	Steady State Test #1 - Water Saturation Decreasing, Oil-Water Relative Permeability vs Saturation (Cartesian Co-ordinates)	59
FIGURE 8:	Steady State Test #1 - Water Saturation Decreasing, Oil-Water Relative Permeability vs Saturation (Semi-Log Co-ordinates)	60
FIGURE 9:	Steady State Test #1 - Comparison of Drainage and Imbibition Water-Oil Relative Permeability Curves (Cartesian Co-ordinates)	61
FIGURE 10:	Steady State Test #1 - Comparison of Drainage and Imbibition Water-Oil Relative Permeability Curves (Semi-Log Co-ordinates)	62
FIGURE 11:	Steady State Test #1 - Total Produced % Oil vs Co-injection Ratio (Water Saturation Increasing)	63
FIGURE 12:	Steady State Test #1 - Total produced % Water vs Co-injection Ratio (Water Saturation Increasing)	64

LIST OF FIGURES (Cont'd)

Page

FIGURE 13: Steady State Test #1 - Percent Free Water vs Injected Water Content (Water Saturation Increasing) 65

FIGURE 14: Steady State Test #1 - Percent Emulsified Oil vs Injected Water Content (Water Saturation Increasing) 66

FIGURE 15: Steady State Test #1 - Percent Water Emulsified In Oil vs Injected Water Content (Water Saturation Increasing) 67

FIGURE 16: Steady State Test #1 - Total Produced % Oil vs Co-injection Ratio (Water Saturation Decreasing) 68

FIGURE 17: Steady State Test #1 - Total produced % Water vs Co-injection Ratio (Water Saturation Decreasing) 69

FIGURE 18: Steady State Test #1 - Percent Free Water vs Injected Water Content (Water Saturation Decreasing) 70

FIGURE 19: Steady State Test #1 - Percent Emulsified Oil vs Injected Water Content (Water Saturation Decreasing) 71

FIGURE 20: Steady State Test #1 - Percent Water Emulsified In Oil vs Injected Water Content (Water Saturation Decreasing) 72

FIGURE 21: Steady State Test #1 - Comparative Data (Water Saturation Increasing and Decreasing), Percent Total Produced Oil 73

FIGURE 22: Steady State Test #1 - Comparative Data (Water Saturation Increasing and Decreasing), Percent Total Produced Water 74

FIGURE 23: Steady State Test #1 - Comparative Data (Water Saturation Increasing and Decreasing), Percent "Free" Water 75

FIGURE 24: Steady State Test #1 - Comparative Data (Water Saturation Increasing and Decreasing), Percent Emulsified Oil 76

FIGURE 25: Steady State Test #1 - Comparative Data (Water Saturation Increasing and Decreasing), Percent Oil Emulsified In Water 77

LIST OF FIGURES (Cont'd)

Page

FIGURE 26: Steady State Test #1 - Comparative Production Phase Volume Data for the Test (Total H_2O, Oil, Free Water and Emulsion Content). 78

FIGURE 27: Steady State Test #2 - Water Saturation increasing, Oil-Water Relative Permeability vs Saturation (Cartesian Co-ordinates) 79

FIGURE 28: Steady State Test #2 - Water Saturation Increasing, Oil-Water Relative Permeability vs Saturation (Semi-Log Co-ordinates) 80

FIGURE 29: Steady State Test #2 - Water Saturation Decreasing, Oil-Water Relative Permeability vs Saturation (Cartesian Co-ordinates) 81

FIGURE 30: Steady State Test #2 - Water Saturation Decreasing, Oil-Water Relative Permeability vs Saturation (Semi-Log Co-ordinates) 82

FIGURE 31: Steady State Test #2 - Comparison of Drainage and Imbibition Water-Oil Relative Permeability Curves (Cartesian Co-ordinates) 83

FIGURE 32: Steady State Test #2 - Comparison of Drainage and Imbibition Water-Oil Relative Permeability Curves (Semi-Log Co-ordinates) 84

FIGURE 33: Steady State Test #2 - Percent Total Oil in Effluent (Water Saturation Increasing) 85

FIGURE 34: Steady State Test #2 - Percent Total Water in Effluent (Water Saturation Increasing) 86

FIGURE 35: Steady State Test #2 - Percent Free Water in Effluent (Water Saturation Increasing) 87

FIGURE 36: Steady State Test #2 - Percent Emulsified Oil in Effluent (Water Saturation Increasing) 88

LIST OF FIGURES (Cont'd)

Page

FIGURE 37: Steady State Test #2 - Percent Water Emulsified in Oil in Effluent (Water Saturation Increasing) 89

FIGURE 38: Steady State Test #2 - Percent Total Oil in Effluent (Water Saturation Decreasing) 90

FIGURE 39: Steady State Test #2 - Percent Total Water in Effluent (Water Saturation Decreasing) 91

FIGURE 40: Steady State Test #2 - Percent Free Water in Effluent (Water Saturation Decreasing) 92

FIGURE 41: Steady State Test #2 - Percent Emulsified Oil in Effluent (Water Saturation Decreasing) 93

FIGURE 42: Steady State Test #2 - Percent Water Emulsified in Oil in Effluent (Water Saturation Decreasing) 94

FIGURE 43: Steady State Test #2 - Comparative (Water Saturation Increasing and Decreasing) Total Oil in Effluent. 95

FIGURE 44: Steady State Test #2 - Comparative (Water Saturation Increasing and Decreasing) Total Water in Effluent 96

FIGURE 45: Steady State Test #2 - Comparative (Water Saturation Increasing and Decreasing) Free Water in Effluent 97

FIGURE 46: Steady State Test #2 - Comparative (Water Saturation Increasing and Decreasing) Emulsified Oil in Effluent 98

FIGURE 47: Steady State Test #2 - Comparative (Water Saturation Increasing and Decreasing) Water Emulsified in Oil in Effluent 99

FIGURE 48: Steady State Test #2 - Comparative Production Phase Volume Data for the Test (Total H_2O, Oil, Free Water and Emulsion Extent) 100

LIST OF FIGURES (Cont'd)

Page

FIGURE 49: Steady State Test #1 - Comparison of Experimental and Regressed Relative Permeability Data, Water Saturation Increasing, Cartesian Co-ordinates 101

FIGURE 50: Steady State Test #1 - Comparison of Experimental and Regressed Relative Permeability Data, Water Saturation Increasing, Semi Log Co-ordinates 102

FIGURE 51: Steady State Test #1 - Comparison of Experimental and Regressed Relative Permeability Data, Water Saturation Decreasing, Cartesian Co-ordinates 103

FIGURE 52: Steady State Test #1 - Comparison of Experimental and Regressed Relative Permeability Data, Water Saturation Decreasing, Semi Log Co-ordinates 104

FIGURE 53: Steady State Test #2 - Comparison of Experimental and Regressed Relative Permeability Data, Water Saturation Increasing, Cartesian Co-ordinates 105

FIGURE 54: Steady State Test #2 - Comparison of Experimental and Regressed Relative Permeability Data, Water Saturation Increasing, Semi Log Co-ordinates 106

FIGURE 55: Steady State Test #2 - Comparison of Experimental and Regressed Relative Permeability Data, Water Saturation Decreasing, Cartesian Co-ordinates 107

FIGURE 56: Steady State Test #2 - Comparison of Experimental and Regressed Relative Permeability Data, Water Saturation Decreasing, Semi Log Co-ordinates 108

FIGURE 57: Steady State Test #1 - Comparison of Smoothed Drainage and Imbibition Data, Cartesian Co-ordinates 109

FIGURE 58: Steady State Test #1 - Comparison of Smoothed Drainage and Imbibition Data, Semi-Log Co-ordinates 110

FIGURE 59: Steady State Test #2 - Comparison of Smoothed Drainage and Imbibition Data, Cartesian Co-ordinates 111

LIST OF FIGURES (Cont'd)

Page

FIGURE 60: Steady State Test #2 - Comparison of Smoothed Drainage and Imbibition Data, Semi-Log Co-ordinates 112

FIGURE 61: Typical Pilot Well Geology 121

FIGURE 62: Typical Model Grid Configuration 122

FIGURE 63: Typical Model Calibration with Field Data 123

FIGURE 64: Comparison of Steady-State and Unsteady-State Laboratory Test Data at 200°C 124

FIGURE 65: Normalized Relative Permeability Curves at 200°C 125

FIGURE 66: Smoothed Normalized Curves and De-Normalized Curves: Steady State Relative Permeability Test Data 126

FIGURE 67: CSS Performance Comparison: Steady-State and Unsteady-State Relative Permeabilities 127

LIST OF APPENDICES

Page

APPENDIX A 114

Paper SPE 23783, "Formation Damage Due to Mineral Alteration and Wettability Changes During Hot Water and Steam Injection in Clay Bearing Sandstone Reservoirs

Paper CIM 83-34-46, "Effect of Relative Permeability on the Numerical Simulation of the Steam Stimulation Process

INTRODUCTION

This steady-state relative permeability and emulsion study was initiated by the PCEJ Hangingstone partners: Petro-Canada, Canadian Occidental Petroleum Ltd., Esso Resources Canada Ltd., and Japan Canada Oil Sands Ltd. The project was 50% funded by CANMET. The laboratory research work was completed by Hycal Energy Research Laboratories Ltd.

The project consisted in the determination of the oil and water relative permeabilities, at reservoir conditions, of two different core samples from the Athabasca Oil Sands. Upon initiation of the study, no thermal steady-state relative permeability data or hysterisis analysis was available for Athabasca's McMurray formation. These parameters were necessary as existing data and models were not capable of estimating heat propagation or pressure distributions in the formation accurately.

The three main objectives of the project were:

1. to formulate a relationship between temperature and flow characteristics,
2. to determine steady-state thermal relative permeabilities that would provide definition of flow throughout the entire saturation range; this would eliminate the need for extrapolation associated with unsteady-state measurements, and
3. to investigate hysterisis and recognize its possible effect on reservoir behavior.

PART A : LABORATORY EXPERIMENT

DESCRIPTION OF EQUIPMENT

A schematic of the coreflow equipment which was used in the PetroCanada Hangingstone High Temperature Steady State Relative Permeability Study appears as Figure 1. The core material is mounted, while frozen, in a specially machined lead sleeve. Figure 2 provides an illustrative schematic of the final core sleeve assembly utilized. Since the experimental program was designed for steady state displacements it was important to have both inlet and outlet sections of core on either side of the desired test section to absorb capillary outlet effects, inlet effects and to ensure uniformly dispersed fluid flow into and out of the test section. This was accomplished utilizing internal pressure taps so that the pressure differential across the central test section, exclusive of the inlet and outlet sections, could be measured. The pressure tap line is run concentrically down the central bore of the injection line. This facilitates only having a single ported large bore tap for both the injection or production of fluid as well as for the measurement of pressure.

Stainless steel (316) sealing heads and nuts confine and seal the encasing lead sleeve preventing the influx of external annular core pressure into the core stack. The core material is retained through the use of specially fused sintered 300 mesh glass retaining disks which were specially manufactured for this project. The sintered glass retaining disks are placed at the injection and production ends of the core. These disks are in place to prevent the relatively plastic core material from being extruded from the core holder upon application of the annular overburden pressure but coarse enough to allow production of a wide size distribution of fines from the core material without plugging and blockage

occurring. The disks also ensure smooth, well dispersed injection and production of fluids from the core. This mounting arrangement eliminates the need for gravel packs and facilitates mounting the cores with a minimum amount of core disturbance. The core pack is compressed hydraulically once mounted to eliminate capillary discontinuities between the individual plugs in the stack. The ductility of the sleeve material facilitates the application of a confining overburden pressure directly to the core material by pressurizing the annular space in the pressure vessel. The injection and production ends of the core heads are equipped with radial distribution plates to ensure that no areas of localized high velocity occur when injecting or producing fluids.

The pressure vessel is equipped with two separate internal heating systems controlled by ERD digital temperature controllers which are capable of elevating core temperature to 340°C. The pressure vessel is rated for 20.7 MPa at 340°C. The pressure jacket is equipped with an external electrically heat traced insulating jacket to minimize external heat losses at elevated temperature.

Pressure differential across the entire core is monitored through the use of two model DP15 Validyne pressure transducers. The transducers are connected in a manifold type arrangement, one having a range of 0 - 140 kPa while the second has a range of 0 - 1400 kPa. This arrangement facilitates the accurate measurement of both high and low pressure differentials which may occur over the course of a series of displacement tests. Both the low and high pressure transducers can be isolated should the pressure differentials in the system exceed their rated value. The transducer system is insulated and electrically heat traced

(85°C) to ensure smooth transmission of pressure through the tubing to the transducers when heavy oil is present in the system. Visual gauges are also connected to the injection and production system from which the operator can take readings as a backup for the pressure transducer system. The transducers output to a digital display terminal from which the operator can obtain the instantaneous pressure differential. The transducers are calibrated prior to each run at run pressure using a set of highly accurate dead weight testers.

Another set of transducers identical to those described previously is located to measure the pressure differential across the center test section of the core under steady state flow.

Both oil and brine are displaced through the sample using a pair of highly accurate digitally controlled, variable speed, synchronous control Ruska type positive displacement pumps. The pumps can inject at a range of speeds from 0.5 to 2000 cc/hr (0.008 to 33.33 cc/min) at pressures of up to 70 MPa with a 0.01 cc accuracy. The positive displacement type action of the pumps provides a very smooth and steady displacement minimizing velocity and pressure shocks to the core matrix.

Injection fluids are stored in 3.8 litre high pressure 316 SS storage cylinders. The system is designed so that either gas, brine or oil can be injected into the core material. Due to the high oil viscosity and the tendency of heavy oils to form emulsions with water or mercury when they are used as displacing fluids a high pressure 1000 cc 316 SS transfer piston is used to displace oil into the core. The transfer piston is heat jacketed and the

injection line to the core heat traced to allow smooth flow of the heavy oil to the core sample. All oil is ultracentrifuged prior to use to remove any solids or water which can affect test pressure response.

Due to potential problems with sand production from unconsolidated samples a set of dual high pressure collection pistons is utilized on the production end of the core to collect the produced effluent. The pistons, transfer lines and production tubing are insulated and heat traced to allow smooth production of heavy oil from the core material. The dual piston arrangement allows continuous operation with one piston always on line collecting samples from the core while the second can have its contents emptied for analysis. The rear side of the piston is initially filled with distilled water and pressurized to run pressure using the sampling pump. As effluent from the core enters the piston barrel the piston is displaced pushing water out through a 316 SS 70 MPa regulating backpressure system accurate to 0.5% of the setpoint value facilitating smooth reservoir condition collection of the produced samples. Since sand and particulates are collected on the front side of the piston they do not cause problems with scoring and plugging of the backpressure regulation system. Samples are collected by displacing water into the back side of the collection piston and removing the collected oil, gas and water through the sample line.

EXPERIMENTAL PROCEDURE

The following section documents the detailed experimental procedures which were utilized for all of the phases of the Petro Canada Hangingstone Study

Preliminary Preparations

1. Fluids - A produced brine composition was supplied to Hycal by Petro Canada. A large volume (20 litres) of this brine was reconstituted for use in the experimental program utilizing laboratory grade reagents and pure de-ionized water.

   Samples of produced Hangingstone area crude oil were also supplied to Hycal for use in the experiments. The oil samples, as received, contained anywhere from 50 to 95% total water (in both free and emulsified states). The oil phase samples contained up to 50% emulsified water content.

   In order to provide representative relative permeability results and good in-situ emulsification data, it was necessary to clean the oil to approximately 1% total water. This was accomplished by:

   a. Decant/syphon off free water from supplied 20 litre canisters (some samples were mostly water, some contained up to 50% emulsified oil).

   b. Heat emulsified oil (while sealed to avoid oxidation) to approx. 60°C, remove any additional free water.

   c. Solubilize approximately 10% $CaCl_2$ in the emulsion ($CaCl_2$ dissolves in the emulsified water phase and greatly increases its density facilitating greater gravity segregation).

   d. Ultracentrifuge oil to remove remaining entrained water (down to approximately 1% total water content).

   A total of approximately 50 litres of produced emulsion was treated in this fashion to yield about 25 litres of clean crude oil for use in the tests. Due to the time required to clean the oil (only about 250 ml could be cleaned effectively each day) cleaning continued continuously to provide a sufficient supply for the ongoing tests.

2. Viscosity Measurements - In order to facilitate accurate permeability calculations at the test temperature of 200°C it was necessary to have a dynamic fluid viscosity measurement on the dead oil phase (water viscosity at test temperature and pressure was computed utilizing the published available data (see references 1, 2, 3 & 4)). Dead oil viscosities were measured at test operating pressure (2000 kPag) at temperatures of 50, 90, 130, 160 and 200°C. The viscosities were measured on clean (<1% BS&W) dead oil utilizing a calibrated high pressure capillary viscometer.

3. Core Handling - Samples of frozen preserved core were supplied to Hycal by Petro Canada for use in the study. A total of 11 sections of frozen preserved core were supplied from well 1-34-84-11 W4M from the 283.23 to 292.95 m interval.

   The samples, as received, were encased in opaque PVC core sleeving and capped. In order to select representative core material for testing two sets of x-rays were taken of each core sample to screen out shale or heterogeneous sections. Based upon this work core samples P5 (289.84 m) and P6 (292.65 m) were selected for use in the first and second relative permeability experiments respectively.

Displacement Tests

The following section describes the actual experimental procedure utilized in the core displacement tests. Identical procedures were followed for both of the tests which were performed as part of the study.

1. Core Mounting - Approximately 6 - 7 core samples 3.81 cm in diameter by 6 - 7 cm in length were obtained from the parent full diameter core (core P5 or P6). The plugs were obtained by first drilling a 2" OD hole through the side of the PVC confining sleeve. A sharp cutting tool was then used to cleanly punch a 3.81 cm OD core from the core. Each plug was then squared to yield a perfect right cylinder and remove any localized surface areas of mud filtrate invasion. Each plug was carefully visually examined for any evidence of heterogeneities or permeability barriers or stratifications which may have rendered it unsuitable for testing. All of the above procedures were conducted in a nitrogen blanketed environment to avoid any oil oxidation or potential wettability alteration.

2. A custom lead sleeve was fabricated for each core stack as described in the "Experimental Equipment" section of the report. While still frozen 6 - 7 core plugs were inserted into the confining sleeve. The plugs were then allowed to thaw very slightly before placing the composite stack in a hydraulic pressure. A total of 6200 kPa of axial pressure was then applied to the core stack to plastically meld all of the individual plugs together and to eliminate any potential inter-plug capillary discontinuities. The core material was not pounded or pressure shocked in any fashion so as to minimize the potential for any intergranular disturbances.

3. Insert other sealing head and seal core material. Install in pressure jacket, slowly apply 4200 kPa confining pressure to simulate net overburden pressure. Allow core to thaw fully to room temperature while under overburden pressure to allow uniform overburden pressure application.

4. Prepare system for run, activate heat tracing on all lines (approx. 85°C), injection pistons, production pistons. Heat core sample to mobilization temperature (approximately 80°C). Commence injection of clean dead oil to pressurize core to run operating pressure of 2000 kPa. Simultaneously increase overburden pressure to 6200 kPa, always maintaining at net 4200 kPa overburden pressure on the core material. Set backpressure regulator at 2000 kPa. Flood dead oil through core and confirm stabilized operation.

5. Slowly over an approximately 30 hour period, heat core material to test operating temperature of 200°C and maintain temperature at 200°C and pressure at 2000 kPa with 6200 kPa backpressure for all subsequent test steps. Continue to flow clean dead oil through the core stack. Once run temperature is achieved, determine permeability to clean oil at the irreducible water saturation.

6. Once initial stabilized oil permeability has been obtained, commence steady state co-injection phase #1 for the water saturation increasing phase of the test. Effect co-injection by switching to the injection of 80% clean oil and 20% injection water. Continue this co-injection process until:

   a. Pressure differential across the test section stabilizes.

   b. Samples of the effluent production indicate that the produced total fluid content is equivalent to the injected fluid ratios (i.e., 80% oil, 20% water).

7. Once a stabilized condition has been obtained, repeat step "6" but at a 60% oil, 40% water co-injection ratio.

8. Once a stabilized condition has been obtained, repeat step "6" but at a 40% oil, 60% water co-injection ratio.

9. Once a stabilized condition has been obtained repeat step "6" but at a 20% oil, 80% water co-injection ratio.

10. Once a stabilized condition has been obtained switch to 100% water injection. Flood to S_{or}, note final stabilized permeability to water at the residual oil saturation.

11. Once the endpoint permeability to water at 200°C has been completed, the water saturation increasing phase of the test has been completed and the oil saturation increasing phase commences. Start the oil saturation increasing phase by switching to 20% oil - 80% water and co-injecting these two fluids until a stabilized differential pressure is obtained and a 20% oil - 80% water effluent ratio is obtained.

12. Once a stabilized condition has been obtained, repeat step "11" but at a 40% oil, 80% water co-injection ratio.

13. Once a stabilized condition has been obtained, repeat step "11" but at a 60% oil, 40% water co-injection ratio.

14. Once a stabilized condition has been obtained, repeat step "11" but at a 80% oil, 20% water co-injection ratio.

15. Once a stabilized condition has been obtained, switch to 100% clean oil injection and displace clean oil until no further water production (free or emulsified) is apparent. Determine final endpoint permeability to oil at the irreducible water saturation.

    [Note: No "recycled" fluids were utilized in any phase of this test series. All fluids injected were either freshly cleaned oil (<1% BS&W) or clean synthetic reconstituted produced water].

16. Cool core to ambient temperature over a 36 hour period. slowly depressurize core to ambient pressure and bleed overburden pressure slowly to ambient. Dismantle apparatus and remove mounted core from the pressure vessel.

17. Freeze mounted core to facilitate dismounting. Remove lead confining sleeve and remove core "test sections" only for final extractive analysis.

18. Mount post test "test section" in thin lead sleeve with 300 mesh retaining screens. Subject to Dean Stark extraction to determine final residual oil and water saturations on a post test basis. Once these measurements have been completed, measure Boyles Law porosity and extracted core air permeability.

19. Subject companion non tested samples of virgin core (from cores P5 and P6) to saturation, porosity and permeability determination for comparative analysis to obtain pre-test values.

Effluent Separation - Emulsion Determination

In order to determine if stabilization at a given injection ratio has been attained, it is necessary to know the total production of oil and water phases from the core. In addition a portion of the study was to address the degree of in-situ emulsification under dynamic simultaneous flow conditions of oil and water at 200°C. Accordingly on each effluent sample, analyses of the following types were performed:

1. Percent of "free" water in the effluent (i.e., the percent of non-emulsified water phase readily separable from the oil by static type gravity separation).

2. Percent of "emulsified" oil. This represents the percentage of the sample which is oil based, but contains emulsified water.

3. Percent of water contained in the "emulsified" produced oil phase. This represents the percentage of water trapped in the produced oil phase for a given effluent sample.

4. Percent of total water in the sample. This represents on a total effluent sample basis how much of the total sample is water. This would include both the "free" water and the water emulsified in the oil.

5. Percent of total oil in the sample. This represents the true volume of produced oil once the emulsified water has been removed.

The procedure for sampling and the treatment of each sample is as follows:

1. Effluent from the core is produced into sample pistons held at approximately 85°C. Once a given sample increment has been concluded (generally every 24 - 48 hours of operation), flow is switched to a clean piston and the filled piston is sampled.

2. The piston is sampled at a constant pressure (2000 kPa) by direct displacement of the piston utilizing the sampling pump (see Figure 1). The total mass of the effluent sample is measured immediately after sampling (T_m).

3. After sitting (sealed) for 24 hours all free water is removed from the sample. Percent of free water is computed (% FW = (Mass FW/T_m) x 100).

4. Percentage of emulsified oil is determined by difference (% Emul Oil = ((T_m - Mass FW)/T_m) x 100.

5. Emulsion content of the oil is determined by cutting the oil with a strong solvent (toluene) in a 4:1 toluene:oil ratio. The resulting blend is then agitated and then ultracentrifuged and the amount of entrained water measured directly. (%Emulsion in oil = ((Mass Emulsified water)/(T_m - Mass FW)) x 100)

6. Total percent water is determined by:
   % Total Water = ((Mass Emulsified Water + Mass FW)/T_m) x 100

7. Total percent oil is determined by:
   % total oil = 100 - % Total Water.

Each produced effluent sample for each of the tests was analyzed in this fashion.

RESULTS AND DISCUSSION

Preliminary Work

Table 1 summarizes the composition of the water which was utilized in the study. Table 2 provides a summary of the core locations and depths for the frozen preserved core samples which were originally supplied to Hycal by Petro Canada.

Table 3 provides a summary of the viscosity measurements conducted on the clean dead oil at various temperatures. The data of Table 3 have been plotted on both Cartesian and log μ vs 1/K co-ordinates and appears as Figures 3 and 4 respectively. At the test temperature of 200 °C the dead oil had a viscosity of 7.8 mPa.s. This viscosity value for oil (and 0.134 mPa.s for the water phase at 200°C) was utilized in all permeability calculations in the study.

High Temperature Steady State Test #1

Table 4 provides a summary of pertinent core, test and fluid parameters for the core stack utilized for the first steady state flow test. The core samples were obtained from full diameter core P5 which was from the 289.84 m interval of Hangingstone area well 1-34-84-11 W4M. Based on companion sample analysis initial permeability (to air) for the core stack had a value of 3048.3 x 10^{-3} $(\mu m)^2$ [3088.5 mD] and porosity a value of 39.5%

Table 5 provides a summary of the experimentally determined data for the water saturation increasing phase of Test #1. Data in this table includes final stabilized in-situ

oil and water saturations at each co-injection ratio, measured permeabilities to both the oil and water phases (in $(\mu m)^2$ and mD)) and the computed relative permeability values for both the oil and water phases. Each stabilized saturation point corresponds to a specific water saturation increasing co-injection ratio (i.e., 0%, 20%, 40%, 60%, 80% and 100% H_2O injection respectively). The relative permeability and saturation pressure data of Table 5 have been plotted on both Cartesian and Semi-log co-ordinates and appear as Figures 5 and 6 respectively.

Examination of the data of Table 5 and Figures 5 and 6 indicates initial oil and water saturations in the core material of 0.942 and 0.058 respectively. Initial permeability to dead oil at the initial water saturation at 200°C for Test #1 had a value of 1544.6 x 10^{-3} $(\mu m)^2$ [1565 mD]. Absolute permeability for the core stack was estimated to have a value of 1930.8 x 10^{-3} $(\mu m)^2$ [1956.3 mD] utilizing the assumption that $k_o = 0.80\ k_{abs}$. This assumption is based on past experience at Hycal as well as on extrapolation of the existing relative permeability curves to a point of 100% oil saturation (i.e., $S_{wi} = 0$).

The estimated absolute permeability of 1930.8 x 10^{-3} $(\mu m)^2$ [1956.3 mD] is somewhat less than the absolute air permeability discussed previously of 3048.3 x 10^{-3} $(\mu m)^2$ [3088.5 mD].

This phenomena has been observed frequently at Hycal and is believed to be related to the following factors:

1. Standard air permeability measurements are non-Klinkenberg slip-corrected. Correction of air permeability data for sandface gas slippage can result in

substantially lower effective gas permeabilities, particularly on very low permeability core material.

2. The application of reservoir pore pressure (6200 kPa) instead of a nominal overburden pressure (1378 kPa) can substantially reduce permeability due to physical compression of the flow channels. Increases in temperature have also been noted to have a reducing effect on permeability, particularly at the higher (200 °C) temperatures under consideration in this test.

3. Extracted and dried core material in general seems to exhibit higher air permeabilities (even if overburden pressure and temperature are held constant) than fluid saturated cores. This phenomenon is believed to be related to desiccation of the clays in the matrix caused by the extraction and drying process. Introduction of water into the matrix appears to rehydrate the clays causing a change in internal matrix flow geometry and a reduction in apparent permeability.

The co-injection phases were conducted as described in the "Experimental Procedure" section of the report. Times for stabilization, with the large pore volume and heavy bitumen used in these tests, were quite extended with each individual point generally requiring 10 to 14 days to achieve stability.

Final oil and water saturations after the 100% waterflood had been completed were 0.311 and 0.689 respectively. This represents a recovery of 67.0% of the original oil in place in the core material. Final stabilized endpoint permeability to water had a value of 120.62 x 10^{-3} $(\mu m)^2$ [122.21 mD] yielding a k_{rw} value of 0.0625.

Once the water saturation increasing phase of the test had been completed, the water saturation decreasing (or oil saturation increasing) phase commenced. Data from this test is summarized in Table 6 (in a manner analogous to the water saturation increasing test) The relative permeability data of Table 6 have been plotted on Cartesian and Semi-Log

co-ordinates and appear as Figures 7 and 8 respectively.

Examination of this data indicates that, as mentioned previously, initial oil and water saturations at the conclusion of the 100% waterflood had values of 0.311 and 0.689 respectively with a water endpoint permeability value of 120.62 x 10^{-3} $(\mu m)^2$ [122.21 mD] (k_{rw} = 0.0625). After the multiple co-injection steps of the water saturation decreasing phase of Test #1 had been completed, including the 100% oil injection phase, residual oil and water saturations of 0.861 and 0.139 were obtained. Final stabilized permeability to oil had a value of 1299.2 x 10^{-3} $(\mu m)^2$ [1316.3 mD] yielding a k_{ro} value of 0.6729. The reduction in k_{ro} from the pre-water saturation increasing test value of 0.8000 can likely be attributed to relative permeability effects associated with the presence of a slightly higher irreducible water saturation within the core on the post test basis (0.139 post test vs 0.058 pre-test). The higher residual water saturation may be due to a combination of capillary trapping phenomena and a transition to a more water wet state caused by the extended exposure to elevated temperatures.

Figures 9 and 10 provide comparative data for the drainage and imbibition cycles of the steady state relative permeability tests conducted in the first phase of the study. Examination of this data indicates substantial hysteresis effects in the oil phase relative permeability curve. Hysteresis effects are also apparent in the water phase curve but are relatively slight in comparison to those observed in the oil phase. Relative permeability is greater when a given phase's saturation is increasing than when decreasing.

Table 7 provides a summary of the produced liquid sample analyses for emulsion and

individual phase contents. This table contains optimum injection ratio data (i.e., the actual injected fluid volumetric ratios), total oil and water in the produced oil, percent free water, percent emulsified oil and the water content in the emulsified oil. A large number of samples were taken during the test, and this data has been condensed and averaged together to yield the data presented in Table 7. Stabilized data appears for each co-injection ratio as well as transitional data for the intermediate injection phases between each stabilized co-injection point where internal core saturations were in a transient stage.

Figures 11 and 12 provide plots of percent actual production of oil and water vs optimum injection ratio. The "transition" points are not necessarily located at the average point between the stabilized co-injection ratios due to variations in the sampling intervals between the stabilized points. In general, it can be seen that injection vs production volumes match well. A slight increase in the amount of water produced at some points over that injected can be attributed to the fact that the produced water total in the effluent also includes the small fraction (approx. 1%) of water which remained emulsified in the original "clean" oil phase.

Figure 13 provides a plot of the percentage of free water in the produced samples vs co-injection ratio. Figure 14 illustrates the percentage of emulsified oil as a function of injected water content. Figure 15 plots the percentage of water emulsified in the oil phase as a function of injected water content. Examination of this data indicates that free water content and emulsified oil contents are non-linear functions of increasing injected water content. The relative fraction of "emulsified" oil and lowest relative fraction of "free" water

occurs near the 40% water - 60% oil co-injection ratio. Also at this point the amount of water actually emulsified in the oil reaches its maximum value of near 26%. This indicates that in-situ emulsification under conditions of simultaneous flow does occur and is a function of the relative ratio of the injected oil and water phases. Emulsion volume and severity were worst near the 40% water - 60% oil injection level. Emulsion content in the oil increased fairly linearly to a local maximum of about 26% near the 40% water injection ratio, and then fell to 15 - 18% range by the 80% injection of water ratio.

Table 8 summarizes the results of the effluent water/oil content and emulsion measurements for the water saturation decreasing phase of Test #1 in a manner analogous to that previously decreased for the water saturation increasing data of Table 7. Percent of total oil and water production, percent free water, percent emulsified oil and percent water emulsified in oil data have all been plotted and appear as Figures 16 - 20. Figures 21 - 25 provide comparative plots for both the water saturation increasing and water saturation decreasing data of Tables 7 and 8. Examination of this data indicates relatively good agreement between the two sets of data indicating that the emulsification effects did not appear to be substantively related to changes in saturation direction. Some evidence of slightly more severe emulsification is indicated in the water saturation decreasing tests, but is not significant enough to be conclusive.

Figure 26 provides a comparative plot of total produced water content, free water content, emulsified oil content and water content in emulsified oil on a single summary chart illustrating the entire experimental program for test #1.

Table 9 summarizes pre and post test parameters for the first steady state relative permeability test. Examination of this data indicates a slight reduction in core permeability and porosity on a pre to post test basis from 3048.3 x 10^{-3} $(\mu m)^2$ [3088.5 mD] to 2500.0 x 10^{-3} $(\mu m)^2$ [2533.0 mD] and 39.5 to 38.0% respectively. This may be related to compaction effects and some leaching and alteration of the matrix during extended high temperature exposure. The matrix does not appear to have been adversely affected by elevated temperature exposure at 200°C, to any significant extent although damage may be more severe for exposure for more extended time periods (longer than 4 months) or at temperatures higher than 200°C.

High Temperature Steady State Test #2

Table 10 provides a summary of pertinent core, test and fluid parameters for the core stack utilized for the second steady state flow test. The core samples were obtained from full diameter core P6 from the 292.65 m interval of Hangingstone area well 1-34-84-11 W4M. Based on companion sample analysis initial permeability (to air) for the core stack had a value of 2533.6 x 10^{-3} $(\mu m)^2$ [2567.0 mD] and porosity a value of 40.4%

Table 11 provides a summary of the experimentally determined data for the water saturation increasing phase of Test #2. Data in this table includes final stabilized in-situ oil and water saturations at each co-injection ratio, measured permeabilities to both the oil and water phases (in x 10^{-3} $(\mu m)^2$ and mD)) and the computed relative permeability values for both the oil and water phases. Each stabilized saturation point corresponds to a specific water saturation increasing co-injection ratio (i.e., 0%, 20%, 40%, 60%, 80% and 100% H_2O injection respectively). The relative permeability and saturation pressure data of Table 11 have been plotted on both Cartesian and Semi-log co-ordinates and appear as Figures 27 and 28 respectively.

Examination of the data of Table 11 and Figures 27 and 28 indicates initial oil and water saturations in the core material of 0.970 and 0.030 respectively. Initial permeability to dead oil at the initial water saturation at 200°C for Test #2 had a value of 1491.94 x 10^{-3} $(\mu m)^2$ [1511.60 mD]. Absolute permeability for the core stack was estimated to have a value of 1864.93 x 10^{-3} $(\mu m)^2$ [1889.5 mD] utilizing the assumption that k_o = 0.80 k_{abs}. This assumption is based on past experience at Hycal as well as on extrapolation of the existing

relative permeability curves to a point of 100% oil saturation (i.e., $S_{wi} = 0$).

The estimated absolute permeability of 1864.93 x 10^{-3} x $(\mu m)^2$ [1889.5 mD] is somewhat less than the absolute air permeability discussed previously of 2533.6 x 10^{-3} $(\mu m)^2$ [2567.0 mD]. This phenomena has been discussed previously for the first test.

The co-injection phases were conducted as described in the "Experimental Procedure" section of the report. Times for stabilization were once again quite extended with each individual point generally requiring 10 to 14 days to achieve stability.

Final oil and water saturations after the 100% waterflood had been completed were 0.346 and 0.654 respectively. This represents a recovery of 64.3% of the original oil in place in the core material. Final stabilized endpoint permeability to water had a value of 171.01 x 10^{-3} $(\mu m)^2$ [173.26 mD] yielding a k_{rw} value of 0.0917.

Once the water saturation increasing phase of the test had been completed, the water saturation decreasing (or oil saturation increasing) phase commenced. Data from this test is summarized in Table 12 in a manner analogous to the water saturation increasing test. The relative permeability data of Table 12 have been plotted on Cartesian and Semi-Log co-ordinates and appear as Figures 29 and 30 respectively.

Examination of this data indicates that, as mentioned previously, initial oil and water saturations at the conclusion of the 100% waterflood, had values of 0.346 and 0.654 respectively with a water endpoint permeability value of 171.01 x 10^{-3} $(\mu m)^2$ [173.26 mD] (k_{rw} = 0.0917). After the multiple co-injection steps of the water saturation decreasing

phase of Test #2 had been completed and the 100% oil injection phase had been completed, residual oil and water saturations of 0.894 and 0.103 were obtained. Final stabilized permeability to oil had a value of 1464.36 x 10^{-3} $(\mu m)^2$ [1464.36 mD] yielding a k_{ro} value of 0.7750. The slight reduction in k_{ro} from the pre-water saturation increasing test value of 0.8000 can likely be attributed to relative permeability effects associated with the presence of a slightly higher irreducible water saturation within the core on the post test basis (0.103 post test vs 0.030 pre-test). The higher residual water saturation may be due to a combination of capillary trapping phenomena and a transition to a more water wet state caused by the extended exposure to elevated temperatures.

Figures 31 and 32 provide comparative data for the drainage and imbibition cycles of the steady state relative permeability tests conducted in the first phase of the study. Examination of this data indicates substantial hysteresis effects in the oil phase relative permeability curve. Hysteresis effects are also apparent in the water phase curve but are relatively slight in comparison to those observed in the oil phase. This data is consistent with that observed in Test #1. Relative permeability is greater when a given phase's saturation is increasing than when decreasing.

Table 13 provides a summary of the produced liquid sample analyses for emulsion and individual phase contents. This table contains optimum injection ratio data (i.e., the actual injected fluid volumetric ratios), total oil and water in the produced oil, percent free water, percent emulsified oil and the water content in the emulsified oil. A large number of samples were taken during the test, and this data has been condensed and averaged

together to yield the data presented in Table 13. Stabilized data appears for each co-injection ratio as well as transitional data for the intermediate injection phases between each stabilized co-injection point where internal core saturations were in a transient stage.

Figures 33 and 34 provide plots of percent actual production of oil and water vs optimum injection ratio. Once again "transition" points are not necessarily located at the average point between the stabilized co-injection ratios due to variations in the sampling intervals between the stabilized points. As with Test #1 it can be seen that injection vs production volumes match well.

Figure 35 provides a plot of the percentage of free water in the produced samples vs co-injection ratio. Figure 36 illustrates the percentage of emulsified oil as a function of injected water content. Figure 37 plots the percentage of water emulsified in the oil phase as a function of injected water content. Examination of this data indicates that, similar to Test #1, free water content and emulsified oil contents are non-linear functions of increasing injected water content. The relative fraction of "emulsified" oil and lowest relative fraction of "free" water occurs near the 40% water - 60% oil co-injection ratio. Also at this point the amount of water actually emulsified in the oil reaches its maximum value of near 24%. This indicates that in-situ emulsification under conditions of simultaneous flow does occur and is a function of the relative ratio of the injected oil and water phases. Emulsion volume and severity were once again worst near the 40% water - 60% oil injection level. Emulsion content in the oil increased fairly linearly through a local maximum, and then fell to 15 - 18% by 80% injection of water in a manner analogous to Test #1.

Table 14 summarizes the results of the effluent water/oil content and emulsion measurements for the water saturation decreasing phase of Test #2 in a manner analogous to that previously decreased for the water saturation increasing data of Table 13. Percent of total oil and water production, percent free water, percent emulsified oil and percent water emulsified in oil data have all been plotted and appear as Figures 38 - 42. Figures 43 - 47 provide comparative plots for both the water saturation increasing and water saturation decreasing data of Tables 13 and 14. Examination of this data indicates relatively good agreement between the two sets of data indicating that the emulsification effects did not appear to be substantively related to changes in saturation direction. (Some evidence of slightly more severe emulsification is indicated in the water saturation decreasing tests).

Figure 48 provides a comparative plot of total produced water content, free water content, emulsified oil content and water content in emulsified oil on a single summary chart illustrating the entire experimental program.

Table 15 summarizes pre and post test parameters for the second steady state relative permeability test. Examination of this data indicates a slight increase in core permeability and slight reduction in porosity on a pre to post test basis 2533.6 x 10^{-3} $(\mu m)^2$ [2567.0 mD] to 2701.1 x 10^{-3} $(\mu m)^2$ [2736.6 mD] and 40.4 to 39.1% respectively. This reduction in porosity may be related to compaction effects and some leaching and alteration of the matrix during extended high temperature exposure. The mechanism for the increase in permeability is not clear, but may be due to some mechanical alteration of the core material on a post test basis prior to the permeability measurements. The matrix does not appear

to have been substantially adversely affected by elevated temperature exposure at 200°C, although damage may be more severe for exposure for more extended time periods (longer than 4 months) or at temperatures higher than 200°C.

Smooth Regression Equations for Relative Permeability

The experimental data for the two relative permeability tests contain a degree of experimental scatter and non-linearity. The data for each test were regressed utilizing a power law formulation of the form:

$$kr_i = k_{max_i} \, (Se_i)^{E_i}_{i=o,w}$$

where	i	=	o, w (oil or water phases)
	kr_i	=	Calculated (regressed) oil or water relative permeability
	$kmax_i$	=	Endpoint maximum oil or water phase relative permeability value
	E_i	=	Power law constant (regressed)
	Se_w	=	$(Sw - Sw_{min})/(Sw_{max} - Sw_{min})$
	Se_o	=	$1 - Se_w$

These equations, which appear on the following pages, will provide monotonic smooth relative permeability data which approximates the experimental data. Examples of the comparative fit of the model are also provided as illustrative checks against the experimental data. Figures 49 to 54 illustrate the comparison between the "experimental" and regressed data (on semi-log and cartesian co-ordinates). It should be noted that while the single parameter power-law functional form utilized is simple and easy to use, it may not provide the best optional fit. More complex (i.e., multi-parameter or cubic spline) type formulations would likely provide a better match to the true data set. The intent of these correlations is to provide reasonably accurate, smooth data sets which may be useful for preliminary simulation work. Figures 57 - 60 provide comparative plots of the smoothed drainage and imbibition data for each test on both cartesian and semi-log co-ordinates.

STEADY STATE TEST #1

WATER SATURATION INCREASING PHASE

Oil Phase				
S_w	$Se_w \left(\frac{S_w - S_{wmin}}{S_{wmax} - S_{wmin}}\right)$	Se_o	K_{ro} (Actual)	K_{ro} (Equation)
0.058	0.000	1.000	0.800	0.8000
0.089	0.049	0.951	0.617	0.614
0.181	0.195	0.805	0.171	0.255
0.241	0.290	0.710	0.115	0.132
0.305	0.391	0.609	0.0623	0.0588
0.689	1.000	0.000	0.0000	0.0000
Regression Equation $k_{ro} = 0.800\ (S_{e_o})^{5.263}$				

Water Phase			
S_w	$Se_w \left(\frac{S_w - S_{wmin}}{S_{wmax} - S_{wmin}}\right)$	Kr_w (Actual)	Kr_w (Equation)
0.058	0.000	0.800	0.000
0.089	0.049	0.0009	0.0001
0.181	0.195	0.0019	0.0006
0.241	0.290	0.0029	0.0019
0.305	0.391	0.0041	0.0045
0.689	1.000	0.0625	0.0625
Regression Equation $k_{rw} = 0.0625\ (Se_w)^{2.81}$			

STEADY STATE TEST #1

WATER SATURATION DECREASING PHASE

Oil Phase				
S_w	$Se_w \left(\frac{S_w - S_{wmin}}{S_{wmax} - S_{wmin}}\right)$	Se_o	K_{ro} (Actual)	K_{ro} (Equation)
0.689	0.000	0.000	0.000	0.000
0.409	0.491	0.509	0.120	0.063
0.333	0.353	0.647	0.177	0.146
0.278	0.253	0.747	0.247	0.242
0.206	0.122	0.878	0.392	0.426
0.139	0.000	1.000	0.673	0.673
Regression Equation $k_{ro} = 0.673\ (Se_o)^{3.511}$				

Water Phase			
S_w	$Se_w \left(\frac{S_w - S_{wmin}}{S_{wmax} - S_{wmin}}\right)$	K_{rw} (Actual)	K_{rw} (Equation)
0.689	1.000	0.0625	0.0625
0.409	0.491	0.0079	0.0080
0.333	0.353	0.0050	0.0031
0.278	0.253	0.0027	0.0012
0.206	0.122	0.0017	0.0001
0.139	0.000	0.0000	0.0000
Regression Equation $k_{rw} = 0.0625\ (Se_w)^{2.89}$			

STEADY STATE TEST #2

WATER SATURATION INCREASING PHASE

Oil Phase				
S_w	Se_w $\left(\frac{S_w - S_{wmin}}{S_{wmax} - S_{wmin}}\right)$	Se_o	K_{ro} (Actual)	K_{ro} (Equation)
0.030	0.000	1.000	0.800	0.8000
0.096	0.106	0.894	0.476	0.4650
0.182	0.244	0.756	0.133	0.2066
0.295	0.425	0.575	0.049	0.0550
0.372	0.548	0.452	0.0171	0.0171
0.654	1.000	0.000	0.0000	0.0000
Regression Equation $k_{ro} = 0.800\ (Se_o)^{4.839}$				

Water Phase			
S_w	Se_w $\left(\frac{S_w - S_{wmin}}{S_{wmax} - S_{wmin}}\right)$	Kr_w (Actual)	Kr_w (Equation)
0.030	0.000	0.0000	0.000
0.096	0.106	0.00196	0.0003
0.182	0.244	0.0047	0.0026
0.295	0.425	0.0082	0.0105
0.372	0.548	0.0157	0.0200
0.654	1.000	0.0917	0.0917
Regression Equation $k_{rw} = 0.0917\ (Se_w)^{2.53}$			

STEADY STATE TEST #2

WATER SATURATION DECREASING PHASE

Oil Phase				
S_w	Se_w $\left(\frac{S_w - S_{wmin}}{S_{wmax} - S_{wmin}}\right)$	Se_o	K_{ro} (Actual)	K_{ro} (Equation)
0.654	1.000	0.000	0.000	0.000
0.431	0.595	0.405	0.125	0.116
0.269	0.301	0.699	0.316	0.366
0.215	0.203	0.797	0.470	0.482
0.185	0.149	0.851	0.696	0.553
0.103	0.000	1.000	0.775	0.775
Regression Equation $k_{ro} = 0.775\ (Se_o)^{2.097}$				

Water Phase			
S_w	Se_w $\left(\frac{S_w - S_{wmin}}{S_{wmax} - S_{wmin}}\right)$	Kr_w (Actual)	Kr_w (Equation)
0.654	1.000	0.0917	0.0917
0.431	0.595	0.0207	0.0223
0.269	0.301	0.0074	0.0035
0.215	0.203	0.0049	0.0012
0.185	0.149	0.0029	0.0005
0.103	0.000	0.0000	0.0000
Regression Equation $k_{rw} = 0.917\ (Se_w)^{2.72}$			

General Discussion

This section provides some general discussion relevant to the two tests conducted. Salient points include:

1. Wettability - The configuration of the water-oil relative permeability curves, low endpoint permeability to water, high residual oil saturation and trapping phenomena resulting in a higher irreducible water saturation after testing would suggest water wet behavior. Initial water saturations were quite low, which is normally atypical of a conventional water wet system, but in past experience not unusual for heavy oil unconsolidated systems of this type. Increases in temperature may also have been a mechanism for a shift to a more water wet state.

2. Recovery by waterflood at 200°C - Residual oil saturations ranged between 30 and 35% after waterflooding at 200°C indicating recoveries of approximately 65% of the oil in place by hot waterflooding. Steamflooding at 200°C, or at higher temperatures, will, in our experience, result in a substantial additional reduction in residual oil saturation. Hycal Paper SPE 23783 entitled "Formation Damage Due to Mineral Alteration and Wettability Changes During Hot Water and Steam Injection in Clay Bearing Sandstone Reservoirs," is enclosed in Appendix "A" and further documents this phenomena.

3. Hysteresis - Substantial physical hysteresis was observed in the non-wetting (oil) phase in both tests. Much less hysteresis was observed in the water phase. Individual phase relative permeabilities were greater when their saturation was increasing than when decreasing. A Hycal paper entitled, "The Effect of Relative Permeability on the Steam Stimulation Process," also appears as a portion of Appendix "A".

4. Formation Damage - At the temperature level tested (200°C) and the time duration of the studies (4-5 months/core), no significant evidence of thermally induced formation damage was apparent. Higher temperatures, longer exposure times and actual steamflooding may result in a greater propensity for damage. SPE paper 23783 in Appendix "A" mentioned previously further documents this phenomena.

5. Emulsion Formation - The in-situ formation of stable emulsions was observed in both tests. Severity of emulsions was greatest at approximately 40% water, 60% oil co-injection ratios. Maximum emulsification of water in the oil phase

observed in this study was about 25 - 27% (by mass). Emulsification level increased fairly linearly with fraction of injected water up to a local maximum of about a 40% injected fraction and then declined to about a 15 - 18% in-situ emulsification level for higher injection ratios. This local maximum may be initiated by an increased in-situ turbulence at these particular saturation levels. An increase in emulsification problems during the water saturation decreasing cycles appears to occur, but there is insufficient data available with only the two tests which were evaluated to be conclusive.

Data Diskette Summary

A 5¼" floppy, double sided, double density data diskette is included at the end of the report. This diskette contains all pertinent numerical information from the test series summarized in Lotus 1-2-3 style spreadsheet format. This will facilitate the plotting and manipulation of the data by Petro Canada personnel as required. A summary of the worksheet files contained on the data disk is as follows:

File Name	Contents
PC1.WK1	Oil Viscosity Data (Table 3)
PC2.WK1	Steady State Test #1 - Water-Oil Relative Permeability Data, Water Saturation Increasing (Table 5)
PC3.WK1	Steady State Test #1 - Water-Oil Relative Permeability Data, Water Saturation Decreasing (Table 6)
PC4.WK1	Steady State Test #1 Produced Phase/Emulsion Data - Water Saturation Increasing (Table 7)
PC5.WK1	Steady State Test #1 Produced Phase/Emulsion Data - Water Saturation Decreasing (Table 8)
PC6.WK1	Steady State Test #2 - Water-Oil Relative Permeability Data, Water Saturation Increasing (Table 11)
PC7.WK1	Steady State Test #2 - Water-Oil Relative Permeability Data, Water Saturation Decreasing (Table 12)
PC8.WK1	Steady State Test #2 Produced Phase/Emulsion Data - Water Saturation Increasing (Table 13)
PC9.WK1	Steady State Test #2 Produced Phase/Emulsion Data - Water Saturation Decreasing (Table 14)

CONCLUSIONS

At the request of Petro Canada, Hycal conducted steady state water-oil relative permeability tests at 200°C on preserved Hangingstone Area core material. It was concluded that:

1. The configuration of the water-oil relative permeability curves, low endpoint permeability to water, high residual oil saturation and trapping phenomena resulting in a higher irreducible water saturation after testing would suggest water wet behavior at 200°C for both core tests.

2. Residual oil saturations ranged between 30 and 35% after waterflooding at 200°C indicating recoveries of approximately 65% of the oil in place by hot waterflooding. Steamflooding at 200°C, or at higher temperatures, will, in Hycal's experience, result in a substantial additional reduction in residual oil saturation.

3. Substantial physical hysteresis was observed in the wetting (oil) phase in both tests. Much less hysteresis was observed in the water phase. Individual phase relative permeabilities were greater when their saturation was increasing than when decreasing.

4. At the temperature level tested (200°C) and the time duration studies (4-5 months/core) no significant evidence of thermally induced formation damage was apparent. Higher temperatures, longer exposure times and actual steamflood may result in a greater propensity for damage.

5. The in-situ formation of stable emulsions was observed in both tests. Severity of emulsions was greatest at approximately 40% water, 60% oil co-injection ratios. Maximum emulsification of water in the oil phase observed in this study was about 25 - 27% (by mass). Emulsification level increased fairly linearly with fraction of injected water up to a local maximum of about a 40% injected fraction and then declined to about a 15 - 18% in-situ emulsification level for higher injection ratios. This local maximum may be initiated by an increased in-situ turbulence at these particular saturation levels. An increase in emulsification problems during the water saturation decreasing cycles appears to occur, but there is insufficient data available with only the two tests which were evaluated to be conclusive.

TABLE 1
PETRO CANADA HIGH TEMPERATURE STEADY STATE
RELATIVE PERMEABILITY STUDY
PRODUCED WELL 12-34-84-11 W4M
WATER ANALYSIS

Ion	Concentration (ppm)
Na	3690
K	60
Ca	54
Mg	42
Sr	2
Cl	5300
SO_3	900
HCO_3	36.9
CO_3	0.2

TABLE 2
PETRO CANADA HIGH TEMPERATURE STEADY STATE
RELATIVE PERMEABILITY STUDY
WELL 1-34-84-11 W4M
SUPPLIED PRESERVED CORE SAMPLES

Core No.	Sample Number	Depth (m)	Intvl Rep (m)
9	P2	283.23 - 283.58	0.35
9	AST19	283.88 - 283.98	0.1
9	P3	283.98 - 284.33	0.35
9	AST20	284.48 - 284.58	0.1
10	AST24	286.04 - 286.14	0.1
10	AST27	286.55 - 286.65	0.1
10	AST29	287.29 - 287.39	0.1
11	P4	288.55 - 288.90	0.1
11	P5	289.84 - 290.19	0.35
12	AST40	292.01 - 292.11	0.1
12	P6	292.65 - 292.95	0.3

TABLE 3
PETRO CANADA HIGH TEMPERATURE STEADY STATE
RELATIVE PERMEABILITY STUDY
CLEAN OIL VISCOSITY DATA

Temperature		Inv Temp 1/K	Oil Viscosity T&P (mPa.s)
(°C)	(K)		
50	323	0.003096	6391.0
90	363	0.002755	336.0
130	403	0.002481	51.0
160	433	0.002309	19.9
200	473	0.002114	7.8

TABLE 4
PETRO CANADA WELL 1-34-84-11 W4M HIGH TEMPERATURE STEADY STATE RELATIVE PERMEABILITY STUDY
TEST #1 - CORE AND RUN PARAMETERS

Core ID	P5
Depth (m)	289.84
Length (cm)	32.4
Diameter (cm)	3.81
Effective Flow Area (cm^2)	11.40
Porosity (%)	38.0
Bulk Volume (cm^2)	369.36
Pore Volume (cm^3)	140.36
Water Viscosity at 200°C (mPa.s)	0.134
Oil Viscosity at 200°C (mPa.s)	7.8
Test Temperature (°C)	200
Backpressure (kPag)	2000
Overburden Pressure (kPag)	6200

TABLE 5
PETRO CANADA WELL 1-34-84-11 W4M HIGH TEMPERATURE STEADY STATE RELATIVE PERMEABILITY STUDY
TEST #1 - WATER SATURATION INCREASING TEST RESULTS

Saturations		Permeability to Oil		Permeability to Water		Kro	Krw
S_o	S_w	$(\mu m)^2 \times 10^{-3}$	(mD)	$(\mu m)^2 \times 10^{-3}$	(mD)		
0.942	0.058	1544.6	1565.0	0.00	0.00	0.8000*	0.0000
0.911	0.089	1191.9	1207.6	1.71	1.73	0.6173	0.0009
0.819	0.181	330.7	335.1	3.65	3.70	0.1713	0.0019
0.759	0.241	221.9	224.9	5.52	5.59	0.1150	0.0029
0.695	0.305	120.3	121.9	7.98	8.08	0.0623	0.0041
0.311	0.689	0.00	0.00	120.62	122.21	0.0000	0.0625

* K_{abs} estimated to be 1930.80×10^{-3} $(\mu m)^2$ [1956.3 mD] using the assumption that $k_o = 0.80\ k_{abs}$

TABLE 6
PETRO CANADA WELL 1-34-84-11 W4M HIGH TEMPERATURE STEADY STATE RELATIVE PERMEABILITY STUDY
TEST #1 - WATER SATURATION DECREASING TEST
RESULTS

Saturations		Permeability to Oil		Permeability to Water		Kro	Krw
S_o	S_w	$(\mu m)^2 \times 10^{-3}$	(mD)	$(\mu m)^2 \times 10^{-3}$	(mD)		
0.311	0.689	0.00	0.00	120.62	122.21	0.0000	0.0625
0.591	0.409	232.3	235.4	15.38	15.58	0.1203	0.0079
0.667	0.333	340.8	345.3	9.87	10.00	0.1765	0.0050
0.722	0.278	477.1	483.4	5.26	5.33	0.2471	0.0027
0.794	0.206	755.8	765.8	3.31	3.35	0.3915	0.0017
0.861	0.139	1299.2	1316.3	0.00	0.00	0.6729	0.0000

TABLE 7
PETRO CANADA WELL 1-34-84-11 W4M HIGH TEMPERATURE STEADY STATE RELATIVE PERMEABILITY STUDY
TEST #1 - WATER SATURATION INCREASING TEST
MEASURED EMULSION PARAMETERS

Optimum Actual Co-Injection Ratio*		Actual Production Ratio**		% Free Water	% Emulsified Oil	% Water Emulsified In Oil
% Oil	% H_2O	% Oil	% H_2O			
100	0	99.1	0.9	0.0	100.0	0.9
transition		86.4	13.6	6.2	93.8	7.9
80	20	79.1	20.9	7.4	93.6	15.5
transition		69.7	30.3	9.9	90.1	22.6
60	40	61.4	38.6	17.8	82.1	25.3
transition		49.0	51.0	37.1	62.9	22.1
40	60	38.9	61.1	53.5	46.5	16.3
transition		28.0	72.0	66.5	33.5	16.5
20	80	18.2	81.8	78.0	22.0	17.4
transition		5.9	94.1	92.6	7.4	20.7
0	100	0.0	100.0	100.0	0.0	--

* Represent injected volumes, injected cleaned oil contained approximately 1.0% H_2O by mass.

** Represent true volumes of "clean" pure oil or water separated after production.

TABLE 8
PETRO CANADA WELL 1-34-84-11 W4M HIGH TEMPERATURE STEADY STATE RELATIVE PERMEABILITY STUDY
TEST #1 - WATER SATURATION DECREASING TEST
MEASURED EMULSION PARAMETERS

Optimum Actual Co-Injection Ratio*		Actual Production Ratio**		% Free Water	% Emulsified Oil	% Water Emulsified In Oil
% Oil	% H_2O	% Oil	% H_2O			
0	100	0.0	100.0	100.0	0.0	--
transition		7.3	92.7	91.2	8.8	17.4
20	80	20.8	79.2	75.6	24.4	14.6
transition		33.9	66.1	56.1	43.9	22.8
40	60	39.9	60.1	49.1	50.9	21.6
transition		53.1	46.9	29.4	70.6	24.8
60	40	59.2	40.8	21.0	79.0	25.1
transition		68.6	31.4	19.1	80.9	15.2
80	20	79.8	20.2	7.9	92.1	13.4
transition		87.4	12.6	1.8	98.2	11.0
100	0	99.0	1.0	0.0	100.0	1.1

* Represent injected volumes, injected cleaned oil contained approximately 1.0% H_2O by mass.

** Represent true volumes of "clean" pure oil or water separated after production.

TABLE 9
PETRO CANADA WELL 1-34-84-11 W4M HIGH TEMPERATURE STEADY STATE RELATIVE PERMEABILITY STUDY
STEADY-STATE TEST #1
PRE/POST TEST PARAMETERS

	Pre-Test	Post-Test
S_o	0.942	0.861
S_w	0.058	0.139
K_{air}		
$(\mu m)^2 \times 10^{-3}$	3048.3	2500.0
(mD)	3088.5	2533.0
Porosity (%)	39.5	38.0

TABLE 10
PETRO CANADA WELL 1-34-84-11 W4M HIGH TEMPERATURE STEADY STATE RELATIVE PERMEABILITY STUDY
TEST #2 - CORE AND RUN PARAMETERS

Core ID	P6
Depth (m)	292.65
Length (cm)	34.5
Diameter (cm)	3.81
Effective Flow Area (cm^2)	11.40
Porosity (%)	39.1
Bulk Volume (cm^2)	393.3
Pore Volume (cm^3)	153.78
Water Viscosity at 200°C (mPa.s)	0.134
Oil Viscosity at 200°C (mPa.s)	7.8
Test Temperature (°C)	200
Backpressure (kPag)	2000
Overburden Pressure (kPag)	6200

TABLE 11
PETRO CANADA WELL 1-34-84-11 W4M HIGH TEMPERATURE STEADY STATE RELATIVE PERMEABILITY STUDY
TEST #2 - WATER SATURATION INCREASING TEST
RESULTS

Saturations		Permeability to Oil		Permeability to Water		Kro	Krw
S_o	S_w	$(\mu m)^2 \times 10^{-3}$	(mD)	$(\mu m)^2 \times 10^{-3}$	(mD)		
0.970	0.030	1491.94	1511.60	0.00	0.00	0.8000*	0.0000
0.904	0.096	887.71	899.40	3.65	3.70	0.476	0.00196
0.818	0.182	248.03	251.30	8.76	8.88	0.133	0.0047
0.705	0.295	91.37	92.58	15.29	15.49	0.049	0.0082
0.628	0.372	31.88	32.31	29.27	29.66	0.0171	0.0157
0.346	0.654	0.00	0.00	171.01	173.26	0.0000	0.0917

* K_{abs} estimated to be 1864.93×10^{-3} $(\mu m)^2$ [1889.5 mD] using the assumption that $k_o = 0.80\ k_{abs}$

TABLE 12
PETRO CANADA WELL 1-34-84-11 W4M HIGH TEMPERATURE STEADY STATE RELATIVE PERMEABILITY STUDY
TEST #2 - WATER SATURATION DECREASING TEST
RESULTS

Saturations		Permeability to Oil		Permeability to Water		Kro	Krw
S_o	S_w	$(\mu m)^2 \times 10^{-3}$	(mD)	$(\mu m)^2 \times 10^{-3}$	(mD)		
0.346	0.654	0.00	0.00	171.01	173.26	0.0000	0.0917
0.569	0.431	293.11	236.18	38.60	39.11	0.125	0.0207
0.731	0.269	589.32	597.08	13.79	13.98	0.316	0.0074
0.785	0.215	876.52	888.06	9.14	9.26	0.470	0.0049
0.815	0.185	1297.99	1315.09	5.40	5.47	0.696	0.0029
0.894	0.103	1445.32	1464.36	0.00	0.00	0.775	0.0000

TABLE 13
PETRO CANADA WELL 1-34-84-11 W4M HIGH TEMPERATURE STEADY STATE RELATIVE PERMEABILITY STUDY
TEST #2 - WATER SATURATION INCREASING TEST
MEASURED EMULSION PARAMETERS

Optimum Actual Co-Injection Ratio*		Actual Production Ratio**		% Free Water	% Emulsified Oil	% Water Emulsified In Oil
% Oil	% H_2O	% Oil	% H_2O			
100	0	99.0	1.0	0.0	100.0	1.0
transition		91.7	8.3	2.9	97.1	5.6
80	20	80.6	19.4	8.1	90.9	11.4
transition		69.4	30.6	15.8	84.2	17.6
60	40	59.5	40.5	22.2	77.8	23.6
transition		46.2	53.8	42.5	57.5	19.6
40	60	39.9	60.1	50.1	49.9	20.0
transition		26.6	73.4	66.5	33.5	20.5
20	80	19.5	80.5	75.0	25.0	22.0
transition		2.4	97.6	97.5	2.5	2.4
0	100	0.0	100.0	100.0	0.0	0.0

* Represent injected volumes, injected cleaned oil contained approximately 1.0% H_2O by mass.

** Represent true volumes of "clean" pure oil or water separated after production.

TABLE 14
PETRO CANADA WELL 1-34-84-11 W4M HIGH TEMPERATURE STEADY STATE RELATIVE PERMEABILITY STUDY
TEST #2 - WATER SATURATION DECREASING TEST
MEASURED EMULSION PARAMETERS

Optimum Actual Co-Injection Ratio*		Actual Production Ratio**		% Free Water	% Emulsified Oil	% Water Emulsified In Oil
% Oil	% H_2O	% Oil	% H_2O			
0	100	0.0	100.0	100.0	0.0	--
transition		7.7	92.3	90.5	9.5	19.0
20	80	21.8	78.2	72.1	27.9	21.9
transition		30.1	69.9	63.7	36.3	17.0
40	60	41.0	59.0	45.3	54.7	25.0
transition		51.2	48.8	31.0	69.0	25.8
20	40	58.6	41.4	18.9	81.1	27.8
transition		73.6	26.4	10.8	89.2	17.5
80	20	78.5	21.5	4.9	95.1	17.5
transition		92.8	7.2	0.0	100.0	7.2
100	0	99.1	0.9	0.0	100.0	0.9

* Represent injected volumes, injected cleaned oil contained approximately 1.0% H_2O by mass.

** Represent true volumes of "clean" pure oil or water separated after production.

TABLE 15
PETRO CANADA WELL 1-34-84-11 W4M HIGH TEMPERATURE STEADY STATE RELATIVE PERMEABILITY STUDY
STEADY-STATE TEST #2
PRE/POST TEST PARAMETERS

	Pre-Test	Post-Test
S_o	0.970	0.897
S_w	0.030	0.103
K_{air}		
$(\mu m)^2 \times 10^{-3}$	2533.6	2701.1
(mD)	2567.0	2736.6
Porosity (%)	40.4	39.1

FIGURE 1

PETRO CANADA STUDY
HYCAL HIGH TEMPERATURE
STEADY-STATE RELATIVE PERMEABILITY APPARATUS

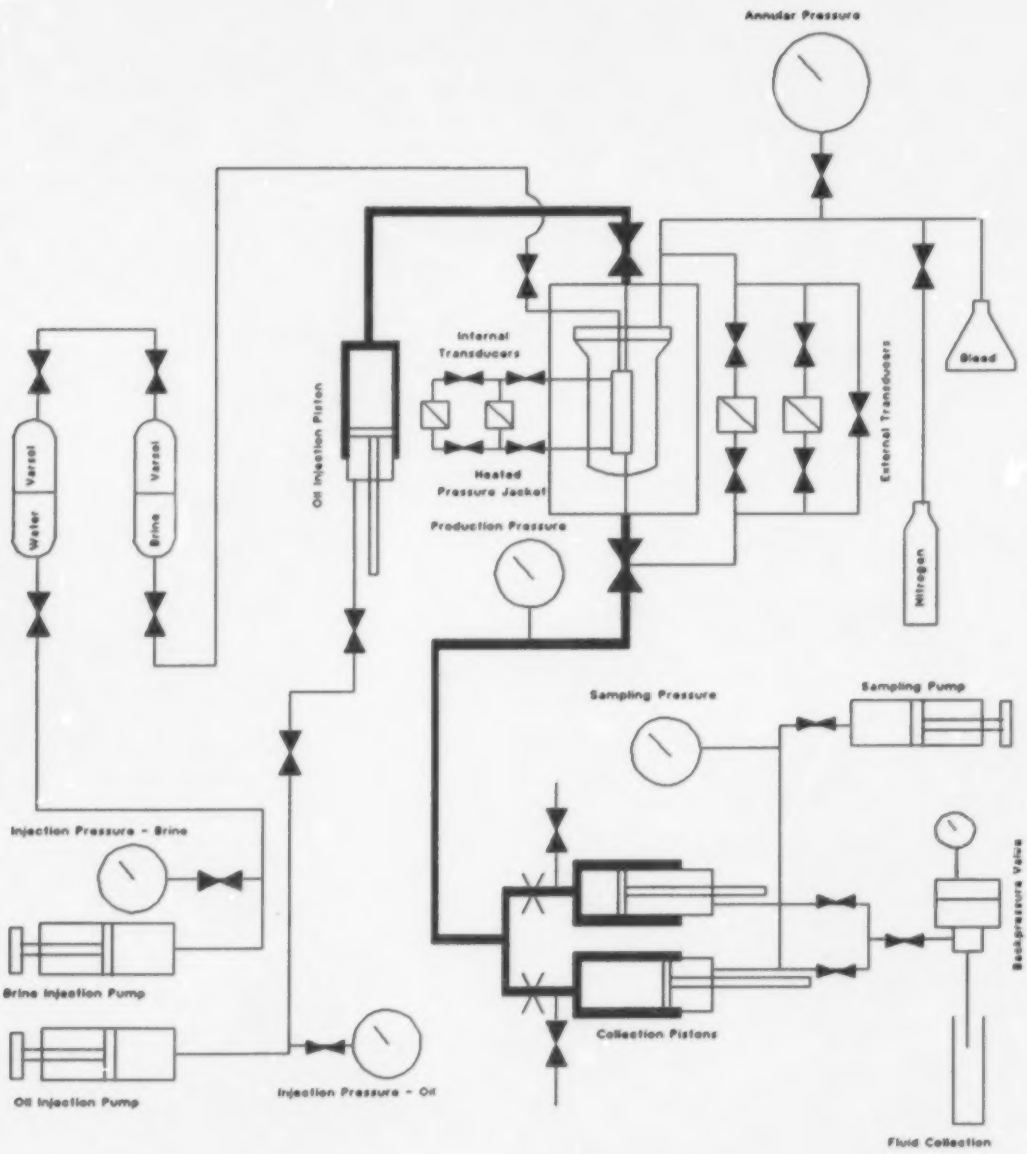

(Thick Lines Represent Heat Traced Flow Tubing)

FIGURE 2

PETRO CANADA HIGH TEMPERATURE STEADY-STATE FLOW STUDY
COREHOLDER SCHEMATIC

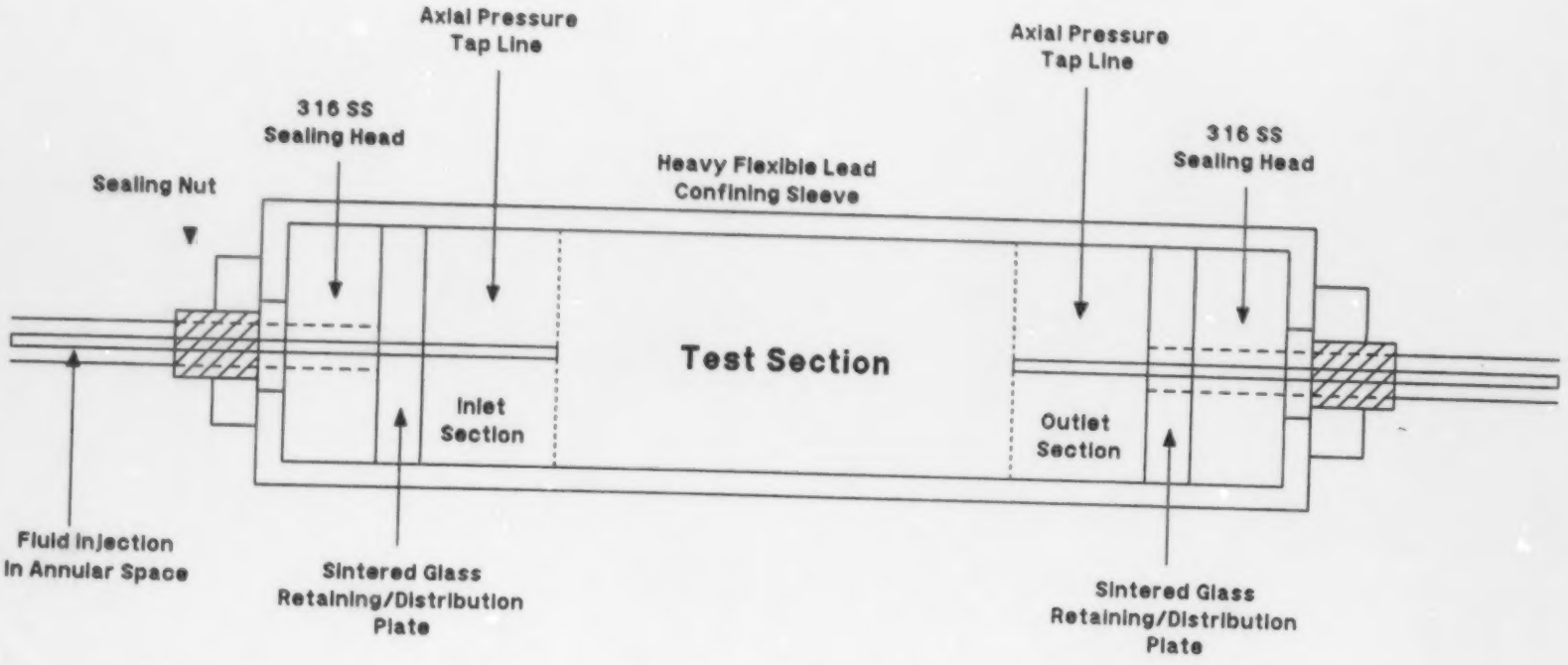

Hycal

FIGURE 3

PETRO CANADA HANGINGSTONE WELL 1-34-84-11 W4M
HIGH TEMP STEADY-STATE RELATIVE PERM STUDY
OIL VISCOSITY vs TEMPERATURE

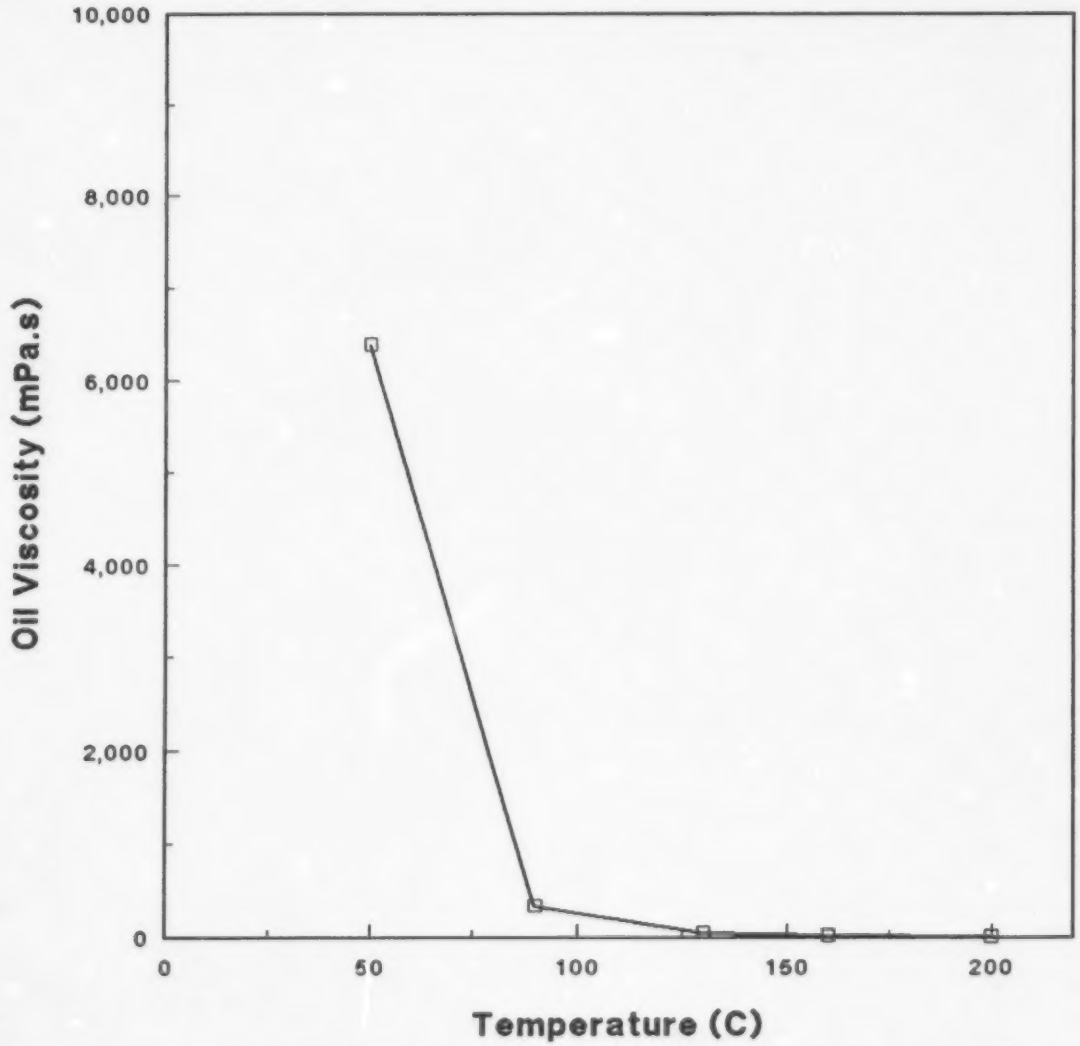

CLEAN OIL VISCOSITY DATA

FIGURE 4

PETRO CANADA HANGINGSTONE WELL 1-34-84-11 W4M
HIGH TEMP STEADY-STATE RELATIVE PERM STUDY
OIL VISCOSITY vs TEMPERATURE

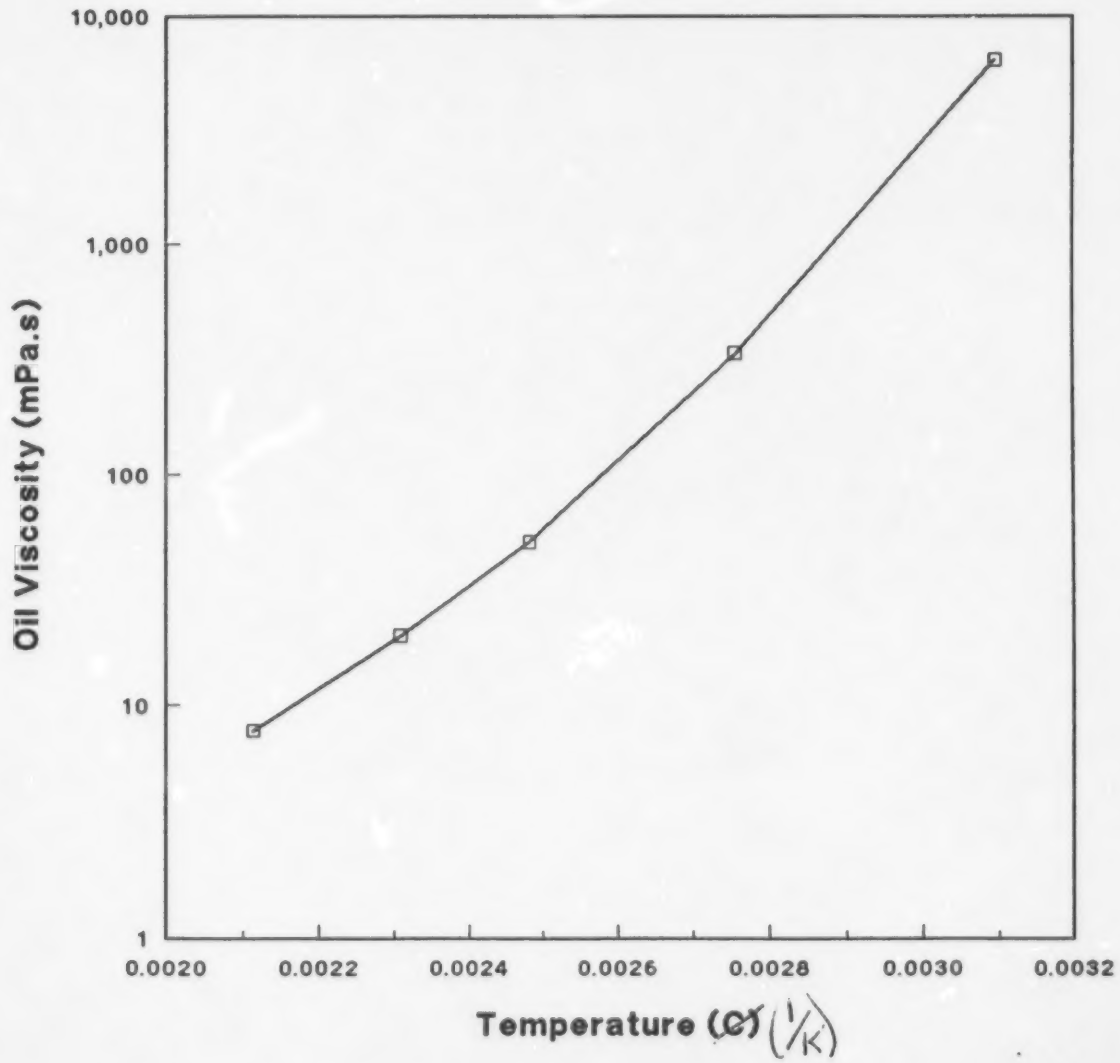

CLEAN OIL VISCOSITY DATA

FIGURE 5

PETRO CANADA WELL 1-34-84-11 W4M
HIGH TEMP STEADY-STATE REL PERM STUDY - TEST #1
RELATIVE PERMEABILITY vs WATER SATURATION

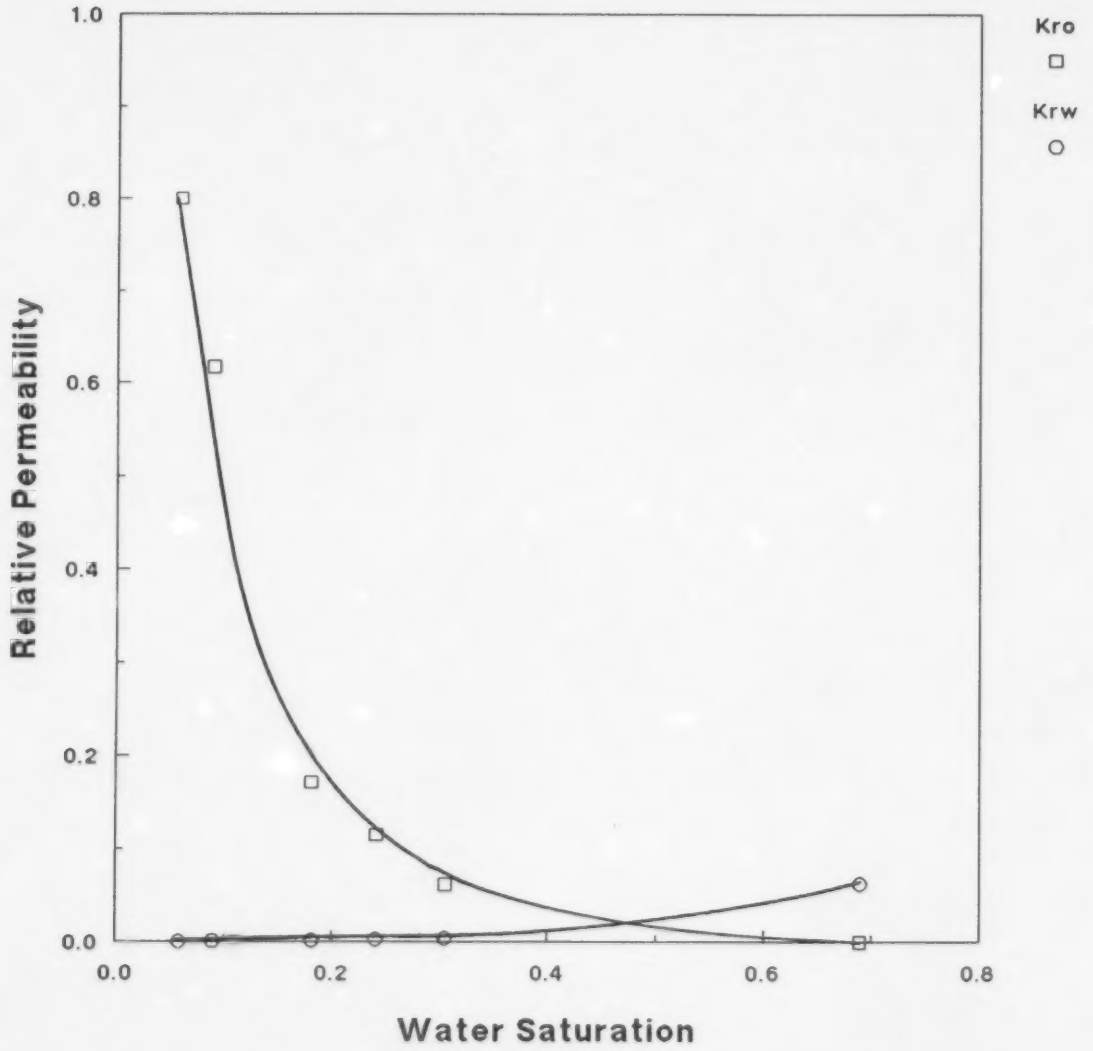

WATER SATURATION INCREASING

FIGURE 6

PETRO CANADA WELL 1-34-84-11 W4M
HIGH TEMP STEADY-STATE REL PERM STUDY - TEST #1
RELATIVE PERMEABILITY vs WATER SATURATION

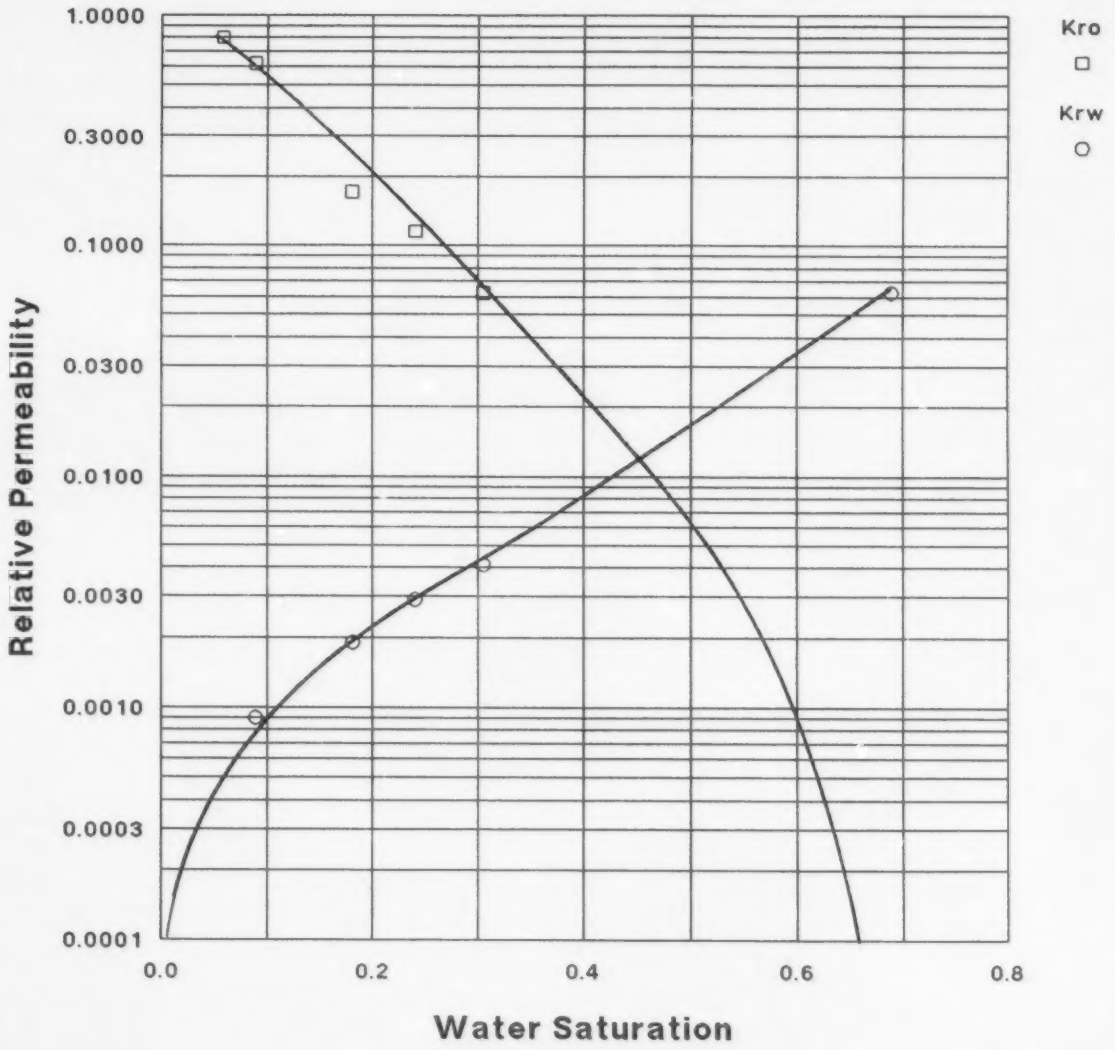

WATER SATURATION INCREASING

FIGURE 7

PETRO CANADA WELL 1-34-84-11 W4M
HIGH TEMP STEADY-STATE REL PERM STUDY - TEST #1
RELATIVE PERMEABILITY vs WATER SATURATION

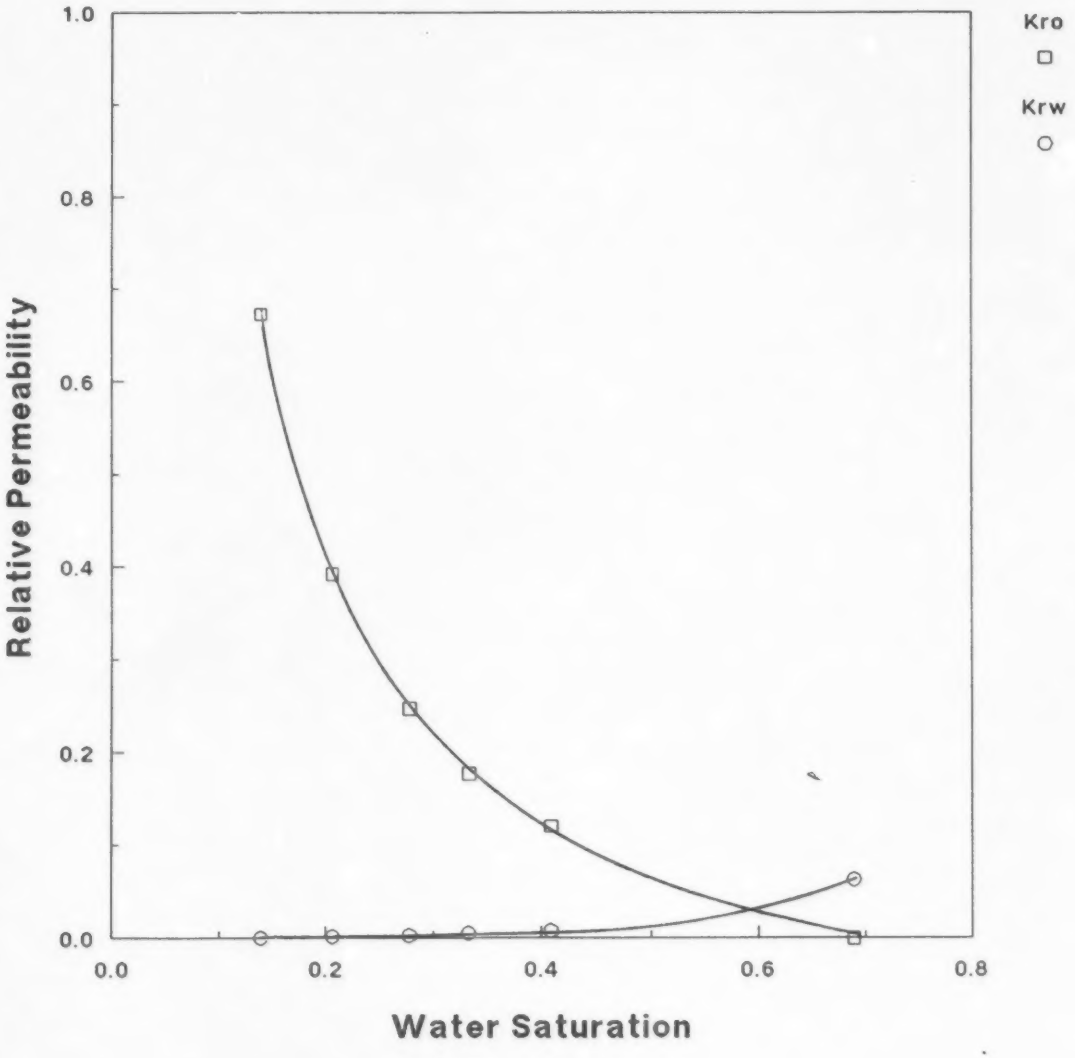

WATER SATURATION DECREASING

FIGURE 8

PETRO CANADA WELL 1-34-84-11 W4M
HIGH TEMP STEADY-STATE REL PERM STUDY - TEST #1
RELATIVE PERMEABILITY vs WATER SATURATION

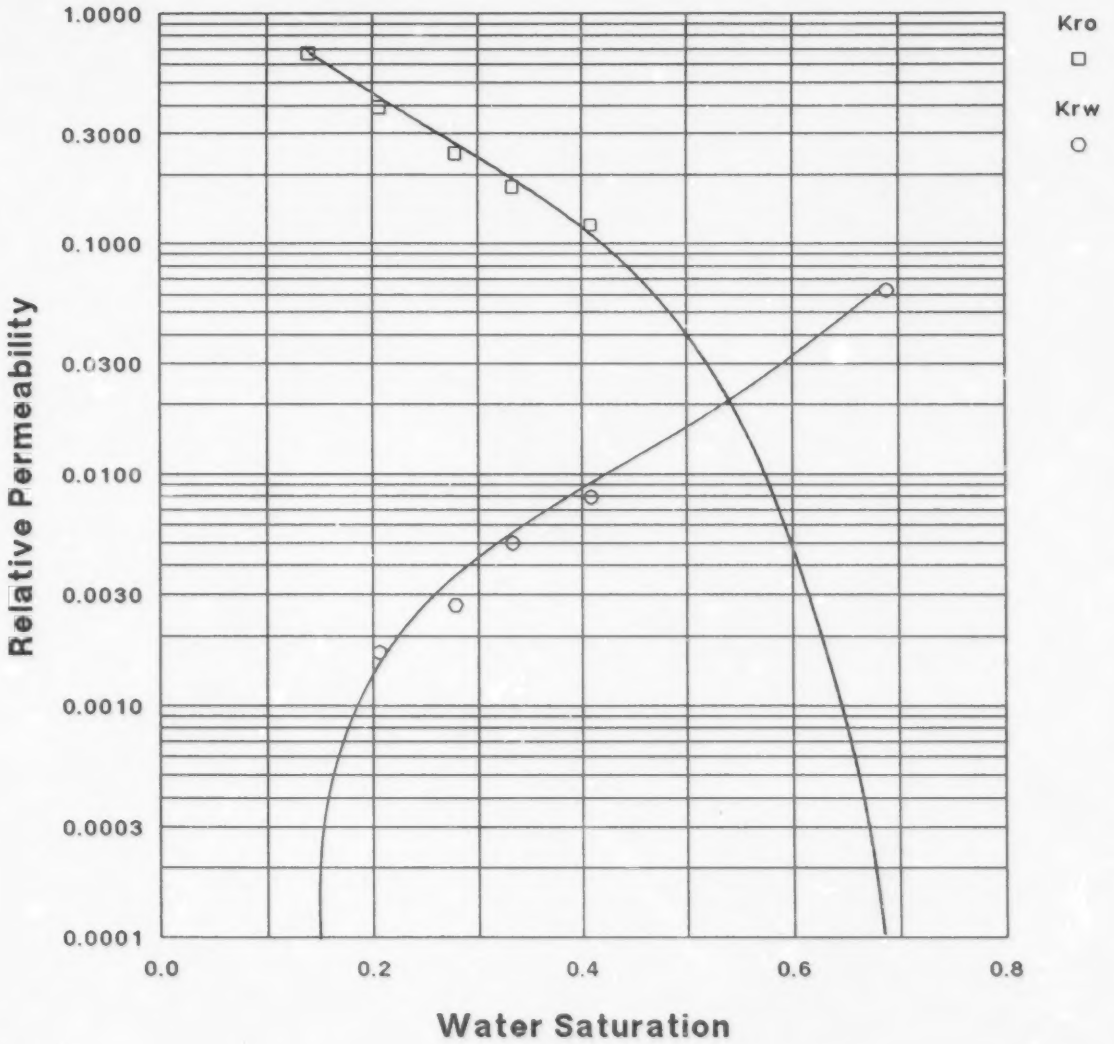

WATER SATURATION DECREASING

FIGURE 9

PETRO CANADA WELL 1-34-84-11 W4M
HIGH TEMP STEADY-STATE REL PERM STUDY - TEST #1
RELATIVE PERMEABILITY vs WATER SATURATION

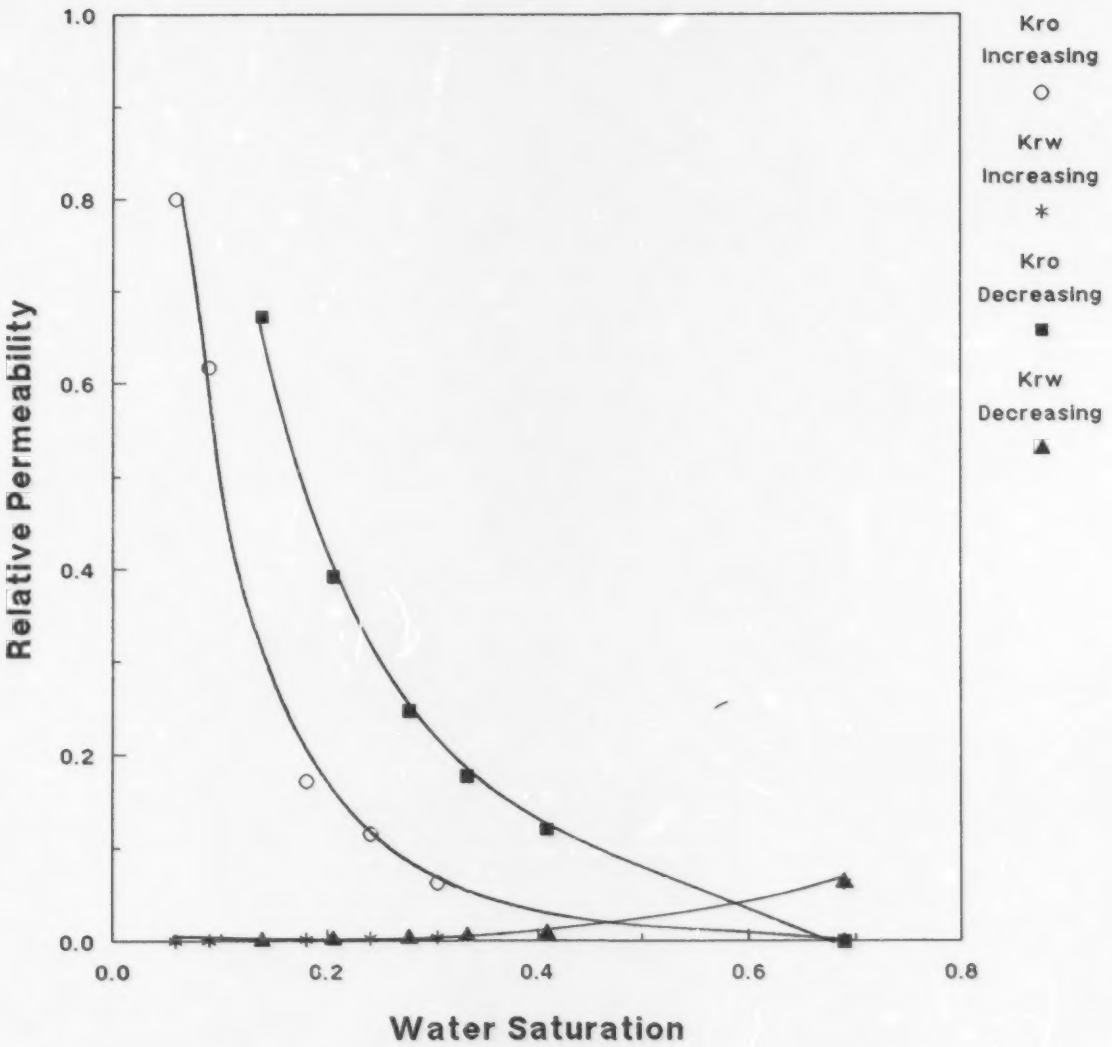

COMPARISON OF WATER SATURATION INCREASING AND WATER SATURATION DECREASING

FIGURE 10

PETRO CANADA WELL 1-34-84-11 W4M
HIGH TEMP STEADY-STATE REL PERM STUDY - TEST #1
RELATIVE PERMEABILITY vs WATER SATURATION

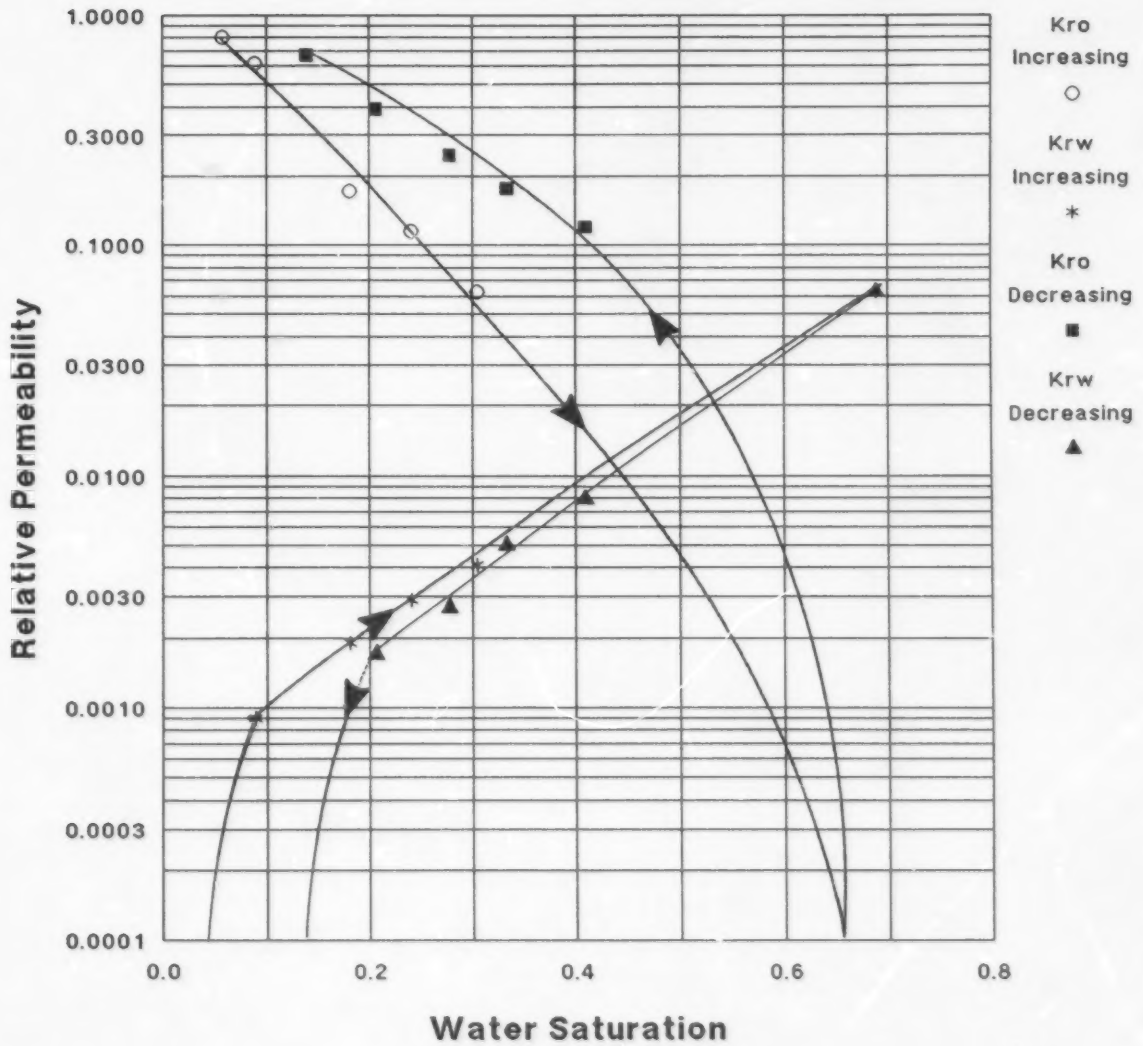

COMPARISON OF WATER SATURATION INCREASING AND WATER SATURATION DECREASING

FIGURE 11

PETRO CANADA HANGINGSTONE WELL 1-34-84-11 W4M
HIGH TEMP STEADY-STATE RELATIVE PERM STUDY
ACTUAL % OIL PROD vs OPTIMUM % H2O CO-INJ RATIO

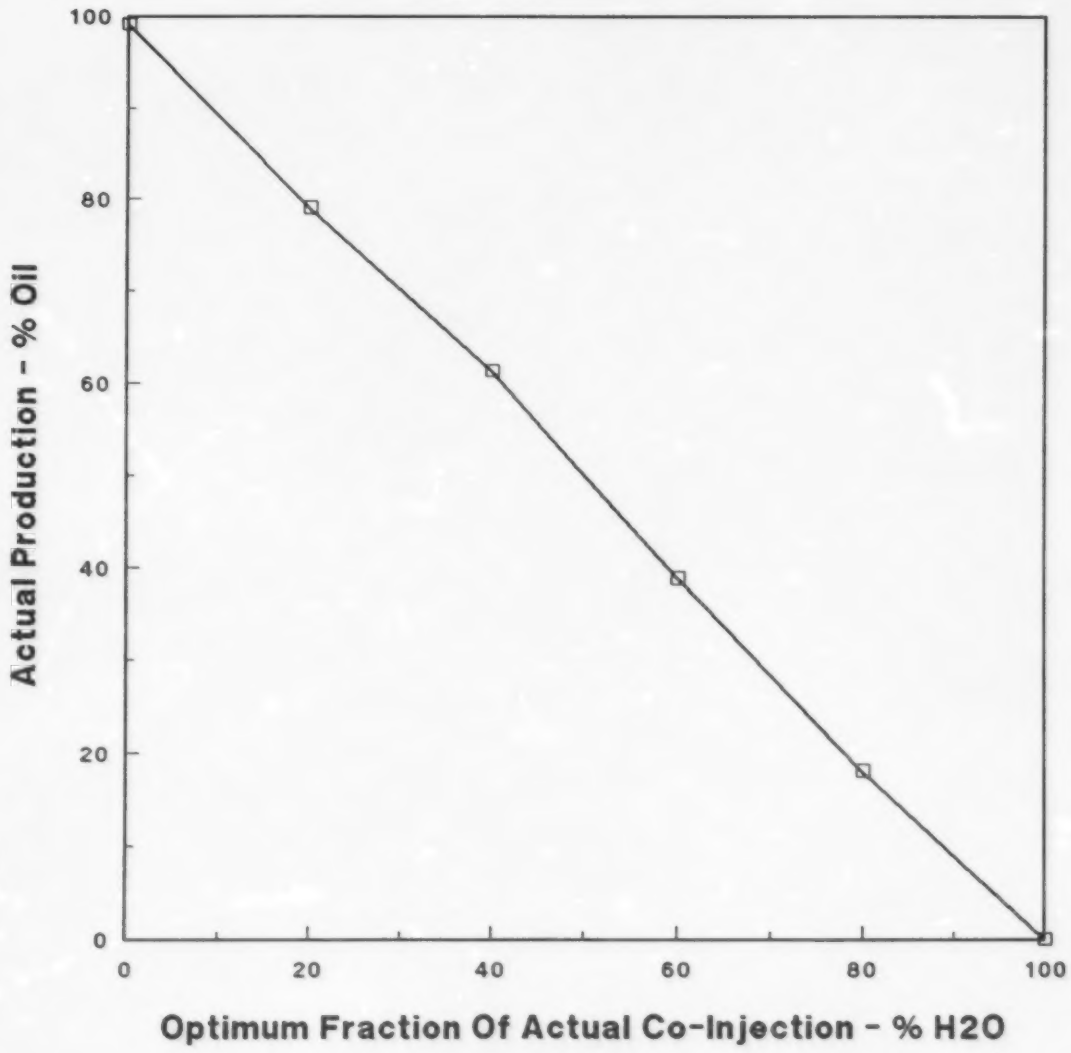

TEST #1 - WATER SATURATION INCREASING

FIGURE 12

PETRO CANADA HANGINGSTONE WELL 1-34-84-11 W4M
HIGH TEMP STEADY-STATE RELATIVE PERM STUDY
ACTUAL % H2O PROD vs OPTIMUM % H2O CO-INJ RATIO

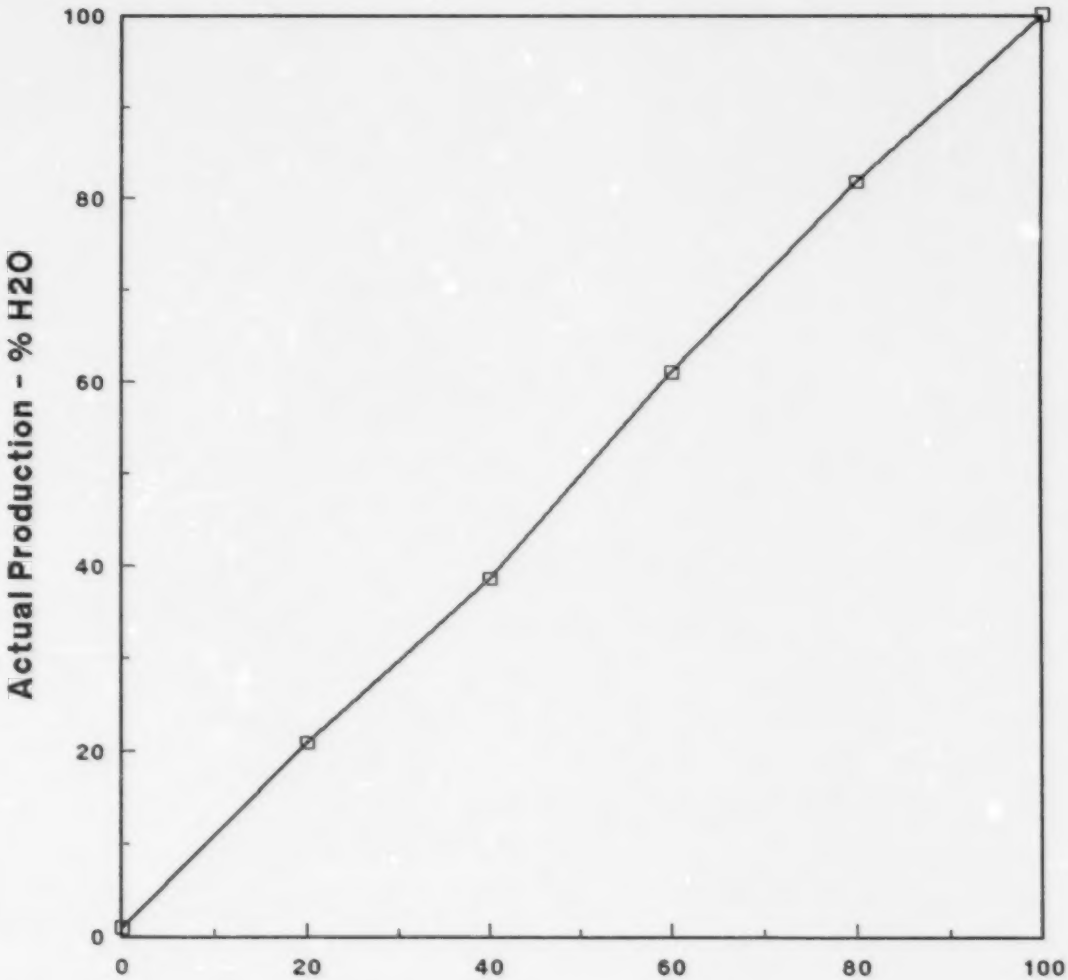

TEST #1 - WATER SATURATION INCREASING

FIGURE 13

PETRO CANADA HANGINGSTONE WELL 1-34-84-11 W4M
HIGH TEMP STEADY-STATE RELATIVE PERM STUDY
% FREE H2O vs OPTIMUM % H2O CO-INJ RATIO

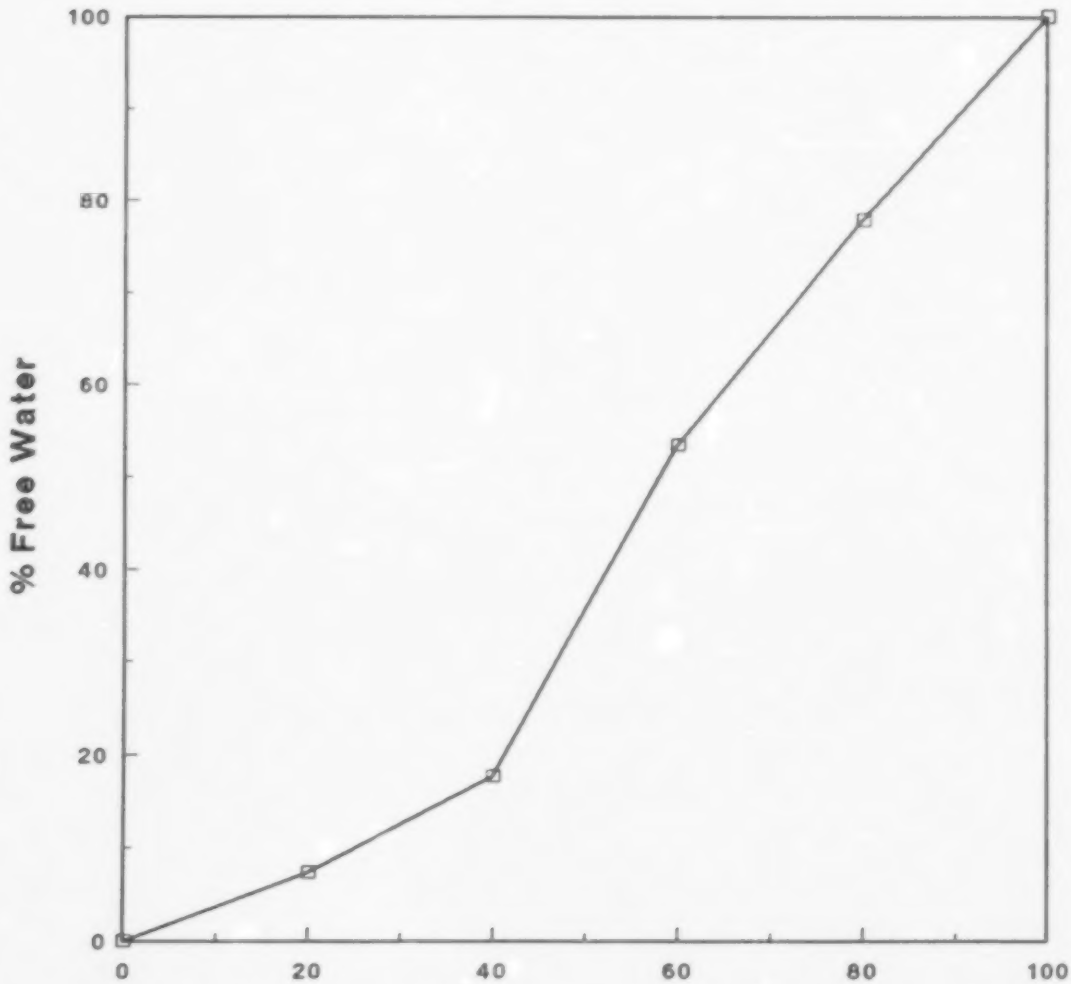

TEST #1 - WATER SATURATION INCREASING

FIGURE 14

PETRO CANADA HANGINGSTONE WELL 1-34-84-11 W4M
HIGH TEMP STEADY-STATE RELATIVE PERM STUDY
% EMULSIFIED OIL vs OPTIMUM % H2O CO-INJ RATIO

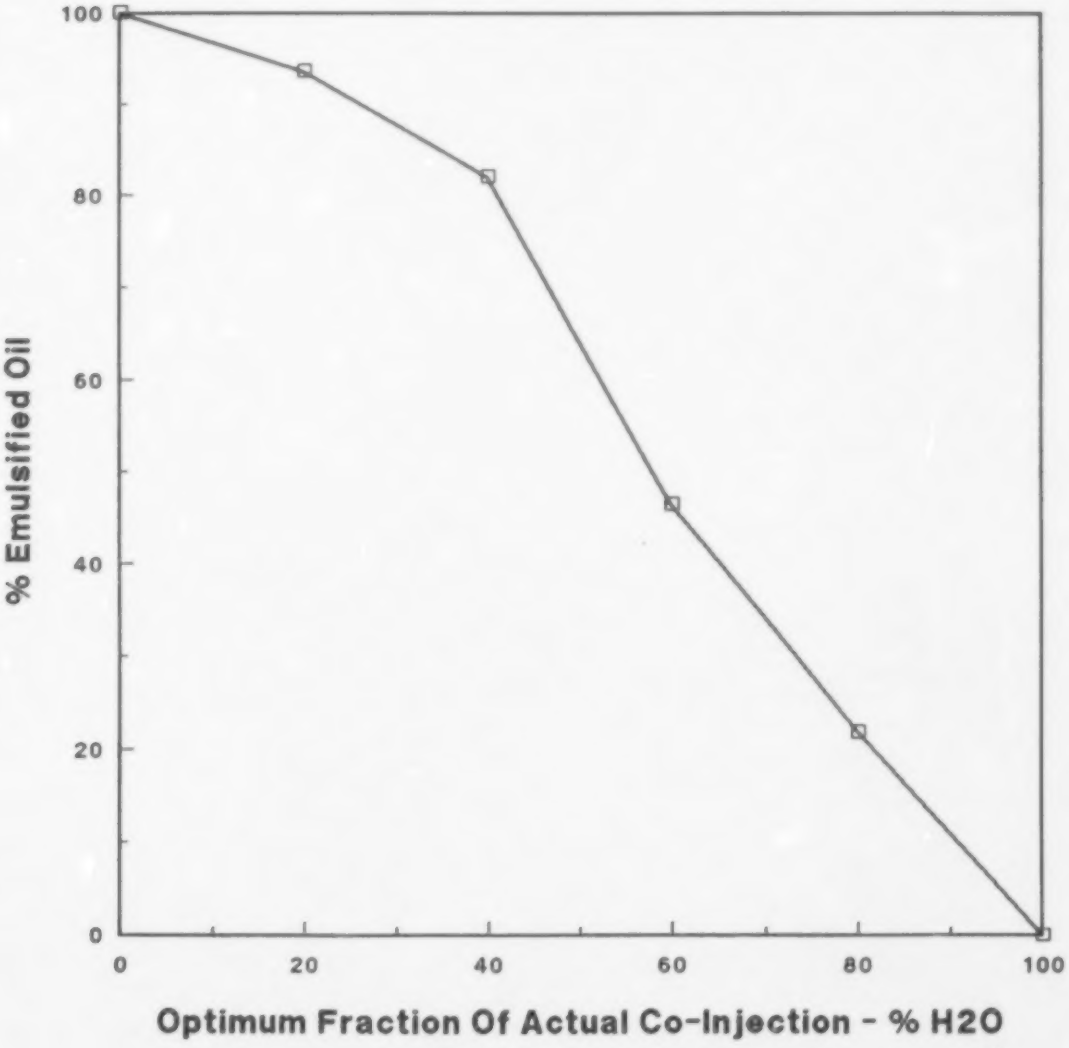

TEST #1 - WATER SATURATION INCREASING

FIGURE 15

PETRO CANADA HANGINGSTONE WELL 1-34-84-11 W4M
HIGH TEMP STEADY-STATE RELATIVE PERM STUDY
% H2O EMULS IN OIL vs OPTIMUM % H2O CO-INJ RATIO

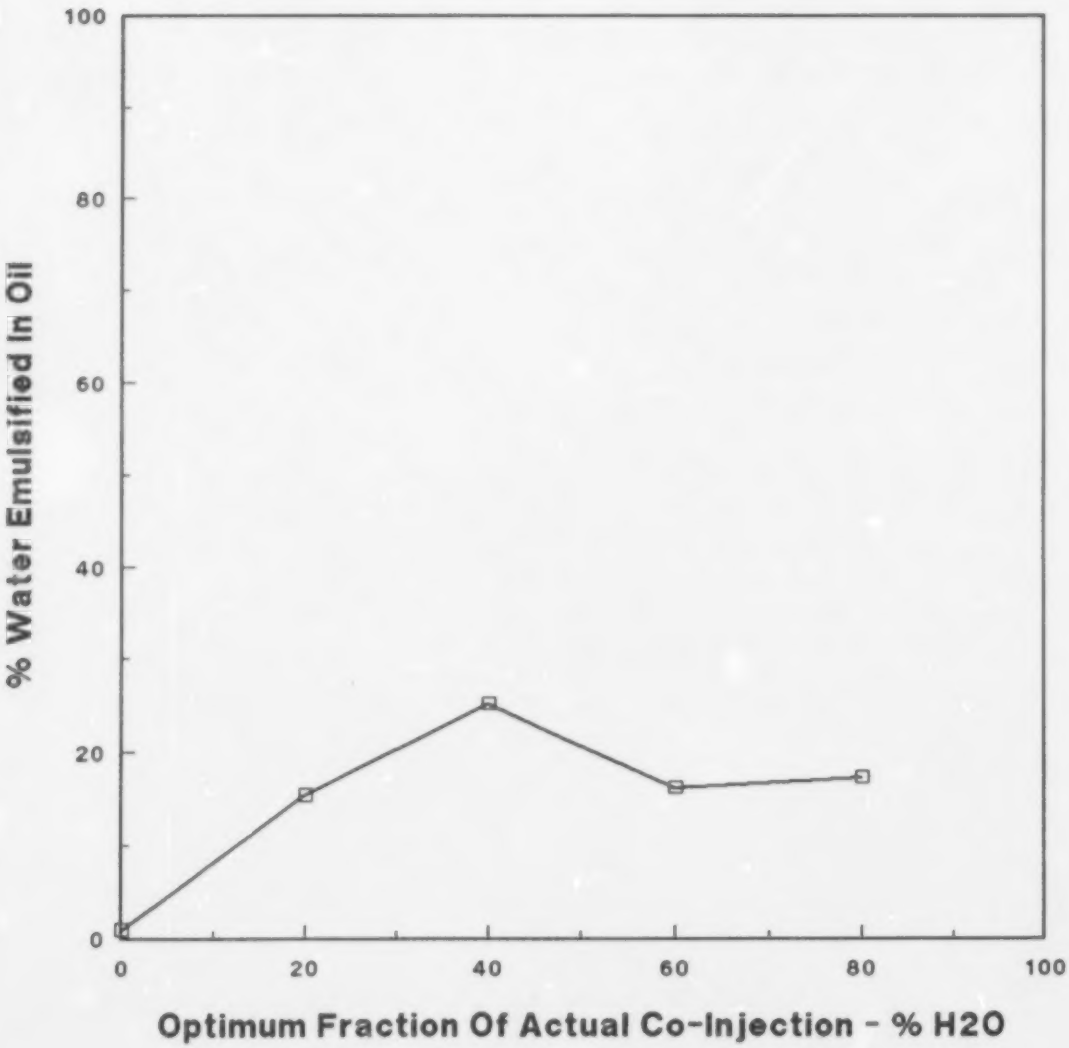

TEST #1 - WATER SATURATION INCREASING

FIGURE 16

PETRO CANADA HANGINGSTONE WELL 1-34-34-11 W4M
HIGH TEMP STEADY-STATE RELATIVE PERM STUDY
ACTUAL % OIL PROD vs OPTIMUM % H2O CO-INJ RATIO

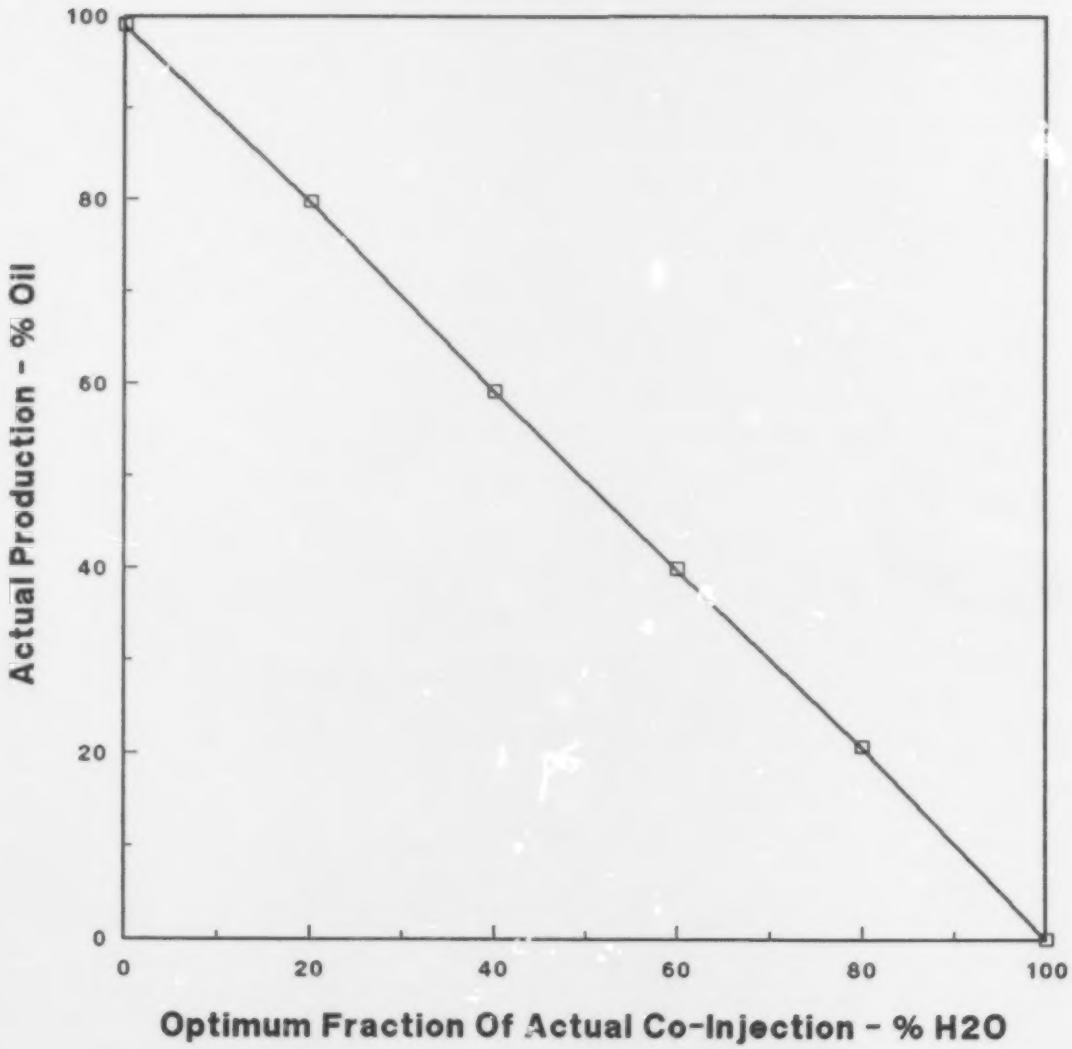

TEST #1 - WATER SATURATION DECREASING

FIGURE 17

PETRO CANADA HANGINGSTONE WELL 1-34-84-11 W4M
HIGH TEMP STEADY-STATE RELATIVE PERM STUDY
ACTUAL % H2O PROD vs OPTIMUM % H2O CO-INJ RATIO

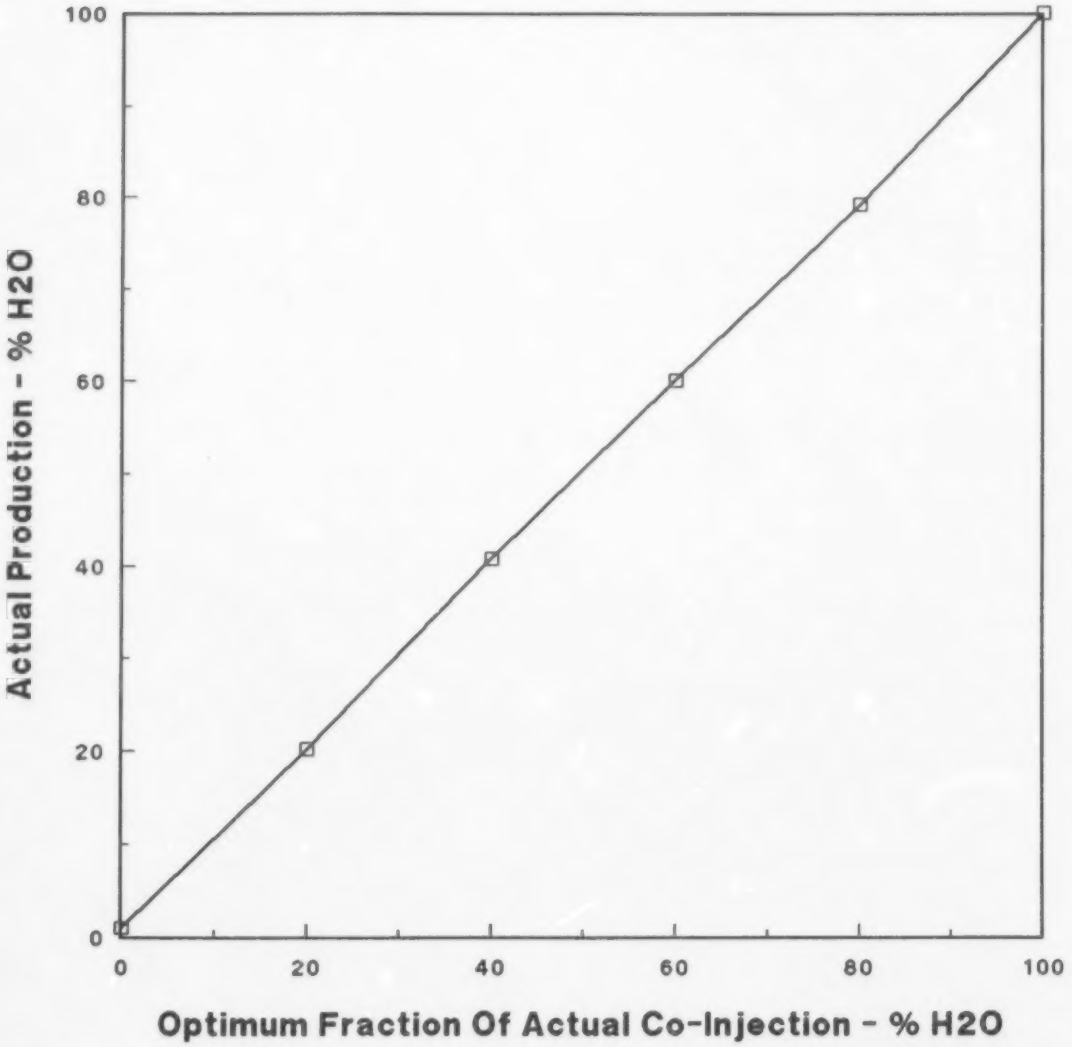

TEST #1 - WATER SATURATION DECREASING

FIGURE 18

PETRO CANADA HANGINGSTONE WELL 1-34-84-11 W4M
HIGH TEMP STEADY-STATE RELATIVE PERM STUDY
% FREE H2O vs OPTIMUM % H2O CO-INJ RATIO

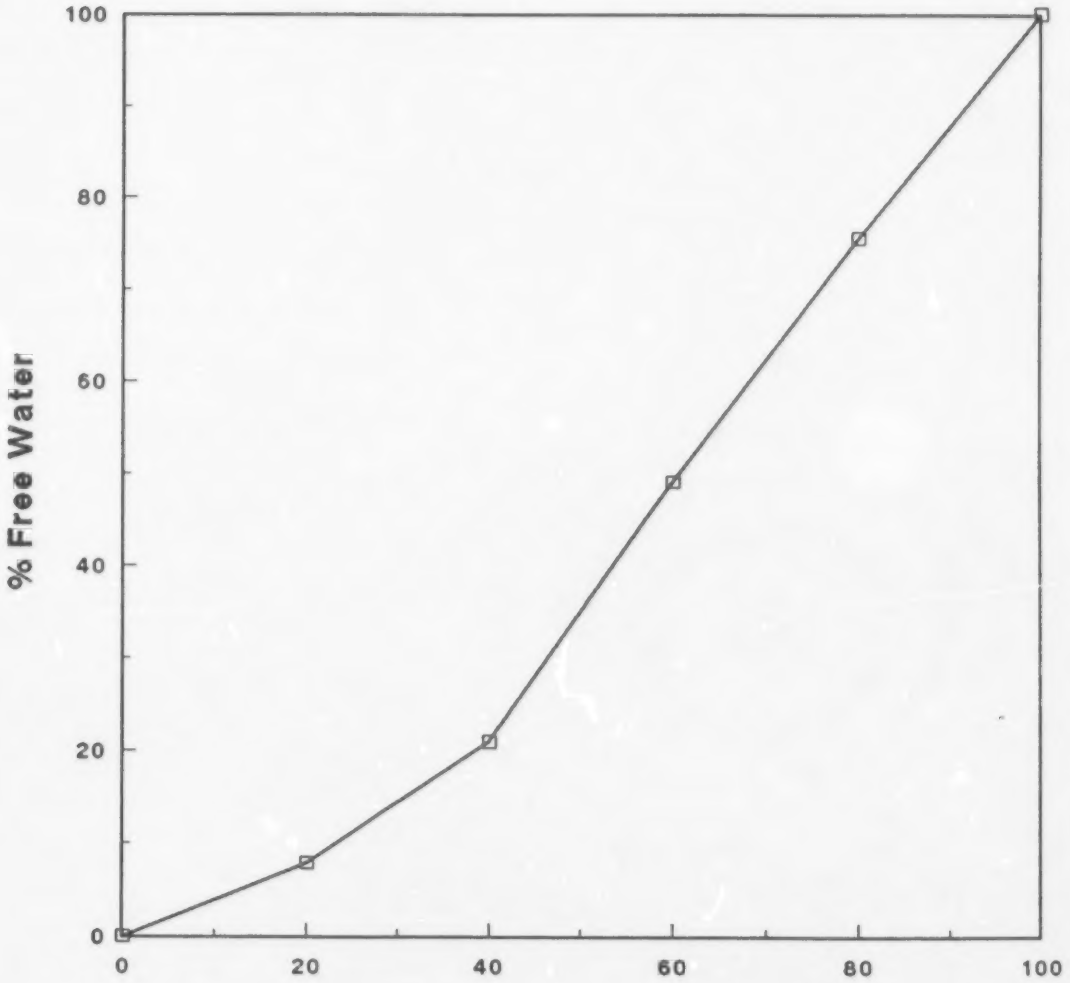

TEST #1 - WATER SATURATION DECREASING

FIGURE 19

PETRO CANADA HANGINGSTONE WELL 1-34-84-11 W4M
HIGH TEMP STEADY-STATE RELATIVE PERM STUDY
% EMULSIFIED OIL vs OPTIMUM % H2O CO-INJ RATIO

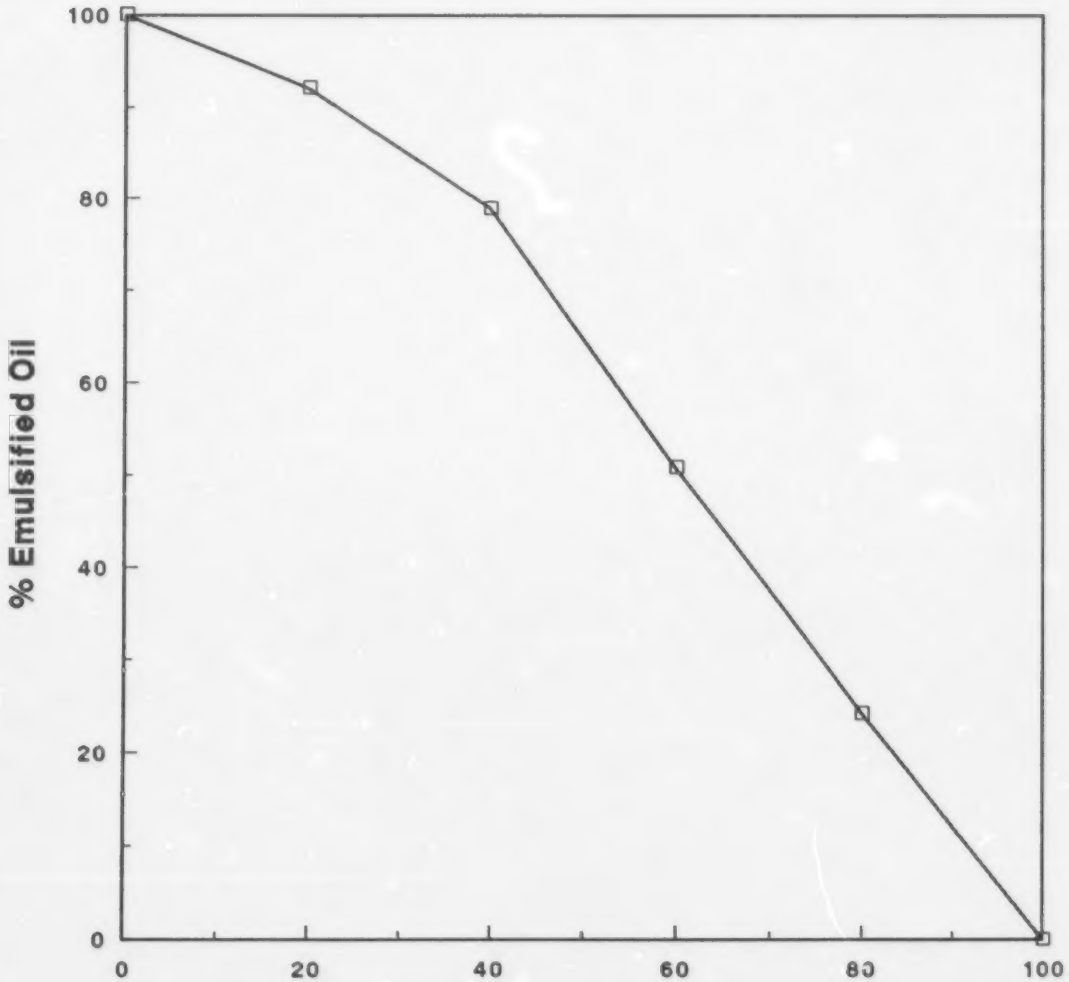

TEST #1 - WATER SATURATION DECREASING

FIGURE 20

PETRO CANADA HANGINGSTONE WELL 1-34-84-11 W4M
HIGH TEMP STEADY-STATE RELATIVE PERM STUDY
% H2O EMULS IN OIL vs OPTIMUM % H2O CO-INJ RATIO

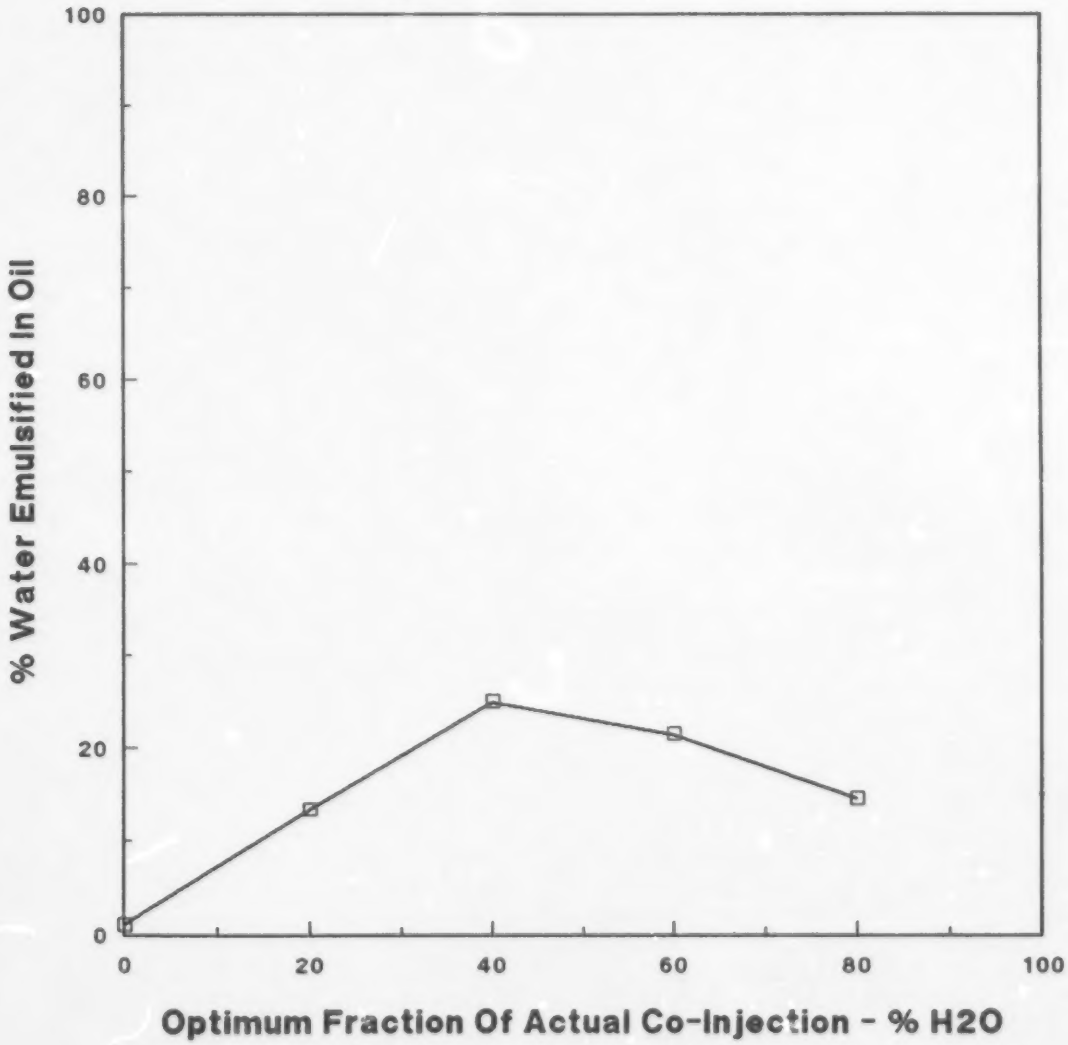

TEST #1 - WATER SATURATION DECREASING

FIGURE 21

PETRO CANADA HANGINGSTONE WELL 1-34-84-11 W4M
HIGH TEMP STEADY-STATE RELATIVE PERM STUDY
ACTUAL % OIL PROD vs OPTIMUM % H2O CO-INJ RATIO

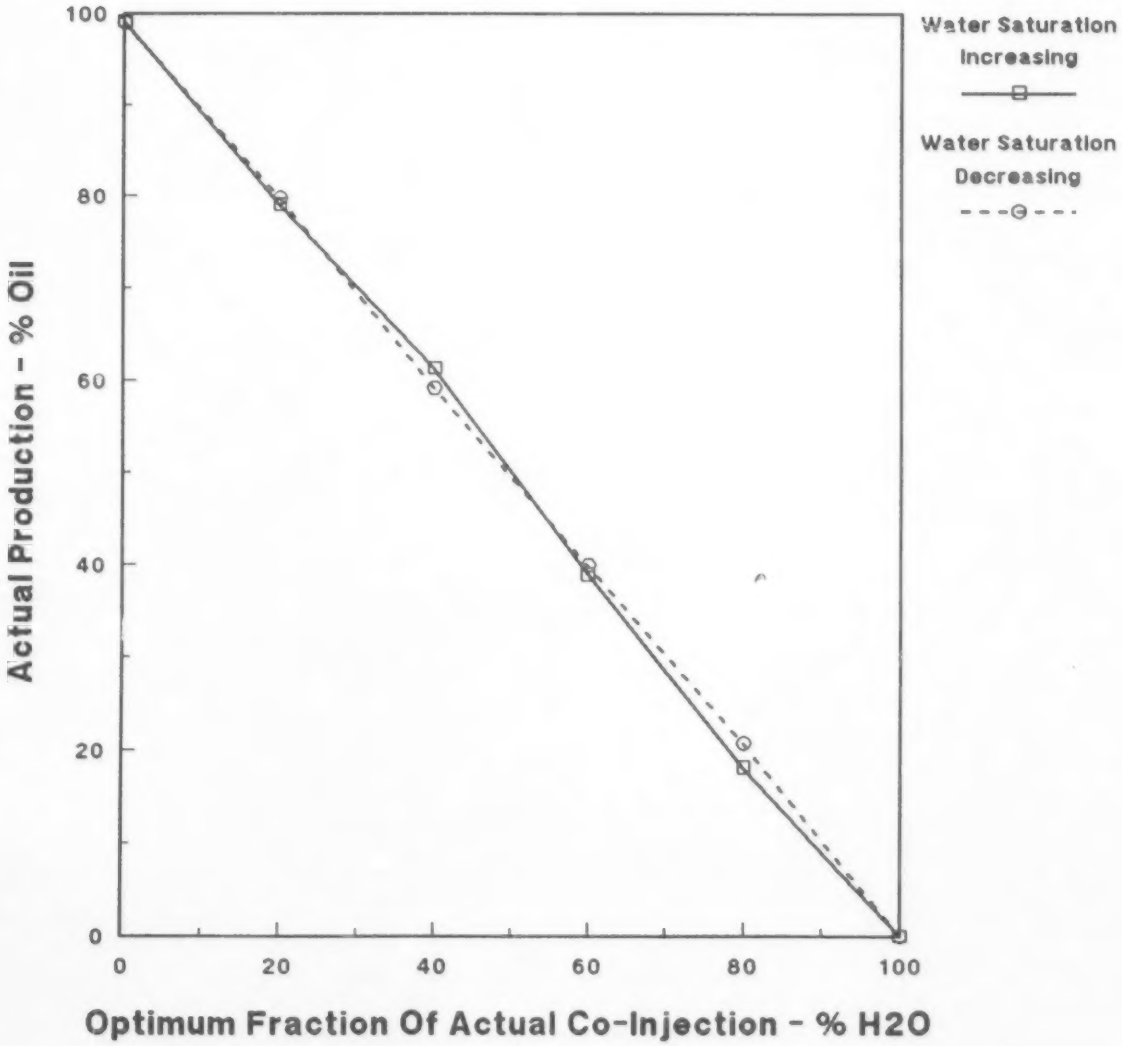

TEST #1

FIGURE 22

PETRO CANADA HANGINGSTONE WELL 1-34-84-11 W4M
HIGH TEMP STEADY-STATE RELATIVE PERM STUDY
ACTUAL % H2O PROD vs OPTIMUM % H2O CO-INJ RATIO

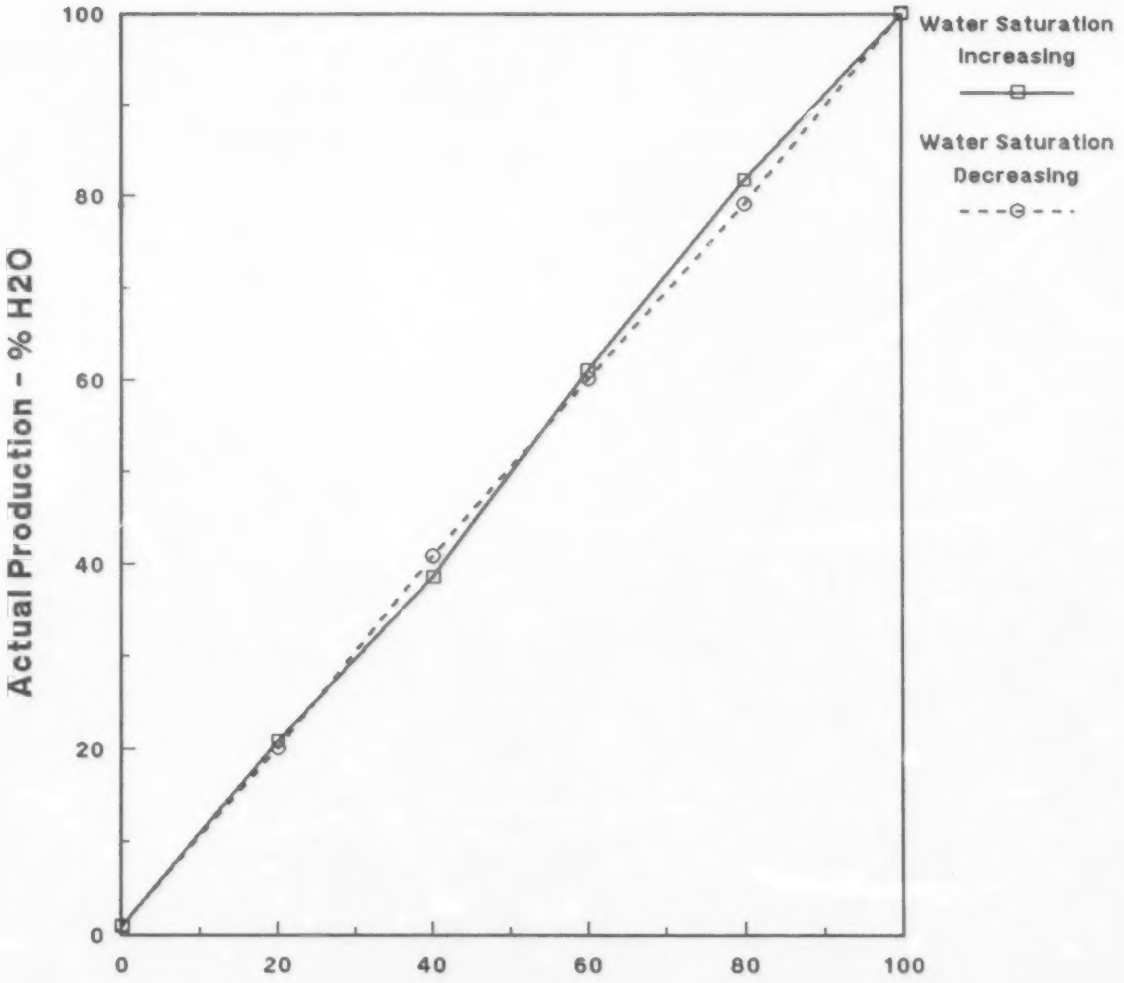

TEST #1

FIGURE 23

PETRO CANADA HANGINGSTONE WELL 1-34-84-11 W4M
HIGH TEMP STEADY-STATE RELATIVE PERM STUDY
% FREE H2O vs OPTIMUM % H2O CO-INJ RATIO

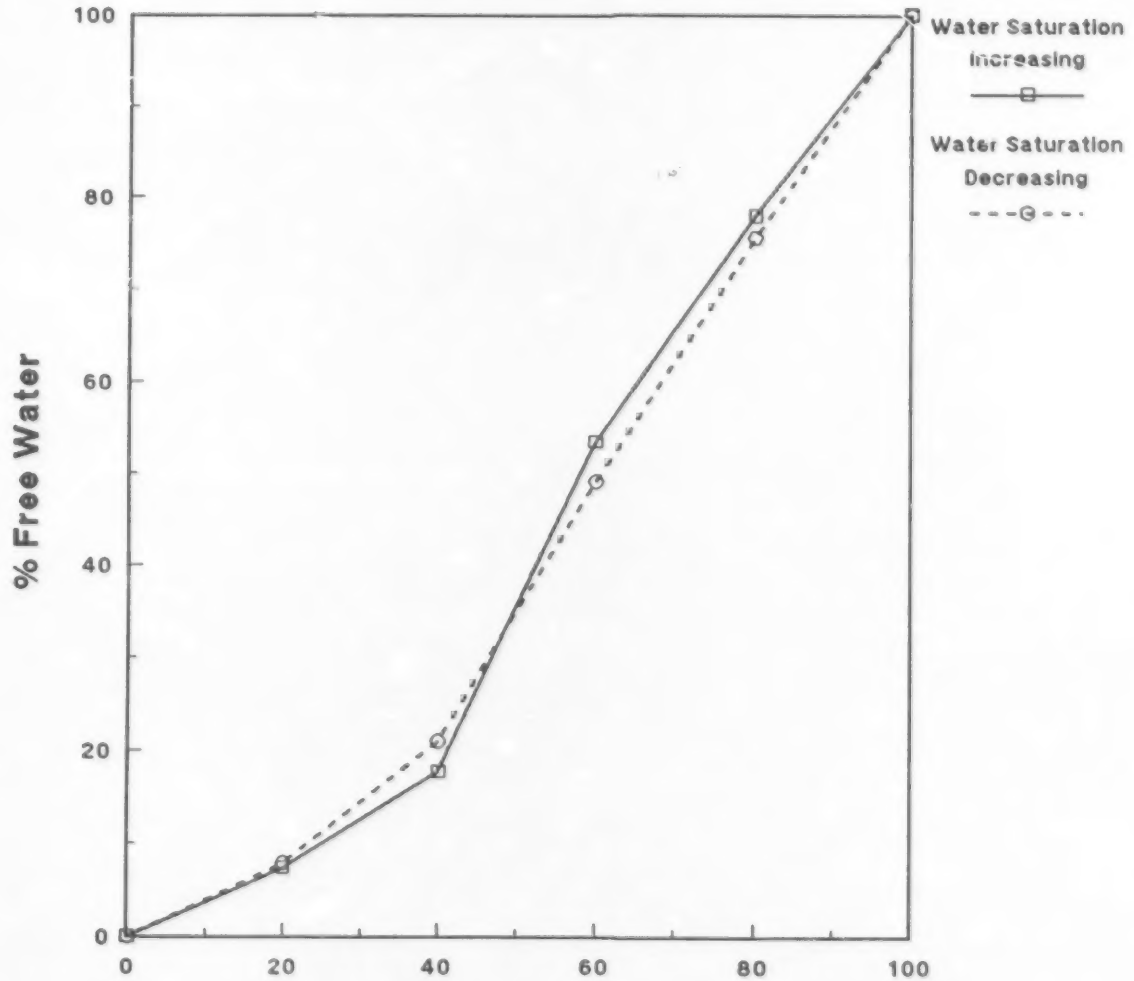

TEST #1

FIGURE 24

PETRO CANADA HANGINGSTONE WELL 1-34-84-11 W4M
HIGH TEMP STEADY-STATE RELATIVE PERM STUDY
% EMULSIFIED OIL vs OPTIMUM % H2O CO-INJ RATIO

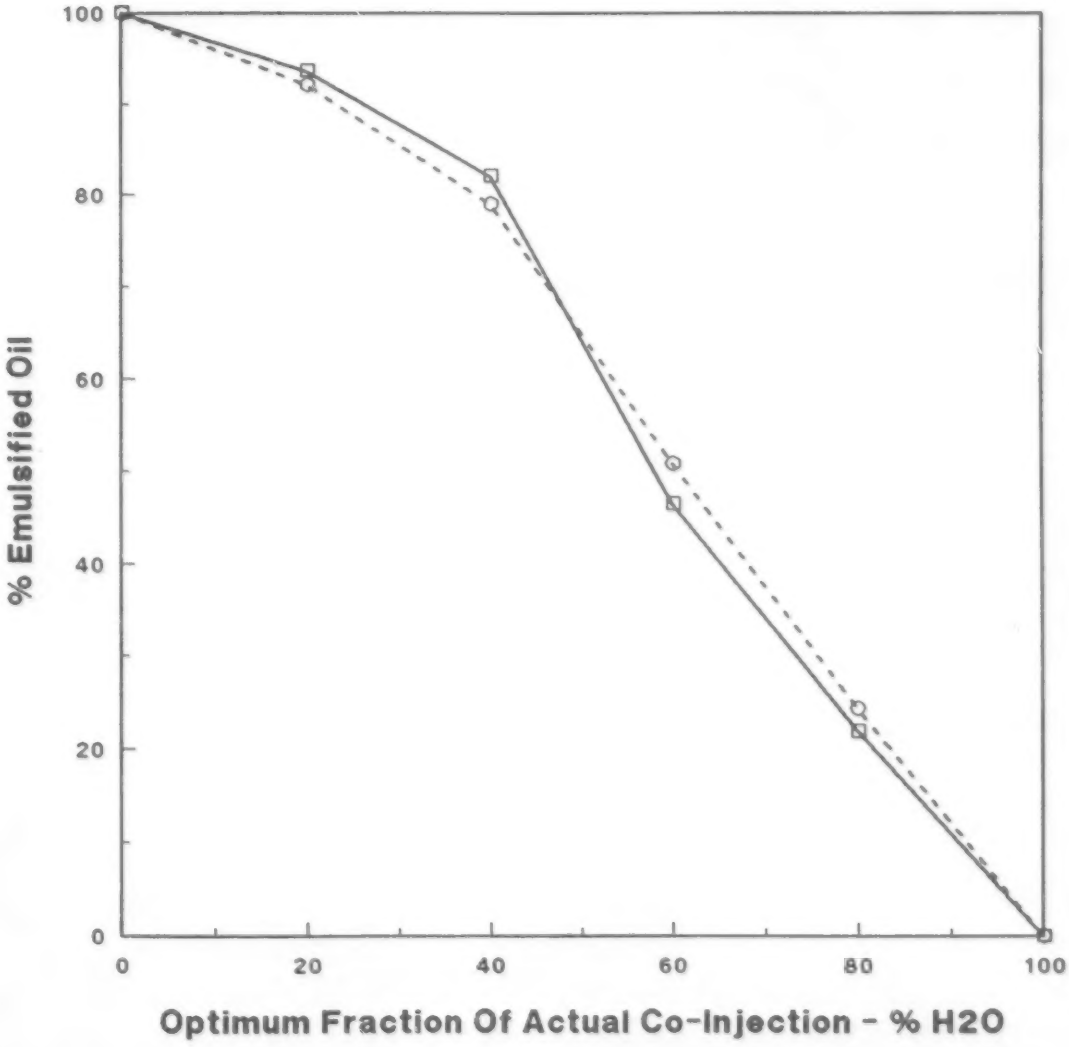

TEST # 1

FIGURE 25

PETRO CANADA HANGINGSTONE WELL 1-34-84-11 W4M
HIGH TEMP STEADY-STATE RELATIVE PERM STUDY
% H2O EMULS IN OIL vs OPTIMUM % H2O CO-INJ RATIO

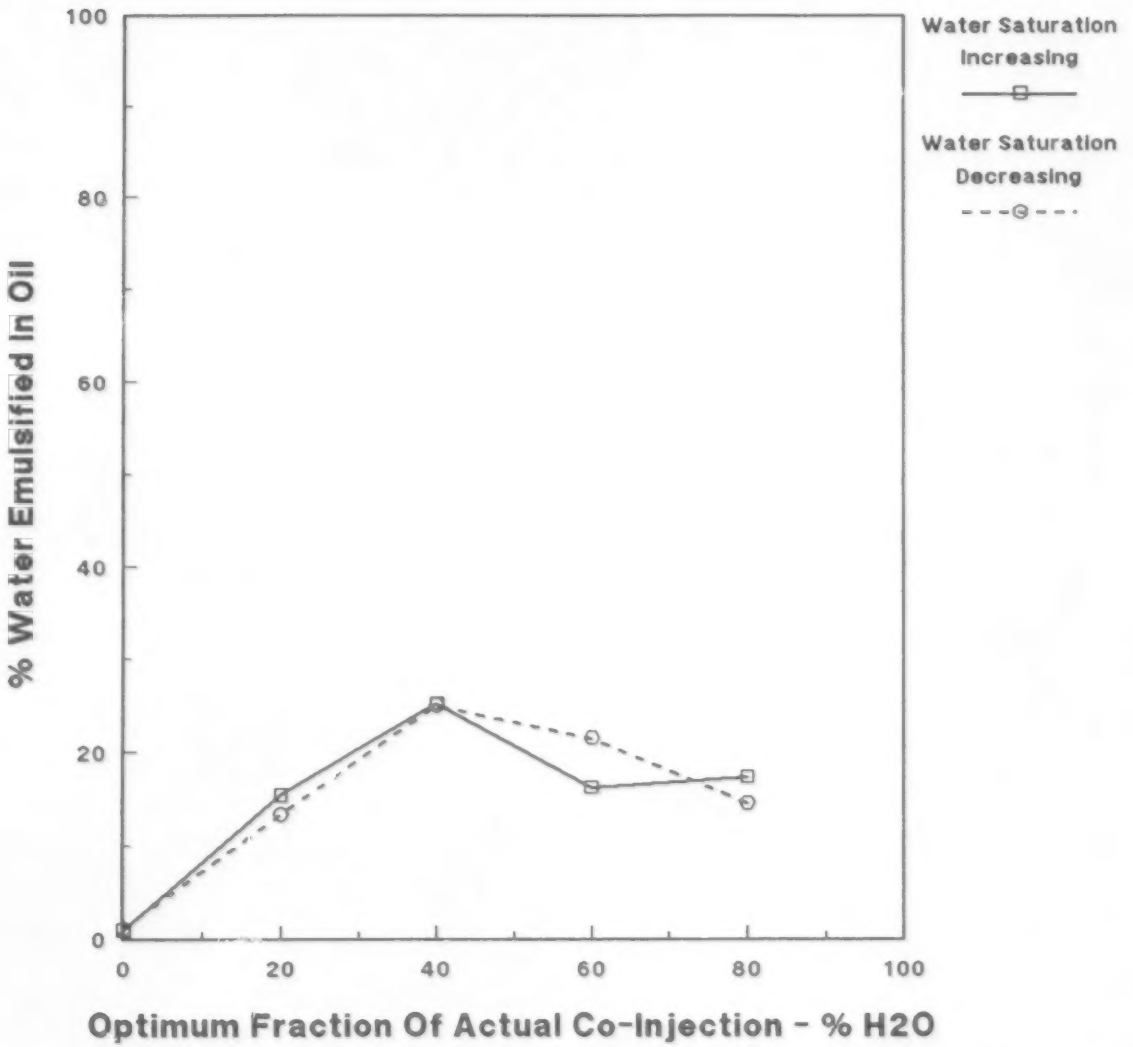

TEST #1

FIGURE 26

PETRO CANADA HANGINGSTONE WELL 1-34-84-11 W4M
HIGH TEMP STEADY-STATE RELATIVE PERM STUDY
PERCENT OF PHASE vs PERCENT INJECTED WATER

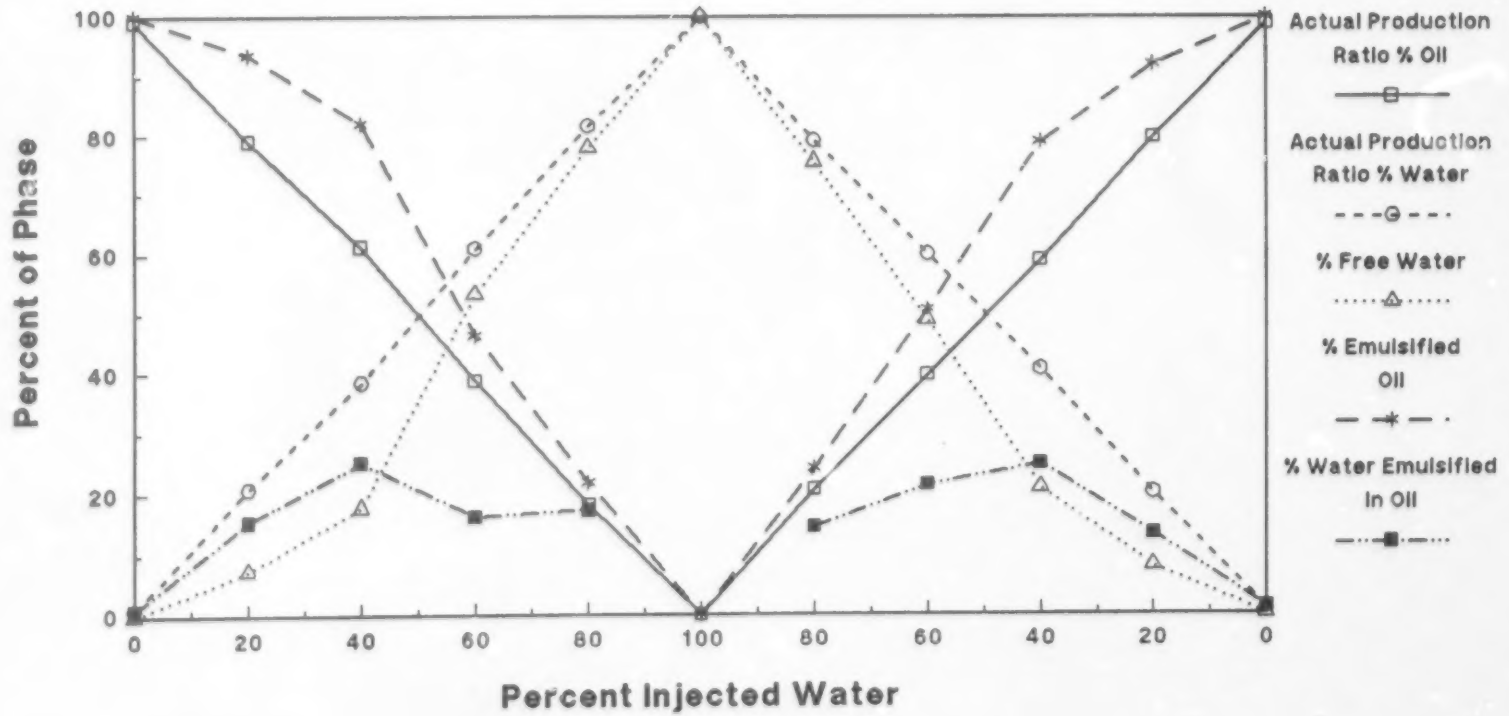

TEST # 1

Hycal

FIGURE 27

PETRO CANADA WELL 1-34-84-11 W4M
HIGH TEMP STEADY-STATE REL PERM STUDY - TEST #2
RELATIVE PERMEABILITY vs WATER SATURATION

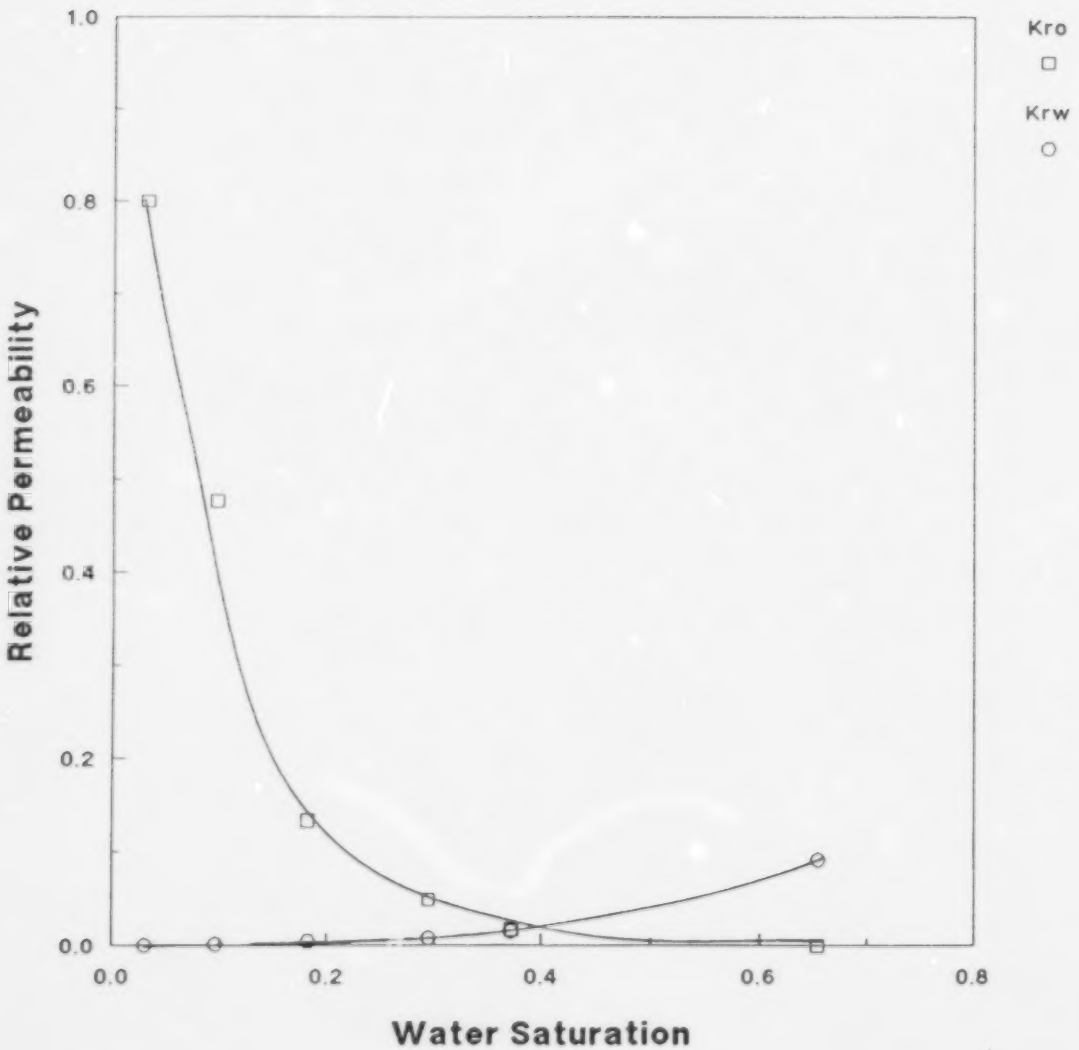

PRELIMINARY RESULTS

WATER SATURATION INCREASING

FIGURE 28

PETRO CANADA WELL 1-34-84-11 W4M
HIGH TEMP STEADY-STATE REL PERM STUDY - TEST #2
RELATIVE PERMEABILITY vs WATER SATURATION

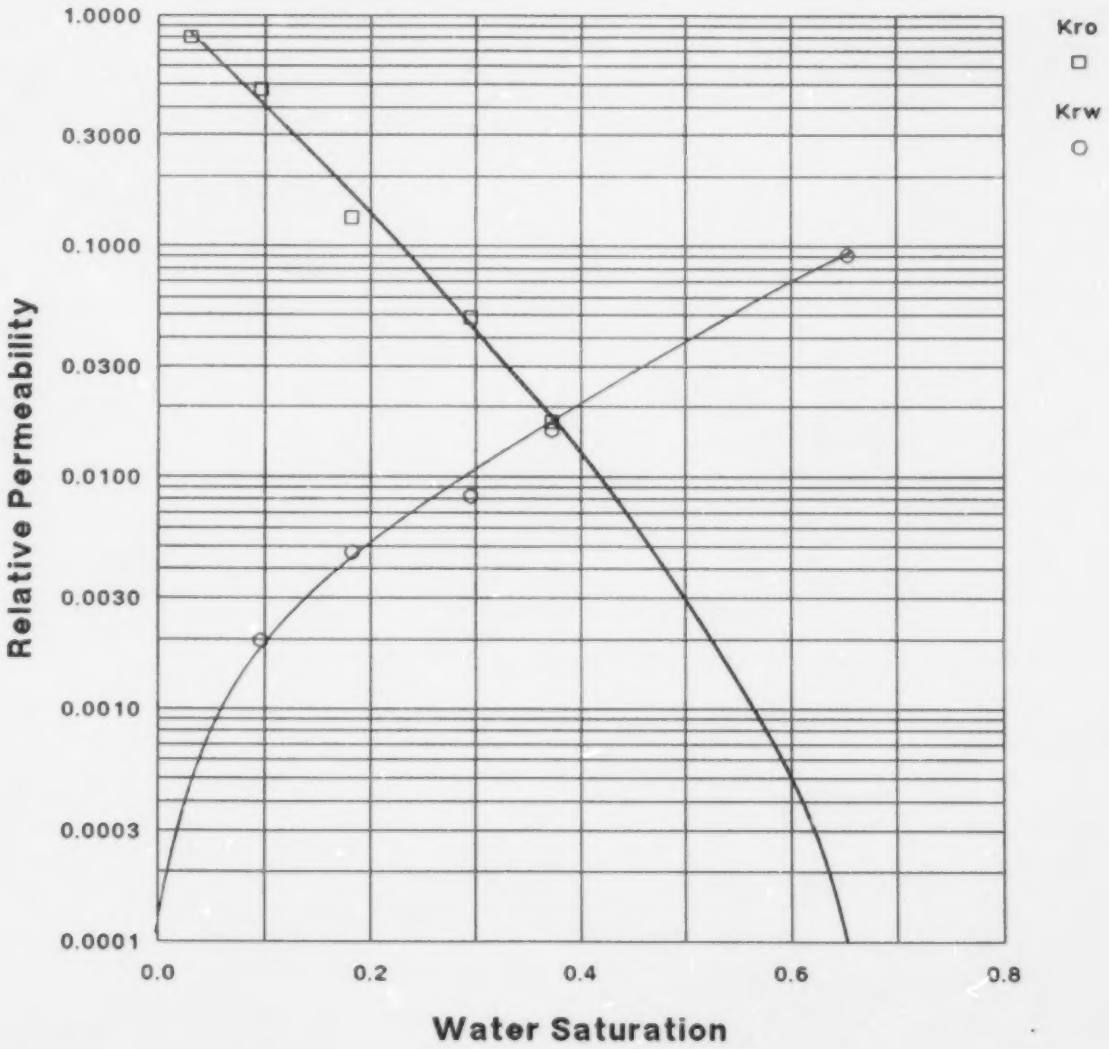

PRELIMINARY RESULTS

WATER SATURATION INCREASING

FIGURE 29

PETRO CANADA WELL 1-34-84-11 W4M
HIGH TEMP STEADY-STATE REL PERM STUDY - TEST #2
RELATIVE PERMEABILITY vs WATER SATURATION

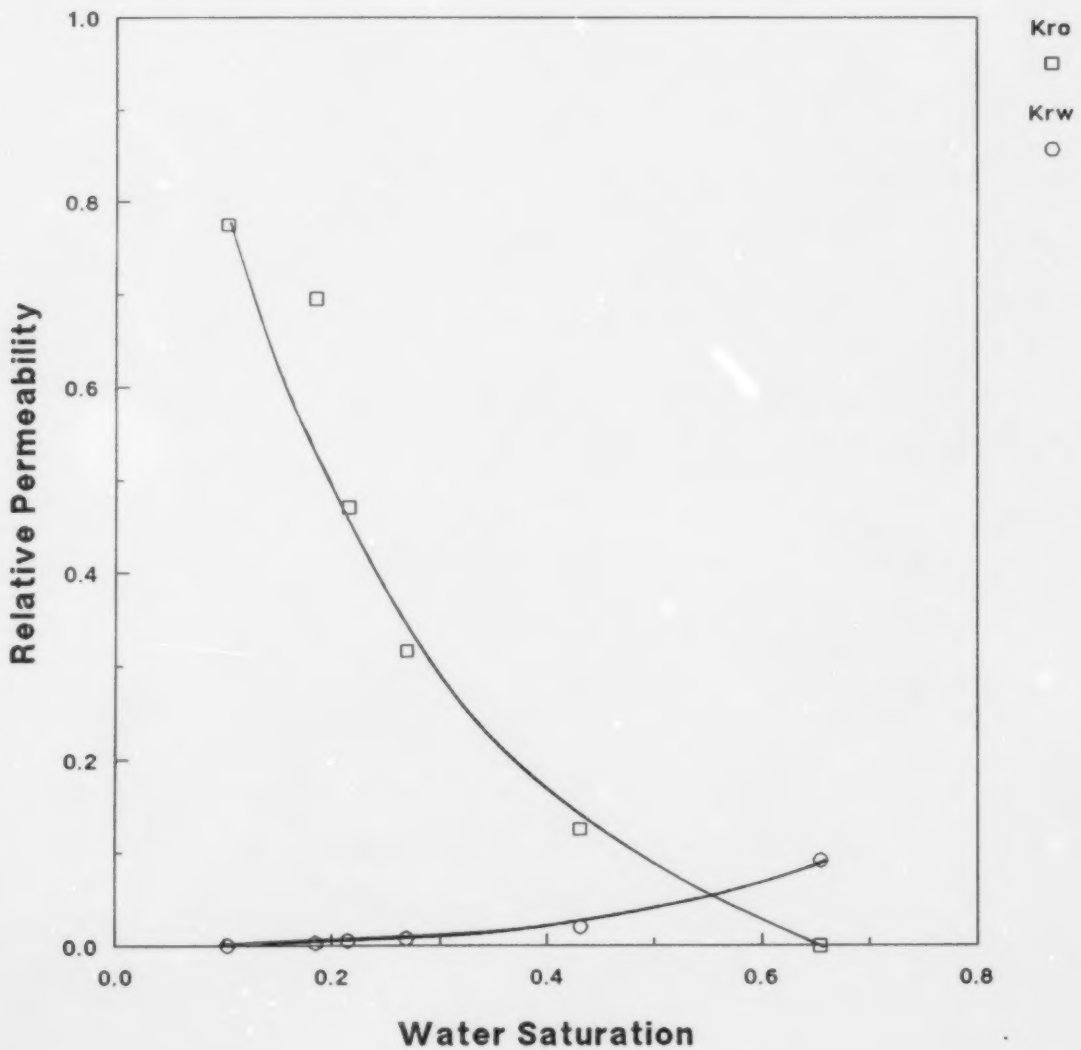

PRELIMINARY RESULTS
WATER SATURATION DECREASING

FIGURE 30

PETRO CANADA WELL 1-34-84-11 W4M
HIGH TEMP STEADY-STATE REL PERM STUDY - TEST #2
RELATIVE PERMEABILITY vs WATER SATURATION

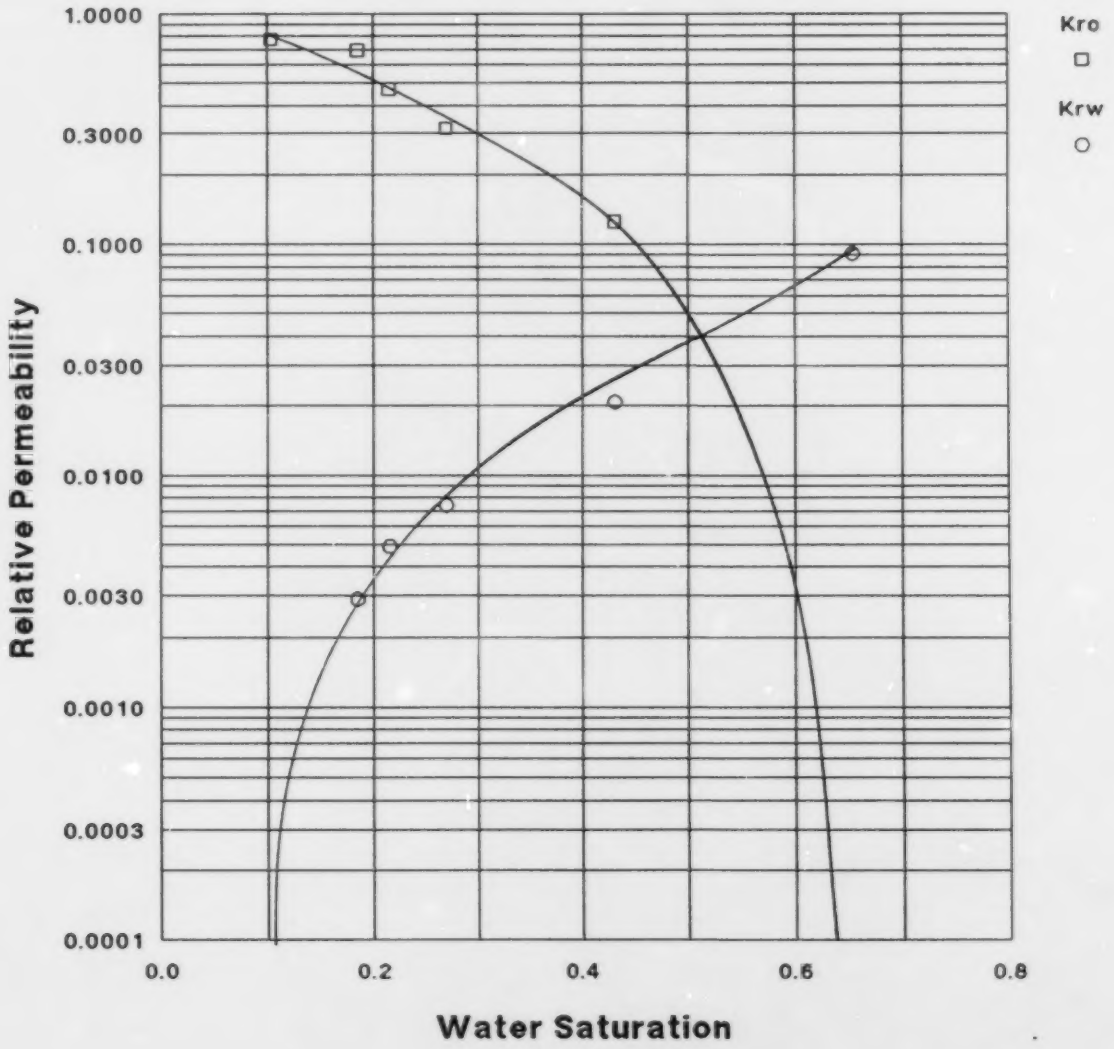

PRELIMINARY RESULTS

WATER SATURATION DECREASING

FIGURE 31

PETRO CANADA WELL 1-34-84-11 W4M
HIGH TEMP STEADY-STATE REL PERM STUDY - TEST #2
RELATIVE PERMEABILITY vs WATER SATURATION

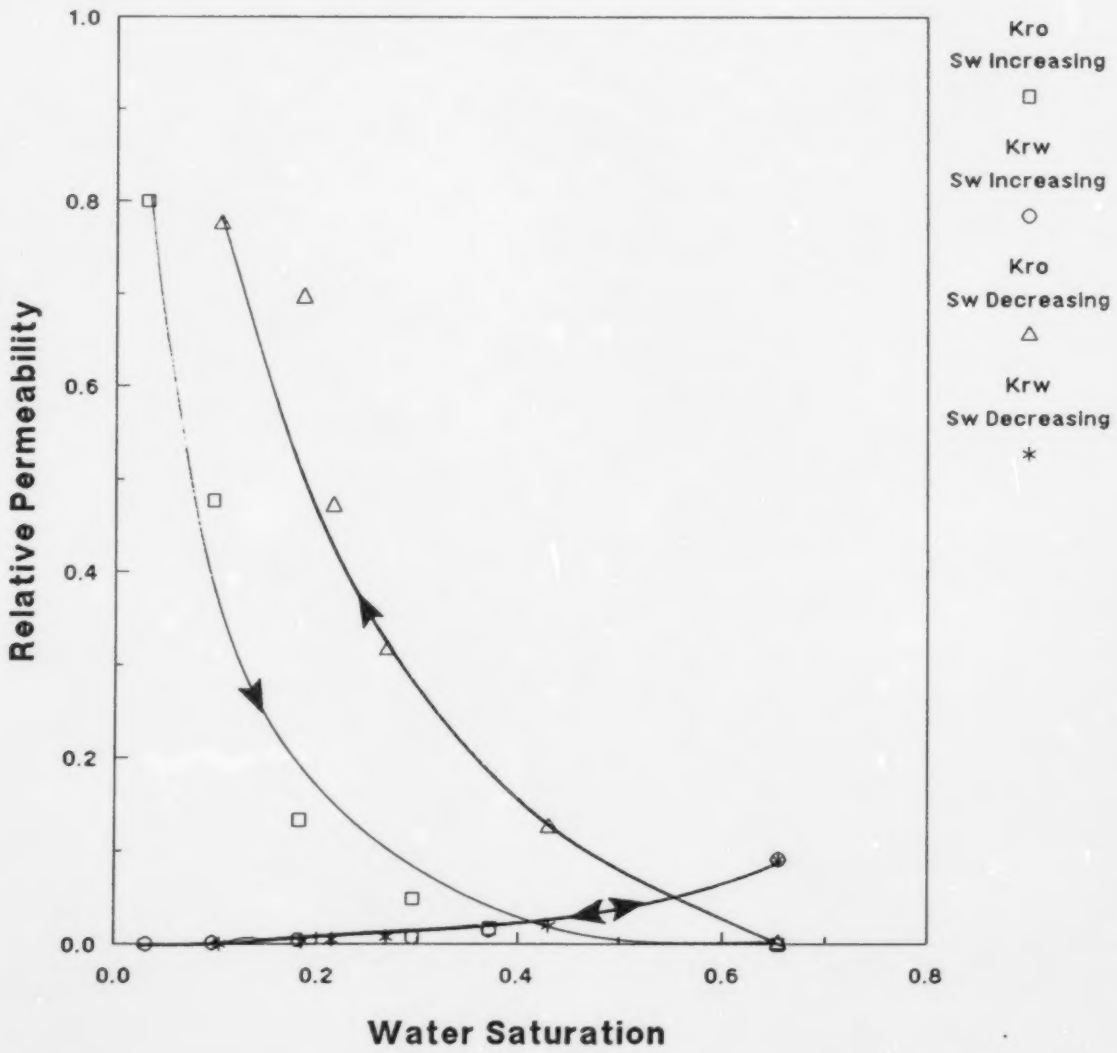

PRELIMINARY RESULTS

COMPARISON OF Sw INCREASING AND DECREASING

FIGURE 32

PETRO CANADA WELL 1-34-84-11 W4M
HIGH TEMP STEADY-STATE REL PERM STUDY - TEST #2
RELATIVE PERMEABILITY vs WATER SATURATION

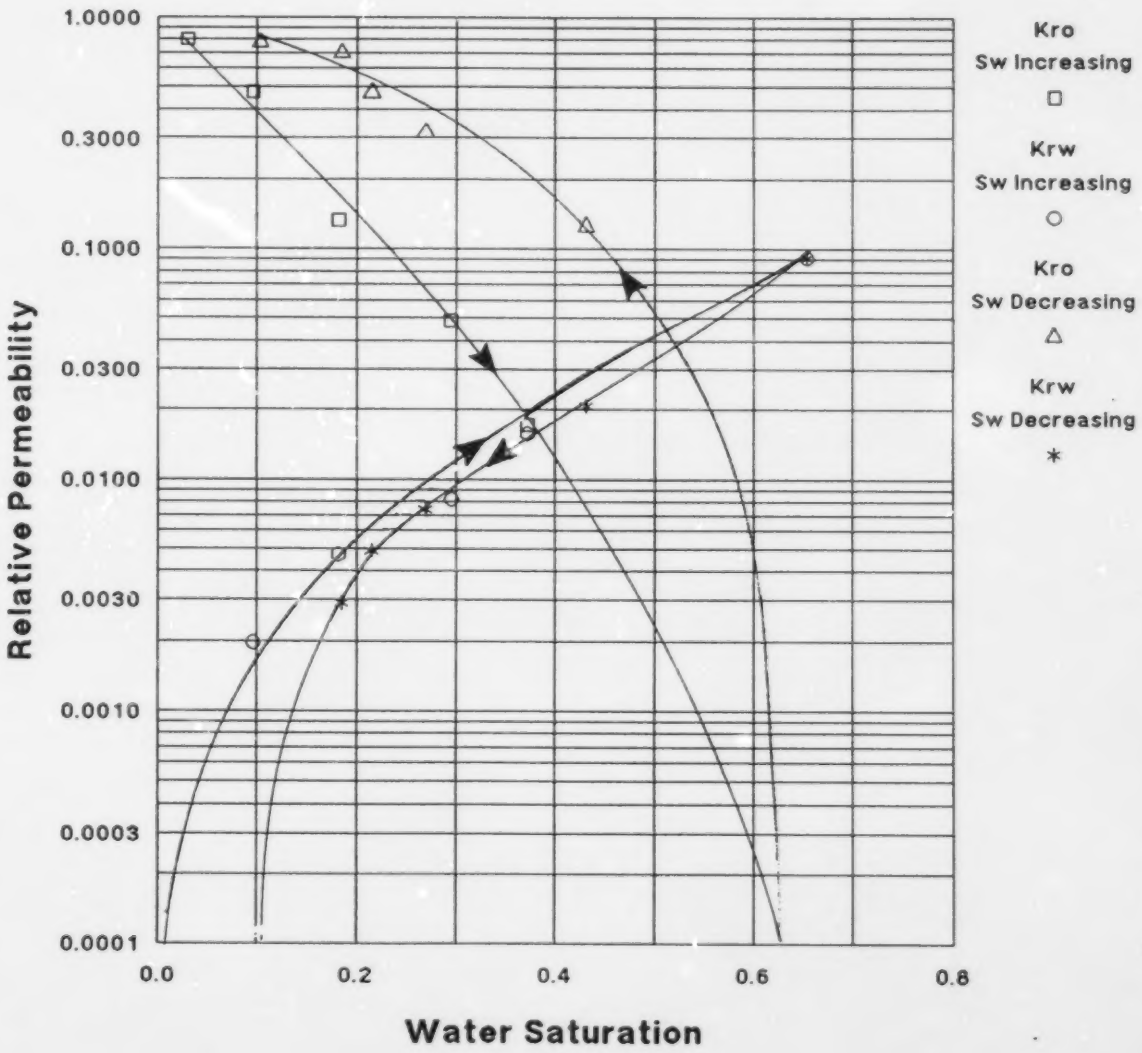

PRELIMINARY RESULTS
COMPARISON OF Sw INCREASING AND DECREASING

FIGURE 33

PETRO CANADA HANGINGSTONE WELL 1-34-84-11 W4M
HIGH TEMP STEADY-STATE RELATIVE PERM STUDY
ACTUAL % OIL PROD vs OPTIMUM % H2O CO-INJ RATIO

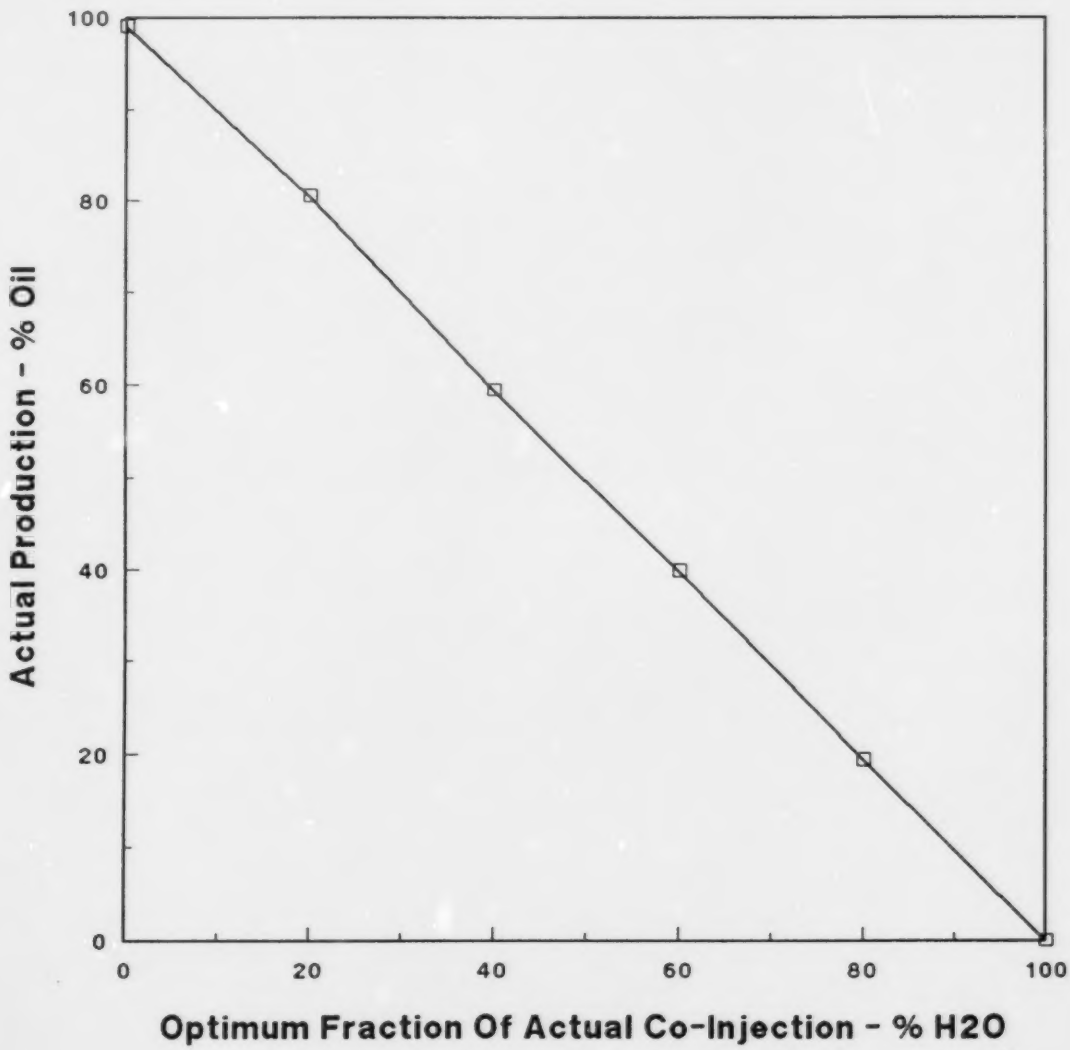

TEST #2 - WATER SATURATION INCREASING

FIGURE 34

PETRO CANADA HANGINGSTONE WELL 1-34-84-11 W4M
HIGH TEMP STEADY-STATE RELATIVE PERM STUDY
ACTUAL % H2O PROD vs OPTIMUM % H2O CO-INJ RATIO

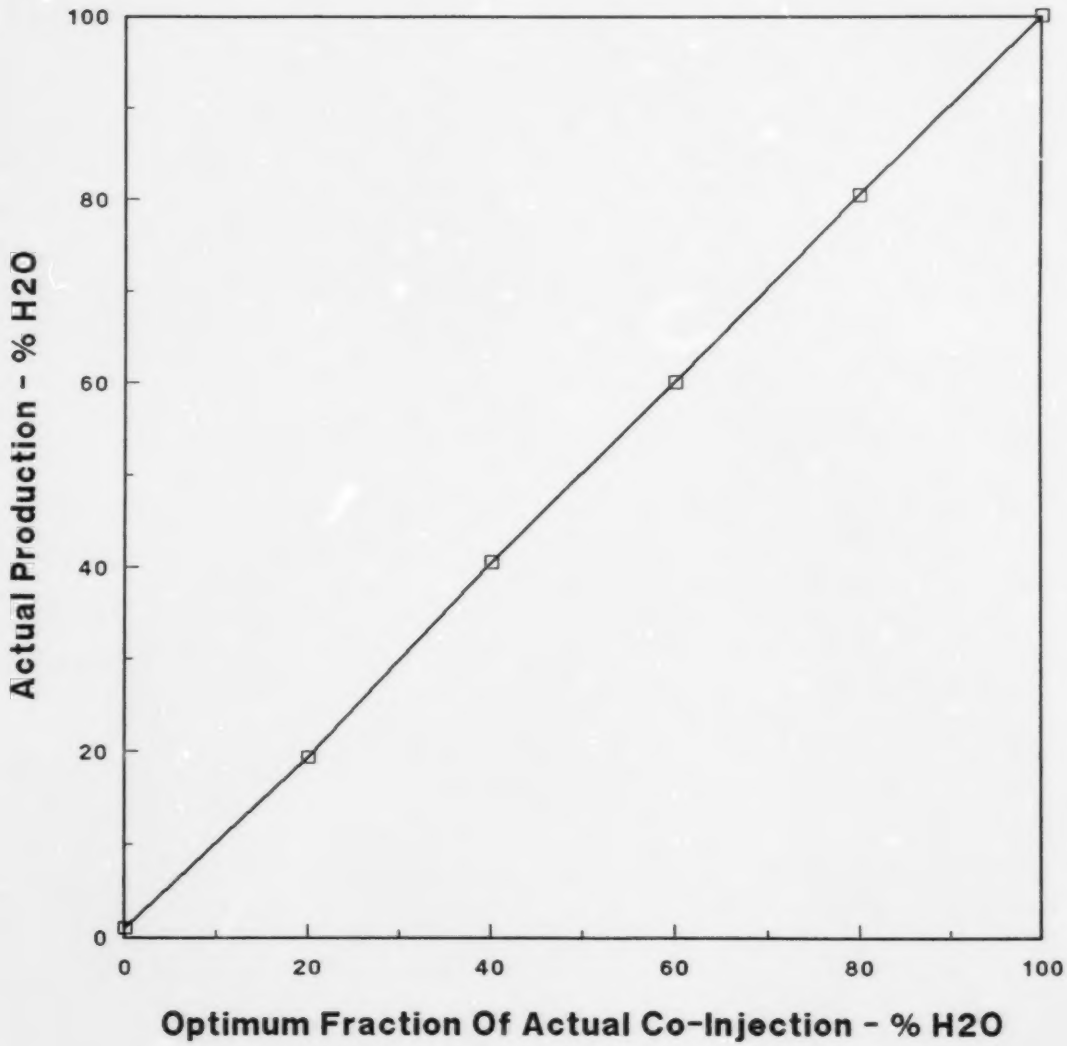

TEST #2 - WATER SATURATION INCREASING

FIGURE 35

PETRO CANADA HANGINGSTONE WELL 1-34-84-11 W4M
HIGH TEMP STEADY-STATE RELATIVE PERM STUDY
% FREE H2O vs OPTIMUM % H2O CO-INJ RATIO

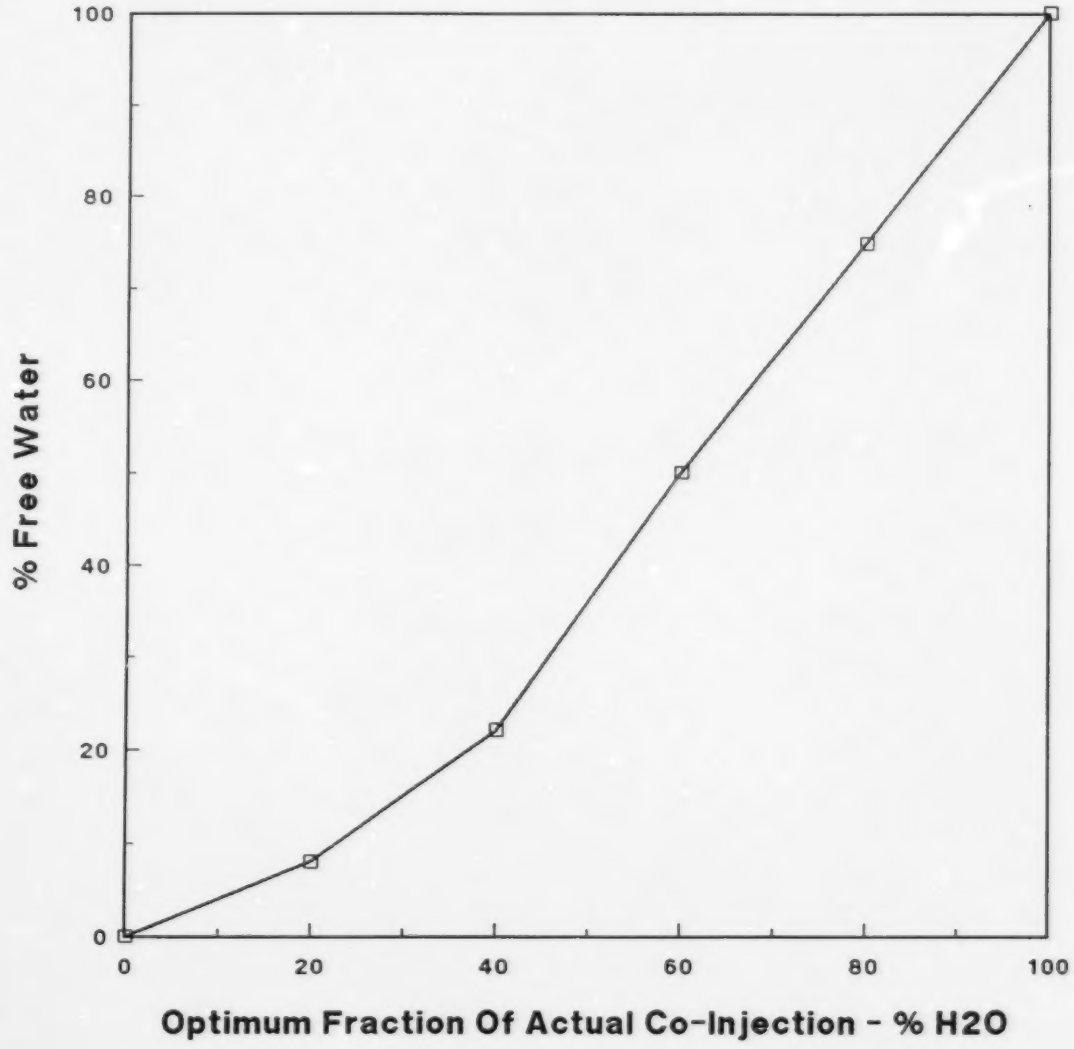

TEST #2 - WATER SATURATION INCREASING

FIGURE 36

PETRO CANADA HANGINGSTONE WELL 1-34-84-11 W4M

HIGH TEMP STEADY-STATE RELATIVE PERM STUDY

% EMULSIFIED OIL vs OPTIMUM % H2O CO-INJ RATIO

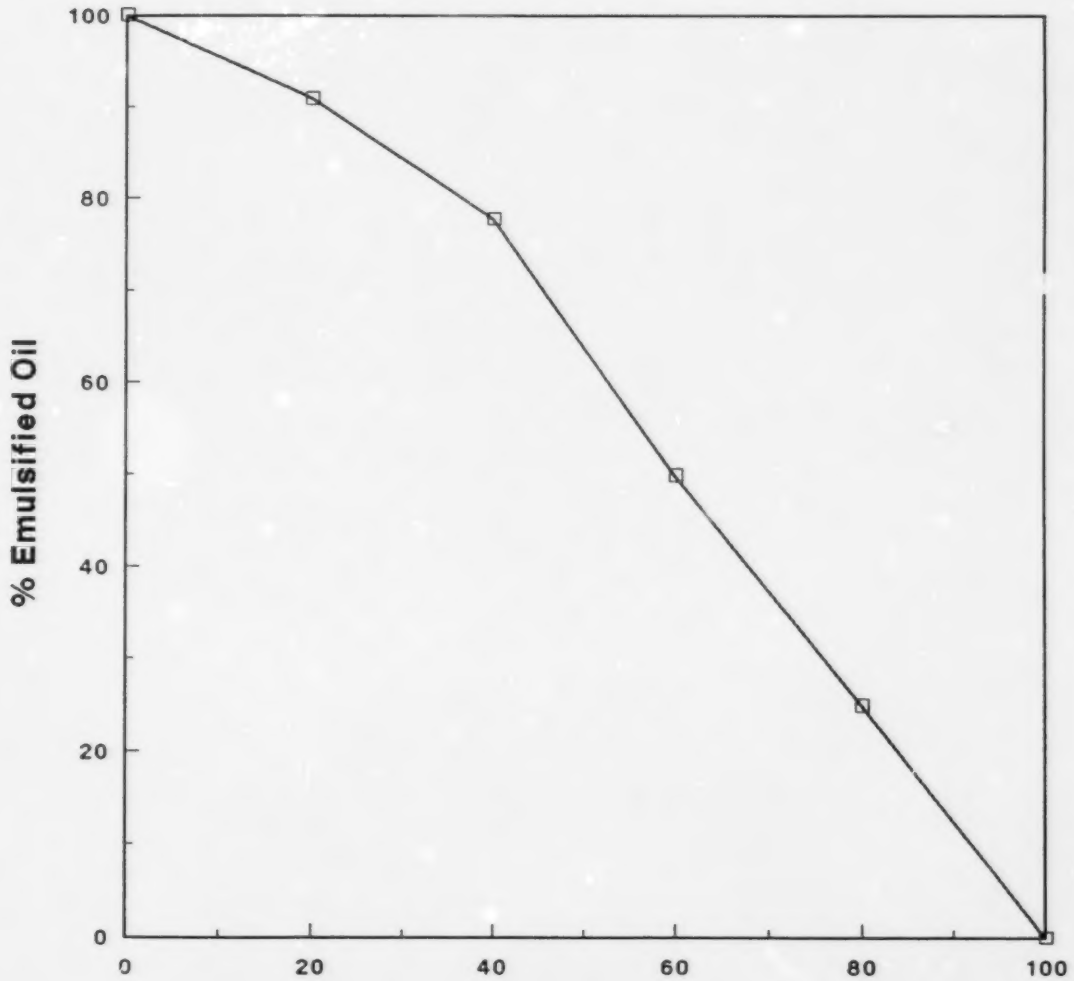

TEST #2 - WATER SATURATION INCREASING

FIGURE 37

PETRO CANADA HANGINGSTONE WELL 1-34-84-11 W4M
HIGH TEMP STEADY-STATE RELATIVE PERM STUDY
% H2O EMULS IN OIL vs OPTIMUM % H2O CO-INJ RATIO

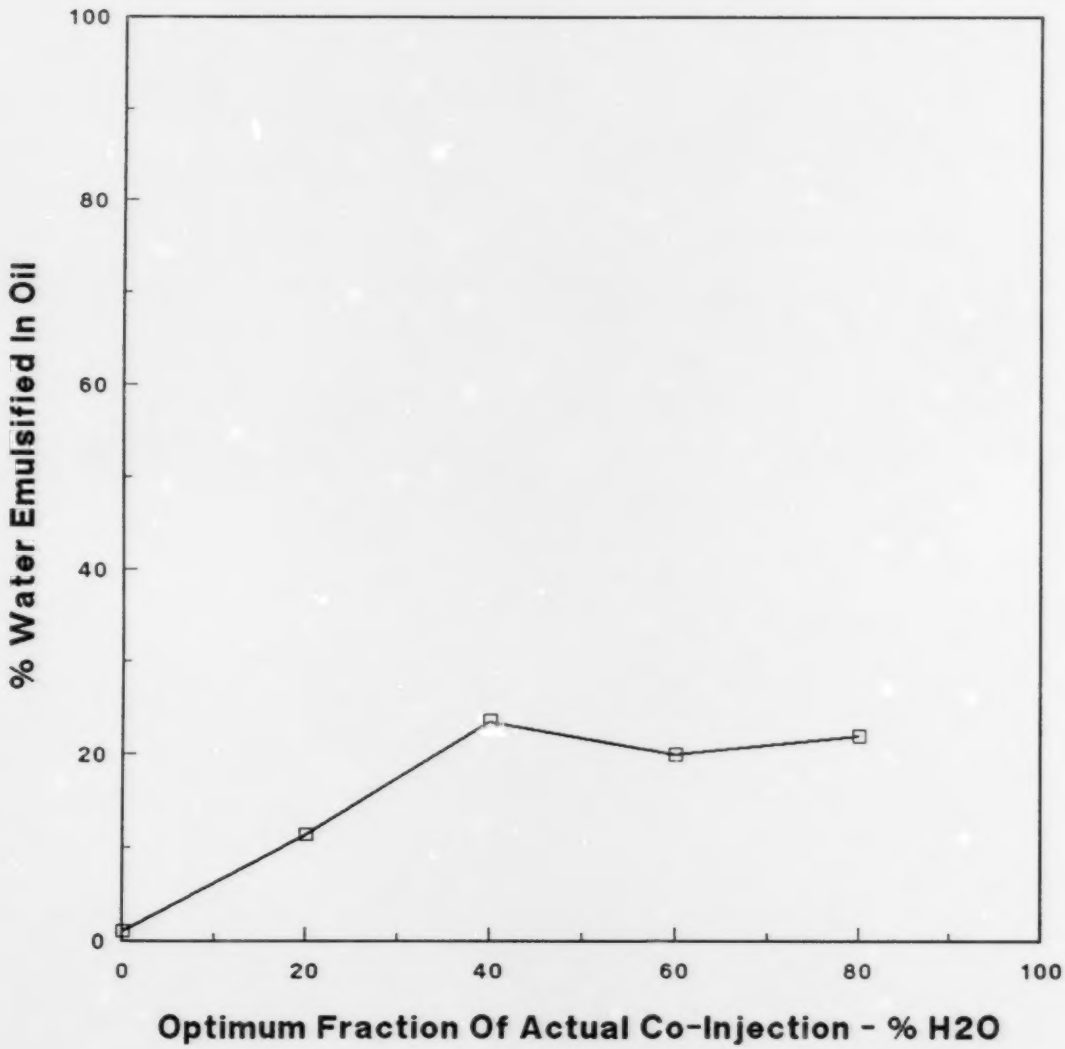

TEST #2 - WATER SATURATION INCREASING

FIGURE 38

PETRO CANADA HANGINGSTONE WELL 1-34-84-11 W4M
HIGH TEMP STEADY-STATE RELATIVE PERM STUDY
ACTUAL % OIL PROD vs OPTIMUM % H2O CO-INJ RATIO

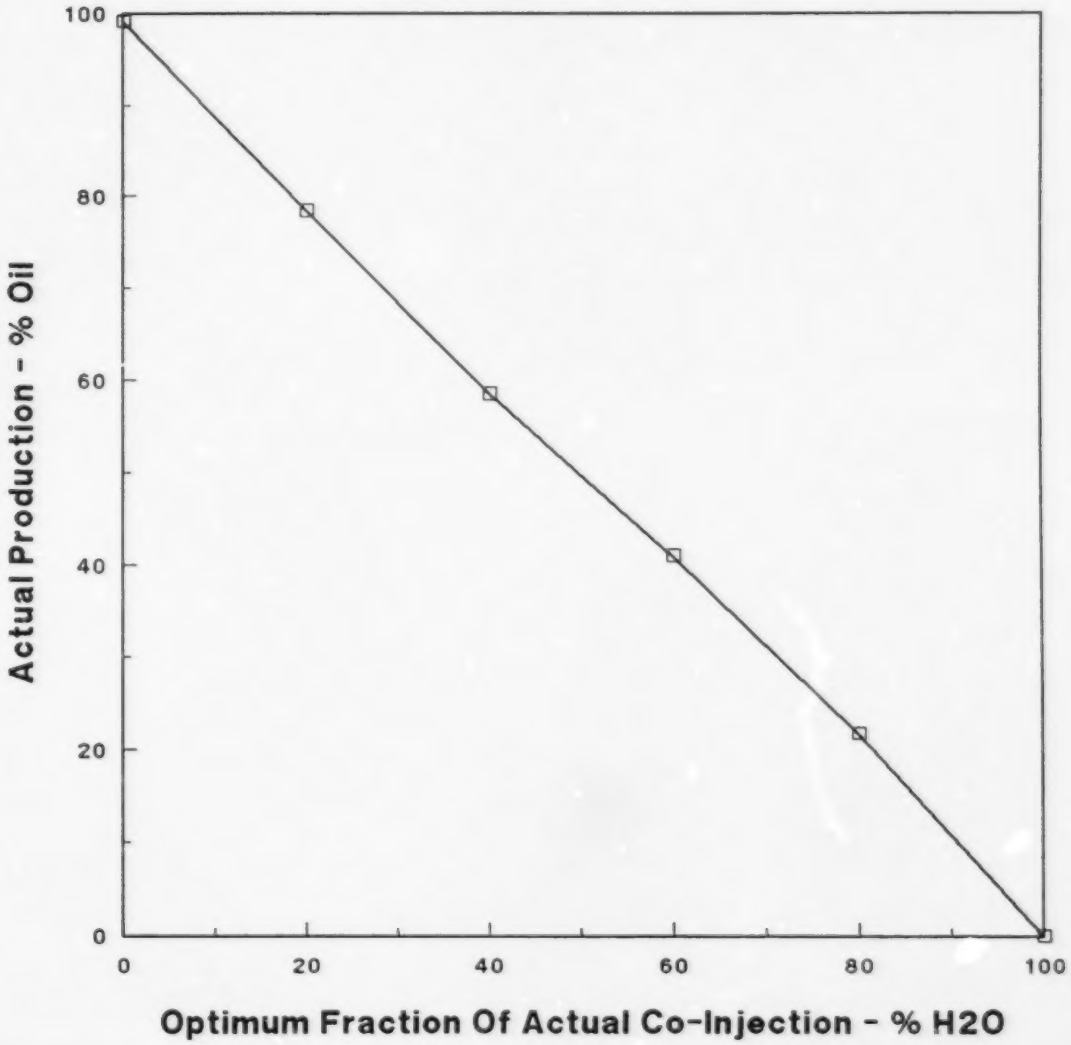

TEST #2 - WATER SATURATION DECREASING

FIGURE 39

PETRO CANADA HANGINGSTONE WELL 1-34-84-11 W4M
HIGH TEMP STEADY-STATE RELATIVE PERM STUDY
ACTUAL % H2O PROD vs OPTIMUM % H2O CO-INJ RATIO

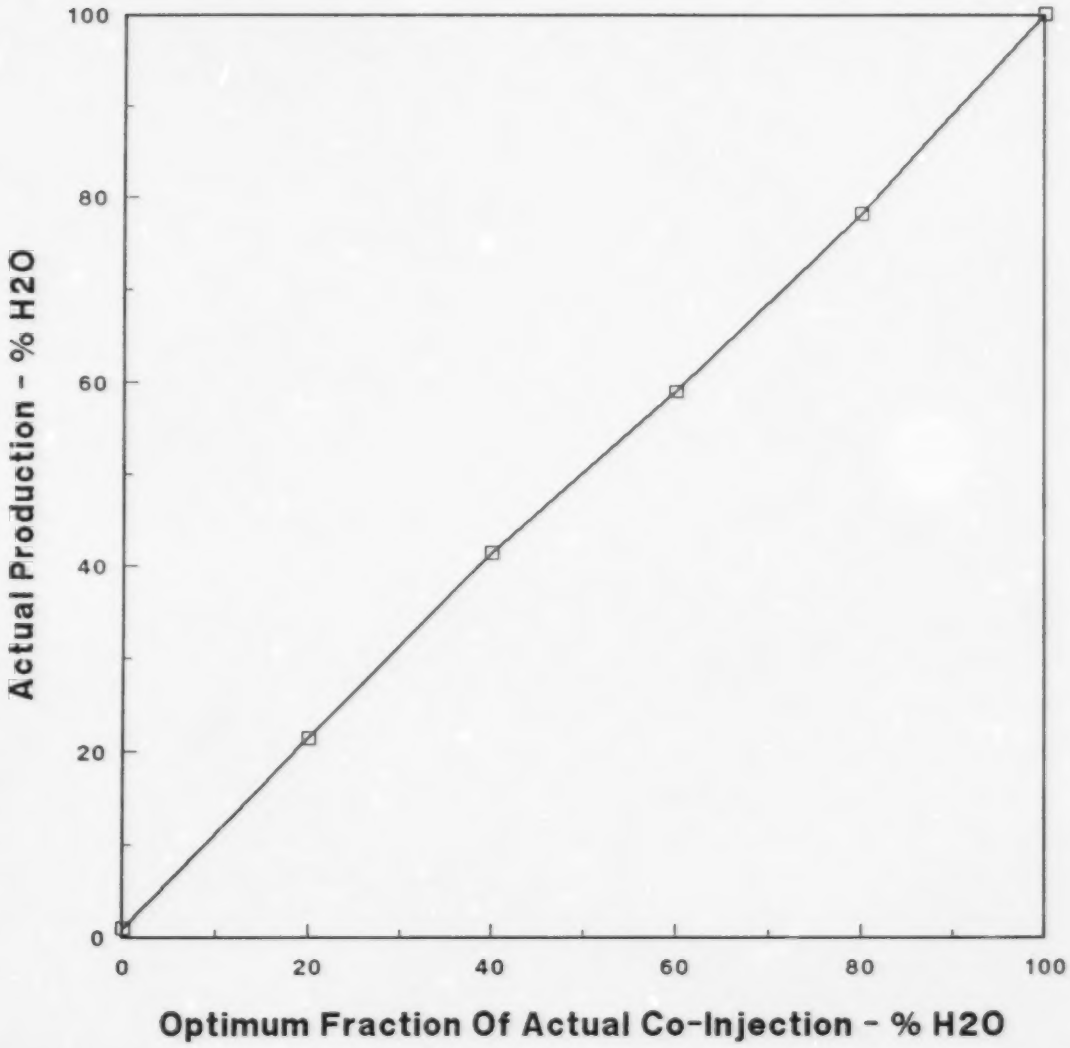

TEST #2 - WATER SATURATION DECREASING

FIGURE 40

PETRO CANADA HANGINGSTONE WELL 1-34-84-11 W4M
HIGH TEMP STEADY-STATE RELATIVE PERM STUDY
% FREE H2O vs OPTIMUM % H2O CO-INJ RATIO

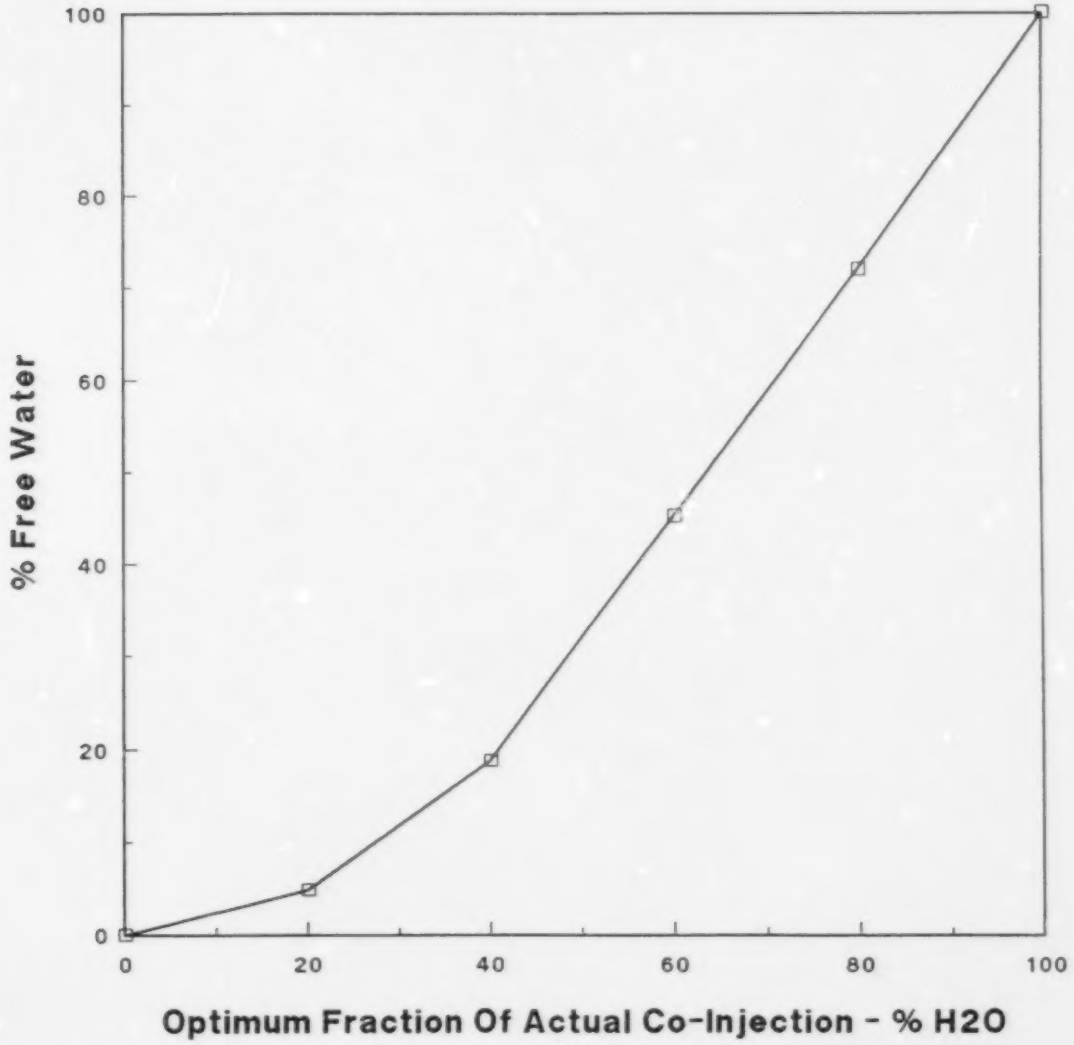

TEST #2 - WATER SATURATION DECREASING

FIGURE 41

PETRO CANADA HANGINGSTONE WELL 1-34-84-11 W4M
HIGH TEMP STEADY-STATE RELATIVE PERM STUDY
% EMULSIFIED OIL vs OPTIMUM % H2O CO-INJ RATIO

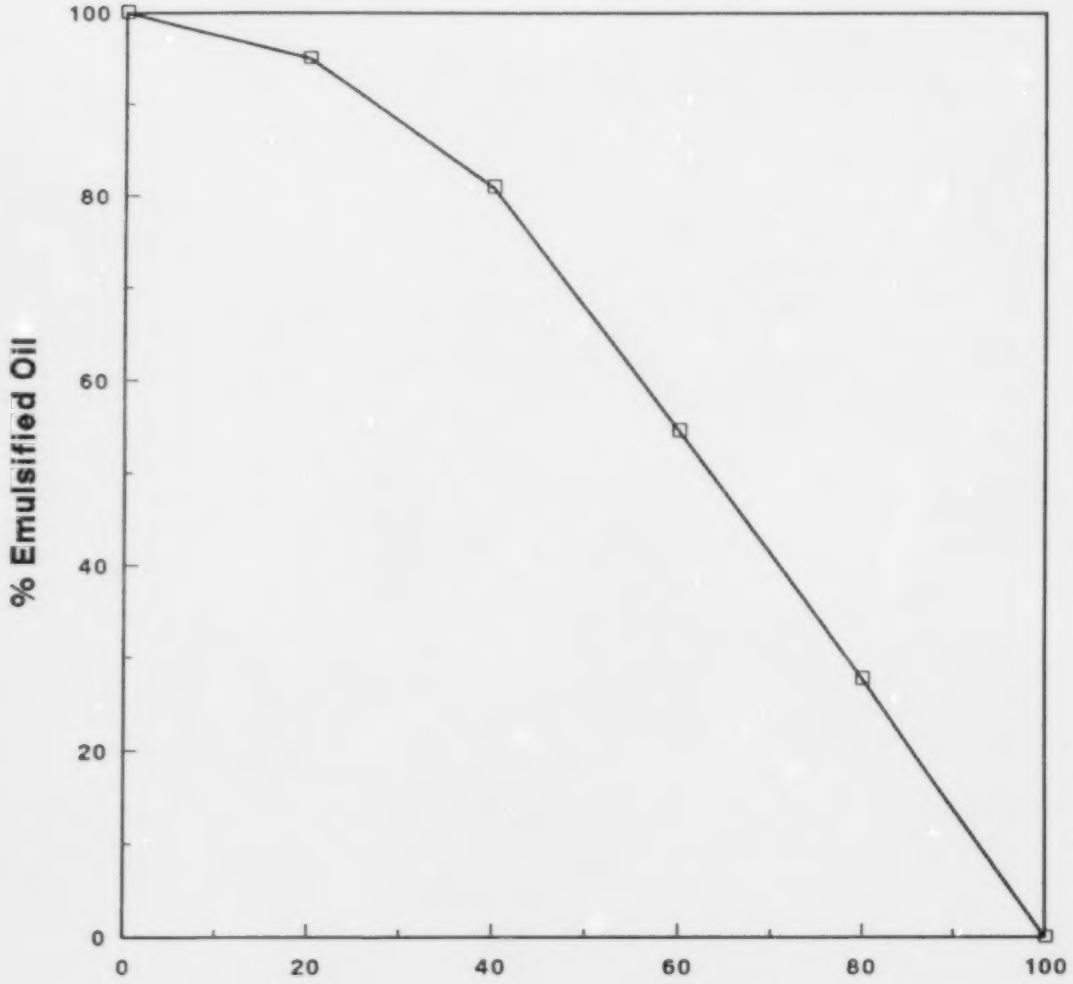

TEST #2 - WATER SATURATION DECREASING

FIGURE 42

PETRO CANADA HANGINGSTONE WELL 1-34-84-11 W4M
HIGH TEMP STEADY-STATE RELATIVE PERM STUDY
% H2O EMULS IN OIL vs OPTIMUM % H2O CO-INJ RATIO

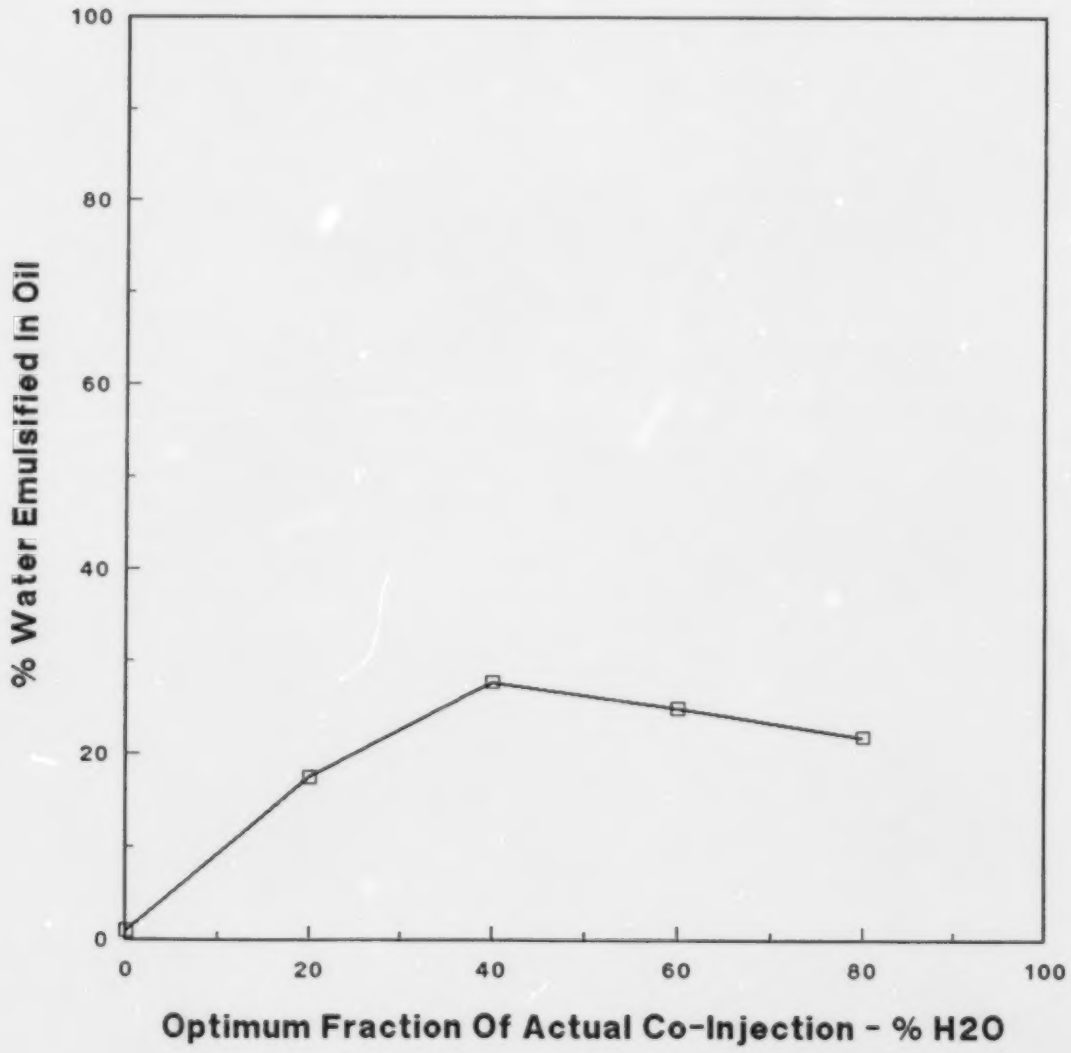

TEST #2 - WATER SATURATION DECREASING

FIGURE 43

PETRO CANADA HANGINGSTONE WELL 1-34-84-11 W4M
HIGH TEMP STEADY-STATE RELATIVE PERM STUDY
ACTUAL % OIL PROD vs OPTIMUM % H2O CO-INJ RATIO

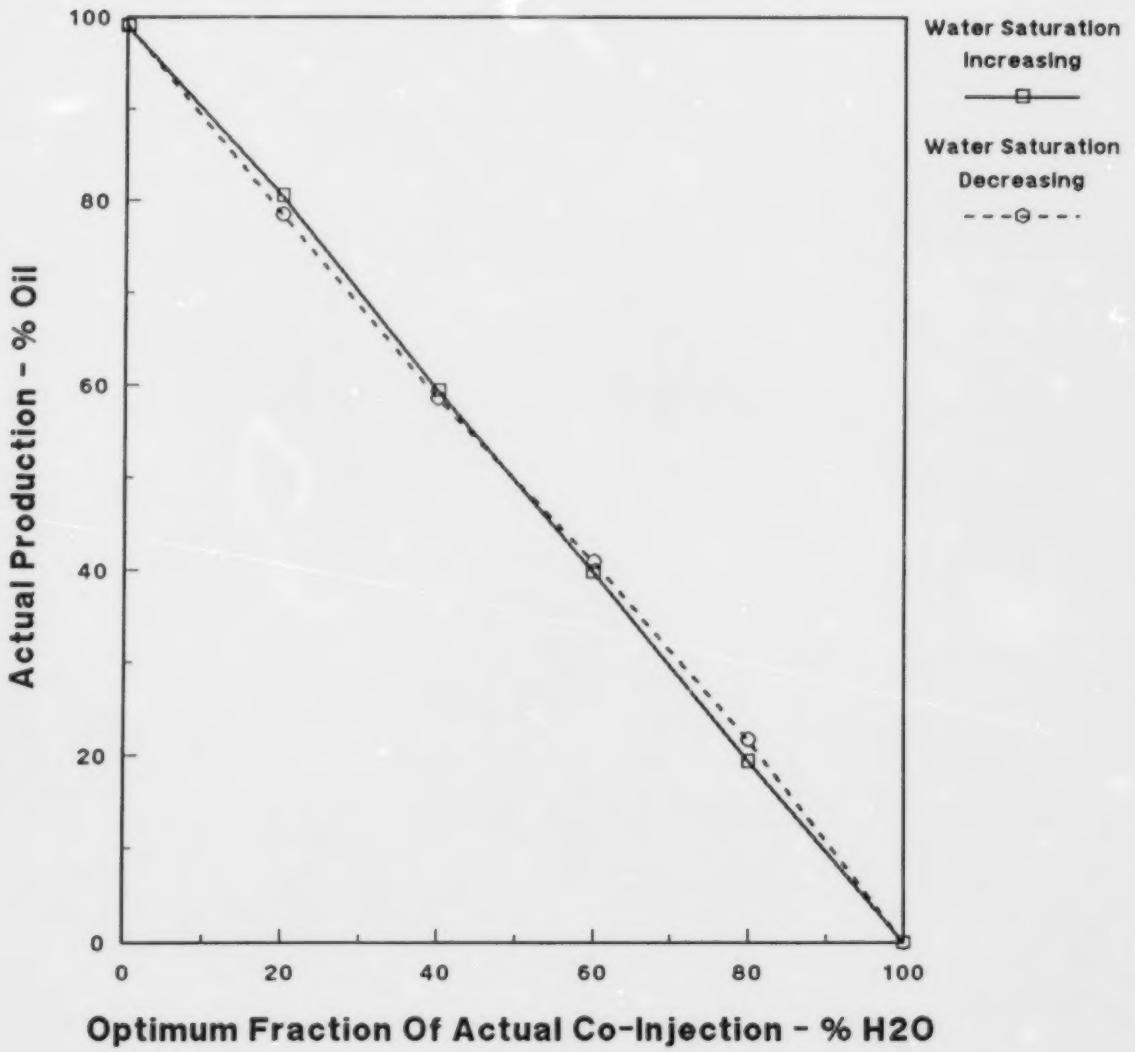

TEST #2

FIGURE 44

PETRO CANADA HANGINGSTONE WELL 1-34-84-11 W4M
HIGH TEMP STEADY-STATE RELATIVE PERM STUDY
ACTUAL % H2O PROD vs OPTIMUM % H2O CO-INJ RATIO

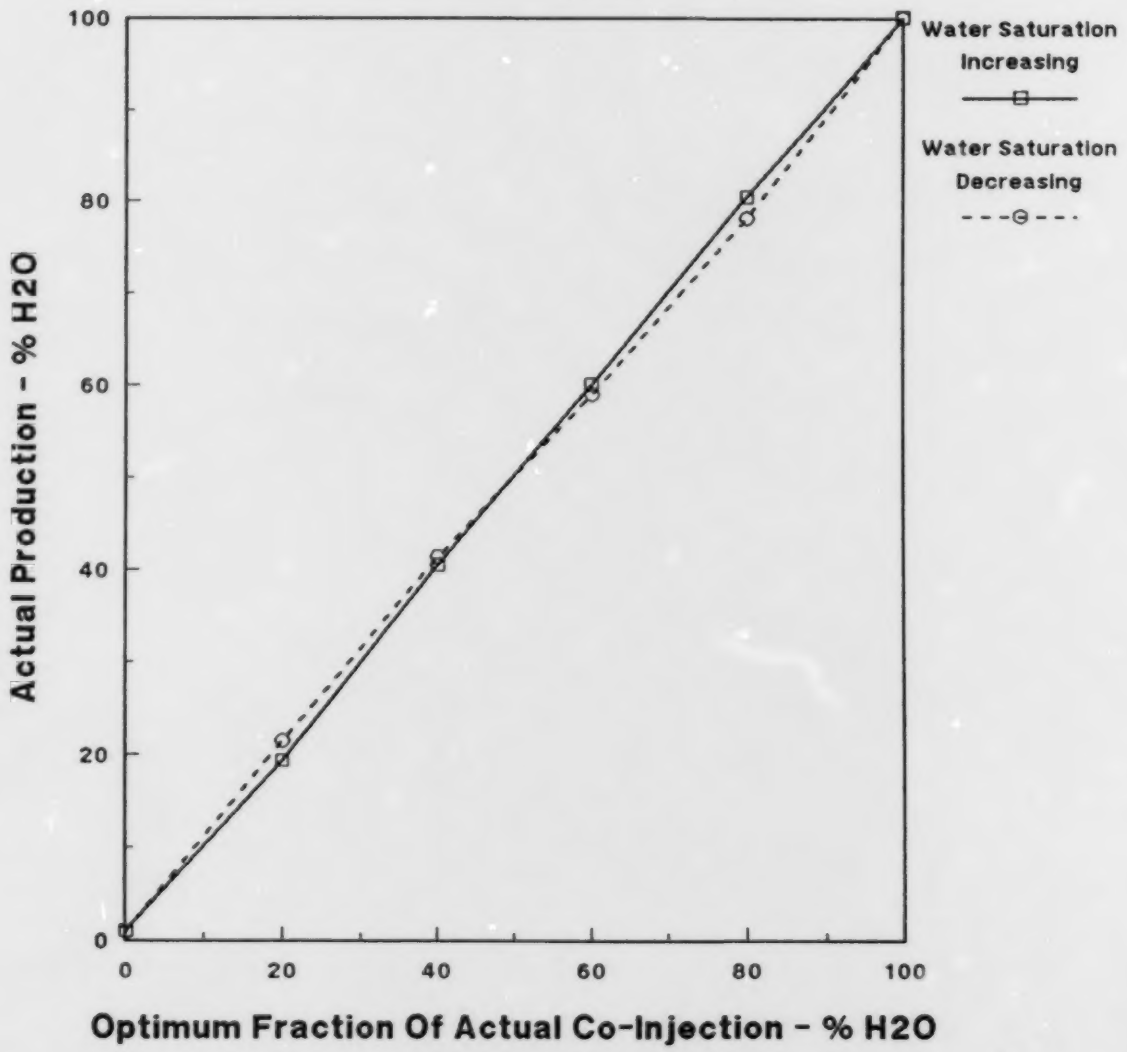

TEST #2

FIGURE 45

PETRO CANADA HANGINGSTONE WELL 1-34-84-11 W4M
HIGH TEMP STEADY-STATE RELATIVE PERM STUDY
% FREE H2O vs OPTIMUM % H2O CO-INJ RATIO

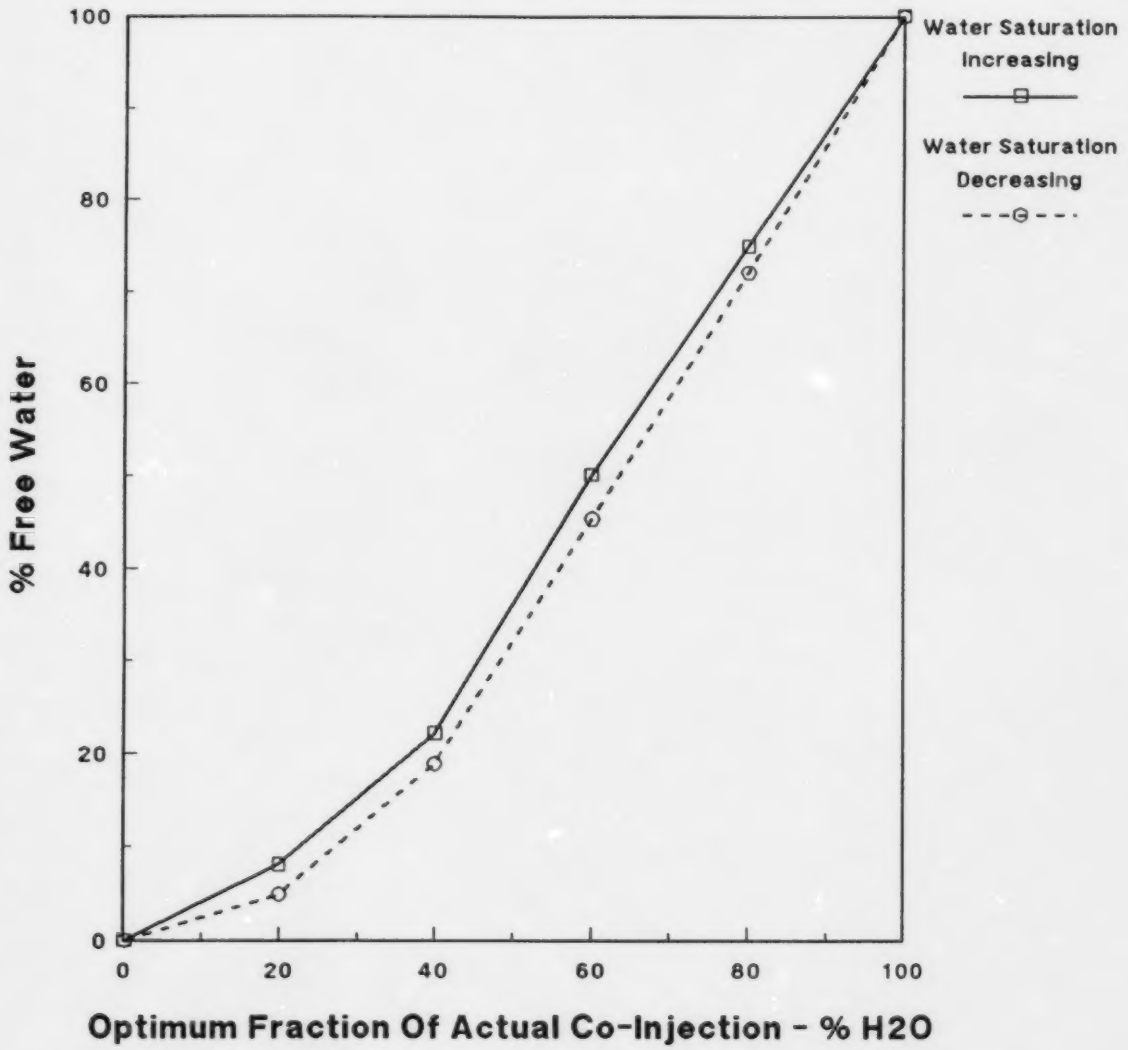

TEST #2

FIGURE 46

PETRO CANADA HANGINGSTONE WELL 1-34-84-11 W4M
HIGH TEMP STEADY-STATE RELATIVE PERM STUDY
% EMULSIFIED OIL vs OPTIMUM % H2O CO-INJ RATIO

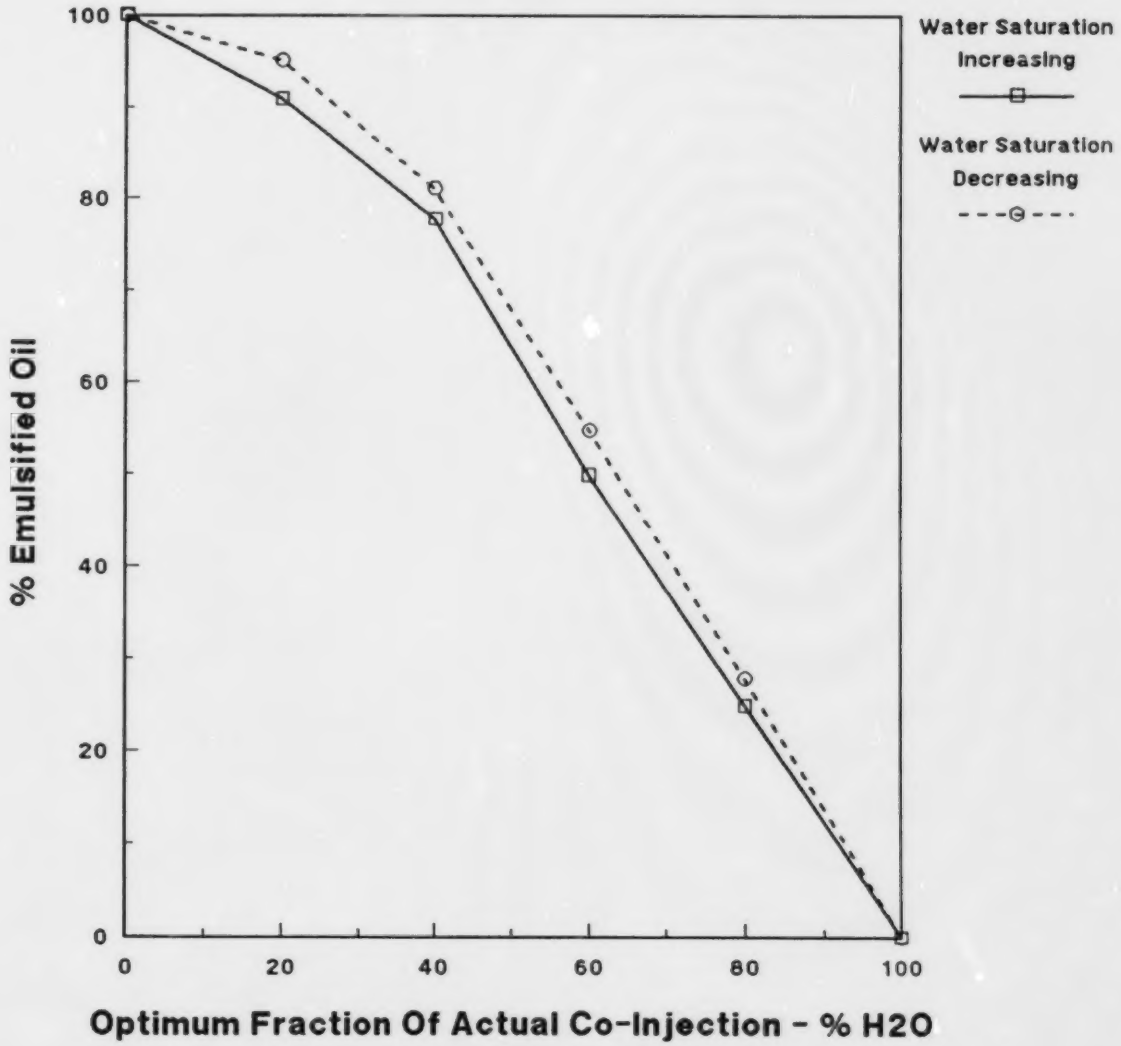

TEST #2

FIGURE 47

PETRO CANADA HANGINGSTONE WELL 1-34-84-11 W4M
HIGH TEMP STEADY-STATE RELATIVE PERM STUDY
% H2O EMULS IN OIL vs OPTIMUM % H2O CO-INJ RATIO

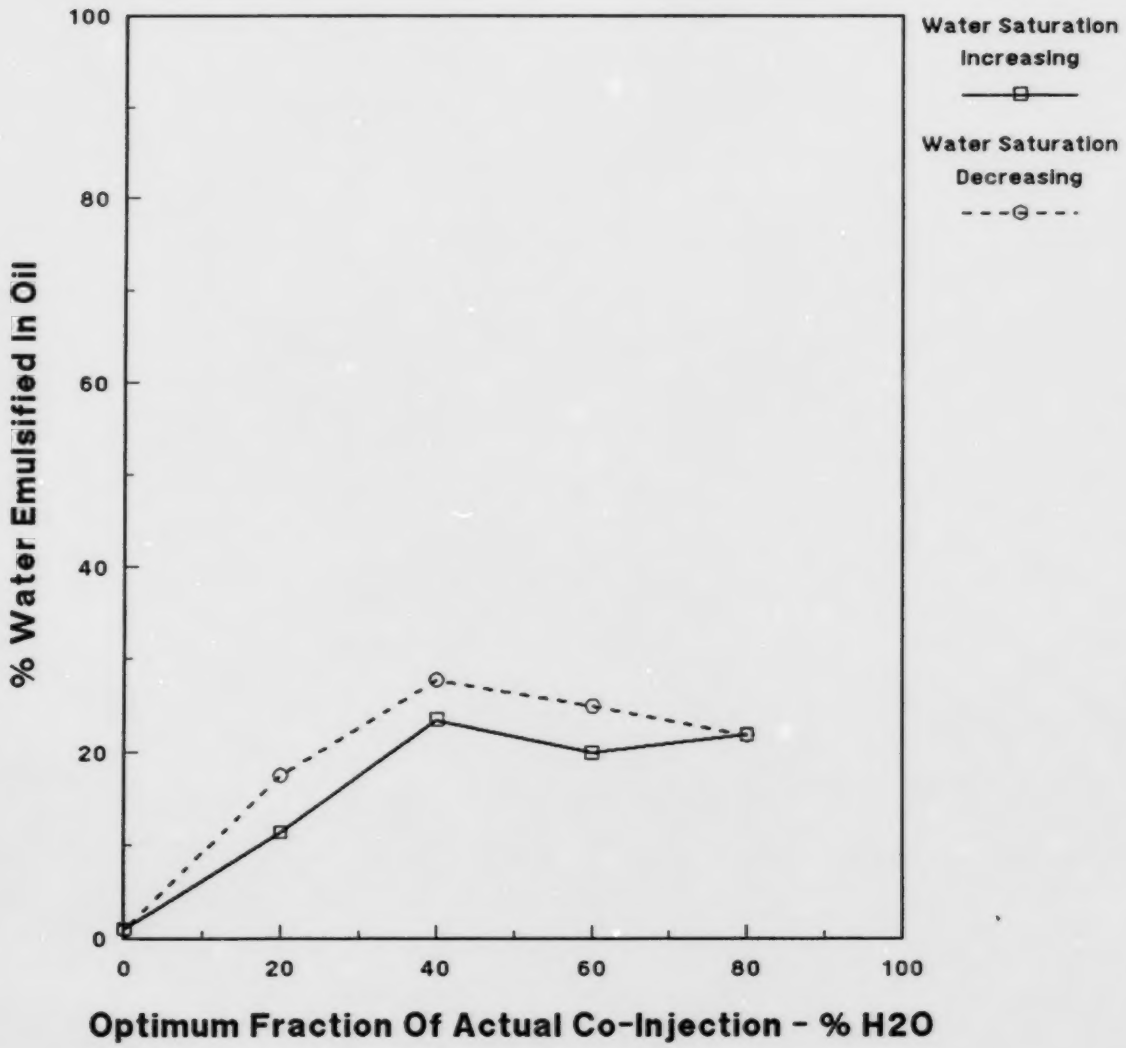

TEST #2

FIGURE 48

PETRO CANADA HANGINGSTONE WELL 1-34-84-11 W4M
HIGH TEMP STEADY-STATE RELATIVE PERM STUDY
PERCENT OF PHASE vs PERCENT INJECTED WATER

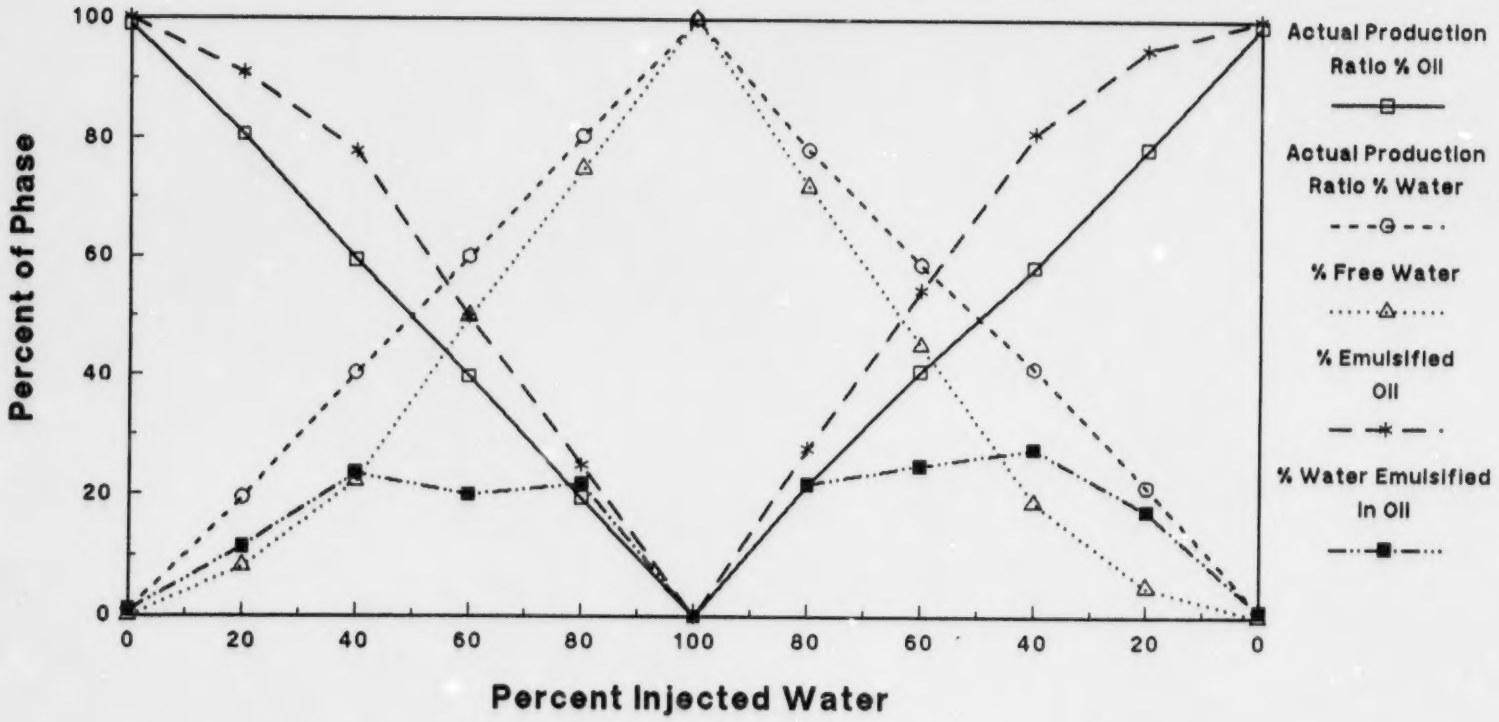

TEST #2

Hycal

FIGURE 49

PETRO CANADA HANGINGSTONE WELL 1-34-84-11 W4M
HIGH TEMP STEADY-STATE RELATIVE PERM STUDY
PERMEABILITY vs WATER SATURATION

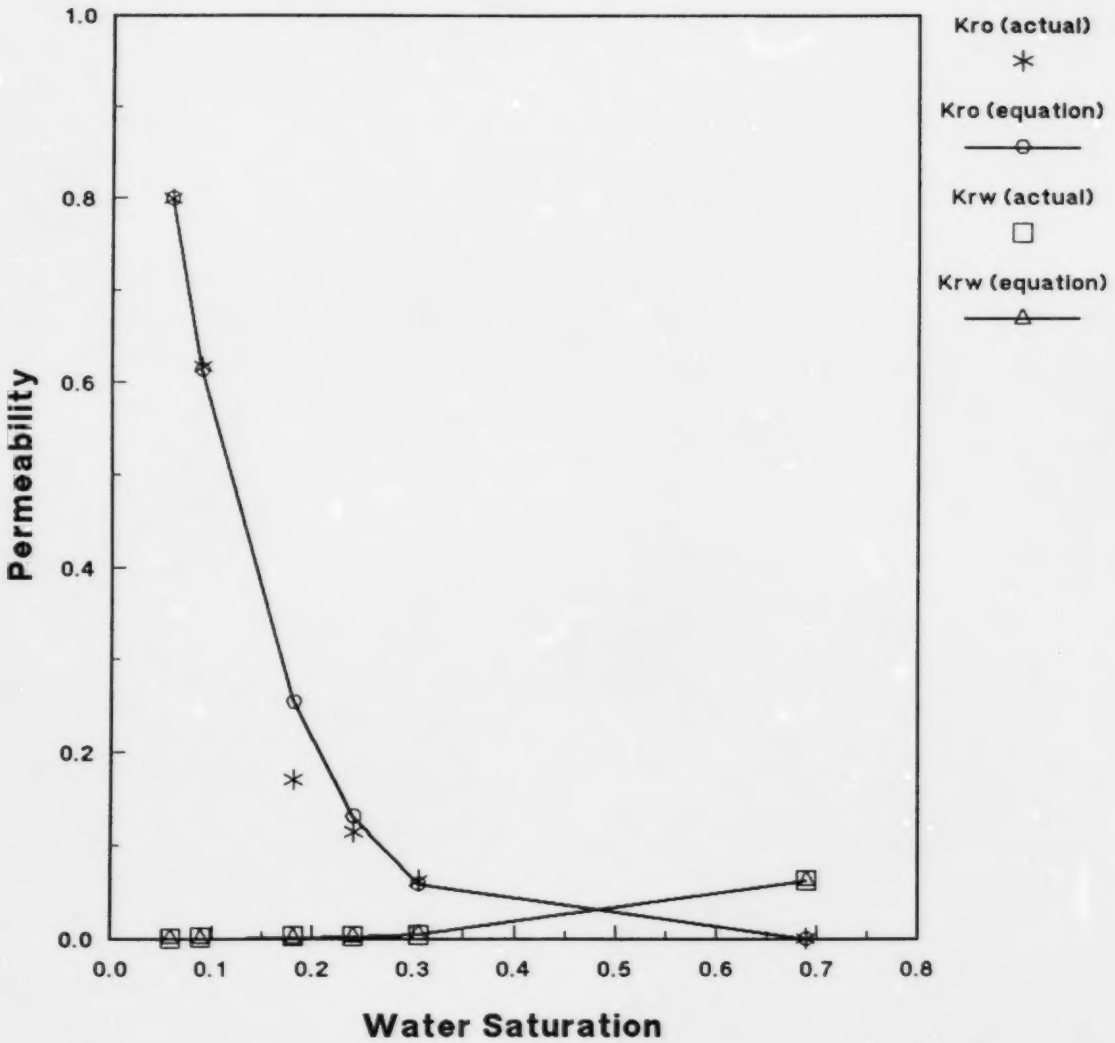

TEST #1 - WATER SATURATION INCREASING

FIGURE 50

PETRO CANADA HANGINGSTONE WELL 1-34-84-11 W4M
HIGH TEMP STEADY-STATE RELATIVE PERM STUDY
PERMEABILITY vs WATER SATURATION

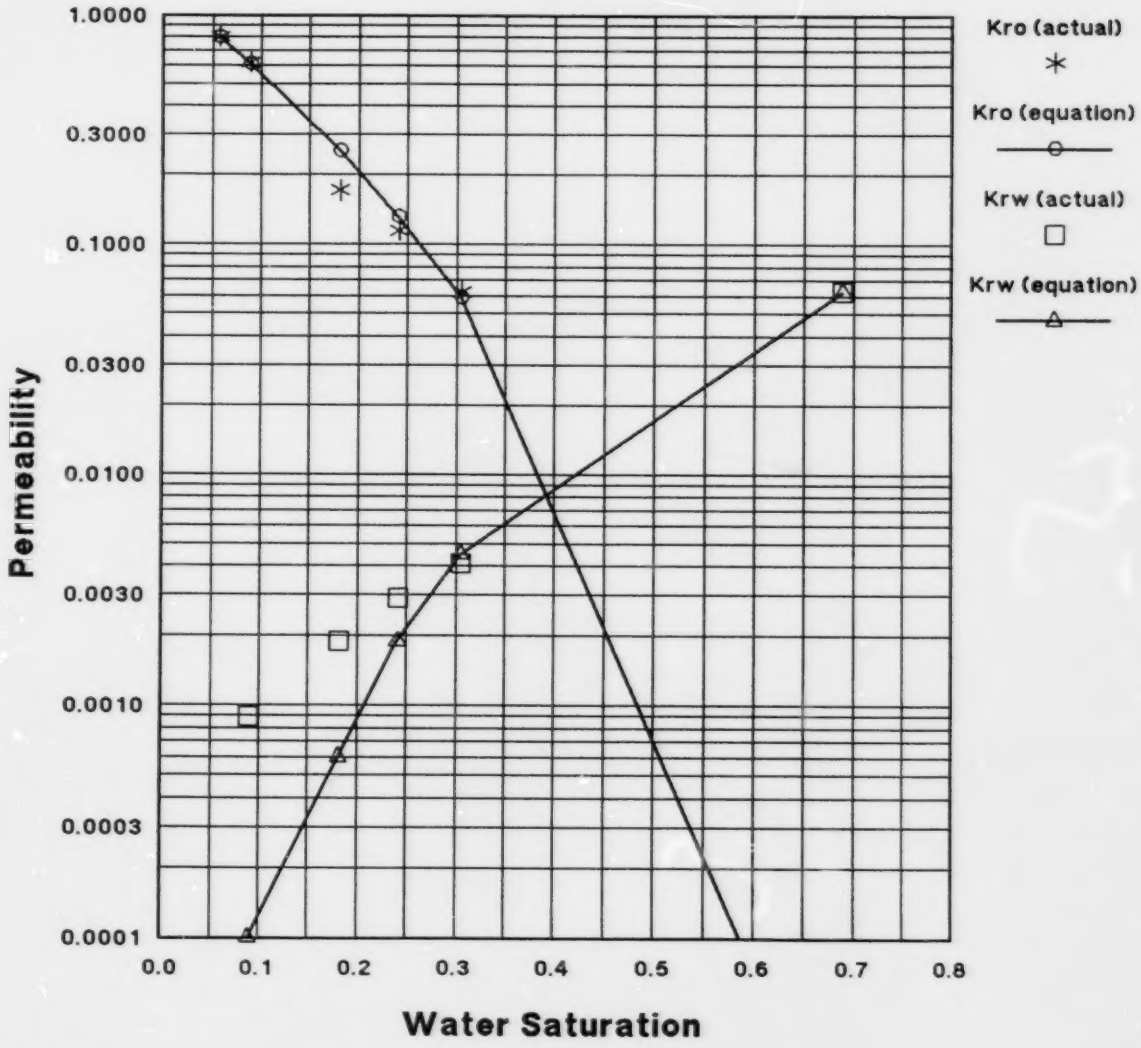

TEST #1 - WATER SATURATION INCREASING

FIGURE 51

PETRO CANADA HANGINGSTONE WELL 1-34-84-11 W4M
HIGH TEMP STEADY-STATE RELATIVE PERM STUDY
PERMEABILITY vs WATER SATURATION

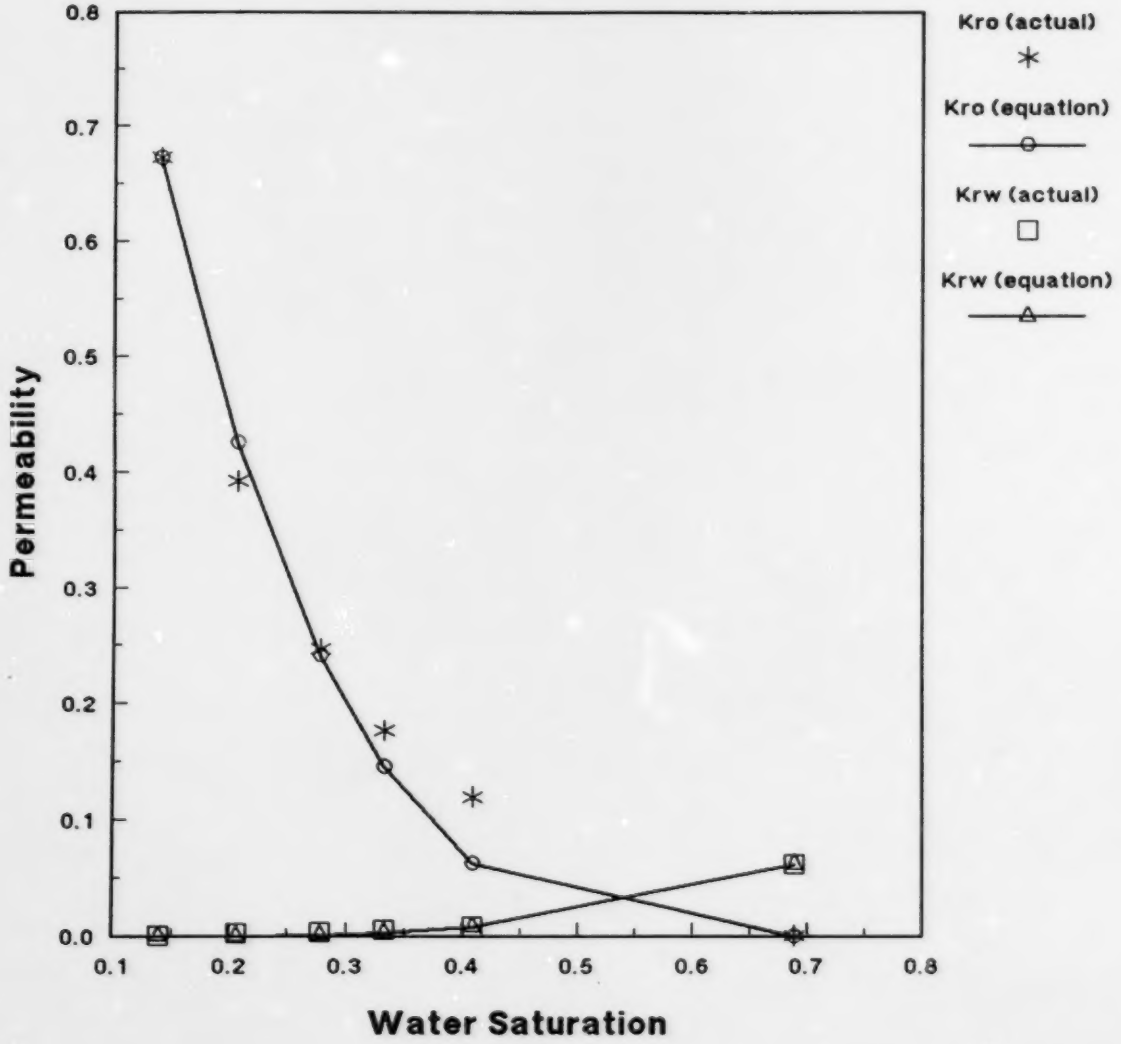

TEST #1 - WATER SATURATION DECREASING

FIGURE 52

PETRO CANADA HANGINGSTONE WELL 1-34-84-11 W4M
HIGH TEMP STEADY-STATE RELATIVE PERM STUDY
PERMEABILITY vs WATER SATURATION

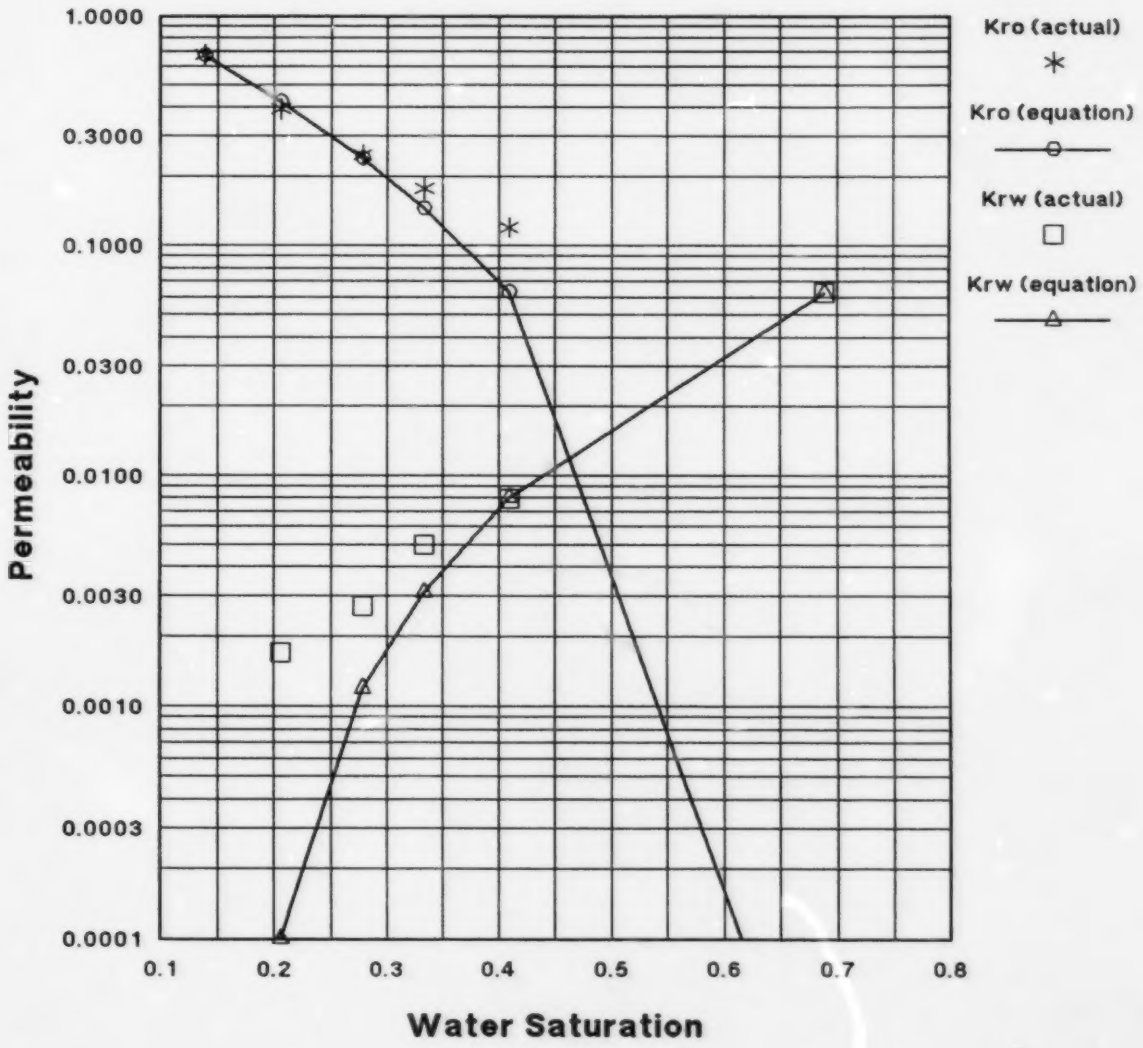

TEST #1 - WATER SATURATION DECREASING

FIGURE 53

PETRO CANADA HANGINGSTONE WELL 1-34-84-11 W4M
HIGH TEMP STEADY-STATE RELATIVE PERM STUDY
PERMEABILITY vs WATER SATURATION

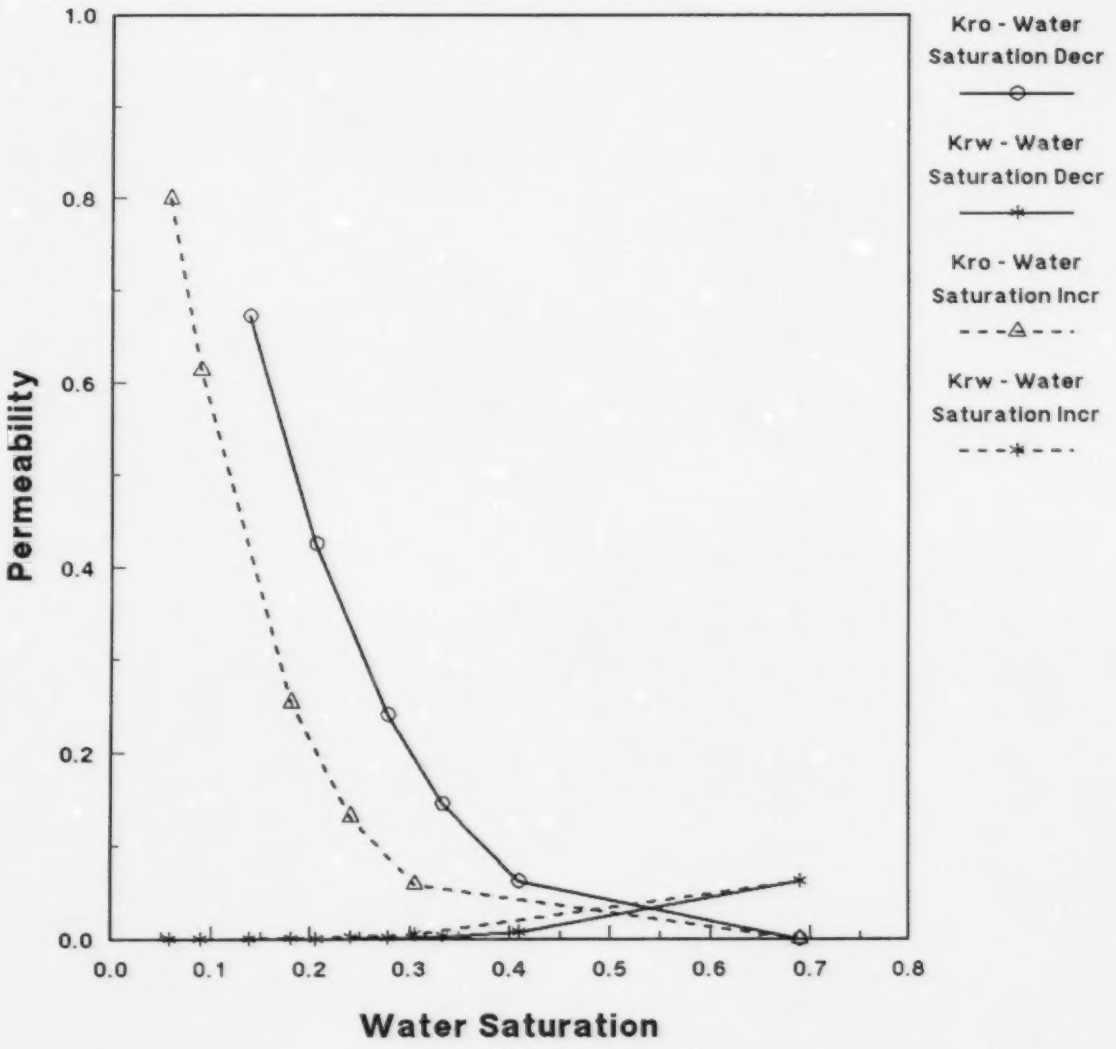

TEST #1

FIGURE 54

PETRO CANADA HANGINGSTONE WELL 1-34-84-11 W4M
HIGH TEMP STEADY-STATE RELATIVE PERM STUDY
PERMEABILITY vs WATER SATURATION

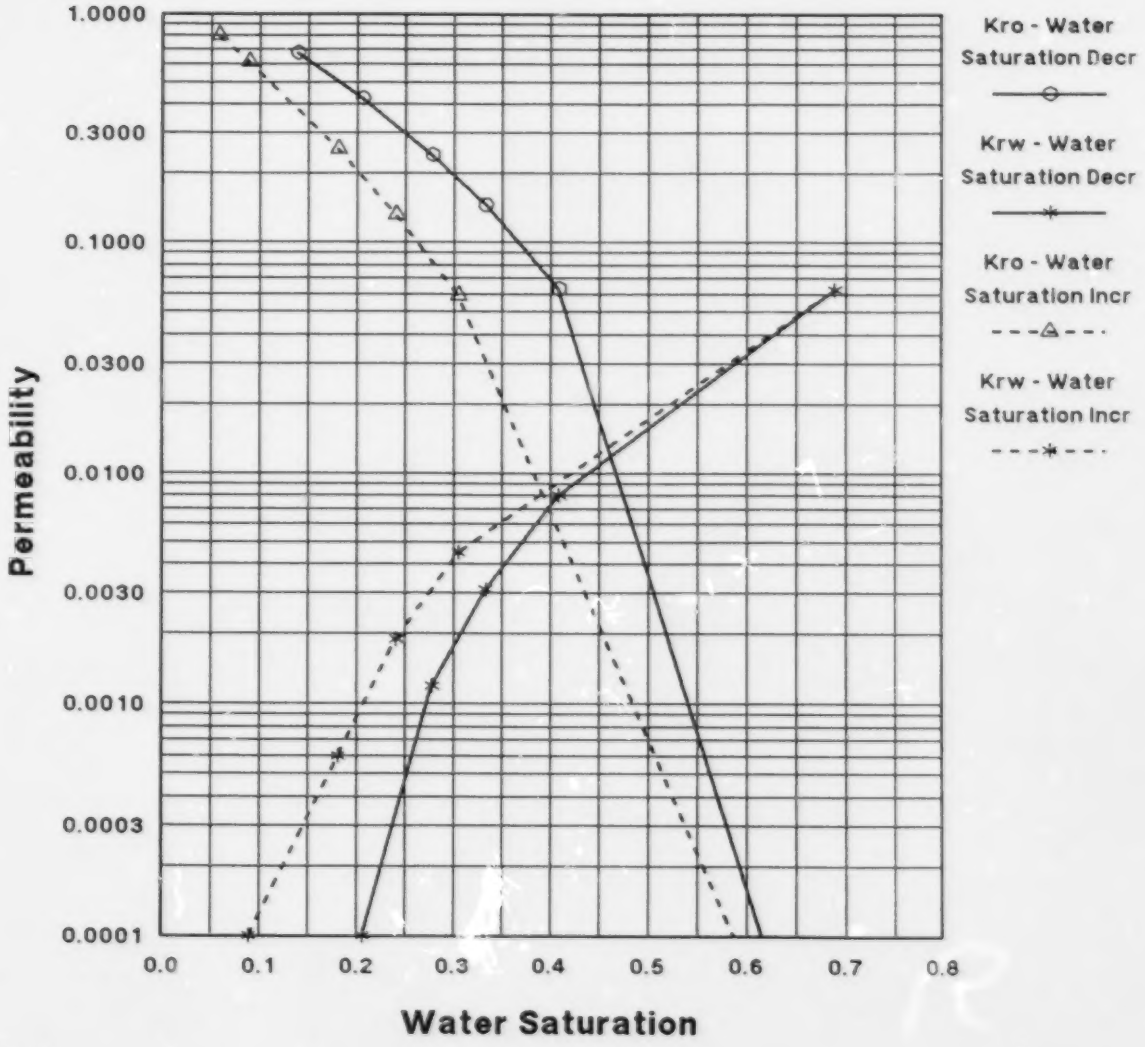

TEST # 1

FIGURE 55

PETRO CANADA HANGINGSTONE WELL 1-34-84-11 W4M
HIGH TEMP STEADY-STATE RELATIVE PERM STUDY
PERMEABILITY vs WATER SATURATION

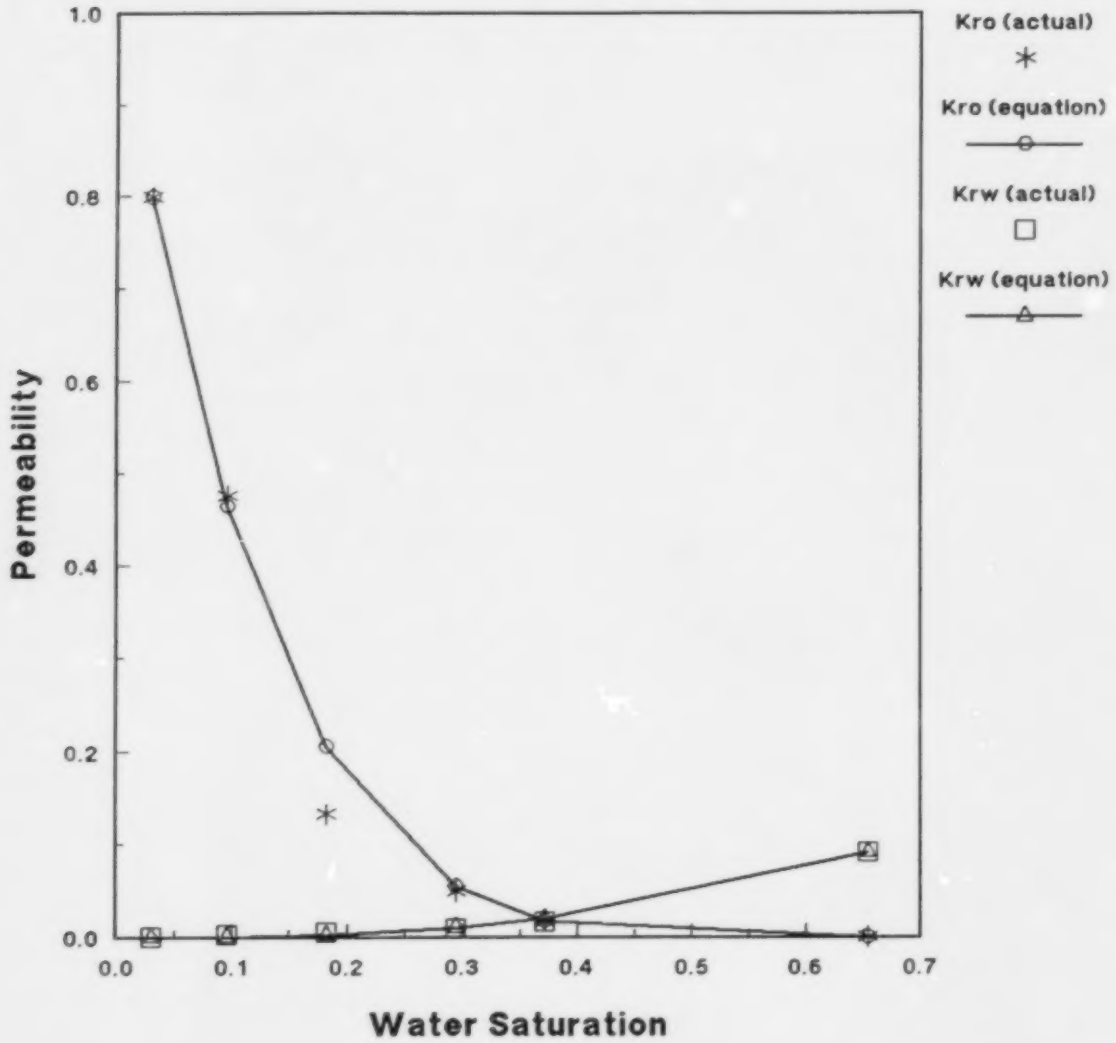

TEST #2 - WATER SATURATION INCREASING

FIGURE 56

PETRO CANADA HANGINGSTONE WELL 1-34-84-11 W4M
HIGH TEMP STEADY-STATE RELATIVE PERM STUDY
PERMEABILITY vs WATER SATURATION

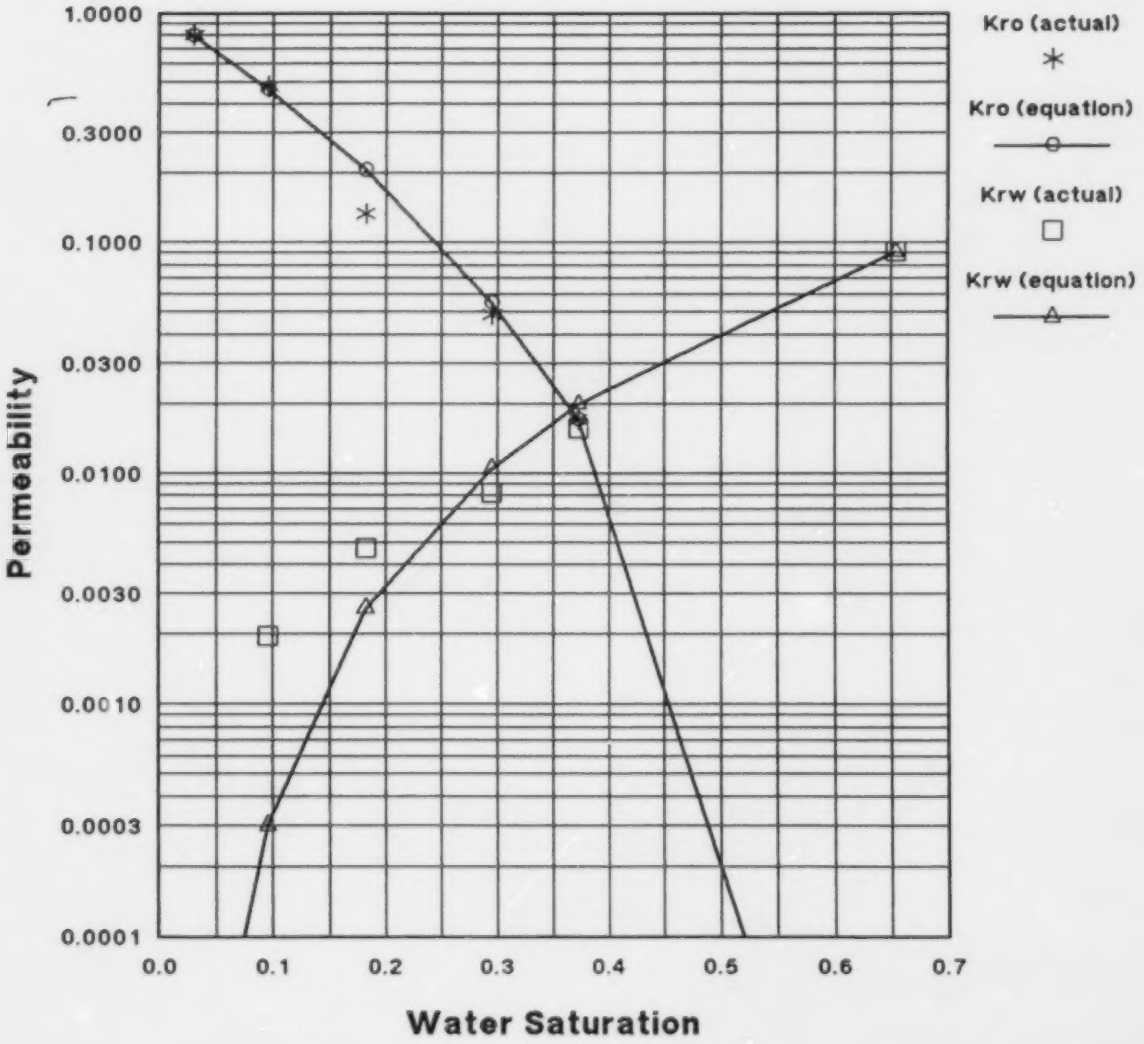

TEST #2 - WATER SATURATION INCREASING

FIGURE 57

PETRO CANADA HANGINGSTONE WELL 1-34-84-11 W4M
HIGH TEMP STEADY-STATE RELATIVE PERM STUDY
PERMEABILITY vs WATER SATURATION

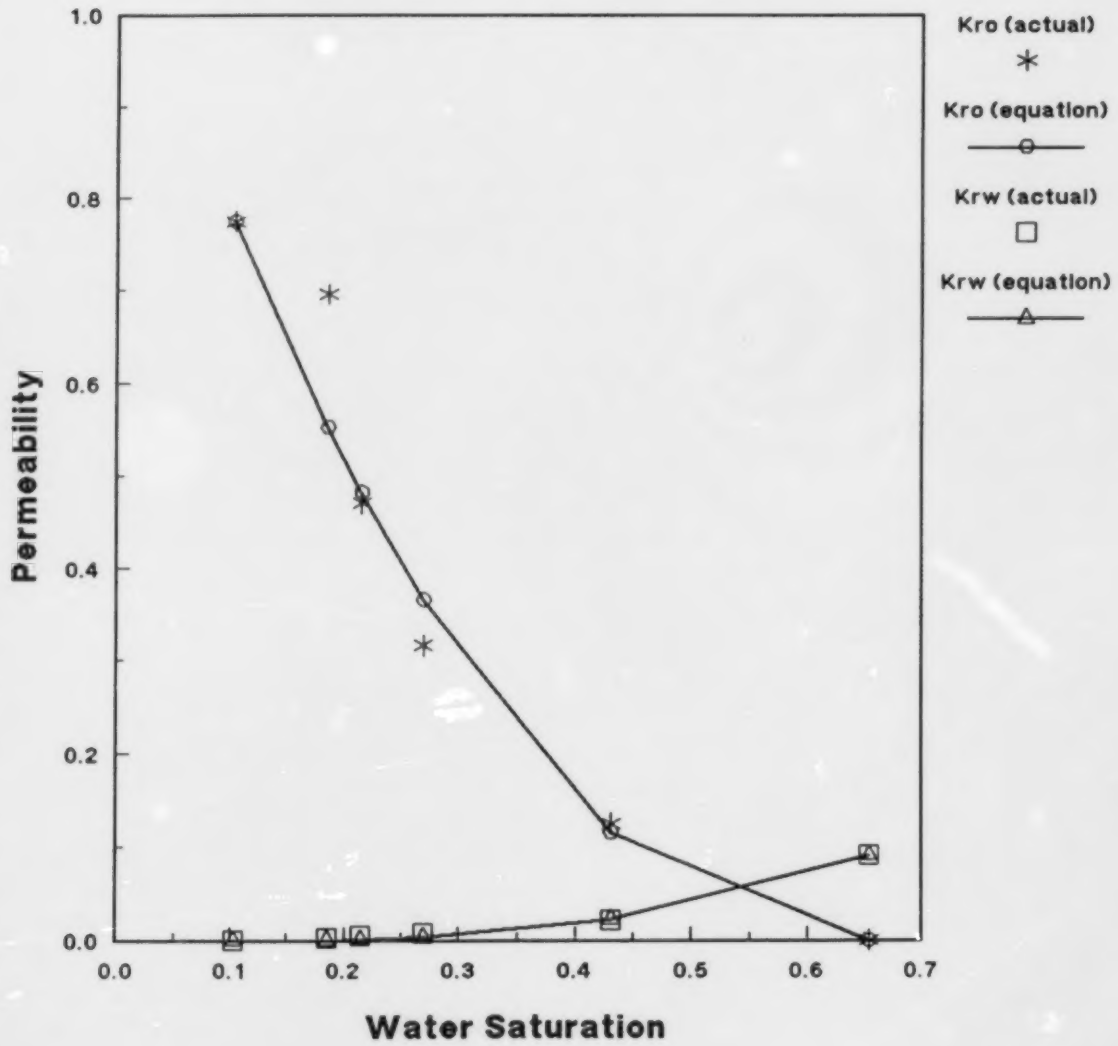

TEST #2 - WATER SATURATION DECREASING

FIGURE 58

PETRO CANADA HANGINGSTONE WELL 1-34-84-11 W4M
HIGH TEMP STEADY-STATE RELATIVE PERM STUDY
PERMEABILITY vs WATER SATURATION

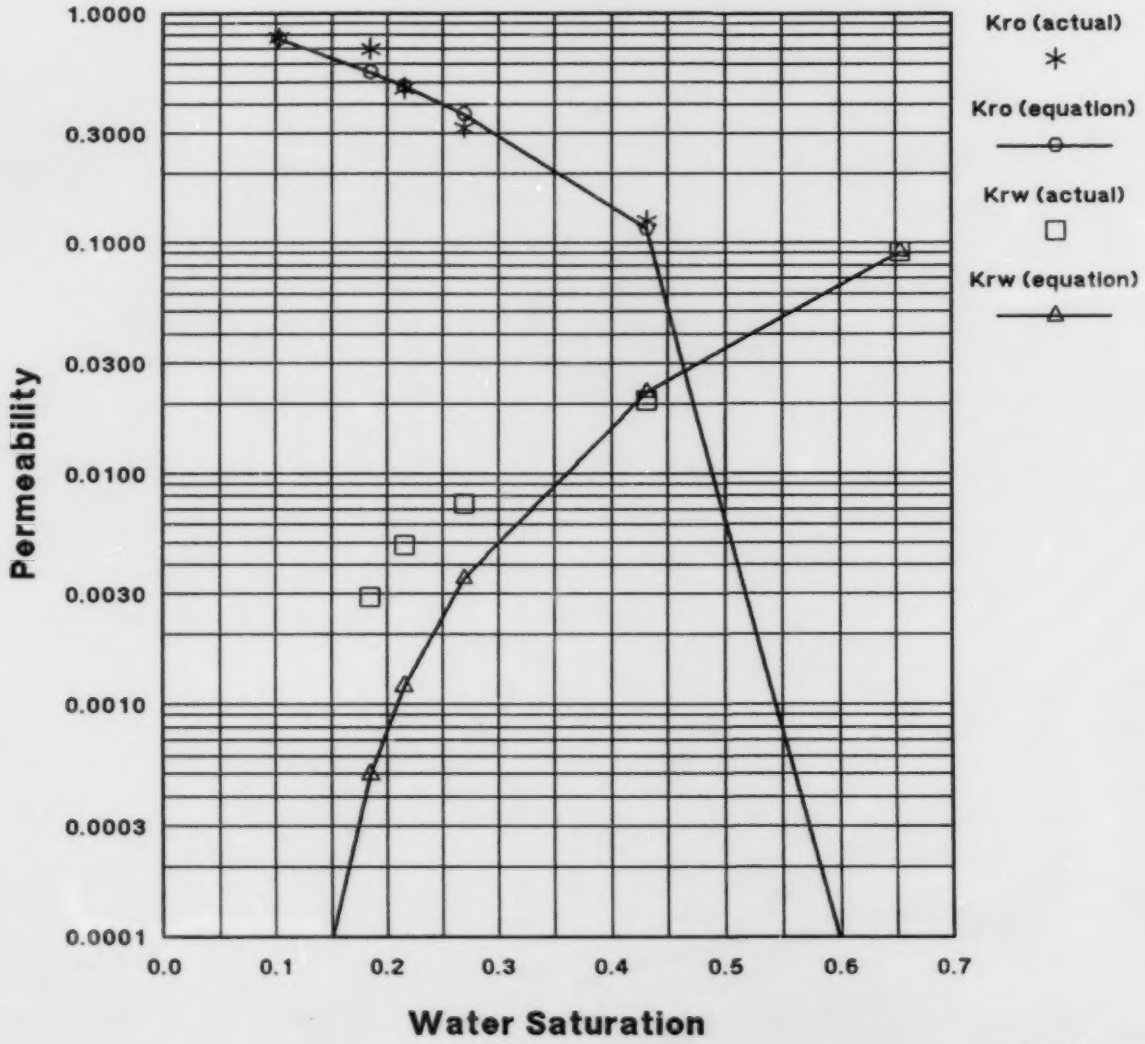

TEST #2 - WATER SATURATION DECREASING

FIGURE 59

PETRO CANADA HANGINGSTONE WELL 1-34-84-11 W4M
HIGH TEMP STEADY-STATE RELATIVE PERM STUDY
PERMEABILITY vs WATER SATURATION

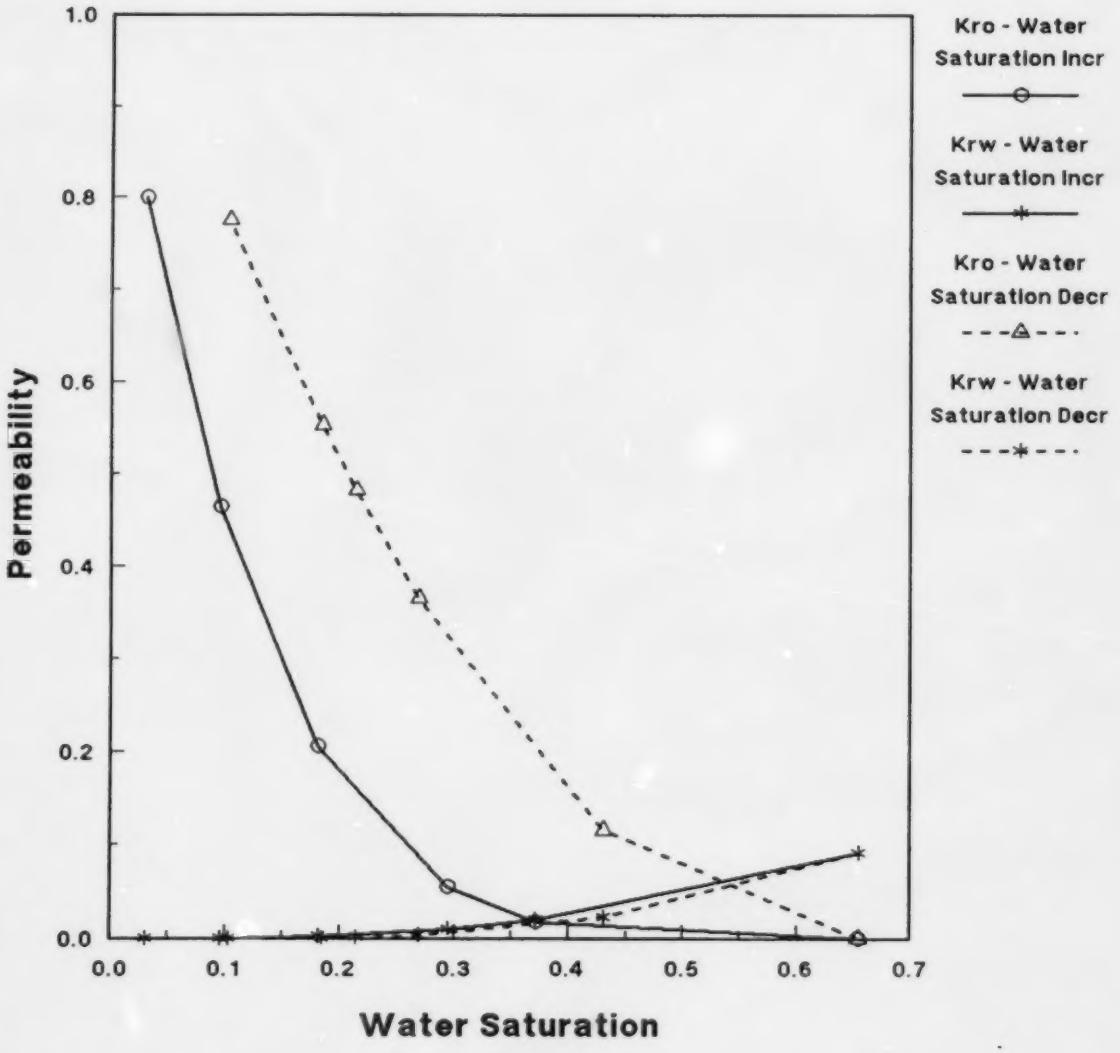

TEST #2

FIGURE 60

PETRO CANADA HANGINGSTONE WELL 1-34-84-11 W4M
HIGH TEMP STEADY-STATE RELATIVE PERM STUDY
PERMEABILITY vs WATER SATURATION

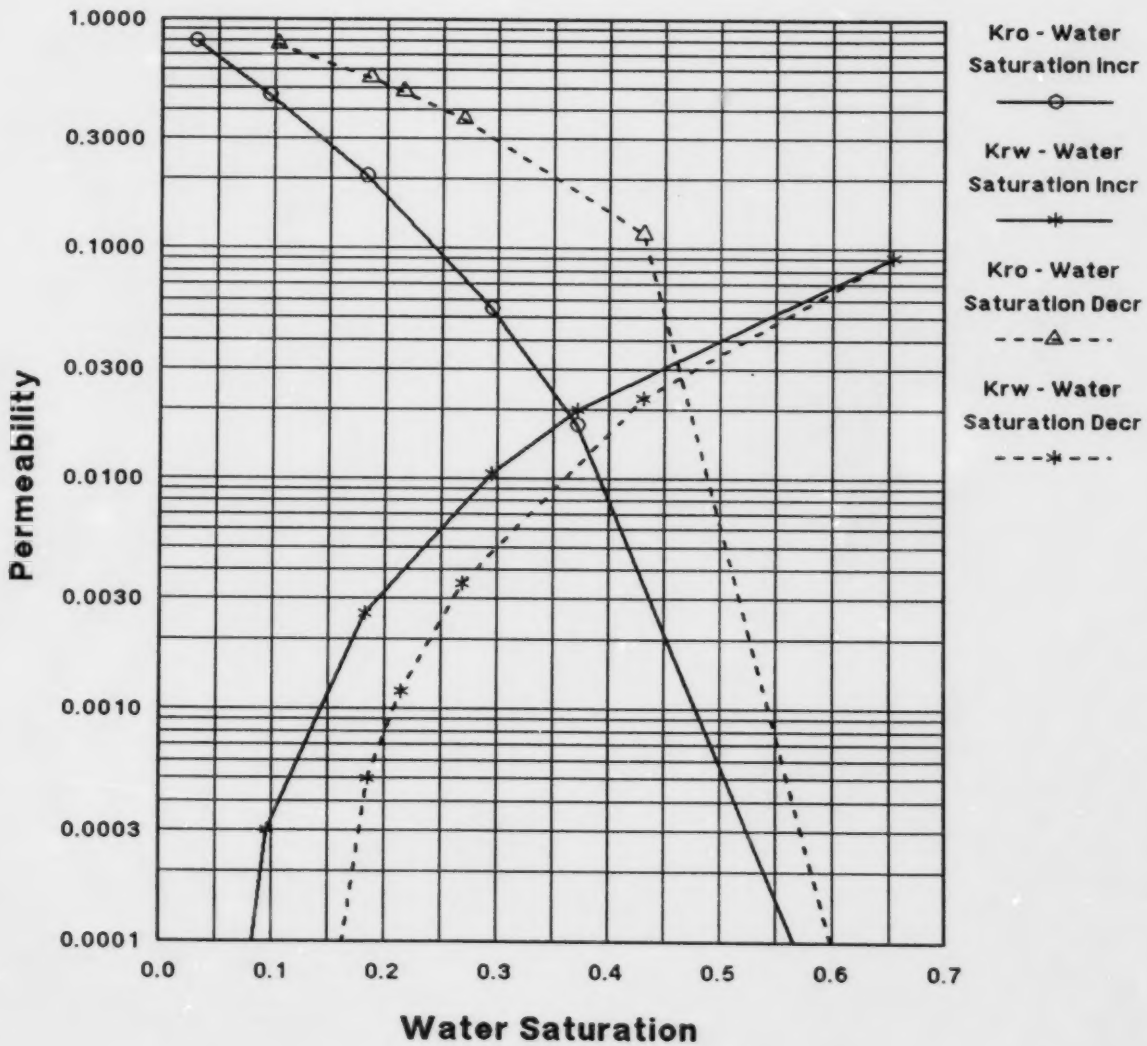

TEST #2

PART B: NUMERICAL SIMULATION

BACKGROUND INFORMATION

Numerical Modelling of the Cyclic Steam Stimulation Process

The PCEJ partners have conducted a series of numerical modelling studies for the CSS process since 1986. The relative permeability curves used were either from the published literature or the unsteady-state laboratory data generated by outside laboratories.

In the current investigation, the THERM simulator was used. Table 16 lists the major model properties, and Table 17 gives the thermal and fluid properties used in this study.

Source of Relative Permeability Data

The unsteady-state laboratory test data was generated by outside laboratories for the PCEJ Hangingstone project in 1988. Gas-oil and oil-water relative permeability curves were generated for temperatures of 100 °C, 200 °C, and 300 °C. The core material tested was from wells located in T84 R11 W4.

The steady-state relative permeability test data was obtained from Hycal Energy Research Laboratories in 1992. The test was conducted at 200 °C. Preserved core samples P5 and P6 were used from well 1-34-84-11 W4, the central well of the PCEJ Hangingstone Phase III pilot. All core material is from the McMurray formation, located at an approximate depth of 300 m in the Athabasca Oilsands deposit. A typical well geology is shown in Figure 61.

Model Configuration

Numerical modelling was conducted using various grid configurations. The number of vertical layers used ranged between one and ten. A typical grid configuration is shown in Figure 62.

Model Calibration

The model used in this investigation was calibrated with field data from the PCEJ Phase III pilot. Thermal models used in the Hangingstone pilot are typically calibrated using CSS pilot test data before it is used to predict or evaluate performance. Figure 63 shows the result of a typical calibration. The scales were normalized where appropriate to protect proprietary information.

RESULTS AND DISCUSSION

Model Performance Comparison

The simulation base case, for the purpose of this study, has the following properties:

1. single well in an infinite reservoir
2. Cyclic Steam Stimulation process
3. steam slug size is constant at 4500 m^3/cycle
4. steam injection rate is constant at 150 m^3/d, cold water equivalent
5. pumping capacity is constant at 25 m^3/d of fluid
6. steam quality is constant at 75 %, at bottom hole conditions
7. the applicable relative permeability curves are those generated by unsteady-state methods.

Figure 64 compares the steady-state and unsteady-state oil-water relative permeability test data. Figure 65 compares the corresponding normalized curves. Figure 66 presents the steady-state normalized curves after smoothing, and the corresponding de-normalized oil-water curves obtained for simulation purposes.

The steady-state oil-water curves were substituted into the base case model. The model performance was evaluated using the same base case operating conditions. Results from the two models were then compared and analyzed.

Analysis of Results

The cumulative steam injection, oil production, and water production from the simulator are plotted in Figure 67. The major results are as follows:

1. The steady-state permeabilities resulted in a slightly lower forecast for the long term oil production than the unsteady-state permeabilities.
2. The steady-state relative permeabilities exhibit slightly longer production cycle life compared to the unsteady-state relative permeabilities.
3. The steady-state relative permeabilities give less water production than the unsteady-state permeabilities.

General Discussion

1. The slightly lower long term oil production predicted by the simulator for the steady-state case is easily explained by the relative permeability curves. At any given water saturation, the steady-state curve exhibits a lower oil relative permeability than the unsteady-state curve. This differs from the report by Maini et al [6], where the steady-state oil permeability curve is above the unsteady-state curve. The reason for the difference between the two experiments has yet to be determined, and is beyond the scope of this project.

2. The steady-state oil relative permeability curve has the same curvature as the unsteady-state curve. Both are convex up. This feature is the opposite of those reported by Maini et al [6] and Polikar et al [7]. In these papers, the steady-state oil curve is convex down, while the unsteady-state oil curve is convex up. The reason for the observed difference is unknown at present.

3. The steady-state oil curve for this project is lower than the steady-state oil curves reported by Maini et al [6] and Polikar et al [7].

4. If the relative permeability curve input data is altered, the simulator output will be affected. The simulator will then require calibration before being used for prediction purposes. It has been proven in the literature that a reasonable history match can be achieved with both the steady-state and unsteady-state relative permeability data. This raises the question of which curves produce more realistic results.

5. The treatment and handling of core material can affect the results of the relative permeability experiment. For example, Bennion et al [8] showed how the relative permeabilities determined from preserved core and extracted core result in different simulated oil production characteristics.

   The effect of core handling on the current results is unknown, however, the results are expected to be reasonably close to the reservoir conditions.

6. One of the secondary objectives of the current project is to explore for evidence of in situ emulsion formation. As evident from the fluid samples collected during the relative permeability test, the chance of emulsion forming in situ and flowing in the reservoir during CSS operations is very high. Seven frozen samples [9] from the pilot were sent to the CANMET laboratory at Devon in 1990. The samples were tested for evidence of in situ emulsification, under frozen conditions, with the use of cryogenic microscopy, SEM, and optical microscopy. The experiment showed sporadic indication of oil-in-water emulsion in the core samples tested. There was not sufficient evidence to either fully support or rule out the occurrence of in situ

emulsification. The current experiment has given much stronger support that in situ emulsification may be an integral part of the CSS process.

The model used in this investigation is not capable of including emulsion flow phenomena, an area worth addressing in future CANMET research.

7. The unsteady-state relative permeability tests were carried out between 100 °C and 300 °C. The results indicate that the end points will shift with a change in temperature. The current comparison runs used the same temperature dependant end points from the unsteady-state tests to generate the simulator forecasts for the steady-state relative permeability case. If this assumption is not valid, the two simulator forecasts may be closer than they should be.

8. In this project, the upper bound of the water-oil hysterisis envelope, the drainage curve, is convex up. The lower bound, or imbibition curve, is also convex up. Conversely, the hysterisis envelope reported by Boberg et al [11] for Cold Lake, has an upper bound that is convex down and a lower bound that is convex up.

CONCLUSIONS

1. The steady-state permeability curves resulted in slightly lower oil and water production, and slightly longer production cycles than the unsteady-state permeability curves.

2. The shape of the relative permeability curve does not affect simulation results as much as the curve endpoints do.

3. The shape of the water-oil hysterisis envelope differs from data found in the published leterature.

4. The effect of emulsion flow and core preservation techniques on relative permeabilities cannot be accounted for in an inadequate reservoir model. These effects are beyond the sccpe of this study and cannot be evaluated at present.

TABLE 16 : THERM MODEL PROPERTIES

PARAMETER	VALUE
Porosity, %	31.6
Rock Compressibility, 1/MPa	1.42×10^{-2}
kx, md	2753.6
ky, md	2753.6
kz, md	1209.2
Heat Capacity, kJ/m^3°C	2055
Heat Conductivity, kJ/dm°C	220
Overburden Heat Conductivity, kJ/dm°C	281.2
Underburden Heat Conductivity, kJ/dm°C	324.4
Overburden Heat Capacity, kJ/m^3°C	2528.0
Underburden Heat Capacity, kJ/m^3°C	2427.0
Initial Pressure, kPa	2009.7
Temperature, °C	10.6
Oil Saturation, %	94.6
Gas Saturation, %	0
Water Saturation, %	5.4
Sorw, %	23.0
Krwro	0.0951
Krocw	1.0000
Krgro	0.1125
Sorg, %	41.0

TABLE 17 : THERMAL MODEL DATA SUMMARY

3 Phase System	Water, Oil and Solution Gas	
Molecular Weight of Oil	544	kg/mole
Molecular Weight of Solution Gas	16.7	kg/mole
Critical Pressure for Solution Gas	4570.8	kPa
Critical Temperature for Solution Gas	193.7	°K
Oil Compressibility	1.1×10^{-3}	MPa^{-1}
Gas Compressibility	4.35×10^{-3}	MPa^{-1}
Thermal Expansion Coefficient	5.8×10^{-4}	$°C^{-1}$
First Coefficient, Ideal Gas, Specific Heat (Oil)	7.52×10^{-1}	kJ/kg°k
Second Coefficient, Ideal Gas, Specific Heat (Oil)	3.36×10^{-3}	kJ/kg°k
First Coefficient, Ideal Gas, Specific Heat (Gas)	1.16	kJ/kg°k
Second Coefficient, Ideal Gas, Specific Heat (Gas)	3.489×10^{-3}	kJ/kg°k
Density, Water	1009.1302	kg/m3
Density, Oil	1017.0000	kg/m3
Partial Volume of Oil	9.83×10^{-4}	m3/kg
Partial Volume of Gas	7.96×10^{-3}	m3/kg
Viscosity Coefficient, A, Oil	4.62156×10^{9}	
Viscosity Coefficient, B, Oil	-3.4640	
Viscosity Coefficient, A, Gas	8.0919×10^{-5}	
Viscosity Coefficient, B, Gas	0.8746	
Rock Compressibility	1.42×10^{-2}	MPa^{-1}
Depth to Top of Layer 1	267	m
Fracture Compressibility	1.42×10^{-2}	MPa^{-1}
Overburden Thermal Conductivity	281.2	kJ/day m°C
Underburden Thermal Conductivity	324.4	kJ/day m°C
Overburden Heat Capacity	2528.0	kJ/m3°C
Underburden Heat Capacity	2427.0	kJ/m3°C
Reservoir Temperature	10.6	°C

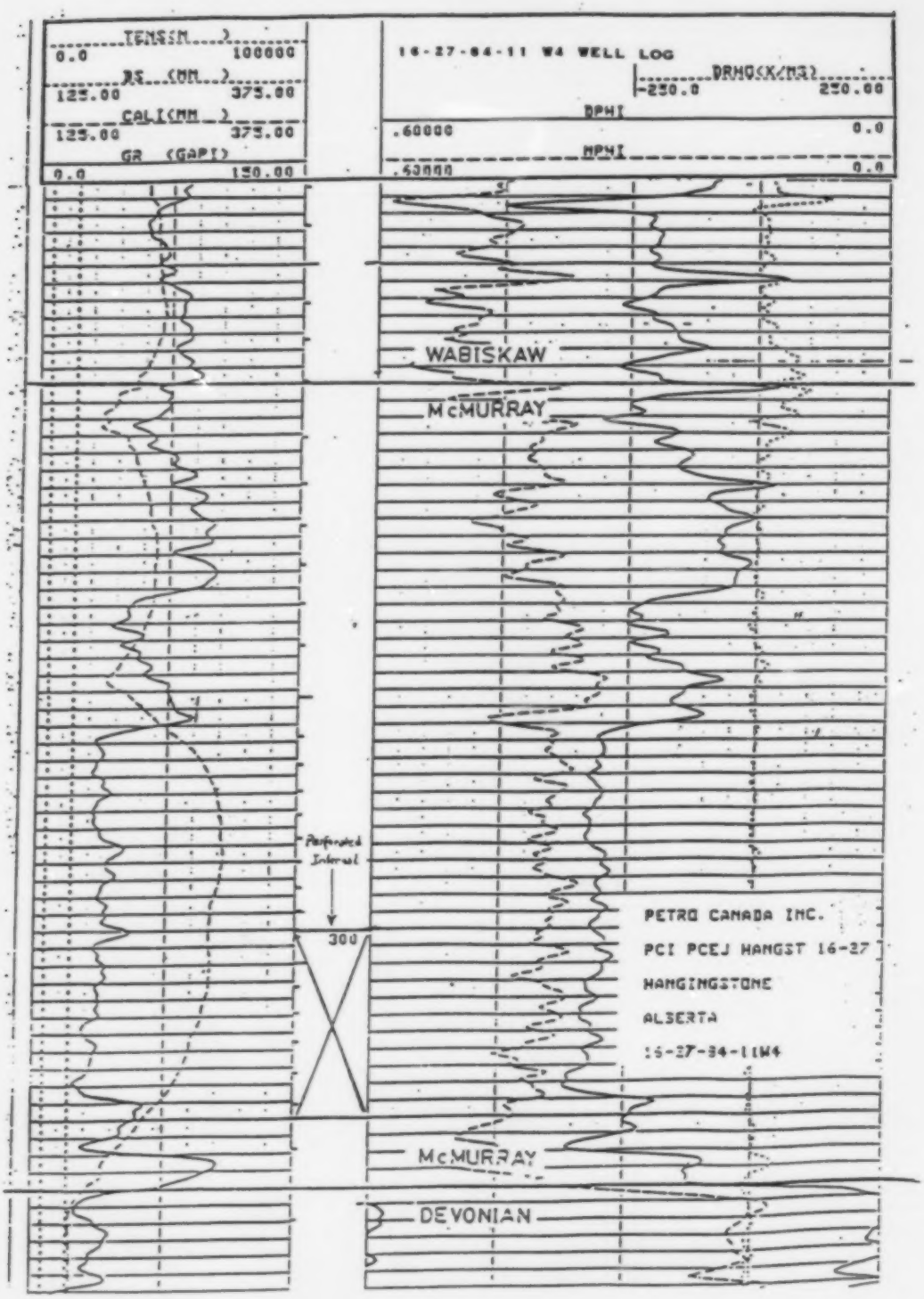

FIGURE 61 : TYPICAL PILOT WELL GEOLOGY

FIGURE 62 : TYPICAL MODEL GRID CONFIGURATION

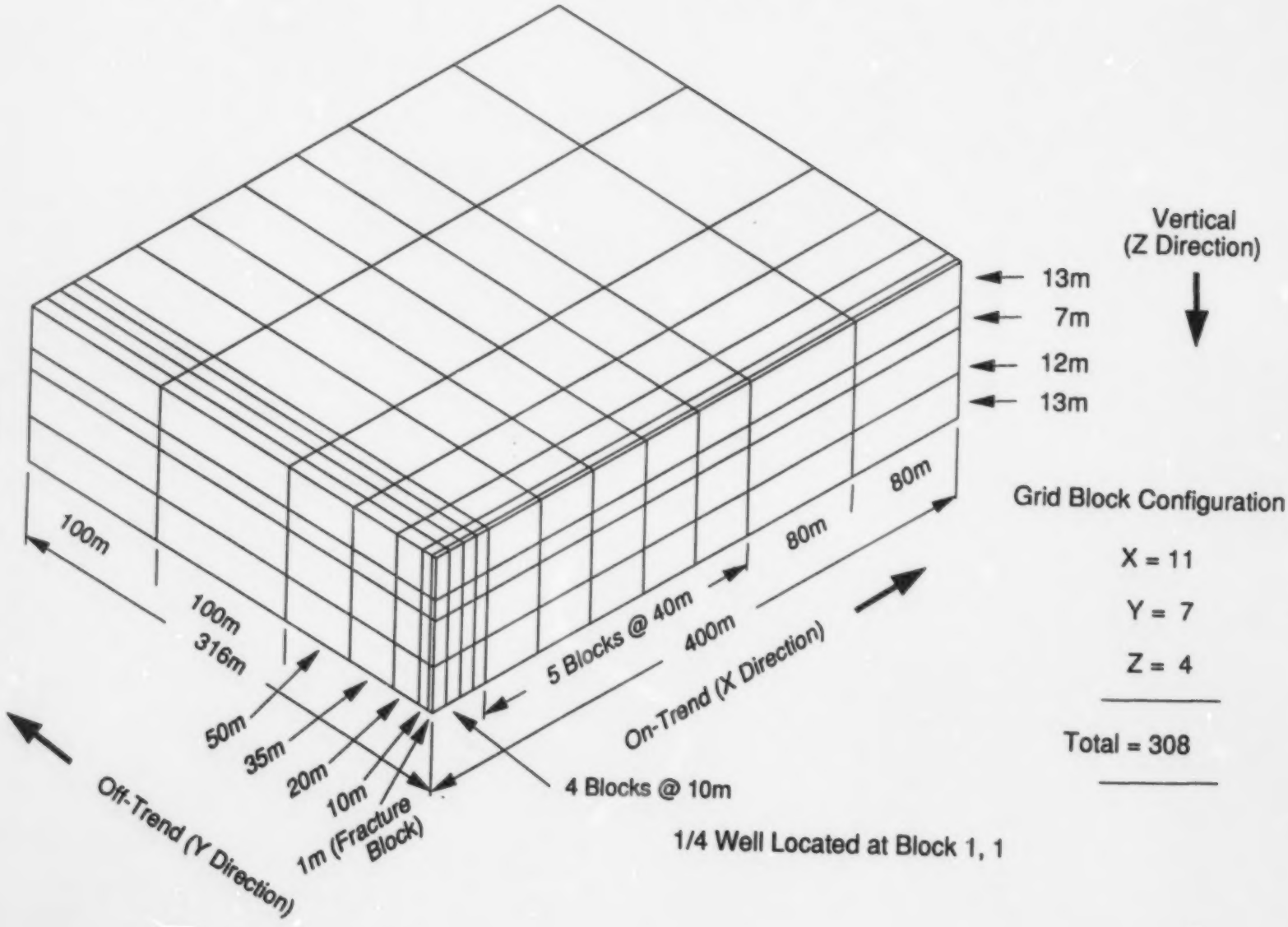

FIGURE 63 : TYPICAL MODEL CALIBRATION WITH FIELD DATA

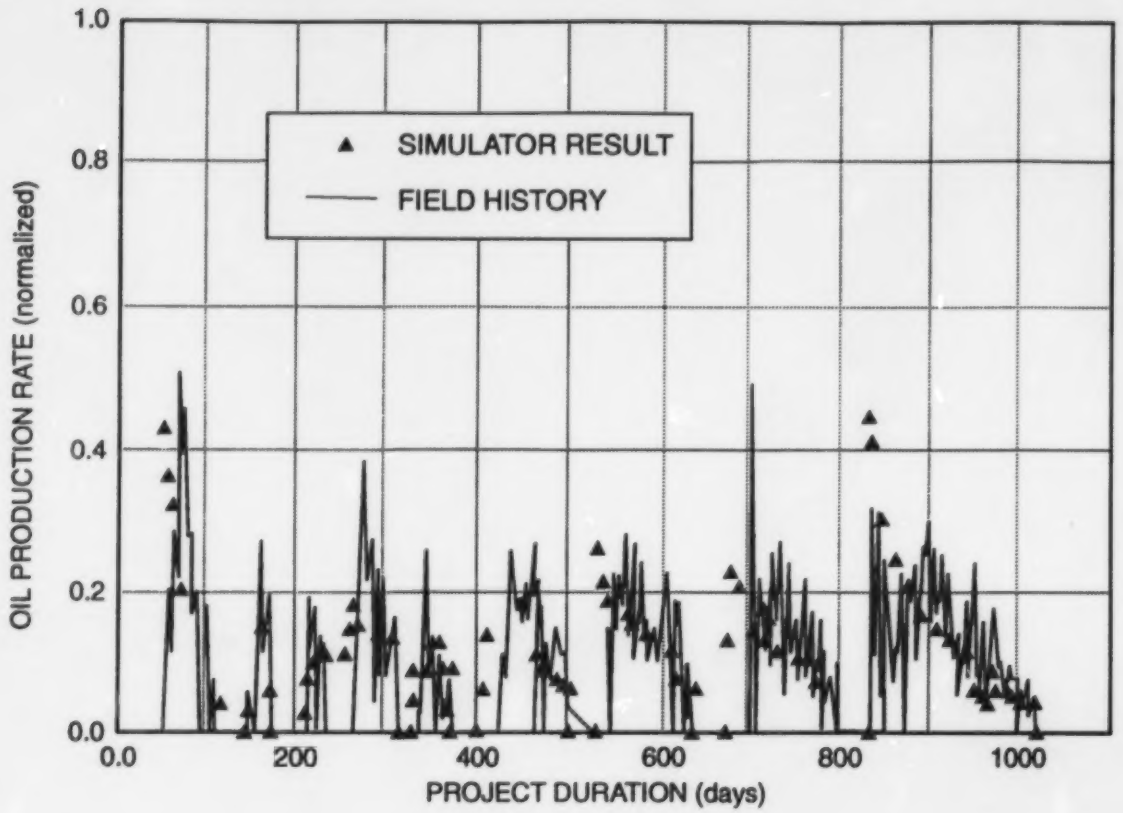

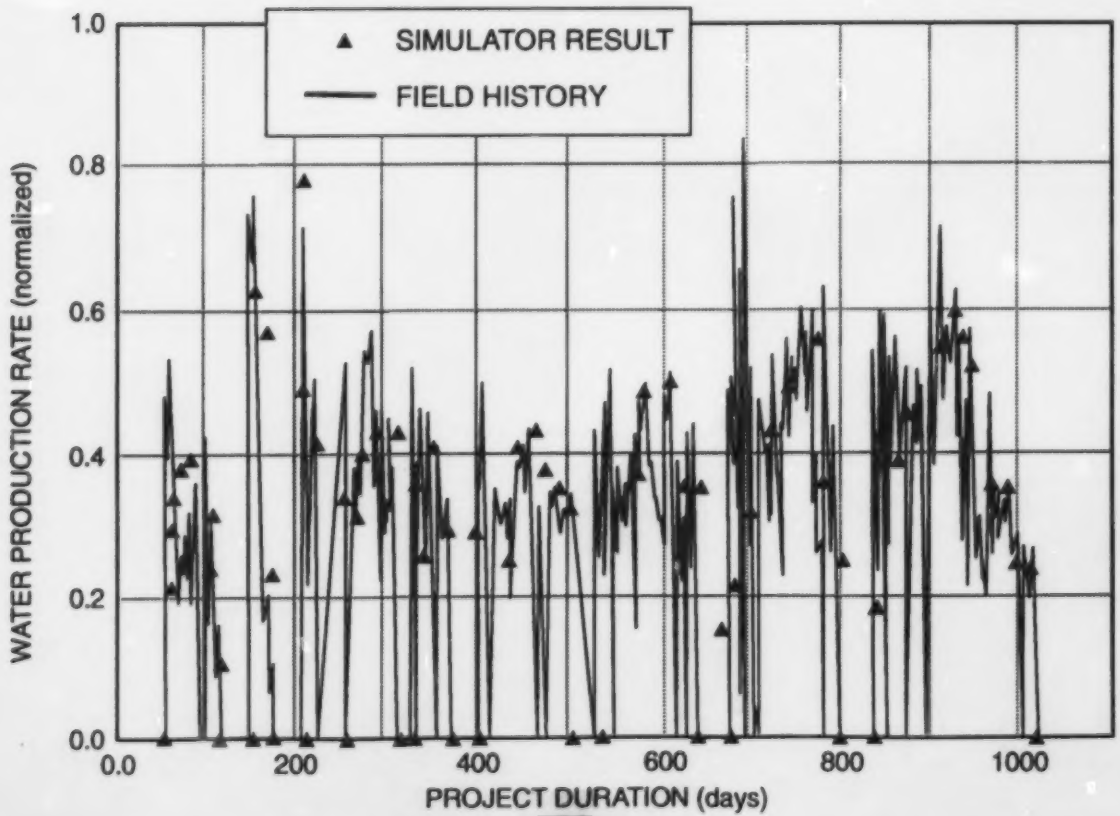

FIGURE 64

COMPARISON OF STEADY-STATE AND UNSTEADY-STATE
LABORATORY TEST DATA AT 200 C

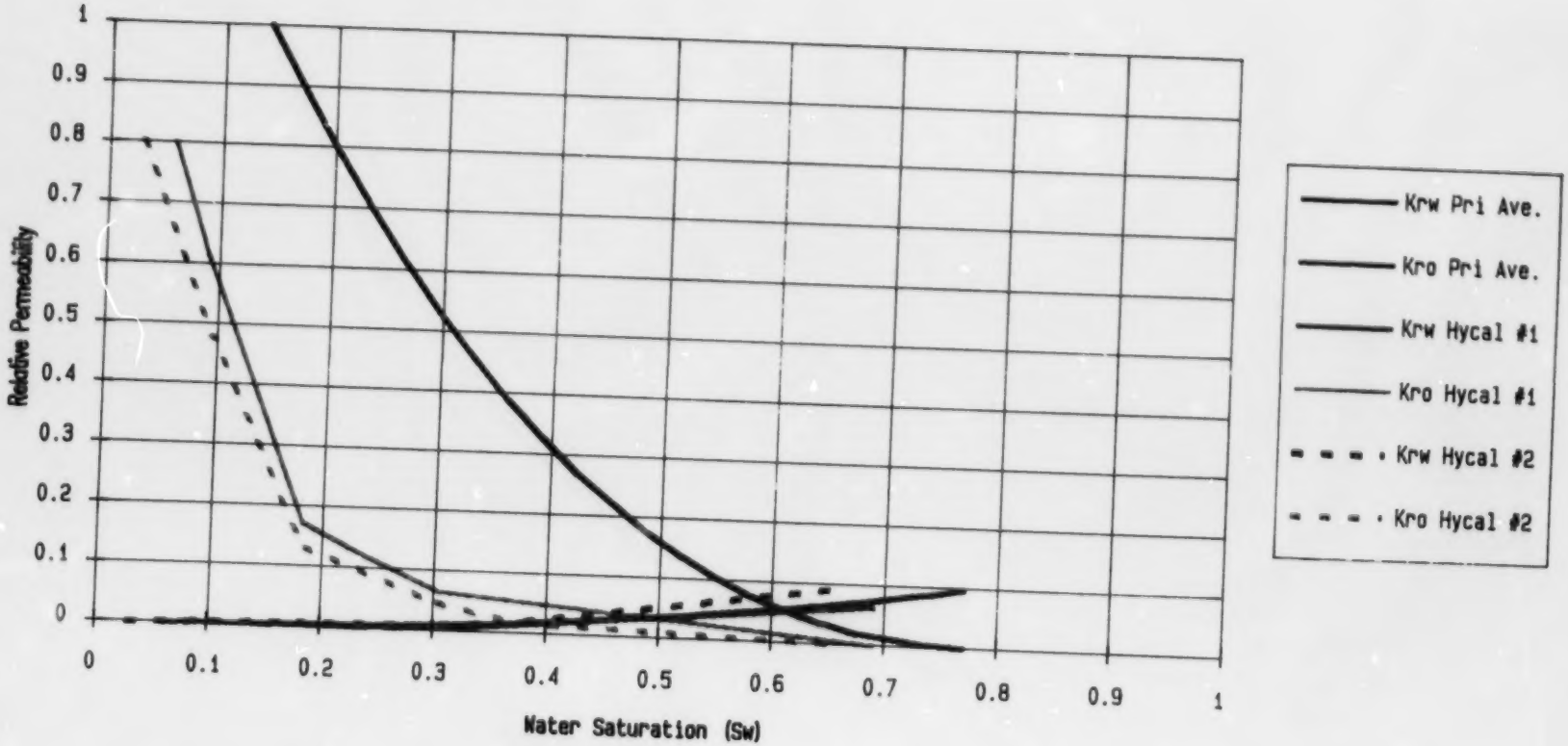

FIGURE 65

NORMALIZED RELATIVE PERMEABILITY CURVES AT 200 C

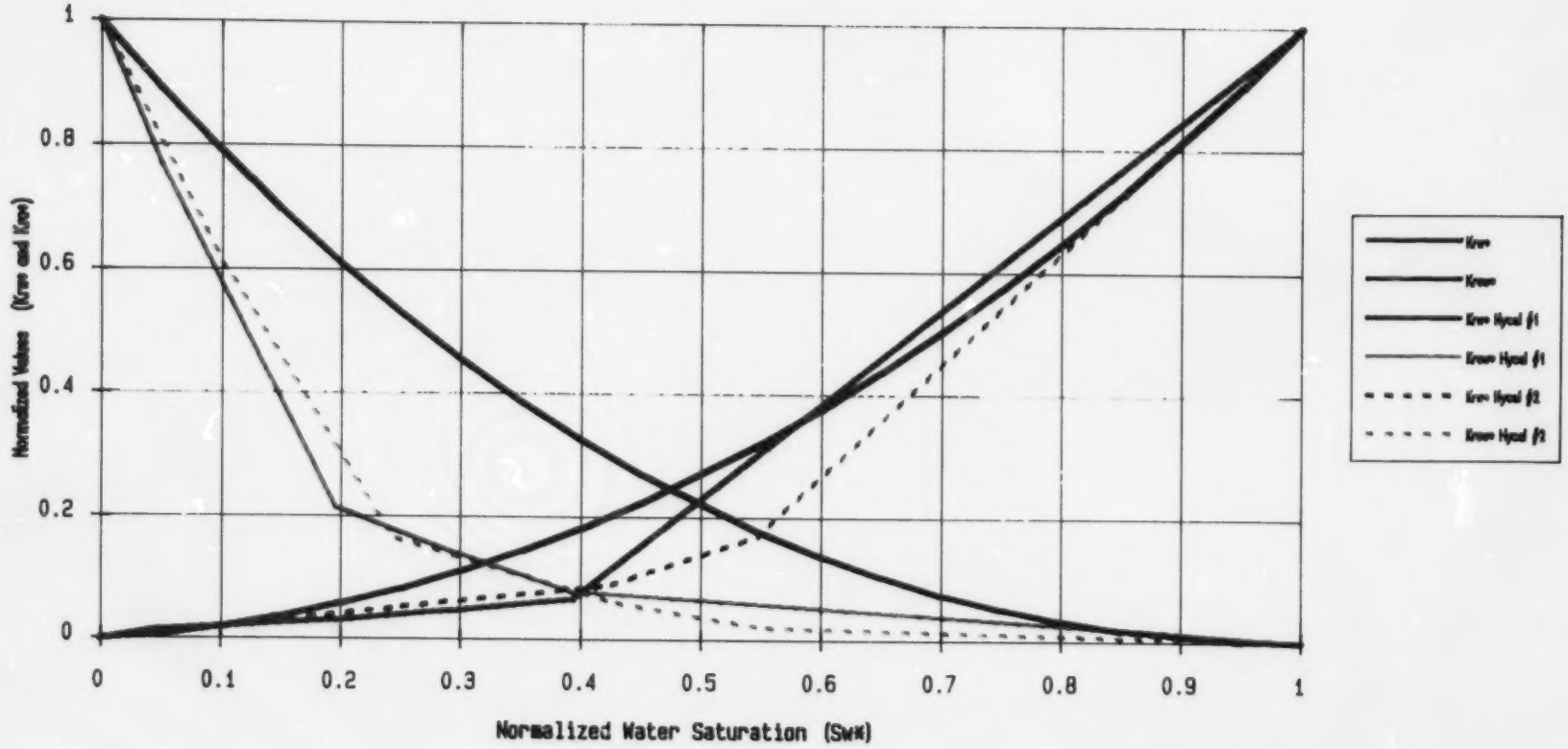

FIGURE 66

SMOOTHED NORMALIZED CURVES AND DE-NORMALIZED CURVES

STEADY-STATE RELATIVE PERMEABILITY TEST DATA

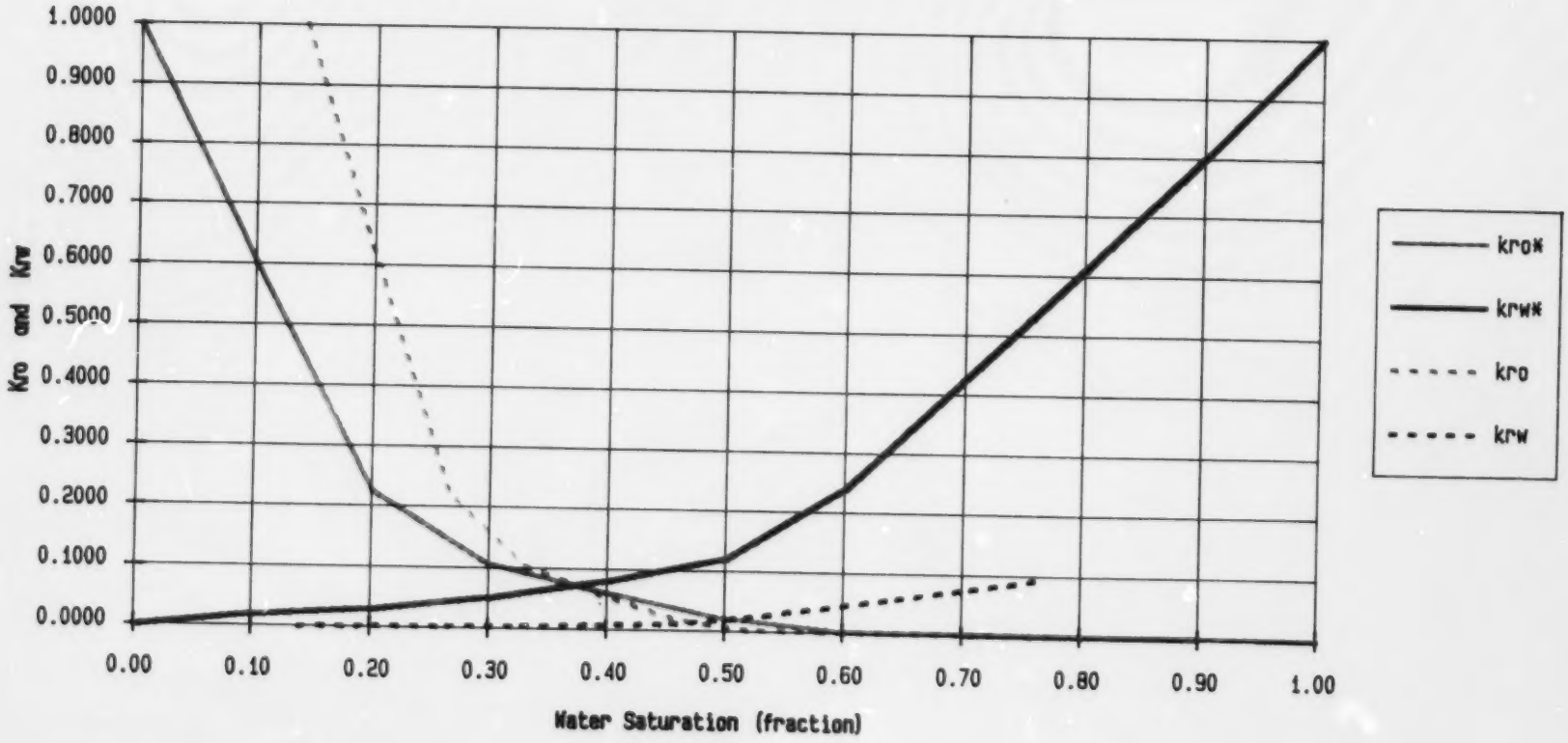

FIGURE 67

CSS PERFORMANCE COMPARISON

STEADY-STATE AND UNSTEADY-STATE RELATIVE PERMEABILITIES

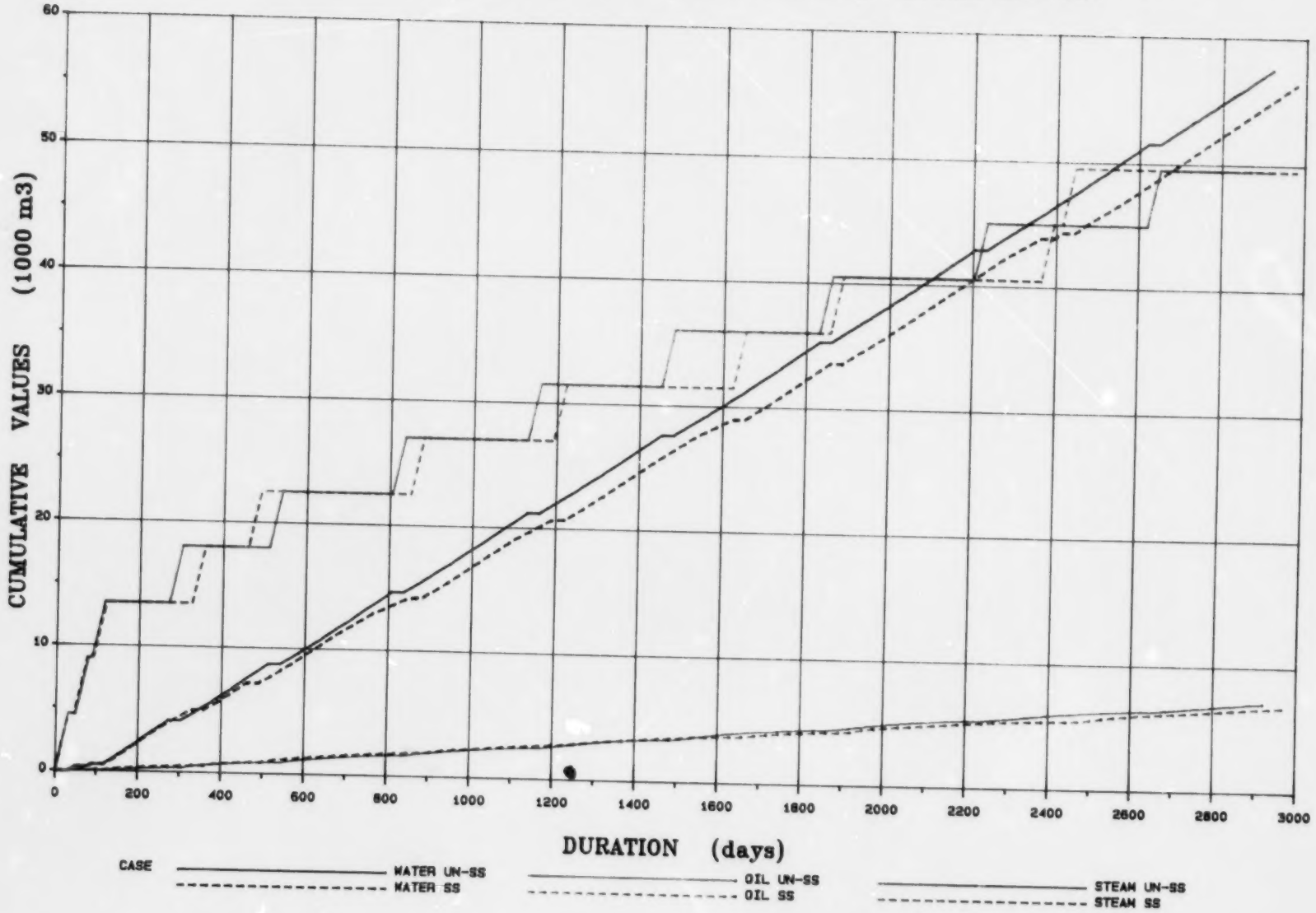

REFERENCES

1. Haywood, R.W., "Sixth International Conference on the Properties of Steam-Supplement on Transport Properties," J. Eng., Power, Trans. AIME, January, 1966, pp. 63-66.

2. Numbere, D., Brigham, W.E., and Standing, M.B., Correlations for Physical Properties of Petroleum Reservoir Brines, Petroleum Research Institute, Stanford University, November, 1977, p. 8.

3. Keenan, J.H., et. al, Steam Tables, John Wiley and Sons, 1969, p. 141.

4. Van Wylen, G.J., and Sonntag, R.E., Fundamentals of Classical Thermodynamics, John Wiley and Sons, 1973, pp. 40-41.

5. "Effects of Temperature on Oil-Water and Oil-Gas Relative Permeability of Athabasca Formation", PRZ report for PCEJ, 1988.

6. Maini, B., Coskuner, G., Jha, K., "A Comparison of Steady-State and Unsteady-State Relative Permeabilities of Viscose Oil and Water in Ottawa Sand", JCPT, March-April 1990, Vol. 29, No. 2.

7. Polikar, M., Puttagunta, V.R., DeCastro, V., Farouq Ali, S.M., "Relative Permeability Curves for Bitumen and Water in Oil Sand Systems", JCPT, January - February 1989, Vol. 28, No. 1.

8. Bennion, D.W., Moore, R.G., Thomas, F.B., "Effect of Relative Permeability on the Numerical Simulation of the Steam Stimulation Process", CIM Paper No. 83-34-46.

9. Munoz, V.A., Lam, W.W., Mikula, R.J., "Microscopic Evaluation of Steamflooded Oil Sand Core Samples", CANMET, April, 1990.

10. Kumar, M., Do, T.N., "Effects of Endpoint Saturations and Relative Permeability Models on Predicted Steamflood Performance", SPE Seventh Symposium on Enhanced Oil Recovery, Tulsa, Oklahoma, April 22-25, 1990.

11. Boberg, T.C., Rotten, M.B., Stark, S.D., "History Match of Multiwell Simulation Models of Cyclic Steam Stimulation Process at Cold Lake", SPE 20743.

APPENDIX A

PETROLEUM SOCIETY OF CIM

PAPER NO. 83-34-46

THIS IS A PREPRINT — SUBJECT TO CORRECTION

EFFECT OF RELATIVE PERMEABILITY ON THE NUMERICAL SIMULATION OF THE STEAM STIMULATION PROCESS

by
D.W. Bennion, R.G. Moore
University of Calgary

F.B. Thomas
Hycal Energy Research Laboratories, Ltd.

PUBLICATION RIGHTS RESERVED
THIS PAPER IS TO BE PRESENTED AT THE 34th ANNUAL TECHNICAL MEETING OF THE PETROLEUM SOCIETY OF CIM HELD JOINTLY WITH THE CANADIAN ASSOCIATION OF DRILLING ENGINEERS IN BANFF, MAY 10 - 13, 1983. DISCUSSION OF THIS PAPER IS INVITED. SUCH DISCUSSION MAY BE PRESENTED AT THE TECHNICAL MEETING AND WILL BE CONSIDERED FOR PUBLICATION IN CIM JOURNALS IF FILED IN WRITING WITH THE TECHNICAL PROGRAM CHAIRMAN PRIOR TO THE CONCLUSION OF THE MEETING.

ABSTRACT

Thermal numerical simulators have been used to predict the performance of the steam stimulation processes. Our experience is that room temperature relative permeability curves measured on extracted core samples need to be adjusted to match field performance. This paper describes a study which was conducted to observe the effects of temperature on initial water saturations and residual oil saturations.

A preserved core was mounted, stressed back to reservoir conditions and saturated with live reservoir oil, then waterfloods and oilfloods were run at reservoir and elevated temperatures.

Two single cycle simulations were run. One utilized relative permeability curves derived from a room temperature waterflood on an extracted core which was saturated with mineral oil. The other simulation used the relative permeability curves from the preserved core, which was run with overburden pressure, and live crude oil. Both sets of simulations used temperature functional relationships for the residual oil saturations and connate water saturations. The simulation which used the preserved core relative permeabilites resulted in matching the water production much closer than the simulation using extracted core relative permeabilities.

INTRODUCTION

Relative permeabilities play an important role in the results of a numerical simulation using a thermal simulator. In thermal processes, the reservoir matrix and fluids undergo temperature changes. These temperature changes reduce the viscosity of the oil, cause rock fluid interactions to occur, and increase stresses within the rock matrix. A number of investigators have found that increases in temperature result in decreases in permeability, Afinogenou (1969), Weinbrandt (1972), and Okoh (1980). Other investigators have found that permeability either increases or remains constant. Gobran (1981) discusses the finding of these investigators. Somerton (1981) has estimated that porosity may decrease as much as 3 to 5 percent as a result of increasing the temperature by 150oC.

Edmondson (1965) found that the residual oil saturation decreases with increases in temperature. Poston (1970) and Sinnokrot (1971) found that as the temperature increased the irreducible water saturation increased. Odeh (1965), Combarnous (1968), Wilson (1956) and Lo (1973) have postulated that the decrease in viscosity ratio is responsible for the decrease in residual oil saturation. Poston (1970) suggested the decrease in residual oil saturation was due to a change in wettability.

Poston (1970) found that for unconsolidated sand both the relative permeability to oil and to water increased as the temperature increased. Weinbrandt (1972) used consolidated Boise sandstone and reported that the relative permeability to oil increased with temperature. The relative permeability to water decreased at low water saturations but increased at flood-out. The study of Lo (1973) using consolidated Berea sandstone and porous teflon cores found that relative permeability to oil and water increased with temperature.

Dietrich (1981) developed a set of empirically derived relative permeability curves to match the performance of a cyclic steam stimulation process in a heavy oil reservoir. To simulate this process both imbibition and drainage relative permeabilities relationships were required. The empirically determined relative permeability curves were very different from those generally reported in the literature for unconsolidated sand.

During the past three years Hycal Energy Research Laboratories has endeavored to develop procedures for measuring relative permeability curves for unconsolidated sands containing heavy oil. This paper describes the experimental procedure used to obtain the curves. It also presents the results of two cyclic steam numerical simulations using relative permeability curves developed from measurements on an extracted, mineral oil saturated core and measurements on a preserved core using the technique developed by Hycal. The relative permeabilities data for the extracted core were taken from curves contained in the Alberta Energy Resource Conservation Board's data file for the Sparky Sand in the Lloydminister area. The gas-oil relative permeabilities from the extracted core were used for both simulations.

DESCRIPTION OF EQUIPMENT

The displacement equipment is designed to operate to 20.6 MPa and temperatures to 300oC. The equipment consists of three sets of components: the injection equipment, core holder and gas measuring equipment. A brief description of the components follows:

(a) Injection Equipment

The injection equipment consists of a variable rate Ruska displacement pump. It is used to flood the core with dead oil, recombined oil and water. Figure 1 presents a schematic of the equipment used in the study.

(b) Core Holder

The core holder assembly consists of a flexible sleeve core holder mounted in a pressure jacket, heaters, pressure transducers and a back pressure valve. The annular space between the pressure jacket and core holder is normally filled with water. The overburden pressure is maintained by pressuring a small void space above the water with nitrogen. The pressure jacket is also equipped with a pressure relief valve which relieves if it exceeds a set pressure. The external surface of the pressure jacket is thermally insulated. Internal heaters activated by an automatic temperature controller allows for elevated temperature operation. The core is mounted in a lead sleeve between injection and production heads which have 0.20 mm slot plates to retain sand. A pressure transducer connected across the core measures the pressure drop. Diaphragm isolators are used to prevent heavy oil from migrating to the differential pressure transducers. The core holder also has Bourdon tube gauges on the injection and production lines for a rough check on the pressure drop. The dome loaded type back pressure valve maintains the production end of the core at the desired reservoir pressure.

(c) Gas Measuring Equipment

The gas measuring equipment consists of a mercury manometer and a collection separator of known volume. Constant produced gas volumes are measured by observing the pressure rise over a measured period of time. If large volumes of gas are being measured a Ruska gasometer or a wet test meter is used.

EXPERIMENTAL PROCEDURE

Three 1 1/2 inch diameter core plugs were drilled horizontally through a preserved field core. The plugs were then stacked to form a composite core for the test. Tabulated below are the approximate lengths and weights of the individual core plugs.

Designated Plug Number	Plug Weight g	Plug Length cm
1	157.7	7.62
2	151.2	7.62
3	166.7	7.62
Total:	475.6	22.86

The individual plugs were stacked in the core holder with plug #1 closest to the injection end, plug #2 in the middle and plug #3 at the production end. The composite core was gently compacted after each plug was placed in the lead sleeve. The total length was measured to be 21.17 cm after final compaction.

The core holder was placed in the pressure jacket and a confining pressure of 10.34 MPa applied using nitrogen. Following leak checking, the pressure jacket was filled almost to capacity with water and pressured with a small nitrogen pocket to 10.34 MPa.

The core was first saturated with dead oil followed by live oil. The live oil flood was continued until the GOR of the produced oil equalled that of the oil being injected. Once this was established, the injection was stopped and the core pressure was allowed to stabilize.

Next a waterflood was performed at 27oC. During this displacement, samples were collected every 15 minutes. The water content of each sample was determined by vacuum distillation. This was necessary because the water and oil formed an emulsion which could not be separated by centrifuging. Following the waterflood the core was flooded using live oil. Samples were collected every 15 minutes and the oil and water separated by distillation. During each of the tests, the pressure drop across the core was continuously monitored.

After the oilflood the temperature was increased to 100oC and another waterflood conducted. Following this flood the temperature was increased to 150oC and the flood continued until no additional oil was produced. Then the temperature was raised to 220oC and flooded to a residual saturation. Finally the back pressure was reduced and the core steamflooded to a residual oil saturation.

Next the core was oilflooded at 220 C until no additional water was produced, the temperature was reduced to 150oC and the core oilflooded to a residual water saturation. Finally the temperature was reduced to 100oC and flooded to a residual water saturation.

At each endpoint during the waterflood 100oC, 150oC and 220oC and after the steamflood, the permeability to water was determined. During the oilflood, permeability to oil was determined at the endpoints of 220oC, 150oC and 100oC.

Following the completion of the test the core was solvent extracted using toluene, CO2 and methanol to remove the oil and water. After the core was extracted the permeability to water was measured.

DISCUSSION OF RESULTS

From the data obtained in the various displacements it was possible to calculate:

1. Residual oil saturation following hot water flooding as a function of temperature.
2. Residual oil saturation is a result of steamflooding.
3. Drainage and imbibition hysteresis.
4. Drainage and imbibition relative permeability curves for oil and water at 27oC.
5. Imbibition relative permeability curves to oil and water 100oC.
6. Residual oil saturation endpoint at 25, 100, 150 and 220oC to and permeability to water at the endpoint.
7. Steam residual oil saturation, and permeability to water this point.
8. Irreducible water saturation at 220, 150, 100 and 25oC, and the permeability to oil at each of these end-points.

Table 1 presents the composite properties of the core following extraction of the core at the completion of the test program.

Table 2 presents the permeabilities measured on the core sample at various

endpoints during the displacement process. The data indicates that the endpoint relative permeability to water increases as the residual oil saturation decreases and the temperature increases. The relative permeability to oil at the irreducible water saturation decreases as the temperature increases.

Figure 2 presents a plot of the relative permeability curves at 27oC and 220oC. It can be seen from the 27oC water curves that the relative permeability to water is larger with increasing water saturation than it is with decreasing water saturation. The corresponding 27oC oil curves shows little hysteresis except at the lower water saturations. The water and oil relative permeability curves at 220oC are also included on this figure for the oilflood following steaming the core.

Figure 3 shows the relative permeability curve from an extracted core. Two things should be noted about these curves. First the irreducible water saturation is much lower than those usually found in unconsolidated sands from the Lloydminister area of Alberta and second the permeability to water at the residual oil saturation is much higher than the ones measured using stressed preserved cores and the actual reservoir fluids.

An examination of the curves in figure 2 show that they possess the characteristics which Coats et al (1977) and Dietrich (1981) had to assume in order to match the steam stimulation process. The relative permeability curves in Figure 2 possess the following properties:

1. Lower values of permeability to water at the endpoint. The preserved core value for water is .0037 compared to .11 for the extracted core.

2. The permeability to water is higher on the injection portion of the cycle then on the production portion of the cycle.

3. Oil hysteresis is not as great as the water hysteresis.

The experimental results presented in this paper confirm Mycal's experience that the practice of measuring relative permeability curves on extracted core material with mineral oil leads to erroneous relative permeability curves. The curves developed in this manner show higher permeability to oil at initial water saturation, lower irreducible water saturation, and very different values for the water relative permeability curve and affects the hysteresis on the water relative permeability curve.

NUMERICAL SIMULATION

In order to determine the effect of relative permeability curves on the results from a numerical simulation, similar (with the exception of the relative permeability curves) two dimensional single cycle simulations were performed using the Computer Modelling Group's general purpose thermal simulator. Figure 4 shows the gird system used for the study. A total of 35 grid blocks were employed. The perforated interval is shown by the cross hatched marks on the left hand axis.

Approximately 6800 m^3 of water converted to steam was injected, the well was soaked for 10 days and then put on production. The bottom hole pressure was systematically reduced until it reached 1300 kPa. The well was placed on a constant liquid withdrawal rate until a bottom hole pressure of 200 kPa was reached. Production was then governed by a minimum bottom hole pressure of 200 kPa.

Table 3 presents most of the parameters used in the study. These were obtained from various sources within the literature. The relative permeability curves for the extracted core case were shifted to fall within the range of saturations observed for the preserved core displacements. The shifted curve is shown in Figure 3. This shifting reduced the width between initial and final water saturation; and gave a higher relative permeability to water at a given change in water saturation than the non-shifted curves.

In both cases, the irreducible water saturation and residual oil saturations were made functions of temperature. The data from the preserved core displacements tests were used for the extracted core as well as the preserved core. For the preserved core case, the waterflood relative permeabilties were used for the injection cycle and the oilflood relative permeabilities were used for the production cycle.

Three hydrocarbon components were used, a heavy oil, light oil and solution gas. Equilibrium constants were determined so as to match the viscosity of the oil at any given temperature.

Figure 4 shows the production rate of oil and water for the two simulations. The preserved core case shows that the water production rate is drastically decreased while the oil rate is only slightly reduced

as compared to the extracted core case. It took forty days to inject the steam using the extracted relative permeabilities and sixty-three days using the preserved core relative permeabilities. Thus the preserved core relative permeabilities resulted in reduced water injectivity and productivity. They appear to affect the productivity much more than the injectivity. The simulation using the extracted core relative permeabilities produced a total of 4640 m3 of water as compared to 904 m3 for the preserved core case. The oil production was 9365 m3 for the extracted core relative permeabilities and 8170 m3 for the preserved core set of relative permeabilities.

Figure 5 compares the water cut with the field data presented by Coats et al (1977). This figure shows that using the preserved core relative permeabilities in the simulation give a good water cut match.

CONCLUSIONS

1. Permeability tests using preserved core, overburden pressure and live reservoir oil, give relative permeabilities curves with hysteresis in both the oil and water curves.

2. Permeability to water using a preserved core and reservoir fluids is much lower at a given saturation than those obtained using extracted cores, and a mineral oil.

3. Relative permeabilties from a preserved core when used in a numerical simulator gave a relatively close match to the shape of a field water cut curve.

Acknowledgment

The authors wish to thank Computer Modelling Group for the use of their thermal simulator ISCOM to perform the simulation, NSERC for their financial assistance and Hycal Energy Research Laboratories for providing the preserved core relative permeabilities curves.

REFERENCES

1. Afinogenou, Y.A.: "How the Liquid Permeability of Rocks is Affected by Pressure and Temperature", SNIIGIMS (1969), No. 6, pp. 34-42.

2. Coats, K.H., Ramesh, A.B., and Winestock, A.G.: "Numerical Modelling of Thermal Reservoir Behavior", Proceedings of the Oil Sands of Canada-Venezuela 1977, Canadian Institute of Mining and Metallurgy.

3. Combarnous, M., and Pavan, J.: "Deplacement par l'Eau Chaude d' Huiles en Place Dans un Millieu Poreux", IIIe Colloque ARTFP (1968) No. 5, Pau, France.

4. Dietrich, J.K.: "Relative Permeability During Cyclic Steam Stimulation of Heavy Oil Reservoirs",JPT Oct.1981,1987.

5. Edmondson, T.A.: "Effect of Temperature on Waterflooding", J. Pet. Tech. (1965), 4, No. 4, 236.

6. Gobran, B.D. and Brigham, W.E.: "Absolute Permeability as a Function of Confining Pressure, Pore Pressure and Temperature", SPE 10156 presented at 56th annual technical meeting of SPE of AIME, San Antonio, Texas, Oct. 5-7, 1981.

7. Lo, H.Y. and Mungan, N.: "Effect of Temperature on Water-Oil Relative Permeability in Oil-Wet and Water-Wet Systems", Paper presented at the 48th SPE Annual Meeting, Las Vegas, Sept. 30-Oct. 3, 1973, SPE No. 4505.

8. Odeh, A.S. and Cook, E.L.: "Discussion - Effect of Temperature on Waterflooding J. Can. Pet. Tech. (1965) 4, No. 4, 242.

9. Okoh, C.: "Effect of Temperature on the Permeability of Porous Rocks", MS Research Report, Univ. of Calif. Berkeley (Dec. 1980).

10. Poston, S.W., Ysrael, S., Hossain, A.K.M.S., Montgomery, E.F. and Ramey, H.J. Jr.,: "The Effect of Temperature on Relative Permeability of Unconsolidated Sands "Soc. Pet. Eng. J. (197) 10, No. 2, 171.

11. Sinnokrot, A.A., Ramey H.J. and Marsden, S.S.: "Effect of Temperature Level Upon Capillary Pressure Curves", SPEJ, March 1971, Vol. 11, No. 1, p. 13.

12. Somerton, W.H.: "Porous rock-fluid Systems at Elevated Temperatures and Pressures", Sympos. or Recent Trends in Hydrogeology, GSA Special Paper (1981).

13. Weinbrandt, R.M. and Ramey, H.J. Jr.: "The Effect of Temperature on Relative Permeability of Consolidated Rocks", Paper presented at the 47th SPE Annual Meeting, San Antonio, Oct. 8-11, 1972, SPE No. 4142.

14. Wilson, J.W.: "Determination of Relative Permeability Under Simulated Reservoir Conditions", AIChE J. (1956) 2, No. 1, 94.

TABLE 2

Permeability μm^2

Permeability to oil at irreducible water saturation	27°C	0.591
Permeability to water at residual oil saturation	27°C	0.0022
Permeability to water at residual oil saturation	100°C	0.0030
Permeability to water at residual oil saturation	150°C	0.0035
Permeability to water at residual oil saturation	220°C	0.0038
Permeability to water at residual oil saturation after steamflood	220°C	0.00739
Permeability to oil at irreducible water saturation	220°C	0.414
Permeability to oil at irreducible water saturation	150°C	0.495
Permeability to oil at irreducible water saturation	100° C	0.532
Permeability to oil at irreducible water saturation	27°C	0.576
Permeability to water after extraction (100% water saturated)	27°C	3.594

TABLE 3

Model Parameters

Number of grid blocks in r direction	7
Number of grid blocks in z direction	5
Maximum injection pressure - kPa	10340
Steam quality at sand face	0.70
Injection rate - m /day	160
Permeability - m	3.60
Porosity - percent	32.0
Ratio of vertical to horizontal permeability	0.1
Initial reservoir pressure - kPa	4030
Initial reservoir temperature - K	300
Initial oil saturation	.695
Initial water saturation	.300
Density gmol/m	
Heavy oil component	1382
Light oil component	4044
Water	$5.537 \times 10^{+4}$
Solution gas	18700
Molecular Weight kg/gmol	
Heavy oil component	.720
Light oil component	.180
Solution gas	.016
Thermal Conductivity J/m-day-K)	
Oil	1.15×10^{-4}
Water	5.35×10^{-4}
Rock	1.495×10^{-5}
Compressibility kPa-1	
Rock	4.05×10^{-6}
Heavy Oil	2.18×10^{-6}
Light Oil	2.18×10^{-6}
Water	4.35×10^{-7}
Coeff. of Thermal Expansion - K-1	
Rock	4.4×10^{-5}
Heavy Oil	8.5×10^{-4}
Light Oil	8.5×10^{-4}

Water	1.044×10^{-3}

Dead Oil Viscosity mPa's	Temperature K
110	353
60	333
30	303

List of figure headings

One set of figures have headings on them other set for printing.

FIGURE 1. Equipment Schematic

FIGURE 2. Relative Permeability-Preserved Core

FIGURE 3. Relative Permeability-Extracted Core

FIGURE 4. Numerical Simulation Grid

FIGURE 5. Simulation Results

FIGURE 6. Water-Cut History

FIGURE 1. Equipment Schematic

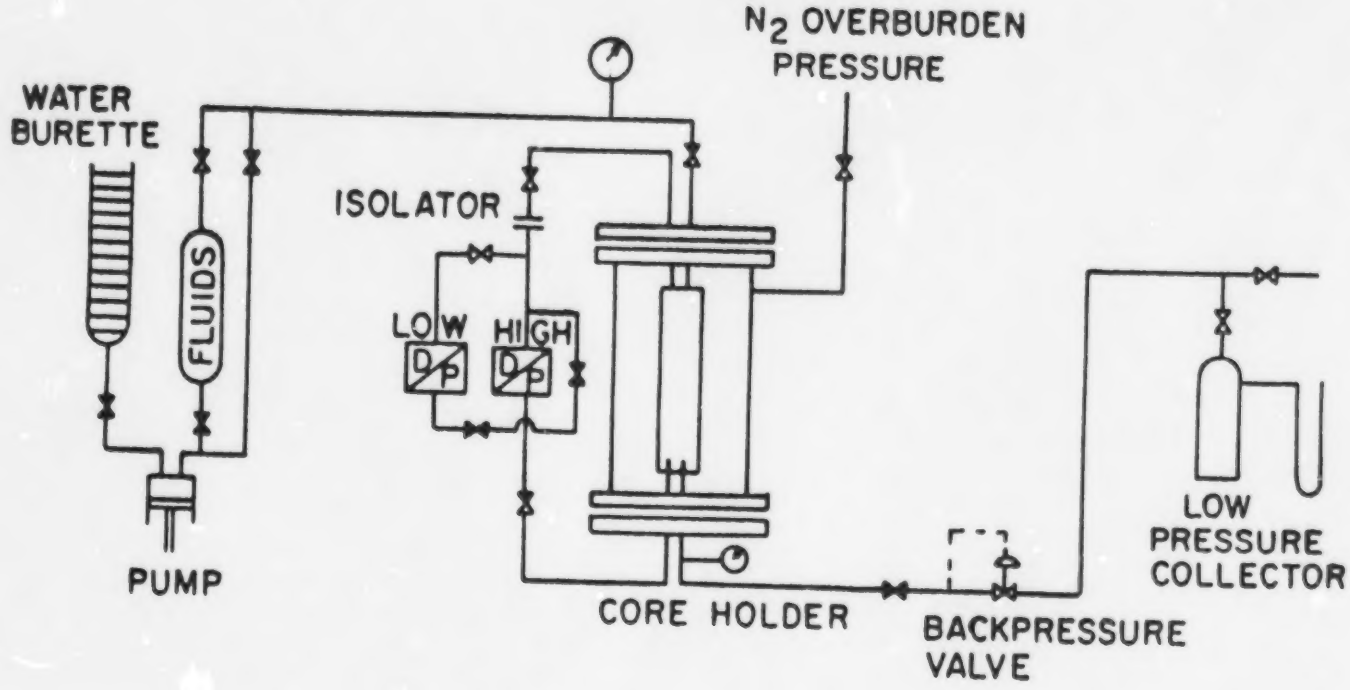

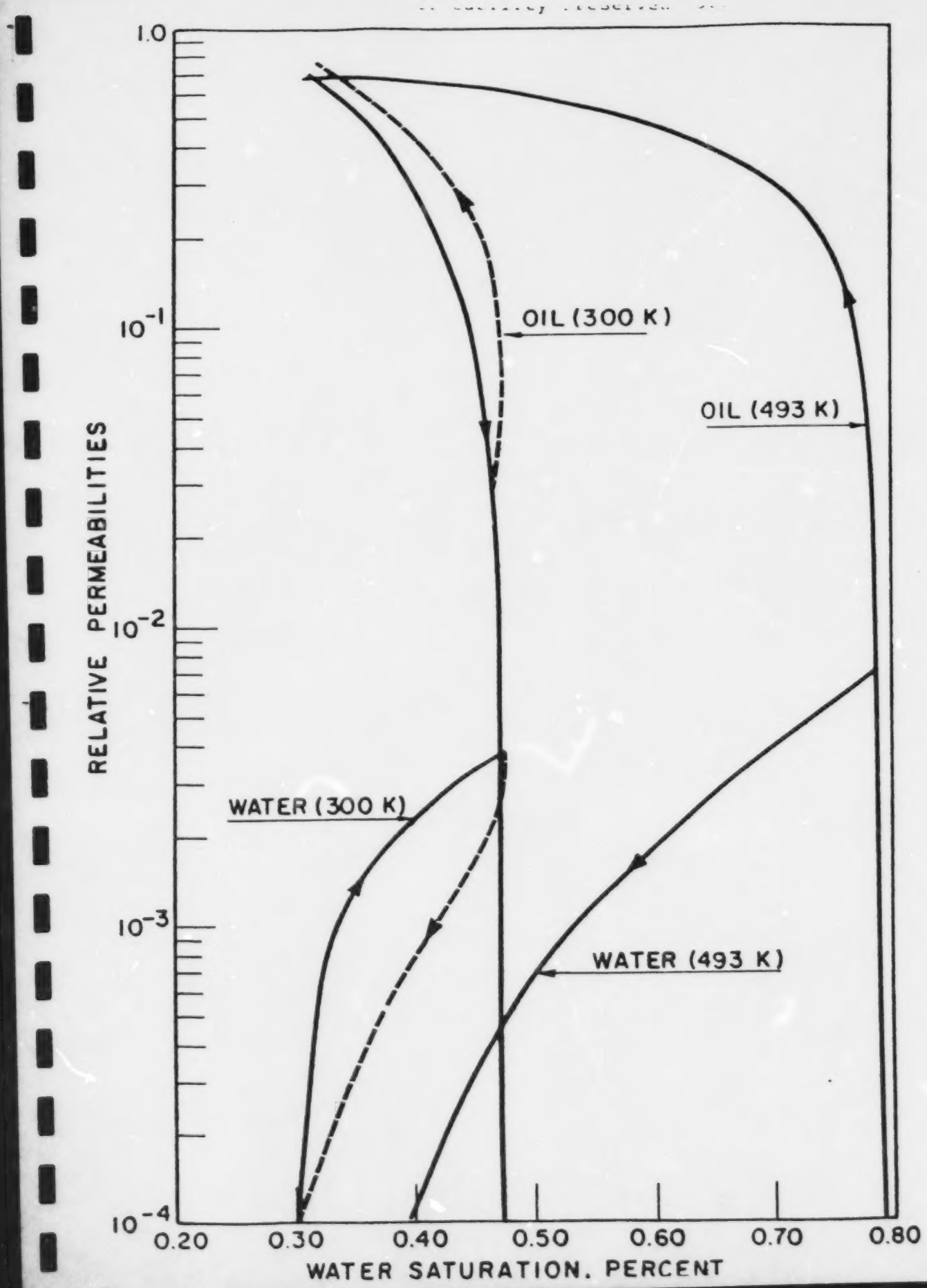
1.0
10^{-1}
10^{-2}
10^{-3}
10^{-4}
RELATIVE PERMEABILITIES
OIL (300 K)
OIL (493 K)
WATER (300 K)
WATER (493 K)
0.20
0.30
0.40
0.50
0.60
0.70
0.80
WATER SATURATION, PERCENT

FIGURE 3. Relative Permeability-Extracted Core

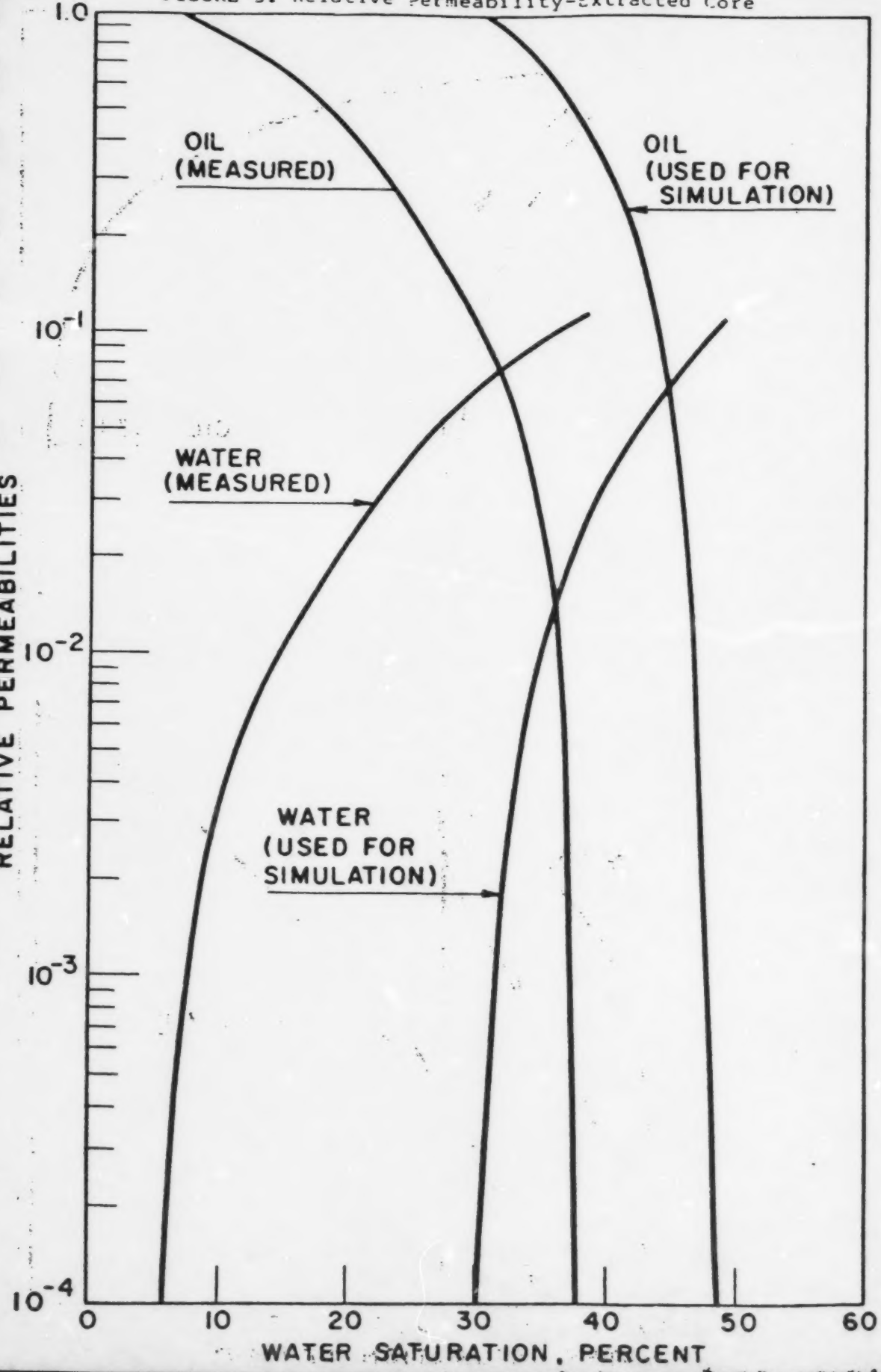

FIGURE 4. Numerical Simulation Grid

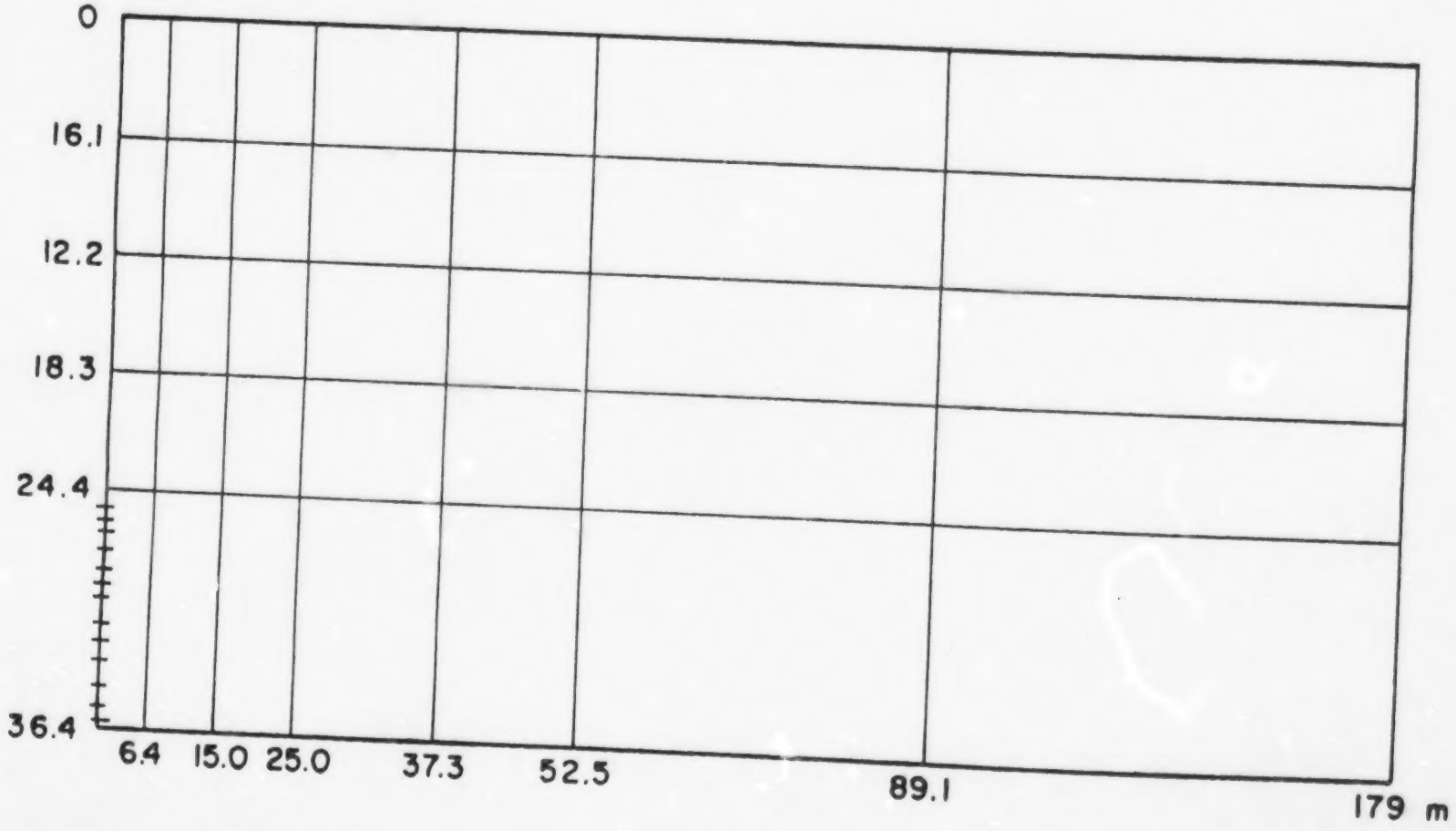

FIGURE 5. Simulation Results

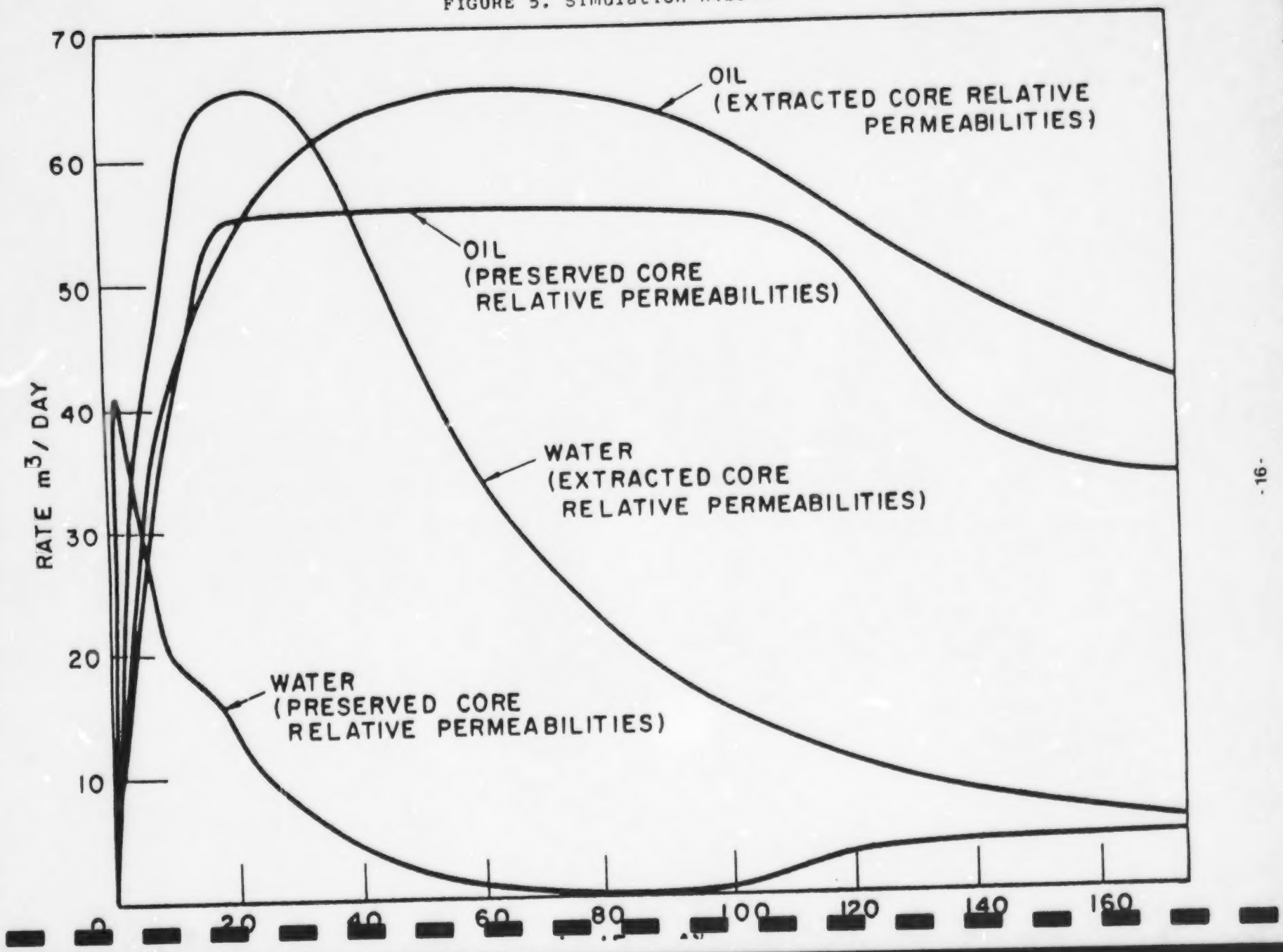

FIGURE 6. Water-Cut History

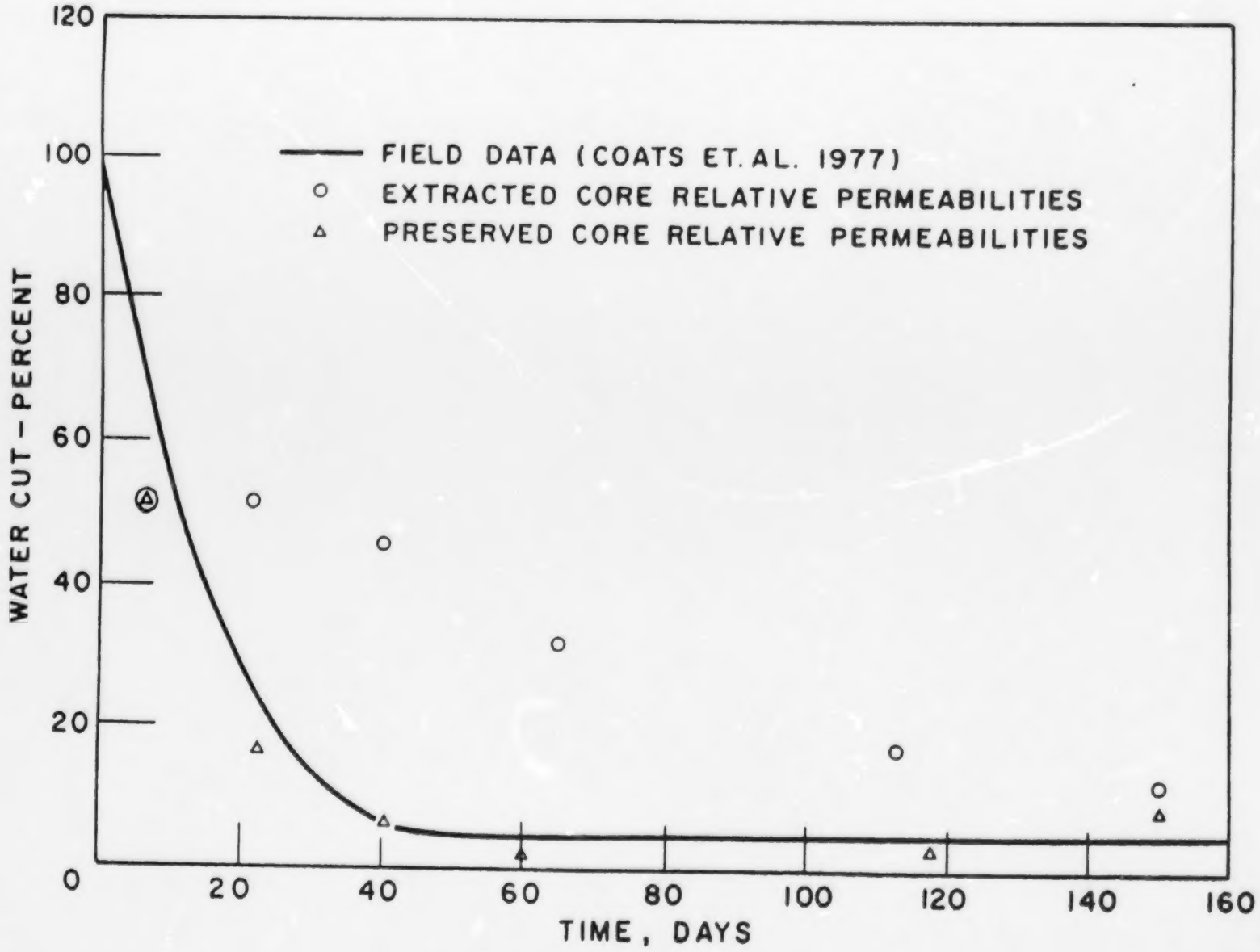

SOCIETY OF PETROLEUM ENGINEERS PAPER NO. SPE 23783

THIS IS A PREPRINT - SUBJECT TO CORRECTION

FORMATION DAMAGE DUE TO MINERAL ALTERATION AND WETTABILITY CHANGES DURING HOT WATER AND STEAM INJECTION IN CLAY BEARING SANDSTONE RESERVOIRS

BY
D. Brant Bennion, F. B. Thomas
Hycal Energy Research Laboratories Ltd.

D. A. Sheppard
Sceptre Resources Ltd.

THIS PAPER IS TO BE PRESENTED AT THE 1992 SPE SYMPOSIUM ON FORMATION DAMAGE CONTROL TO BE HELD FEBRUARY 26-27, 1992 IN LAFAYETTE, LOUISIANA

ABSTRACT

Detailed laboratory studies were conducted to study the effect of hot water and steam injection on the permeability, relative permeability, wettability, residual oil saturation and mineralogic composition and structure of a clay bearing sandstone reservoir in Southern Alberta, Canada. The samples initially contained only kaolinite and illite clays, classically classified as non-water sensitive. This paper presents the results of three detailed laboratory coreflow experiments and documents the degree of formation damage (up to 95% reductions in permeability were observed) due to temperature induced mineralogic and wettability alterations. Multipoint temperature tests from 32 to 265°C (90 to 510°F) were conducted at full reservoir conditions on preserved core material to generate this data. The effect of steamflooding vs merely hot waterflooding at 265°C (510°F) on residual oil saturation is also illustrated indicating up to a 20% additional reduction in residual oil saturation by steamflooding. A complete suite of pre and post test petrographic studies on each sample tested including x-ray diffraction, thin section and scanning electron microscope analysis indicate the definitive transformation of inert kaolinite clay into water sensitive swelling smectitic clay due to reactions between the kaolinite clay and the quartz during the high temperature flooding process. The results of this study have specific application to the design of hot water and steam injection projects in other similar types of sandstone reservoirs.

References and figures at end of paper

INTRODUCTION

Hot water and steamflooding are commonly used techniques to mobilize and recover substantial additional low and mid API gravity oil from shallow hydrocarbon bearing formations. The input of thermal energy into the reservoir reduces the viscosity of the oil and increases the reservoir energy allowing mobilization and production of the crude oil. As with any type of reservoir injection and production process, the ability to successfully inject and produce the fluids is of paramount importance. Formation damage in the reservoir can greatly reduce injectivity into the formation. If the thermal process is of a cyclic nature, the productivity of the formation on the production cycle can also be adversely affected and result in an overall reduction in the fraction of recoverable oil. Formation damage mechanisms during hot water and steamflooding are somewhat different processes than commonly associated with conventional wells. This paper will document some of the common causes of permeability impairment associated with thermal recovery projects and illustrate these phenomena using the results of a comprehensive suite of laboratory data.

MECHANISMS OF THERMALLY INDUCED FORMATION DAMAGE

Formation damage occurring during normal drilling,completion and stimulation operations has been

documented in the literature[1,2]. This paper is concerned with the mechanisms of permeability impairment which can occur during a thermal stimulation operation. These processes would include:

1. Mineral transformations
2. Mineral solubilization/dissolution
3. Wettability alterations
4. In-situ emulsion formation.

Each of these damage mechanisms will now be discussed in greater detail.

Mineral Transformations

Mineral transformations can be a particular problem in reservoirs which contain a substantive amount of in-situ clay. Many reservoir systems are evaluated prior to testing for the presence of smectite clay. Smectite clay's structure is such that due to an uneven charge distribution, layers of fresh water can readily substitute themselves between clay crystals causing an expansion of the clay structure. When fully hydrated, a smectite clay crystal can almost double in size from 9.2 Angstroms to over 17 Angstroms[3]. Obviously, if smectitic clay is present in the matrix of a reservoir, sensitivity to fresh low salinity injected water may be a potential mechanism for formation damage. This problem is often overcome in regular waterflood operations by increasing the ionic strength or divalent ion concentration[1,4] in the injected water stream. This causes the substitution of a smaller mineral ion in the clay structure in lieu of water. This results in clay stabilization and the exclusion of the water from the clay matrix.

Many reservoirs also contain what would normally be classed as non-swelling clays. These clays would include materials such as kaolinite, illite and chlorite[3]. Clays of this type generally exhibit balanced charges and hence are not susceptible to swelling, although they may exhibit deflocculative[4] or migrative[5] tendencies.

The potential for mineral transformation in high temperature thermal operations occurs when relatively inert kaolinite clay is transformed into fresh water sensitive smectite clay. This reaction[6] occurs as follows:

$$\underset{\text{[Kaolinite Clay]}}{7Al_2Si_2O_5(OH)_4} + \underset{\text{[Solubilized Quartz]}}{8SiO_2} + Me \rightarrow \underset{\text{[Smectite Clay]}}{2(Me)Al_7Si_{11}O_{30}(OH)_6} + 7H_2O + 2H \quad \ldots\ldots (1)$$

where Me is Ca, Mg or possibly Fe

The transformation from inert kaolinite clay to smectitic clay is induced by the temperature induced solubility of quartz in the water phase and the presence of Ca, Mg or Fe in the injection fluid from direct injection or solubilization of carbonate/dolomite cementing materials. The fluid which is in contact with the resulting newly formed swelling clay is fresh steam condensate. Since the steam condensate contains no stabilizing ions it will rapidly substitute into the smectite structure causing the clay to swell and reduce permeability. This phenomenon has also been documented by others.[6,7,8,9]

MINERAL DISSOLUTION

Figure 1 illustrates the phenomenon of mineral dissolution. Damage from mineral dissolution can take two forms, these being:

a) Damaging reprecipitation of the solubilized minerals either as the reservoir cools or as the saturated hot water phase cools as it moves deeper into the formation.

b) Often clasts of soluble material will contain encapsulated insoluble fines. As the high temperature injected water dissolves the soluble material, the non-soluble encapsulated fines are released where they then migrate into the flowing fluid stream. If of sufficient size, these fines can bridge and plug at pore throats.

Wettability Alterations

The effects of temperature on wettability have been previously documented by several authors[10,11]. Almost all minerals in a natural, clean state exhibit water wet behavior. Polar high molecular weight compounds that tend to be physically adsorbed on the surface of

minerals, particularly on carbonates, are the motivating cause of neutral or oil-wet behavior. Studies suggest[12] that up to half of all sandstone and about 90% of all carbonate oil reservoirs exhibit neutral to oil-wet behavior. The degree of physical adsorption which adheres these oil-wetting hydrocarbon agents to the surface of the minerals in the reservoir is controlled by temperature. The higher the temperature becomes, the less of these types of hydrocarbons can be retained on the surface of the reservoir rock. Therefore, the hotter a system becomes (while under a hot waterflood), in general, the more water wet it becomes.

It is well understood that wettability strongly influences the flow and relative permeability characteristics of porous media[13]. Figure 2 illustrates how a typical temperature induced shift in wettability can influence the flow behavior of an initially oil wet reservoir. In general, permeability to water drops substantially even though maximum water saturation increases due to a reduction in the residual oil saturation by viscosity reduction effects. Oil permeability may also increase in some cases due to the shift to more water wet behavior.

This type of behavior can be advantageous, particularly in a cyclic thermal production project as it tends to greatly improve the oil-water mobility ratio and improve speed and efficiency of overall oil recovery. Injectivity of water due to a reduction in water phase permeability is generally not a problem as the water viscosity reduction with temperature in most cases offsets the reduction in injectivity thereby maintaining a constant or decreasing injection pressure.

Figure 3 illustrates how an abrupt wettability transformation can occur when the transition from hot waterflood to steamflood occurs. Figure 3a illustrates a typical pore when hot waterflooding. The pore is water wet at high temperature and the residual oil saturation is trapped in the central portion of the pore, encapsulated and shielded from contact with the rock matrix by the surrounding liquid hot water phase. When the transition to steamflooding occurs, (Figure 3b), the shielding water phase is vaporized allowing the residual oil saturation to contact the surface of the rock directly. This allows direct unshielded adsorption which in many cases, even at elevated temperatures, can cause a very rapid alteration to an oil wetted state (Figure 3c).

Figure 4 illustrates how a transition in wettability induced by steamflooding can adversely affect the water-oil relative permeability characteristics of a porous media. The large increase in water phase relative permeability can greatly reduce the recovery efficiency of the mobilized oil on the return production cycle. Wettability changes of this type can be permanent or gradually reversible (due to gradual desorption after hot waterflooding resumes) depending on the specific nature of the system under consideration.

Emulsion Formation

The formation of high viscosity oil external emulsions can be a severe problem both in the reservoir and in surface production systems. Many mid and low API gravity crude oils can contain up to 70% water by volume internally emulsified in an encapsulating external oil phase. These oils are readily characterized by their "creamy" appearance and it is not at all unusual for oils with high water contents to exhibit dynamic viscosities an order of magnitude or more greater than clean, unemulsified oil.

In general, fresh, lower density water tends to emulsify with crude oil more readily than higher density saline brines. This being the case, production from hot water and steamfloods are particularly susceptible to emulsification problems due to the fact that these processes are most commonly associated with low gravity crudes and fresh injection water/steam condensate. The in-situ formation of emulsions tends to cause the formation of a trapped highly viscous immobile phase. This trapped phase greatly impedes the flow of subsequently mobilized oil and increases the turbulence between produced oil and water, thereby causing further emulsification problems.

DESCRIPTION OF THE EXPERIMENTAL STUDY

Three detailed high temperature displacement studies were conducted on preserved state core samples from a selected well in a Glauconitic sandstone reservoir in Southern Alberta, Canada. The tests were specifically designed to investigate:

1. Reservoir condition water-oil relative permeabilities.
2. Recovery efficiency to hot water as a function of temperature.
3. Incremental oil recovery by steamflooding.
4. The potential for and mechanisms of thermally induced formation damage for this system.

EXPERIMENTAL EQUIPMENT

A schematic of the high temperature core displacement apparatus appears as Figure 5. Preserved core material is mounted in a ductile lead sleeve to allow the transmission of a confining overburden pressure in both radial and axial modes to the core material. Sintered glass disks are used to retain the core material and radial distribution heads ensure that flow into and out of the core specimens is evenly distributed eliminating potential areas of localized high fluid velocity. The core assembly is mounted inside a high temperature core jacket encased in a digitally controlled 6 kilowatt heating mantle capable of elevating core temperature up to 340°C (650 °F). The pressure rating of the core jacket at this temperature was 21 000 kPa (3000 psi).

Pressure differential measurements across the core sample, to facilitate permeability calculations, were conducted through the use of a manifold system of two capacitance type pressure transducers. One transducer had a range of 0 -150 kPa (0 - 20 psi) and the second from 0 - 1500 kPa (0 - 200 psi) to facilitate the accurate measurement of a wide range of pressure differentials which might occur over the course of a displacement test.

Fluids were displaced through the core samples using digitally controlled, constant rate, positive displacement pumps. The use of positive displacement pumps obviates problems associated with pressure "shocking" the core samples (as can occur with conventional reciprocating chromatographic style pumps) and reduces the potential for premature damage due to fines mobilization.

Backpressure on the system was controlled using a precision backpressure regulation system accurate to 0.5% of the setpoint value. Fluids were produced into a test separator where exact volumes of produced oil, water and gas as a function of time could be determined. All system components were constructed of corrosion resistant monel or 316 stainless steel.

EXPERIMENTAL PROCEDURE

Selected samples of preserved state glauconitic core were utilized for the three different experiments conducted as a portion of the study. Table 1 documents a summary of pertinent core physical parameters for each of the three tests. Samples of fresh unoxidized reservoir crude oil were obtained from field separators in sealed pressurized stainless steel cylinders and recombined with equilibrium separator gas to yield a saturation pressure of 3250 kPa (471 psig) at 32°C (90°F) and a resulting gas-oil ratio of 22 m^3/m^3 [124 scf/bbl] for the live oil. The actual displacement tests were conducted at 7500 kPa (1090 psi) as this was the current reservoir operating pressure in the reservoir under study. Table 2 documents the pressurized viscosity measurements conducted on the live oil and injection water at 7500 kPa (1090 psig) at the different temperature levels utilized in the study.

The following identical procedure was utilized for each of the three different core samples in the study

1. Mount core stack as previously described in a ductile lead sleeve. Apply 9390 kPag (1360 psig) of initial net overburden pressure. Heat the core sample slowly to the reservoir temperature of 32°C (90°F). Internally pressurize the sample to 7500 kPag (1090 psig) by the injection of unoxidized dead reservoir crude oil while simultaneously increasing the overburden pressure to 16 890 kPa (2450 psig) to always maintain a net overburden pressure of 9390 kPag (1360 psig).

2. Displace dead reservoir crude out of the core sample at 7500 kPag (1090 psig) by injection of 10 pore volumes of live crude oil. Determine initial stabilized permeability to live crude oil. Verify that effluent oil G.O.R. and composition are identical to the initial injected live reservoir oil to ensure complete saturation of the sample.

3. Conduct an unsteady state, water saturation increasing, constant rate relative permeability test on the core at 7500 kPag (1090 psig) and 32 °C. Collect incremental production and transient pressure history data to facilitate computation of full water-oil relative permeability curves via implicit computer history matching techniques[14].

4. While continuing to waterflood, slowly elevate core temperature to 100 °C. Measure final stabilized permeability to water at 100 °C and note residual oil saturation.

5. Heat core to 175 °C, repeat step #4.

6. Heat core to 220 °C, repeat step #4.

7. Heat core to 265 °C, repeat step #4.

8. Steamflood core at 265 °C by slowly reducing internal pressure to 5800 kPag (700 psi) to generate steam in-situ in the porous media. Steamflood the sample until no additional reduction in oil saturation is observed.

9. Repressurize core to 7500 kPag (1090 psig) to re-establish liquid phase flow. Remeasure post steamflood brine permeability to note the effect of steamflooding.

10. Cool core, dismantle, measure final saturations and post test air permeability and porosity.

11. Subject pre and post test core samples from each test to thin section, XRD (X-Ray Diffraction) and SEM (Scanning Electron Microscope) analysis to quantify the mechanisms of any observed formation damage.

RESULTS OF EXPERIMENTAL TESTS

Initial Mineralogy

Table 3 presents the initial bulk and clay XRD analysis summary for each of the three samples which were evaluated during the study. The samples were generally silt sized to fine and medium grained lithanerite sandstones. The framework mineralogy was predominantly monocrystalline quartz with lesser amounts of sedimentary rock fragments, chert, polycrystalline quartz and trace amounts of feldspar. Matrix clay occupies up to 6% of the rock volume (and up to 9% of the mass on a bulk compositional basis - Table 3). This clay lines the pores and occasionally blocks pore throats. The analysis indicated that the clay material was predominantly detrital kaolinite with a minor illitic component and the case of sample "B" a trace smectitic component. Calcite and ferroan (iron bearing) dolomite cements occur in trace quantities precipitated in the intergranular pore system.

Experimental Data

Table 4 compares the water and oil phase endpoint relative permeability data and Table 5 provides the residual saturation data as a function of temperature for the three tests. Figure 6 provides a comparison of the oil-water relative permeability data generated using the implicit history matching technique[14] at 32°C and 7500 kPag (1090 psig) for each of the three samples. Examination of this data indicates very comparable water-oil relative permeability characteristics between the three samples. The configuration of the relative permeability curves would suggest that the three samples likely exhibit neutral to slightly water-wet initial wettability.

The water relative permeability data of Table 4 has been plotted and appears as Figure 7. This clearly illustrates how the water phase permeability in each test declined dramatically with temperature. Substantive reductions in the residual oil saturation (Table 5) were occurring as temperature increased contributing to a higher water saturation which should, in theory, have caused an increase in water phase relative permeability.

The primary cause for the reduction in permeability to water in the 32 to 175°C (90 to 348°F) range is likely primarily attributable to wettability shifts to a more water wet condition. Above 175 °C (347 °F) the permeability decline with temperature becomes more pronounced and is likely motivated by the additional effect of mineral transformations and dissolution phenomena, coupled with continued wettability alteration effects. Table 6 documents the specific clay fraction composition of each of the cores on a pre and post test basis. The XRD results indicate definitively for samples "A" and "C" a substantive reduction in the concentration of kaolinite clay and an increase in smectitic clay concentration.

The residual saturation data of Table 5 have been plotted and appear as Figure 8. Examination of this data indicates that residual oil saturation was in general steadily reduced with temperature. Core "C", which was very heterogeneous and permeable, had the highest residual oil saturation. This is believed to be due to macroscopic channelling effects and the subsequent bypassing of a large amount of trapped oil in lower permeability portions of the sample. All of the tests indicated that a substantial additional volume of oil (15 - 20% of the total pore space could be recovered by steamflooding at 265°C versus merely waterflooding at the same temperature. This substantial additional recovery, while still maintaining a constant temperature, is believed to be due to a combination of steam

distillation and stripping effects, additional energy added to the system by the compressible gaseous steam phase, and a possible reduction in trapping effects due to the transition from a water wet to oil wet media[15].

The fact that a wettability alteration has occurred is readily apparent from the data of Table 4 and Figure 7. Although one would expect the reduction in residual oil saturation to cause an increase in water permeability, permeabilities to water increased by 162%, 1503% and 880% for samples A, B and C respectively. This is a much greater increase than would normally be associated with the reduction in saturation (based upon extrapolation of the configuration of the initial oil-water relative permeability curves). Expulsion of bridging fines and particulates during the steamflood process can in some cases cause large permeability increases similar to this. Both thin section and XRD analysis of the pre and post test core samples indicated no evidence of this type of mechanism, further substantiating the mechanism of wettability alteration for the permeability increase.

Post Test Mineralogy

No substantive difference in the rock fabric and diagenetic mineral suite was seen in thin sections; however, smectitic swelling clays were identified in post test SEM and XRD samples analyses which were previously absent. The percentage of quartz and kaolinite had been reduced in these cases and the percentage of smectite increased. Samples of very small (<5) microns of poorly crystallized silica precipitates were observed in the pore system (particularly sample C) possibly contributing to the observed permeability reduction by blockage of some pore throats. Pre and post test clay mineralogy data is summarized in Table 6.

CONCLUSIONS

The test results illustrate three of the classic forms of formation damage potentially associated with thermal recovery projects, these being:

1) The transformation of kaolinite clay to swelling smectitic clay.
2) Mineral dissolution and re-precipitation.
3) Wettability alteration.

The test results indicate that formation permeability could be reduced by up to 90% by a combination of these factors. The formation of in-situ emulsions can also occur, but was not observed to be a problem in these tests, possibly due to the higher gravity crude oil utilized in this case in comparison to many hot-water and steamflood projects.

The test program also illustrated that residual oil saturation was a function of temperature and was reduced by increasing the temperature. Steamflooding at 265°C (509°F) was found to mobilize substantial (up to 20% of the total pore volume) additional oil resulting in residual oil saturations as low as 8%. Wettability alterations to a more oil-wet state were observed when steamflooding which substantially increased the relative permeability to water. This illustrates that considerations of the viability of recovering the extra oil mobilized by steamflooding need to be balanced against the potential creation of a more adverse mobility ratio.

The use of laboratory displacement tests were illustrated as an effective means of screening and predicting reservoir performance and defining potential thermal sensitivity problems prior to the capital cost of implementation in the reservoir.

Acknowledgements

The authors wish to express appreciation to the Management of Sceptre Resources for their permission to publish this data.

REFERENCES

1. Bennion, D.B. and Thomas, F.B.: "The Design of Effective Laboratory Coreflood Tests to Evaluate and Minimize Formation Damage in Horizontal Wells", Paper Presented at the Third International Conference on Horizontal Well Technology, Houston, Texas (Nov. 12-14, 1991).

2. Bennion, D.B., Thomas, F.B. and Crowell, E.C.: "Laboratory Tests to Evaluate and Minimize Damage in Horizontal and Vertical Wells", Paper Presented at the 30th Annual Conference of the Ontario Petroleum Institute, London, Ontario (Oct. 9-11, 1991).

3. Yang, Joseph, Ph.D. Thesis, University of Calgary, 1979.

4. Scheuerman, Ronald F., and Bergersen, Barbara M., "Injection-Water Salinity, Formation Pretreatment, and Well-Operations Fluid-Selection Guidelines", *JPT*, (July 1990).

5. Gruesbeck, C., and Collins, R.E., "Entrainment and Deposition of Fine Particles in Porous Media", *SPEJ*, (1979) 846-56.

6. Hutcheon, I., Abercrombie, H.J., Shevalier, M., and Nahnybida, C.: "A Comparison of Formation Reactivity in Quartz-Rich and Quartz-Poor Reservoirs During Steam Assisted Thermal Recovery", In, R.F. Meyer and E.J. Wiggins (eds.), The Fourth UNITAR/UNDP International Conference on Heavy Crude and Tar Sands, Volume 2, Paper No. 235, (1989) pp. 747-757.

7. Abercrombie, H.J.: "Water-Rock Interaction During Diagenesis and Thermal Recovery, Cold Lake, Alberta". An unpublished University of Calgary Ph.D. Thesis.

8. Perry, C., and Gillott, J.E.: "The Formation and Behavior of Montmorillonite During the Use of Wet Forward Combustion in the Alberta Oil Sand Deposits", Bulletin of Canadian Petroleum Geology, v.27, No. 3, pp 314-325.

9. Sedimentology Research Group, "The Effects of In-Situ Steam Injection on Cold Lake Oil Sands," Bulletin of Canadian Petroleum Geology, v. 29, No. 4, pp 447-478.

10. Maini, B.B. and Okazawa, T., "Effects of Temperature on Heavy Oil-Water Relative Permeability of Sand," *JCPT*, May 1987.

11. Polikar, M., Ali, S.M.F., Puttagunta, V.R.: "High Temperature Relative Permeabilities for Athabasca Oil Sands," *SPE Res. Eng.* (Feb. 1990).

12. Treiber, L.E., Archer, D.L. and Owens, W.W., "A Laboratory Evaluation of the Wettability of Fifty Oil Producing Reservoirs," *SPE*, Vol. 13 (4) (1973) p 221.

13. Craig Jr., F.F.: "The Reservoir Engineering Aspects of Waterflooding," *SPE Monograph Series*, (1971).

14. Bennion, D.B., Bennion, D.W., Thomas, F.B., "Recent Improvements in Experimental and Analytical Techniques for the Determination of Relative Permeability from Unsteady State Flow Experiments," presented at the SPE 10th Technical Conference and Exposition held in Port of Spain, Trinidad (June 26-28, 1991).

15. Wardlaw, N.C.: "The Effects of Geometry, Wettability, Viscosity and Interfacial Tension on Trapping in Single Pore Throat Pairs," *JCPT*, (May 1982).

TABLE 1 - INITIAL CORE PARAMETERS

Core Property	Core A	Core B	Core C
Length (cm)	10.20	9.41	8.88
Area (cm^2)	11.28	11.32	11.47
Porosity (%)	24.2	24.2	26.0
Pore Volume (cm^3)	27.84	25.80	26.45
Initial Water Saturation	0.121	0.148	0.134
Final Water Saturation	0.907	0.917	0.755
Backpressure (kPa) [psi]	7500 [1090]	7500 [1090]	7500 [1090]
Overburden Pressure (kPa) [psi]	16890 [2450]	16890 [2450]	16890 [2450]
Final Avg. Post Test Air Permeability $(\mu m)^2 \times 10^3$ [mD]	473.3 [479.5]	530.5 [537.5]	-- *

* Plugs crumbled during post test extraction, permeability was extremely high

TABLE 2 - OIL AND BRINE VISCOSITY MEASUREMENTS AT 7500 KPA

Temperature (°C)	Live Oil Viscosity mPa.s (cP)	Water Viscosity mPa.s (cP)
32	6.94	0.792
100	1.46	0.295
175	0.578	0.165
220	0.390	0.131
265	0.298	0.109

TABLE 3 - INITIAL SAMPLE COMPOSITIONAL DATA VIA XRD ANALYSIS

Compound	Percent in Sample		
	A	B	C
Quartz	91	91	96
Plagioclase	0	0	0
Feldspar	0	0	0
Pottassic Feldspar	0	tr	0
Calcite	0	tr	0
Dolomite	0	0	0
Barite	tr	0	0
Pyrite	0	0	0
Ankerite	0	0	0
Gypsum	0	0	0
Siderite	0	0	0
Kaolinite	7	7	3
Chlorite	0	0	0
Illite	2	1	tr
Mixed Layer Clays	0	0	0
Smectite	0	tr	0
Total Clay	9	9	4

TABLE 4 COMPARATIVE RELATIVE PERMEABILITY DATA AS A FUNCTION OF TEMPERATURE FOR CORES A, B, AND C

Fluid	Temperature	Relative Permeability		
	°C (°F)	Core A	Core B	Core C
Live Oil	32 (90)	0.8000*	0.8000*	0.8000*
Water	32 (90)	0.2024	0.1600	0.1829
Water	100 (212)	0.1742	0.1012	0.1198
Water	175 (347)	0.1236	0.0632	0.0528
Water	220 (428)	0.1041	0.0468	0.0343
Water	265 (509)	0.0794	0.0114	0.0116
Steam	265 (509)	--	--	--
Water	265 (509)	0.2085	0.1828	0.1137
Kabs to fluid ($\mu m^2 \times 10^{-3}$) [mD]		207.9 [219.7]	368.8 [373.7]	944.5 [956.9]

Note: Absolute permeability to fluid estimated for each preserved core assuring k_o = 0.80 abs.

TABLE 5 - COMPARISON OF RESIDUAL OIL SATURATION TO WATERFLOOD/STEAMFLOOD AS A FUNCTION OF TEMPERATURE FOR CORES A, B AND C

Temperature	Fluid Type	Final Residual Oil Saturation (Fraction)		
		Core A	Core B	Core C
32	Live Oil	0.879	0.852	0.867
32	Water	0.452	0.451	0.453
100	Water	0.312	0.381	0.419
175	Water	0.294	0.319	0.419
220	Water	0.276	0.299	0.419
265	Water	0.262	0.299	0.367
265	Steam	0.093	0.083	0.245
265	Water	0.093	0.083	0.245

TABLE 6 - ILLUSTRATION OF CHANGE IN CLAY COMPOSITION BETWEEN PRE AND POST TEST SAMPLES OF CORE A, B AND C

Clay Type	Percentage Clay Present in Sample					
	Core A Pretest	Core A Post Test	Core B Pre Test	Core B Post Test	Core C Pre Test	Core C Post Test
Kaolinite	88	83	82	92	90	42
Chlorite	0	6	0	0	0	0
Illite	12	8	12	4	10	25
Mixed Layer	0	0	0	0	0	0
Smectite	0	3	6	4	0	33

FIGURE 1
EXAMPLE OF FORMATION DAMAGE
MINERAL DISSOLUTION

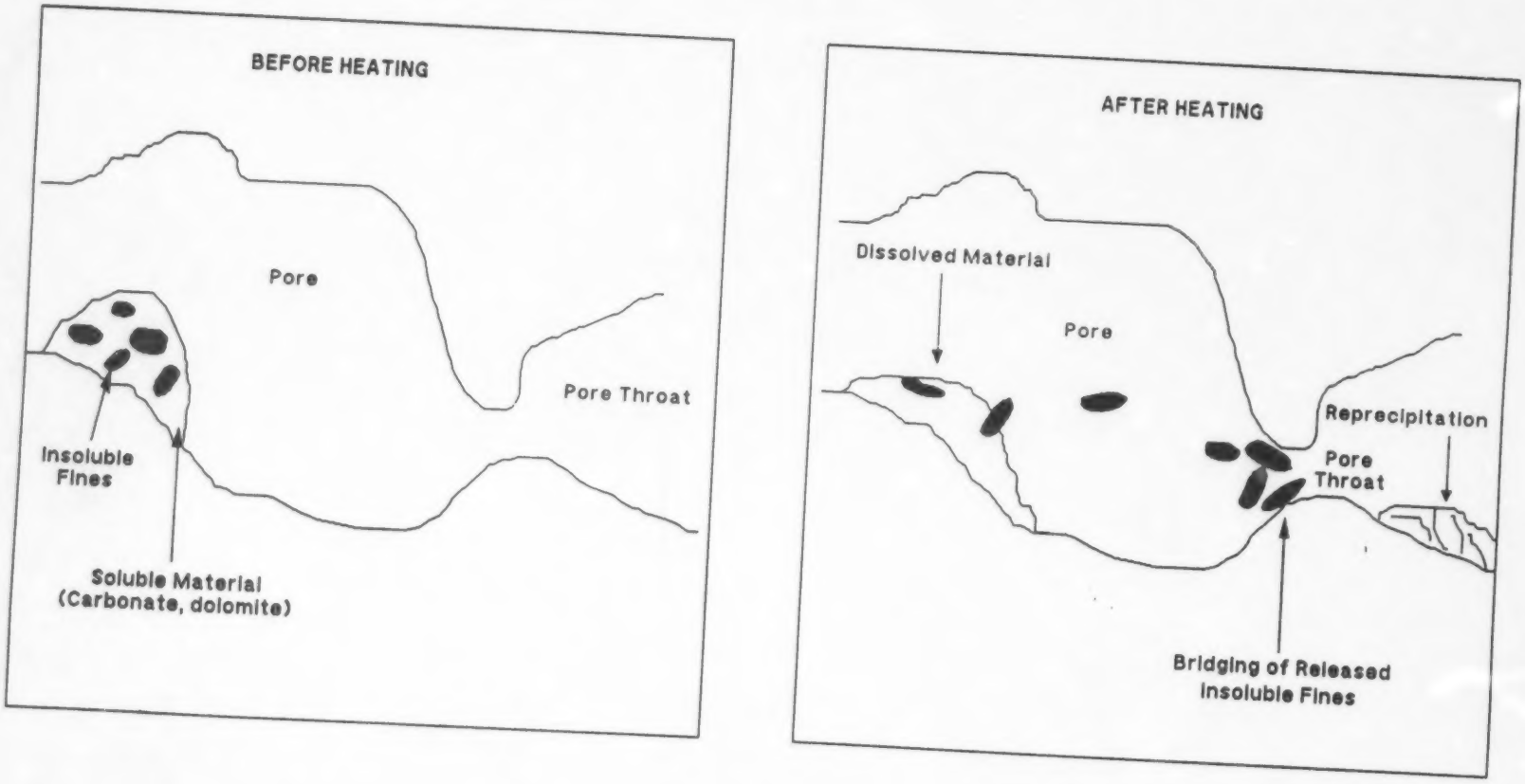

FIGURE 2
INFLUENCE OF TEMPERATURE ON RELATIVE PERMEABILITY/WETTABILITY
(Illustrative Example)

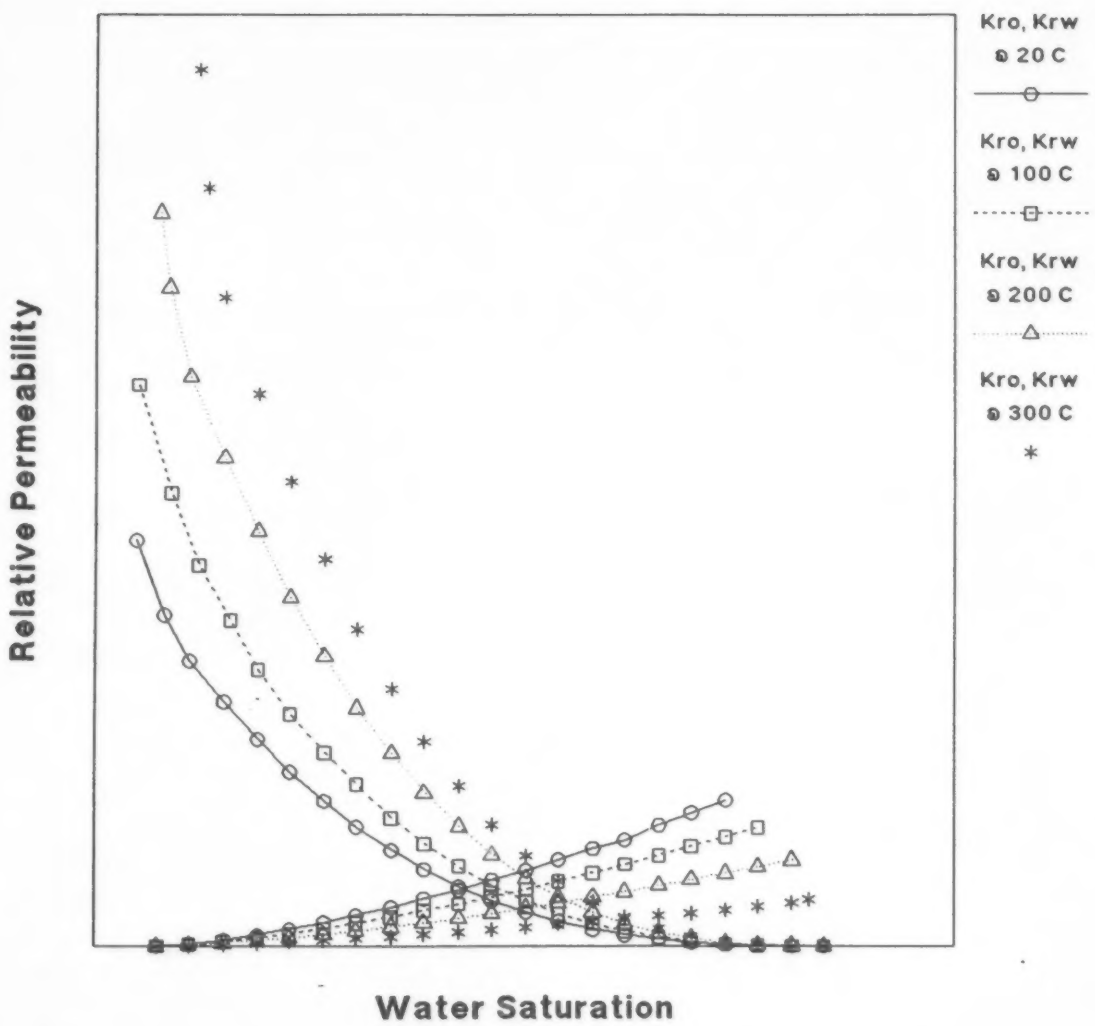

FIGURE 3
ILLUSTRATION OF WETTABILITY ALTERATION WITH STEAMFLOODING

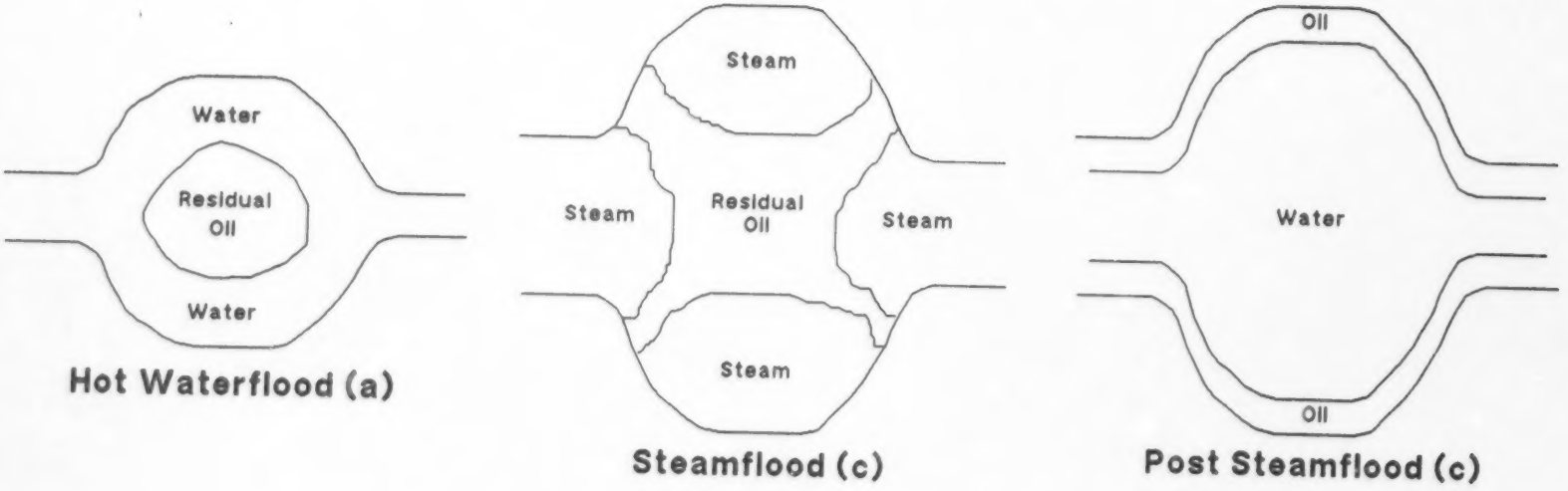

FIGURE 4
ILLUSTRATION OF CHANGE IN RELATIVE PERMEABILITY CHARACTERISTICS DUE TO WETTABILITY ALTERATIONS DUE TO STEAMFLOODING

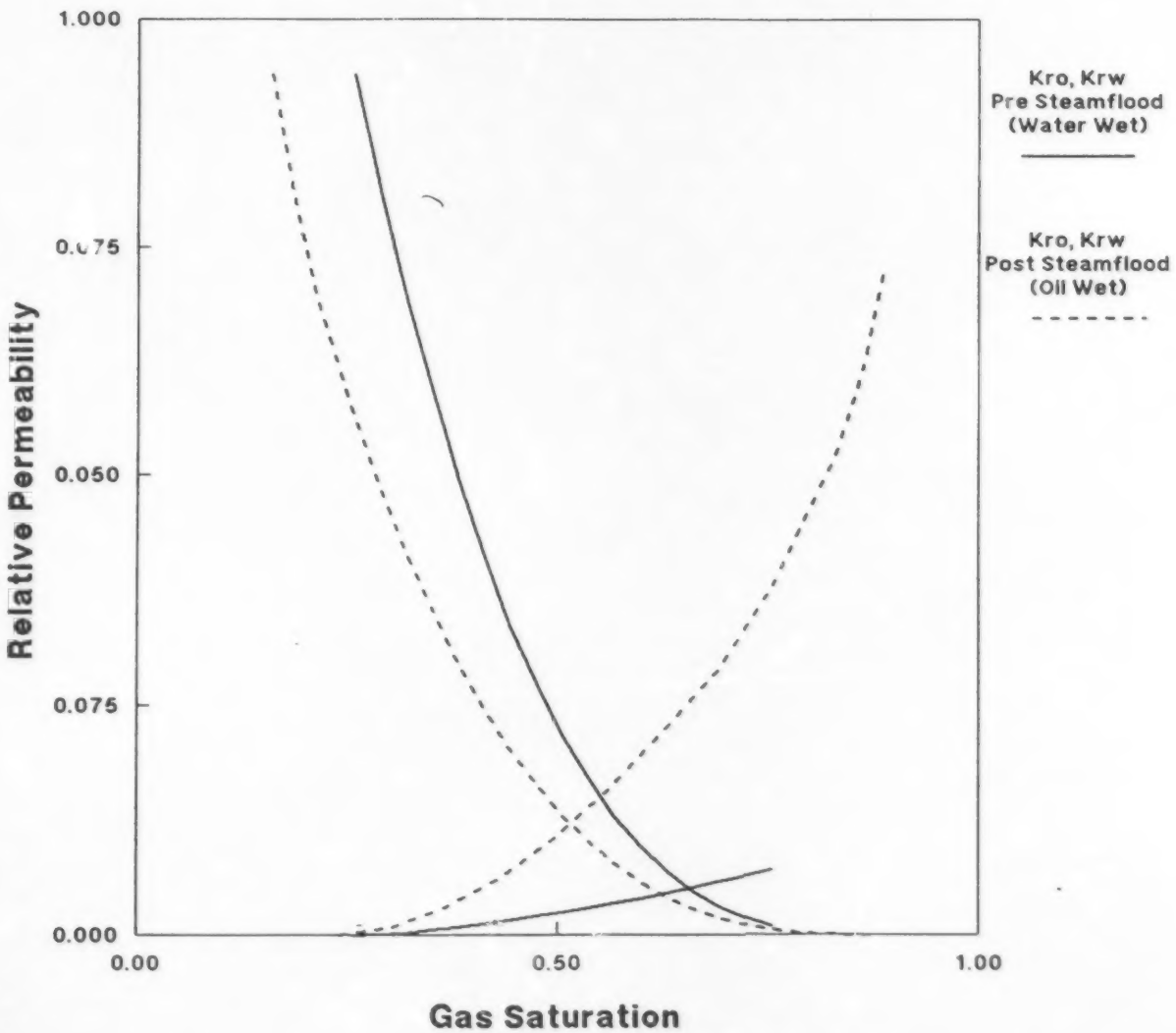

FIGURE 5
HIGH TEMPERATURE RELATIVE PERMEABILITY AND FLUID SENSITIVITY APPARATUS

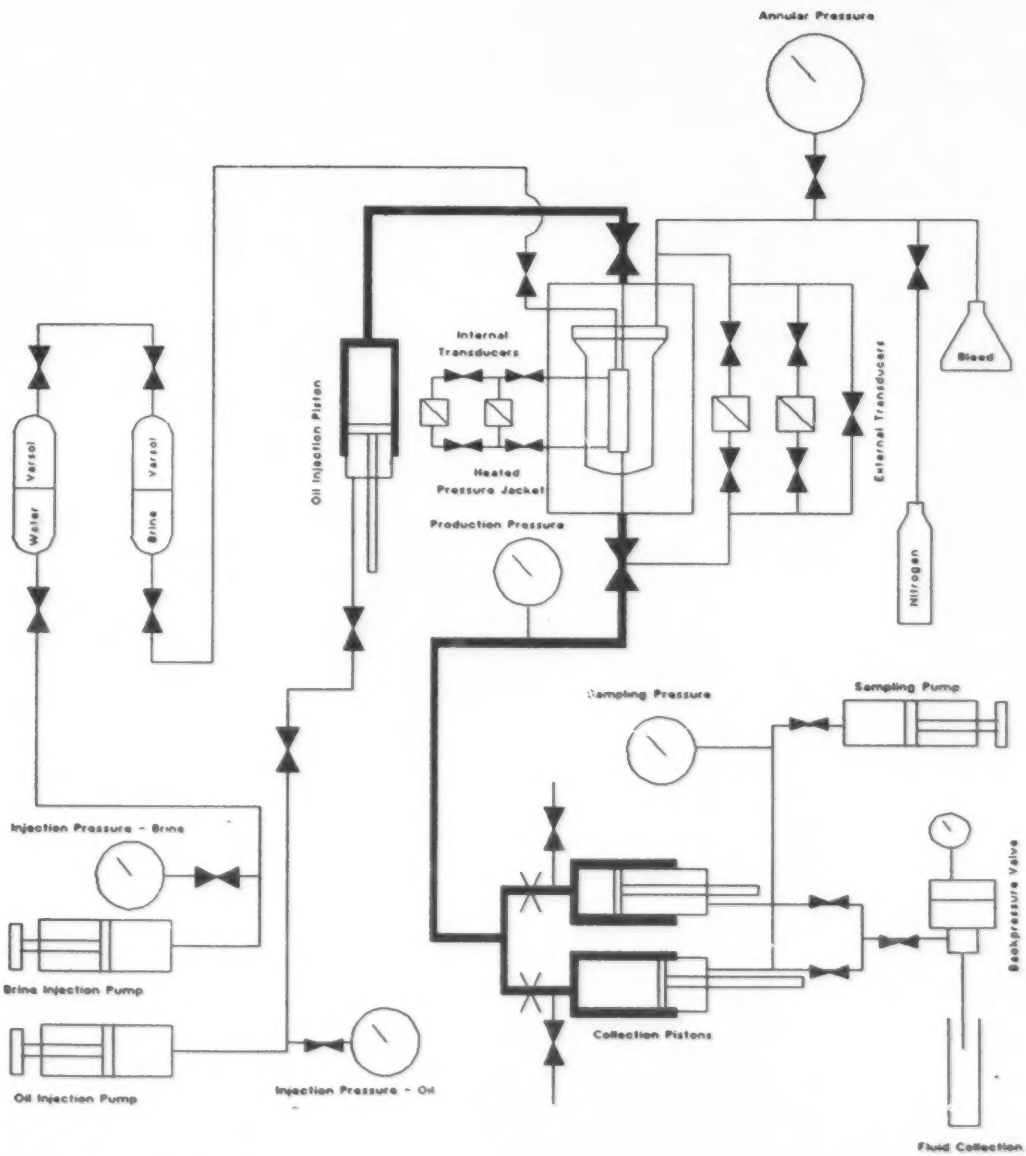

(Thick Lines Represent Heat Traced Flow Tubing)

FIGURE 6
COMPARISON OF WATER-OIL RELATIVE PERMEABILITY DATA AT 32 C FOR CORES A, B & C

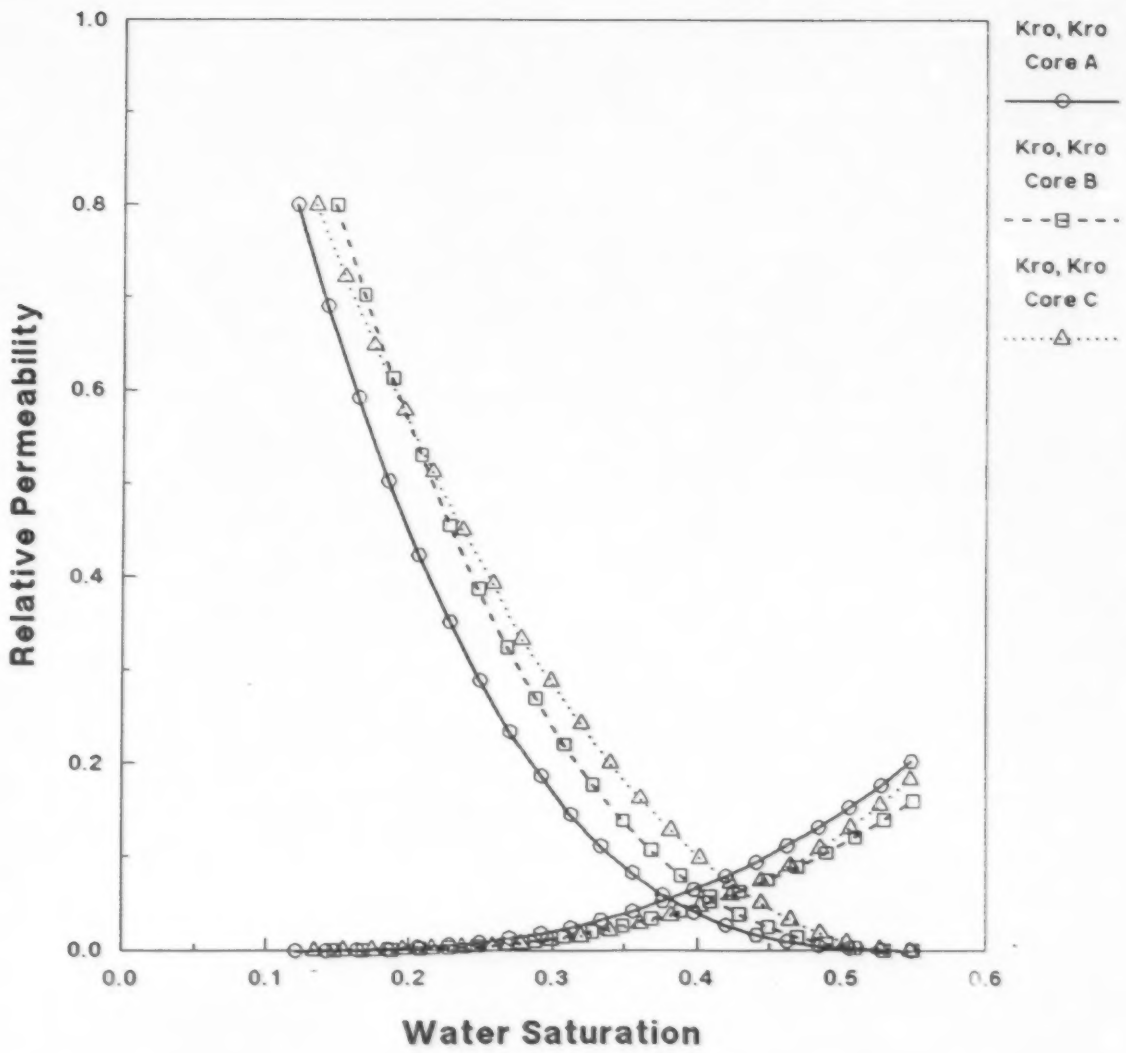

FIGURE 7
COMPARISON OF HIGH TEMPERATURE WATER ENDPOINT RELATIVE PERMEABILITY DATA FOR CORES A, B & C

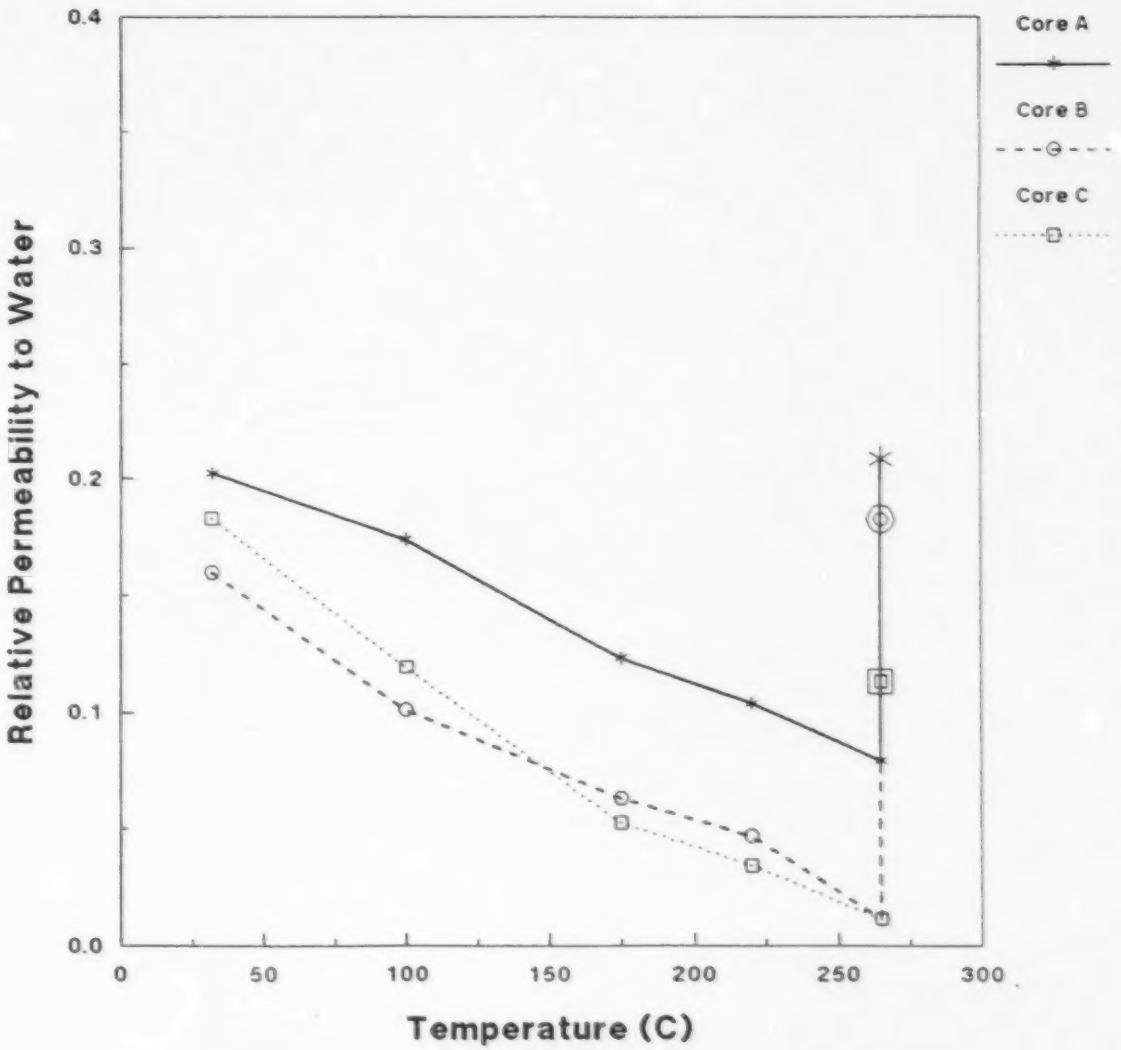
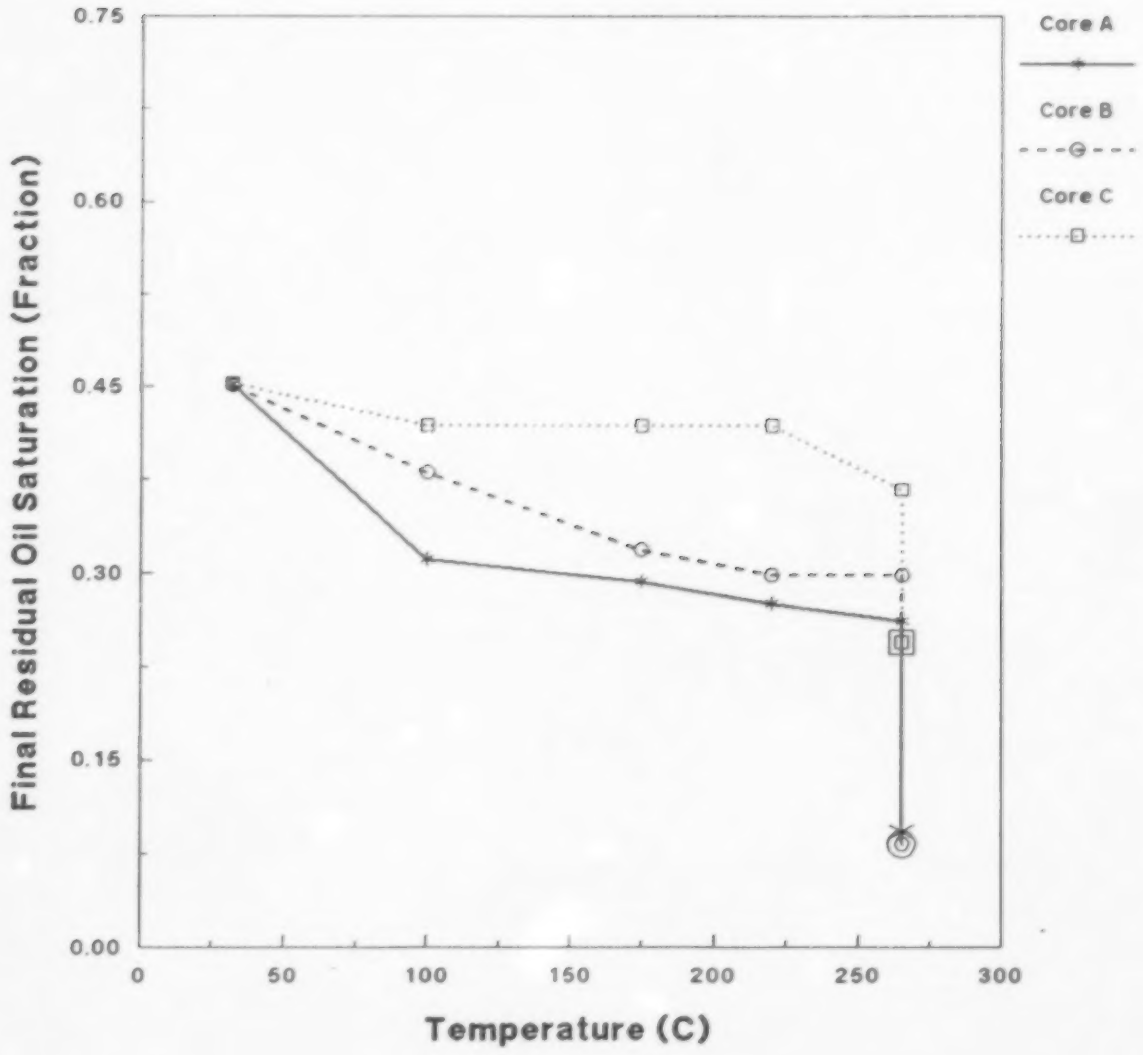
FIGURE 8
COMPARISON OF HIGH TEMPERATURE RESIDUAL SATURATION DATA FOR CORES A, B & C